DIC | SBC 1943 | ABC Imagem Cardiovascular

Volume 37 | Number 1

January/ February/ Mach 2024

Sociedade Brasileira de Cardiologia
ISSN-2675-312X

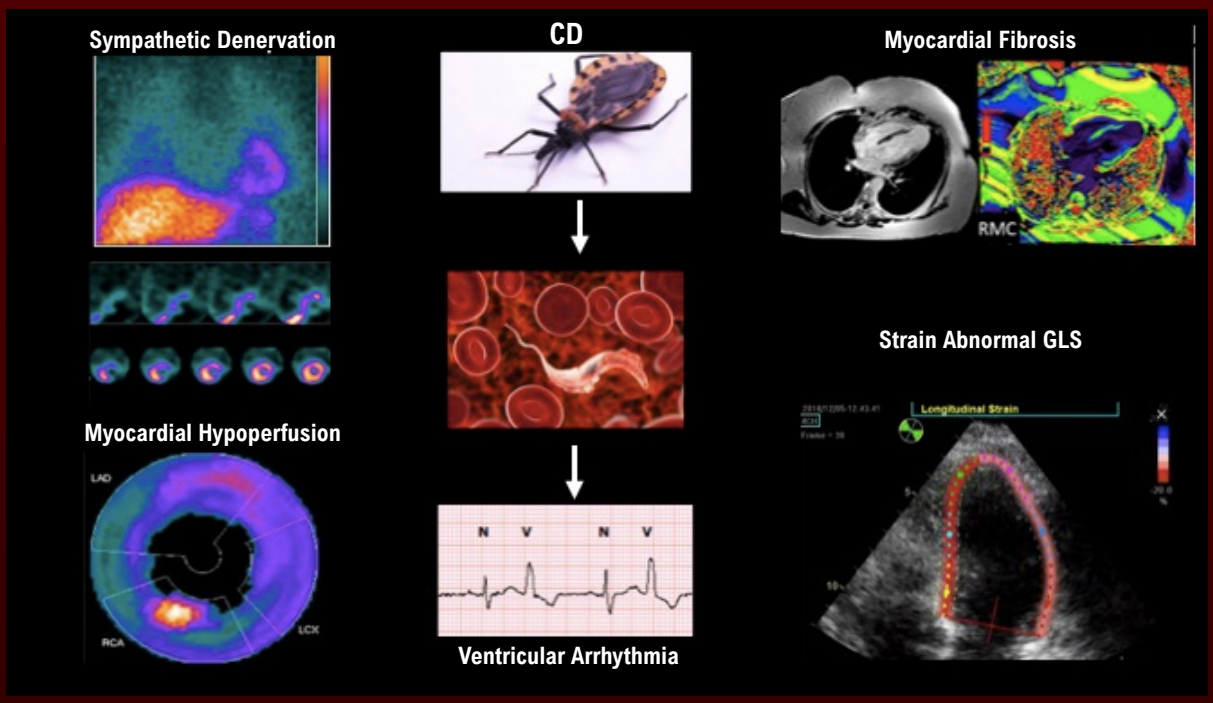

Central Illustration of the article: Association of Sympathetic Denervation, Myocardial Hypoperfusion, and Fibrosis with Ventricular Arrhythmias in Chronic Chagas Cardiomyopathy

DIC | SBC Sociedade Brasileira de Cardiologia 1943 | ABC Imagem Cardiovascular

Contents

Click on the title to read the article

Case Report

Brief Communication

Departament of Cardiovascular Imaging

President
Silvio Henrique Barberato - PR

Vice President of Echocardiography
Daniela do Carmo Rassi Frota - GO

Vice President of Nuclear Cardiology
Cláudio Tinoco Mesquita – RJ

Vice President of Vascular Echography
Salomon Israel do Amaral – RJ

Vice President of Magnetic Resonance Imaging
Isabela Bispo Santos da Silva Costa – SP

Vice President of Computed Tomography
Jorge Andion Torreão – BA

Vice President of Congenital Heart Disease and Pediatric Cardiology
Andressa Mussi Soares – ES

Managing Director
Adenalva Lima de Souza Beck – DF

Financial Director
Gláucia Maria Penha Tavares - SP

Journal Editor
Marcelo Dantas Tavares de Melo – PB

Consulting Board

Members
André Luiz Cerqueira de Almeida - BA
Arnaldo Rabischoffsky - RJ
Carlos Eduardo Rochitte - SP
Marcelo Luiz Campos Vieira - SP
Samira Saady Morhy - SP

Scientific Committee

Coordinator
Daniela do Carmo Rassi Frota - GO

Members
Andressa Mussi Soares - ES
Cláudio Tinoco Mesquita - RJ
Isabela Bispo Santos da Silva Costa - SP
Jorge Andion Torreão - BA
Salomon Israel do Amaral - RJ

Echocardiography Certification Committee

Coordinator
Tatiane Mascarenhas Santiago Emerich - ES
Andrea de Andrade Vilela - SP

Adult Echo Members
Antonio Amador Calvilho JR. - SP
Antonio Tito Paladino Filho - SP
Eliza de Almeida Gripp - RJ
Jaime Paula Pessoa Linhares Filho - CE
João Carlos Moron Saes Braga - SP
Marcio Mendes Pereira - MA
Paulo Henrique Nunes Pereira - PA
Renato de Aguiar Hortegal - SP
Tiago Costa Bignoto - SP
Wanessa Nakamura Guimarães - DF

Congenital Echo Members
Barbara Neiva Tanaka - MA
Daniela Lago Kreuzig - SP
Danielle Lopes Rocha - ES
Halsted Alarcao Gomes Pereira da Silva - SP
Leandro Alves Freire - SP
Marcio Miranda Brito - TO
Maria Elisa Martini Albretch - SP

Seniors
Andrea de Andare Vilela - SP
Glaucia Maria Penha Tavares - SP
José Luiz Barros Pena - MG
Maria Estefania Bosco Otto - DF
Mohamed Hassan Saleh - SP
Solange Bernardes Tatani - SP

Social Media Committee

Coordinator
Alex dos Santos Félix - RJ
Antonio Carlos Leite de Barros Filho - SP

Members
Barbara Athayde Linhares Martins Vrandecic - MG
Cristiane Nunes Martins - MG
José Roberto Matos Souza - SP
Simone Cristina Soares Brandão - PE

Professional Defense and Institutional Relations Committee

Members
Fabio Cañellas Moreira - RS
Jorge Yussef Afiune - DF
Marcelo Haertel Miglioranza - RS
Mohamed Hassan Saleh - SP
Wagner Pires de Oliveira Júnior - DF

Committee of Education and Accreditation

Coordinator
Edgar Bezerra de Lira Filho - SP

Members
Andrea de Andare Vilela - SP
Sandra Nívea dos Reis Saraiva Falcão - CE

Intersociety Committee

Coordinator
Marcelo Luiz Campos Vieira - SP

Members
Ana Cristina de Almeida Camarozano - PR
José Luiz Barros Pena - MG
Marcelo Haertel Miglioranza - RS

DIC Youth Committee

Coordinator
Bruna Morhy Borges Leal Assunção - SP
Márcio Miranda Brito - TO

Adult Echo Members
Carolina da Costa Mendes - SP
Manoela Falsoni - SP
Talita Beithum Ribeiro Mialski - PR
Tauin Raoni Do Couto - PA

CR/MR Members
Maria Júlia Silveira Souto - SP

Vascular Ultrasound Member
Larissa Chaves Nunes de Carvalho - SP

Member Of Congenital Heart Diseases
Isabela de Sousa Lobo Silva - SP

Committee on Echocardiography, Congenital and Pediatric Cardiology

Coordinator
Andressa Mussi Soares - ES

Members
Cláudia Regina Pinheiro de Castro Grau - SP
Laura Mercer Rosa - USA
Márcia Ferreira Alves Barberato - PR

PORTAL DIC

Coordinator
Alex dos Santos Félix - RJ

Board of Directors – Year 2024 (Brazilian Society of Cardiology)

North/Northeast
Nivaldo Menezes Filgueiras Filho (BA)
Sérgio Tavares Montenegro (PE)

East
Denilson Campos de Albuquerque (RJ)
Andréa Araujo Brandão (RJ)

State of São Paulo
Ricardo Pavanello (SP)
João Fernando Monteiro Ferreira (SP)

Center
Carlos Eduardo de Souza Miranda (MG)
Weimar Kunz Sebba Barroso de Souza (GO) – President of the Administrative Council

South
Paulo Ricardo Avancini Caramori (RS)
Gerson Luiz Bredt Júnior (PR) – Vice-President of the Administrative Council

Scientific Committee
Denilson Campos de Albuquerque (RJ)
Ibraim Masciarelli Francisco Pinto (SP)
Nivaldo Menezes Filgueiras Filho (BA)

National Editorial Board

ABC Imagem Cardiovascular

Volume 37, Nº 1, January/February/March 2024

Indexing: Lilacs (Latin American and Caribbean Health Sciences Literature), Latindex (Regional Cooperative Online Information System for Scholarly Journals from Latin America, the Caribbean, Spain and Portugal) and DOAJ (Directory of Open Access Journals)

Address: Av. Marechal Câmara, 160 - 3º andar - Sala 330
20020-907 • Centro • Rio de Janeiro, RJ • Brazil
Phone.: (21) 3478-2700
E-mail: abcimaging@cardiol.br
https://www.abcimaging.org/

Commercial Department
Phone: (11) 3411-5500
E-mail: comercialsp@cardiol.br

Editorial Production
SBC - Scientific Department

Graphic Design and Diagramming
SBC - Scientific Department

Original Article

Relationship Between Echocardiographic Parameters and The Systemic Immune-Inflammation Index in Patients With Pulmonary Arterial Hypertension

Sefa Erdi Ömür,[1] *Gulsen Genc Tapar,*[1] *Mustafa Yilmaz,*[1] *Abdullah Emre Bektaş,*[1] *Osman Demir*[1]

Tokat Gaziosmanpasa Universitesi,[1] *Tokat – Turkey*

Abstract

Background: **Pulmonary arterial hypertension (PAH) is a chronic disease with high morbidity and mortality. The diagnosis of PAH is mainly made based on echocardiographic parameters and natriuretic peptide levels. However, given the low incidence of PAH worldwide, the diagnosis of PAH can be challenging.**

Objectives: **To evaluate the relationship between systemic immune-inflammation (SII) index and PAH.**

Methods: **This was a retrospective, cross-sectional study of 110 patients (43 PAH patients and 67 controls). The SII index was compared between the PAH and control groups. A probability(p) <0.05 were deemed to indicate statistical significance.**

Results: **The findings of this study indicated that SII index was significantly higher in the PAH group than in the control group (1054.15±439.99 vs. 506.7±180.55, p<0.001). The correlation analysis between SII index and echocardiographic parameters revealed that SII index was moderately correlated with right ventricular fractional area change (FAC) (r:-0.567,p<0.001), systolic pulmonary artery pressure (sPAP) (r:0.593, p<0.001), and tricuspid regurgitation velocity (TRV) (r:0.662,p<0.001). Additionally, the SII index was strongly correlated with right atrial (RA) area (r:0.822,p<0.001), pulmonary artery (PA) diameter (r:0.819, p<0.001), left atrium (LA) diameter (r:0.937,p<0.001), inferior vena cava diameter (r:0.869,p<0.001), tricuspid annular plane systolic excursion (TAPSE) (r:-0.902,p<0.001), TAPSE/sPAP (r:-0.831,p<0.001). In addition, the SII index significantly increased as patients' functional capacity (FC) decreased.**

Conclusion: **The SII index is as a simple, inexpensive, noninvasive and easily accessible biochemical parameter that may be useful in the diagnosis and follow-up of PAH patients, especially in centers where echocardiography (ECHO) is not available.**

Keywords: **Pulmonary Arterial Hypertension; Inflammation; Echocardiography.**

Introduction

Pulmonary hypertension (PH) is a term used to describe a group of diseases manifested by different mechanisms and characterized by abnormally increased pressure in the pulmonary arterial system. It is clinically categorized into five subgroups. It is estimated that PH, whose incidence increases with increasing age, affects 1% of the world population,[1] and that the incidence and prevalence of PH subgroups differ from each other.[2]

In PH patients, electrocardiographic data and natriuretic peptide levels are included in a diagnostic algorithm. Echocardiography (ECHO), a non-invasive evaluation tool, is very useful in evaluating patients with pulmonary arterial hypertension (PAH). ECHO findings can be interpreted in accordance with the 2022 European Society of Cardiology (ESC) Guidelines on PH.[3] Systolic pulmonary artery pressure (sPAP), tricuspid regurgitation velocity (TRV), right heart chamber sizes, tricuspid annular plane systolic excursion (TAPSE) and TAPSE/sPAP ratio are the most important ECHO findings that suggest PH. A low TAPSE value indicates right heart failure, while a high TRV value indicates an increased left ventricular filling pressure. TAPSE/sPAP ratio, on the other hand, is a newly defined ECHO parameter recently started to be used in the context of PAH. TAPSE/sPAP contributes to the diagnosis of PAH by reflecting the relationship between the right ventricle and the pulmonary artery (PA) non-invasively.[4]

Systemic immune-inflammation (SII) index is an inflammation marker that has been defined in recent years and associated with various malignancies, coronary artery disease (CAD), rheumatological diseases and hypertension (HT).[5-9] The SII index is calculated using the neutrophil, lymphocyte and platelet counts obtained from the complete blood count test. It reflects two different cellular pathways, i.e., the myeloid and the lymphoid series, that interact with each other. It has also been shown that the SII index is associated with the risk, severity and collateral development of CAD.[10] Pathophysiologically, it is thought that the SII index reflects the balance between inflammation and immune response.[11]

Mailing Address: Sefa Erdi Ömür •
Tokat Gaziosmanpasa Universitesi, 60250 - Turkey
E-mail: sefaerdi61@gmail.com
Manuscript received October 26, 2023; revised January 30, 2024; accepted January 31, 2024
Editor responsible for the review: Marcelo Dantas Tavares de Melo

DOI: https://doi.org/10.36660/abcimg.20230086i

Contents

There is increasing evidence in the literature that inflammation plays a role in the pathogenesis of PAH. Endothelial cells in the pulmonary arterial system are involved in this inflammation. Increased serum cytokine levels cause endothelial dysfunction, vasoconstriction and increased vascular filling. Additionally, patients with PAH have increased levels of perivascular inflammatory cells and inflammatory cytokines.[12]

However, a thorough review of the literature did not reveal any study on the relationship between the SII index and PAH. In this context, the objective of this study is to contribute to the literature by evaluating SII index, an easily accessible and inexpensive marker of inflammation, and the relationship between PAH, SII index, and ECHO findings.

Material and methods

Population and Sample

The population of this cross-sectional, retrospective study consisted of 130 patients who were seen in the cardiology clinic between April 2016 and April 2023 and were diagnosed with PAH. The study protocol was approved by the local university hospital ethics committee. The study was carried out in accordance with the principles outlined in the Declaration of Helsinki.

Right heart catheterization was performed to diagnose PAH. Patients with mean pulmonary artery pressure (mPAP) higher than 20 mmHg, pulmonary capillary wedge pressure (PCWP) lower than 15mmHg, and pulmonary vascular resistance (PVR) higher than 2.0 Woods units were diagnosed with PAH.[3] Right atrial pressure (RAP), mPAP, and PCWP and of the patients were recorded sequentially. Cardiac index (CI) was calculated by the Fick method. PVR was calculated with the formula (mPAP-PCWP)x80/Q .

Individuals under 18 years of age, with acute infection or sepsis, human immunodeficiency virus (HIV) infection, portal HT, drug or toxin-induced peripheral arterial disease, heart failure, pulmonary embolism, severe valve disease, malignancy, coagulation disorder, acute or chronic stroke, storage diseases (lysosomal storage disease, glycogen storage disease, lipid storage disorder, etc.), uncontrolled diabetes mellitus (DM) (glycated haemoglobin >7), acute kidney disease, end-stage renal disease, severe anemia, recent acute coronary syndrome (first six months) or CAD (>30% stenosis in any coronary artery) were excluded from the study. Additionally, ten patients who did not volunteer for the study and an additional ten patients with missing data were excluded from the study. In the end, the PH group consisted of 43 patients diagnosed with PAH. Patients were classified according to their World Health Organization (WHO) functional capacity (FC) (WHO-FC). The control group consisted of 67 patients who were seen at the cardiology clinic with dyspnea and were not diagnosed with PAH, age-matched with the PAH patients.

Echocardiographic Assessment

Echocardiographic evaluations of the PAH and control groups were performed in our center with a Vivid S5 ECHO device (General Electric, Milwaukee, WI, USA), using a 2.5-3.5 MHz transducer, with the patients placed in the left lateral decubitus position. All Doppler ECHO and tissue doppler imaging (TDI) measurements were performed during normal respiration. All two-dimensional, color Doppler, continuous wave (CW)/pulsed-wave (PW) Doppler ECHO data were reviewed and recorded retrospectively by three echocardiographers experienced in PH, blinded to the participants. Left ventricular ejection fraction (LVEF) of all participants were calculated using the modified Simpson method.

Measurements of the left atrium (LA) were performed in the parasternal long-axis view; dimensions of the ascending aortic root and the right atrium were measured at the end of diastole from a right ventricle -focused apical 4-chamber view. The right atrial (RA) dimensions were obtained using RA systolic area parameters; RV basal diameter and RV mid- cavity diameter were measured according to the American Society of ECHO and European Society of Cardiovascular Imaging criteria.[13] Also, the RV end-diastolic longitudinal diameter was measured, and the RA area were calculated. PA diameter was measured from the parasternal short axis and correlated with the result of pulmonary CT angiography. In subxiphoid long axis imaging, inferior vena cava (IVC) imaging and measurements were performed while the probe was over the left lobe of the liver in the subxiphoid area.

Estimated sPAP was calculated based on the tricuspid regurgitation pressure gradient which was calculated from the peak flow rate of the tricuspid regurgitation using Bernoulli's equation. TAPSE and right ventricular fractional area change (FAC) were calculated from the RV-focused apical 4-chamber view.

Laboratory and demographic parameters and inflammatory markers

Biochemical parameters were evaluated automatically using a Beckman Coulter LH-750 Hematology Analyzer (Beckman Coulter, Inc, Fullerton, CA, USA). Patients' lipid profile was evaluated using standard methods. Patients who had a low-density lipoprotein (LDL) value above 130 mg/dL and were treated or previously diagnosed with hypercholesterolemia were considered to have hypercholesterolemia. Patients who were previously diagnosed with DM by an endocrinologist based on the American Diabetes Association criteria[14] were considered to have DM. Patients who had systolic/diastolic blood pressures above 140/90 mmHg as a result of repeated measurements or were previously diagnosed with HT and started on HT treatment were deemed hypertensive.

Treatment data and right heart catheterization outcomes of the patients were obatined from the registry system of the university hospital.

The SII index was calculated by the following formula: peripheral platelet count×neutrophil count/lymphocyte count.

Statistical analysis

The statistical analyses of the collected data were carried out using SPSS 22.0 (Statistical Product and Service Solutions for Windows, Version 22.0, IBM Corp., Armonk, NY, U.S., 2013) software package. The probability (p) < 0.05 indicated statistical significance. Quantitative variables were expressed

as arithmetic mean ± standard deviation (SD) and qualitative variables as numbers and percentages. Continuous variables were described as mean ± SD as they were normally distributed, and qualitative variables were described using absolute and relative frequencies. Shapiro-Wilk test was used to evaluate whether the distributions of continuous variables were normal. The differences between two groups in terms of continuous variables were analyzed using Independent Samples t test. Additionally, the differences between more than two groups in terms of continuous variables were analyzed using the One-Way Analysis of Variance (ANOVA). For post-hoc pairwise comparisons between the groups, the Tukey HSD test was used. The chi-square test was used to determine whether there was a relationship between qualitative variables. Pearson correlation analysis was used to determine the relationships between echocardiographic data and SII index.

Results

Demographic, clinical characteristics and laboratory data were compared between the PAH and control groups. There was no significant difference between the groups in age, gender, body mass index (BMI), comorbid diseases, HT, DM, asthma, chronic obstructive pulmonary disease, dyslipidemia and CAD (Table 1). On the other hand, there was a significant difference between the groups in terms of PAH-specific treatments.

There were significant differences between the groups in terms of laboratory and echocardiographic parameters (Table 2). Accordingly, among the laboratory parameters, neutrophil count, creatinine, uric acid, C-reactive protein (CRP), N-terminal pro–B-type natriuretic peptide (NT-proBNP) levels and SII index values (1054.15±439.99) vs. 506.7±180.55 p<0.001) were significantly higher in the PAH group than in the control group. In addition, among the echocardiographic parameters, TRV, left atrial (LA) diameter, sPAP, TAPSE, TAPSE/sPAP, RA area, RV-FAC, IVC diameter and

Table 1 – Distribution of the basic characteristics of the groups

variable	PAH (n:43)	Control (n:67)	p
Gender (female, n%)	32(74.4)	39(58.2)	0.083
Age (years, mean±SD)	42.42±12.4	42.88±9.8	0.828
BMI (kg/m2, mean±SD)	30.21±6.20	32.72±8.08	0.291
HT (n%)	20(46.5)	24(35.8)	0.264
Hyperlipidemia (n%)	7(10.4)	11(25.6)	0.168
DM (n%)	6(14)	15(22.4)	0.272
CAD (n%)	8(18.6)	15(22.4)	0.634
Asthma (n%)	6(14)	3(4.5)	0.077
Betablocker (n%)	18(41.9)	15(22.4)	0.030
CCB (n%)	14(32.6)	8(11.9)	0.008
ACEi/ARB (n%)	13(30.2)	21(31.3)	0.902

BMI: Body Mass Index; CAD: Coronary Arteries Disease; ACEi: Angiotensin Converting Enzyme inhibitor; ARB: Angiotensin Receptor Blocker; CCB: calcium channel blocker; HT: Hypertension; DM: diabetes mellitus

Table 2 – Comparison of laboratory, echocardiographic features and right heart catheterization parameters between the groups

Variable	PAH (n:43)	Control (n:67)	p
Hemoglobin (g/dl)	13.99±1.53	13.37±1.53	0.053
WBC (X103/µl)	7.66±2.19	8.05±2.47	0.400
Neutrophil (X103/µl)	5.42±1.66	4.6±1.7	0.014
Lymphocyte(X103/µl)	1.44±0.54	2.58±0.92	<0.001
Platelet (X103/µl)	254.16±63.44	272.57±62.52	0.137
Sodium (mmol/L)	140.12±3.38	140.17±2.48	0.917
Potassium(mmol/L)	4.36±0.45	4.36±0.32	0.981
Uric Acid (mg/dl)	19.24±13.52	14±4.82	0.004
Creatinine (mg/dl)	0.88±0.33	0.75±0.16	0.006
CRP (mg/L)	14.35±14.87	6.00±6.44	<0.001
TSH (ng/dL)	2.14±1.64	1.96±0.96	0.463
T4 (ng/dL)	1.36±0.27	1.44±1.21	0.689
Triglyceride (mg/dL)	116.07±45.47	121.81±78.83	0.666
LDL cholesterol(mg/dL)	101.98±46.83	107.63±32.42	0.456
ALT (U/L)	25.27±0.65	23.45±0.76	0.202
AST (U/L)	23.91±0.84	23.42±0.86	0.934
Albumin (gr/dl)	4.1±0.5	4.94±4.24	0.198
NT-proBNP (ng/mL)	1133.84±690.45	30.17±14.97	<0.001
SII	1054.15±439.99	506.7±180.55	<0.001
ASAO diameter (mm)	35.19±4.46	33.09±6.3	0.061
LVEF (%)	58.95±2.79	60.97±3.04	0.001
TRV (m/s)	3.88±0.71	2.32±0.29	<0.001
LA diameter (mm)	39.93±4.57	35.33±5.67	<0.001
sPAP (mmHg)	61.98±21.55	24.85±6.68	<0.001
TAPSE (mm)	1.24±0.33	1.75±0.11	<0.001
TAPSE/sPAP (mm/mmHg)	0.22±0.14	1.3±0.51	<0.001
RA area (cm2)	52.21±7.28	12.86±2.61	<0.001
RV-FAC (%)	24.20±3.61	44.44±2.69	<0.001
IVC diameter (cm)	3.17±0.68	1.73±0.11	<0.001
PA diameter (mm)	32.76±4.82	18.44±4.51	<0.001

sPAP: systolic pulmonary arterial pressure; TAPSE: tricuspid annular plane systolic excursion; TRV: tricuspid regurgitation velocity; RA: Right atrium; IVC: inferior vena cava; PA: pulmonary artery; LA: left atrium; LVEF: left ventricular ejection fraction; ASAO: ascending aorta; SII: systemic immune inflammatory index; ALT: Alanine transaminase; AST: aspartate transaminase ; LDL: low density lipoprotein; TSH: thyroid stimulating hormone; CRP: C-Reactive Protein; WBC: White blood cell; NT-proBNP: N-terminal pro–B-type natriuretic peptide.

PA diameter values were significantly higher in the PAH group than in the control group.

Correlation analysis involving SII index and quantitative parameters, i.e. echocardiographic parameters, laboratory findings, and six-minute walk distance (6MWD) was carried out in the PAH group (Table 3, Figure 1). Consequently, it was found that the SII index was moderately correlated with RV-FAC, sPAP, TRV, and NT-pro BNP. Additionally, SII was strongly correlated with the RA area, PA diameter, LA diameter, IVC diameter, TAPSE, TAPSE/sPAP, and 6MWD.

Considering the results of right heart catheterization in the group with PAH, SII index, mPAP, PVR, CI, PAWP, SvO2 values were strongly correlated.

Analysis of PAH patients by WHO-FC revealed that echocardiographic and laboratory parameters of PAH patients with decreased FC also worsened significantly (Table 4). The comparison of echocardiographic parameters, i.e., RA area, PA diameter, sPAP, IVC diameter, TAPSE and TRV between PAH patients classified as WHO-FC-I, WHO-FC-II and WHO-FC-III revealed significant worsening of FC (from FC I to FC III) of the PAH patients (Table 4). Similarly, the SII index increased (670.65 ± 186.04^{a}, 1375.87 ± 138.15^{b}, and 1712.02 ± 124.77^{c}, respectively, $p<0.001$) as the FC of the PAH patients deteriorated from FC I to FC III (Figure 2).

Table 3 – The parameters associated with SII

variable	r	p
RA area (cm2)	0.822	<0.001
PA diamater (mm)	0.819	<0.001
RV FAC (%)	-0.567	<0.001
LA diameter (mm)	0.937	<0.001
sPAP (mmHg)	0.593	<0.001
IVC diameter (cm)	0.869	<0.001
TAPSE (mm)	-0.902	<0.001
TAPSE/sPAP(mm/mmHg)	-0.831	<0.001
TRV (m/s)	0.662	<0.001
6MWD (m)	-0.905	<0.001
NT-proBNP (ng/mL)	0.649	<0.001
mPAP (mmHg)	0.734	<0.001
PVR (wood unit)	0.767	<0.001
CI (L/min/m2)	-0.699	<0.001
PAWP (mmHg)	-0.831	<0.001
RAP (mmHg)	0.697	<0.001
SvO2 (%)	-0.629	<0.001

sPAP: systolic pulmonary arterial pressure; TAPSE: tricuspid annular plane systolic excursion; TRV: tricuspid regurgitation velocity; RA: Right atrium; IVC: inferior vena cava; PA: pulmonary artery; LA: left atrium; 6MWD: 6-minute walk distance, NT-proBNP: N-terminal pro–B-type natriuretic peptide; mPAP: mean pulmonary artery pressure; PVR: pulmonary vascular resistance; CI: cardiac index; PAWP: pulmonary artery capillary wedge pressure; RAP: right atrial pressure; Sv02: mixed venous oxygen saturation.

Discussion

The results of this study on the relationship between echocardiographic findings of PAH patients and the SII index revealed that the index was significantly and moderately correlated with sPAP, TRV, and RV-FAC, significantly and strongly correlated with RA area, PA diameter and IVC diameter, and significantly and very strongly correlated with LA diameter, TAPSE and TAPSE/sPAP. These findings are important in that they indicate that ECHO parameters change as the SII index increases.

PAH is a progressive cardiopulmonary disease characterized by vaso-occlusive lesions and structural changes in the pulmonary circulation, essentially causing an increase in PA pressure. The pathogenesis of PAH is considered to be multifactorial and complex.[15] Genetic causes, metabolic changes, embolic events, lung diseases, left heart disorders seem to play a role in the etiology of PAH. Then again, vasoconstriction due to inflammation in the early stage and vascular remodeling of the vessel wall in the final stage is detected in all PAH patients.[16] Vascular remodeling is characterized by irreversible tissue change including smooth muscle cells, PA endothelial cells, and fibroblasts. Clustering of macrophages, mast cells, neutrophils, T-lymphocytes and B-lymphocytes has been observed around the pulmonary vessels of patients with PAH, indicating the importance of perivascular inflammation in vascular remodeling.[17] In fact, perivascular inflammation plays a role in all forms of PH. Changes in the structure and function of the endothelium in small to medium-sized pulmonary arterioles due to inflammation occur in conjunction with the growth of the neointimal, medial, and adventitial layers.[18] Vascular stiffening, defined as the increased resistance of the arterial wall against these changes during blood flow, occurs as a result of pathological remodeling in both large proximal arteries and small distal arteries.[19] The mechanical consequence of this structural change is decreased compliance in the proximal vessels and increased resistance to blood flow in the distal vessels, which leads to right heart failure due to high resistance to blood flow. The severity of the disease is related to vascular stiffness. In fact, both experimental studies and studies conducted with PAH patients indicated that vascular stiffness increases with inflammation. In one of these studies, it was demonstrated that inflammation antagonist treatments significantly reduced aortic stiffness in patients with rheumatoid arthritis.[20] In another study, it was shown that plasma CRP levels were high in patients with chronic thromboembolic PAH and that such increase was correlated with the accumulation of endothelial neutrophils and macrophages.[21] Similarly, the correlations found between SII index, a systemic inflammation marker, and the ECHO parameters of PAH patients in this study, and the fact that their neutrophil and lymphocyte counts and CRP values were significantly higher than those of control subjects indicate the effect of inflammation on PAH.

The SII index used in this retrospective study fully demonstrates the balance between the immune and inflammatory states of the host.[22,23] SII index, which has been extensively used in the literature, is accepted as an important marker in determining the risk of pulmonary embolism [9],

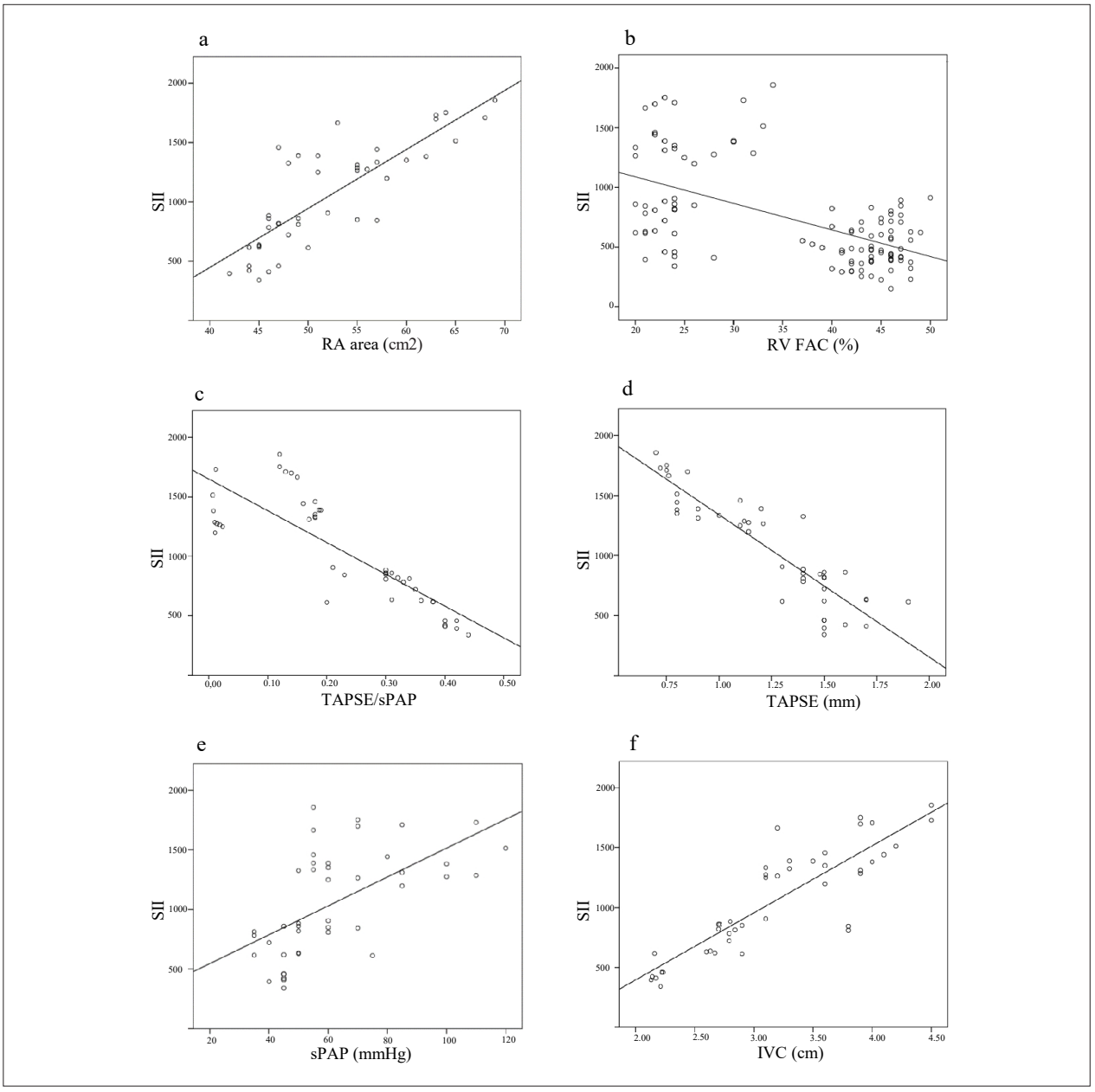

Figure 1 – *Scatter plot diagrams of the relationship of RA area (r:0.8222, p<0.001), RV FAC (r:-0.567, p<0.001), TAPSE/sPAP (R-0.831, P<0.001), TAPSE (R:-0.902, p<0.001), sPAP (0.591, p<0.001), IVC (r:0.869, p<0.001) with SII index in PAH group.*

and prognosis in cancer patients[24] and patients undergoing coronary artery bypass surgery.[24] However, there is no study in the literature that addressed SII index in the context of PAH. Therefore, this is the first study to evaluate the SII index together with ECHO parameters in the diagnosis and follow-up of PAH, and to demonstrate the relationship of the SII index with PAH severity and right ventricular functions.

PAH is a progressive cardiopulmonary disease in which obliterative changes in small to medium pulmonary arterioles are common. Changes occur in the structure and function of the endothelium with the growth of the neointimal, medial, and adventitial layers, resulting in an occlusive arteriopathy associated with high resistance to blood flow, right heart failure, and death. ECHO is an easily applicable non-invasive method for the measurement of many variables associated with PA pressure and right heart hemodynamics.[25] Right atrium dilates due to right ventricular failure, increased right ventricular diastolic pressure and functional tricuspid regurgitation in PAH patients, and increased RA size is one of the indicators of poor prognosis.[26] In this study, the RA area, PA diameter, and TRV values were found to be significantly higher in PAH patients than in control subjects. Additionally, FAC and TAPSE, which are used for the echocardiographic assessment of right ventricular systolic function, were found to be significantly reduced in PAH

Tabela 4 – Comparação do SII e parâmetros ecocardiográficos de acordo com a CF

Variável	CF I (n:14)	CF II (n:18)	CF III (n:11)	p
Área do AD (cm^2)	47,23±3,64 [a]	54,81±4,76 [b]	65,8±2,59 [c]	<0,001
Diâmetro da artéria pulmonar (mm)	29,45±3,33 [a]	35,06±3,15 [b]	40±1,41 [c]	<0,001
FAC do VD (%)	45±2,85 [a]	48,69±3,32 [b]	51,6±3,78 [b]	<0,001
NT-proBNP (ng/mL)	663,27±214,34 [a]	1552±759,67 [b]	1866,2±112,09 [b]	<0,001
Diâmetro do AE (mm)	36,36±1,87 [a]	42,63±3,2 [b]	47±1,22 [b]	<0,001
PSAP (mmHg)	48,86±10,57 [a]	71,88±19,14 [b]	88±27,06 [c]	<0,001
VCI diameter (cm)	2,68±0,47 [a]	3,53±0,35 [b]	4,22±0,28 [c]	<0,001
TAPSE (mm)	1,52±0,14 [a]	1,01±0,19 [b]	0,74±0,04 [c]	<0,001
TAPSE/sPAP (mm/mmHg)	0,34±0,07 [a]	0,11±0,08 [b]	0,08±0,06 [b]	<0,001
TRV (m/s)	3,42±0,27 [a]	4,24±0,63 [b]	4,78±0,86 [c]	<0,001
Neutrófilos (X103/µl)	4,73±1,18 [a]	6,22±2,01 [b]	5,93±1 [ab]	0,003
Linfócitos (X103/µl)	1,63±0,54[a]	1,28±0,51 [b]	1,11±0,36 [c]	<0,001
Plaquetas (X103/µl)	226,5±66,09 [b]	273,94±46,43 [ab]	312,6±34,66 [a]	0,005
TC6M (m)	536,82±82,26 [a]	252,25±68,97 [b]	138±15,12 [c]	<0,001
Índice SII	670,65±186,04 [a]	1375,87±138,15[b]	1712,02±124,77[c]	<0,001

a, b, c letras iguais indicam ausência de diferença significativa, e letras diferentes indicam diferença estatisticamente significativa
PSAP: Pressão Sistólica da Artéria Pulmonar; TAPSE: Excursão Sistólica do Plano do Anel Tricúspide; VRT: Velocidade de Regurgitação Tricúspide; AD: Átrio Direito; VCI: Veia Cava Inferior; AE: Átrio Esquerdo; FAC do VD: variação fracional da área do ventrículo direito; TC6M: Teste de Caminhada de seis mintuos; NT-proBNP: porção N-terminal do pró-hormônio do peptídeo natriurético do tipo B; CF: capacidade funcional.

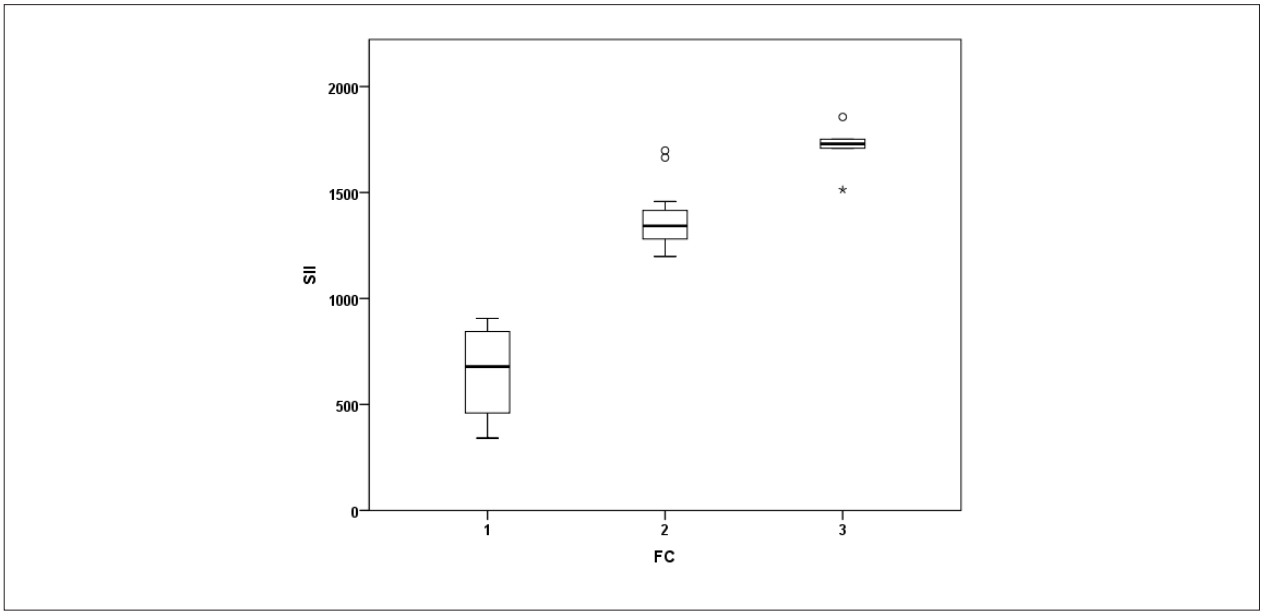

Figure 2 – *The box plot graphic shows increasing SII index from FC I to FC III in PAH group. SII: systemic immune-inflammation; FC: functional capacity.*

patients. These findings indicated that the ECHO parameters used in the diagnosis and follow-up of PAH changed in the negative direction as the SII index value increased.

Furthermore, in this study, PAH patients were divided into subgroups according to their functional capacities and the echocardiographic parameters were evaluated separately between the groups. Consequently, it was determined that the patients' functional capacities decreased and echocardiographic parameters deteriorated as the SII index increased. This finding can be explained by the deterioration

in right heart functions in particular and the decrease in cardiac reserve and functions, in relation to SII index.

Limitations of the study

The single-center and retrospective design and the relatively low number of patients were the primary limitations of this study. Secondly, subgroup analysis of patients with PAH was not performed. Thirdly, mortality of the patients was not evaluated. In the "PAH" patient cohort, the LA size was larger than in the control group and it also increased significantly and abnormally with the worsening of the WHOFC. One possible explanation for this is that we did not evaluate, in the PAH patients, the presence of others comorbidities known to contribute to the worsening of heart failure FC, like atrial fibrillation and heart failure with preserved ejection fraction . Therefore, more comprehensive studies including a larger number of patients are needed to corroborate the findings of this study.

Conclusion

This study is the first in the literature to show that inflammation is an important cause of PAH development and that there is a relationship between the SII index and ECHO parameters in PAH patients. SII index, as a simple, inexpensive, noninvasive and easily accessible biochemical parameter, may be useful in preventing the progression of PAH and determining the treatment strategy, especially in centers where ECHO cannot be not performed.

Acknowledgments

We thank our families for their contributions.

Higlights of the Study

1) The SII index was found to be significantly higher in PAH patients compared to the control subjects.

2) Considering that the SII index is high in PAH patients, it may be a helpful marker in the diagnosis of PAH.

3) The SII index correlates with worsening ECHO parameters in patients with PAH who develop right ventricular heart failure.

4) The SII index may be an important parameter in the diagnosis and follow-up of PAH patients who cannot undergo ECHO.

Author Contributions

Conception and design of the research and analysis and interpretation of the data: Ömür SE, Yilmaz M, Bektaş AE; acquisition of data and obtaining financing: Ömür SE, Tapar GG;

Statistical analysis: Demir O; writing of the manuscript: Ömür SE, Tapar GG, Demir O; critical revision of the manuscript for intellectual content: Ömür SE, Yilmaz M.

Potential Conflict of Interest

No potential conflict of interest relevant to this article was reported.

Sources of Funding

There were no external funding sources for this study.

Study Association

This study is not associated with any thesis or dissertation work.

Ethics Approval and Consent to Participate

This study was approved by the Ethics Committee of the Tokat Gaziosmanpaşa University Clinical Research Ethics Committee under the protocol number 23-KAEK-127. All the procedures in this study were in accordance with the 1975 Helsinki Declaration, updated in 2013. Informed consent was obtained from all participants included in the study.

References

1. Hoeper MM, Humbert M, Souza R, Idrees M, Kawut SM, Sliwa-Hahnle K, et al. A Global View of Pulmonary Hypertension. Lancet Respir Med. 2016;4(4):306-22. doi: 10.1016/S2213-2600(15)00543-3.
2. Hoeper MM, Ghofrani HA, Grünig E, Klose H, Olschewski H, Rosenkranz S. Pulmonary Hypertension. Dtsch Arztebl Int. 2017;114(5):73-84. doi: 10.3238/arztebl.2017.0073.
3. Humbert M, Kovacs G, Hoeper MM, Badagliacca R, Berger RMF, Brida M, et al. 2022 ESC/ERS Guidelines for the Diagnosis and Treatment of Pulmonary Hypertension. Eur Heart J. 2022;43(38):3618-731. doi: 10.1093/eurheartj/ehac237.
4. Tello K, Wan J, Dalmer A, Vanderpool R, Ghofrani HA, Naeije R, et al. Validation of the Tricuspid Annular Plane Systolic Excursion/Systolic Pulmonary Artery Pressure Ratio for the Assessment of Right Ventricular-Arterial Coupling in Severe Pulmonary Hypertension. Circ Cardiovasc Imaging. 2019;12(9):e009047. doi: 10.1161/CIRCIMAGING.119.009047.
5. Huang J, Zhang Q, Wang R, Ji H, Chen Y, Quan X, et al. Systemic Immune-Inflammatory Index Predicts Clinical Outcomes for Elderly Patients with Acute Myocardial Infarction Receiving Percutaneous Coronary Intervention. Med Sci Monit. 2019;25:9690-701. doi: 10.12659/MSM.919802.
6. Wu J, Yan L, Chai K. Systemic Immune-Inflammation Index is Associated with Disease Activity in Patients with Ankylosing Spondylitis. J Clin Lab Anal. 2021;35(9):e23964. doi: 10.1002/jcla.23964.
7. Ji Y, Wang H. Prognostic Prediction of Systemic Immune-Inflammation Index for Patients with Gynecological and Breast Cancers: A Meta-Analysis. World J Surg Oncol. 2020;18(1):197. doi: 10.1186/s12957-020-01974-w.
8. Akyüz A, Işık F. Systemic Immune-Inflammation Index: a Novel Predictor for Non-dipper Hypertension. Cureus. 2022;14(8):e28176. doi: 10.7759/cureus.28176.

9. Gok M, Kurtul A. A Novel Marker for Predicting Severity of Acute Pulmonary Embolism: Systemic Immune-Inflammation Index. Scand Cardiovasc J. 2021;55(2):91-6. doi: 10.1080/14017431.2020.1846774.

10. Kelesoglu S, Yilmaz Y, Elcık D, Kalay N. Systemic Immune Inflammation Index: A Novel Predictor for Coronary Collateral Circulation. Perfusion. 2022;37(6):605-12. doi: 10.1177/02676591211014822.

11. Dziedzic EA, Gąsior JS, Tuzimek A, Paleczny J, Junka A, Dąbrowski M, et al. Investigation of the Associations of Novel Inflammatory Biomarkers-Systemic Inflammatory Index (SII) and Systemic Inflammatory Response Index (SIRI)-with the Severity of Coronary Artery Disease and Acute Coronary Syndrome Occurrence. Int J Mol Sci. 2022;23(17):9553. doi: 10.3390/ijms23179553.

12. Mathew R. Inflammation and Pulmonary Hypertension. Cardiol Rev. 2010;18(2):67-72. doi: 10.1097/CRD.0b013e3181cd612f.

13. Sahn DJ, Maria A, Kisslo J, Weyman A. Recommendations Regarding Quantitation in M-Mode Echocardiography: Results of a Survey of Echocardiographic Measurements. Circulation. 1978;58(6):1072-83. doi: 10.1161/01.cir.58.6.1072.

14. American Diabetes Association. 2. Classification and Diagnosis of Diabetes: Standards of Medical Care in Diabetes-2018. Diabetes Care. 2018;41(Suppl 1):13-27. doi: 10.2337/dc18-S002.

15. Simonneau G, Hoeper MM. The Revised Definition of Pulmonary Hypertension: Exploring the Impact on Patient Management. Eur Heart J Suppl. 2019;21(Suppl K):K4-K8. doi: 10.1093/eurheartj/suz211.

16. Bousseau S, Sobrano Fais R, Gu S, Frump A, Lahm T. Pathophysiology and New Advances in Pulmonary Hypertension. BMJ Med. 2023;2(1):e000137. doi: 10.1136/bmjmed-2022-000137.

17. Hu Y, Chi L, Kuebler WM, Goldenberg NM. Perivascular Inflammation in Pulmonary Arterial Hypertension. Cells. 2020;9(11):2338. doi: 10.3390/cells9112338.

18. Rabinovitch M, Guignabert C, Humbert M, Nicolls MR. Inflammation and Immunity in the Pathogenesis of Pulmonary Arterial Hypertension. Circ Res. 2014;115(1):165-75. doi: 10.1161/CIRCRESAHA.113.301141.

19. Wang Z, Chesler NC. Pulmonary Vascular Wall Stiffness: an Important Contributor to the Increased Right Ventricular Afterload with Pulmonary Hypertension. Pulm Circ. 2011;1(2):212-23. doi: 10.4103/2045-8932.83453.

20. Protogerou AD, Zampeli E, Fragiadaki K, Stamatelopoulos K, Papamichael C, Sfikakis PP. A Pilot Study of Endothelial Dysfunction and Aortic Stiffness after Interleukin-6 Receptor Inhibition in Rheumatoid Arthritis. Atherosclerosis. 2011;219(2):734-6. doi: 10.1016/j.atherosclerosis.2011.09.015.

21. Quarck R, Wynants M, Verbeken E, Meyns B, Delcroix M. Contribution of Inflammation and Impaired Angiogenesis to the Pathobiology of Chronic Thromboembolic Pulmonary Hypertension. Eur Respir J. 2015;46(2):431-43. doi: 10.1183/09031936.00009914.

22. Duyan M, SARIDAŞ A, Vural N. Is it Possible to Predict High-Risk Patients in Acute Pulmonary Embolism with Systemic Immune-Inflammation Index? Eurasian J Crit Care. 2022;4(3):101-5. doi: 10.55994/ejcc.1193320.

23. Chen JH, Zhai ET, Yuan YJ, Wu KM, Xu JB, Peng JJ, et al. Systemic Immune-Inflammation Index for Predicting Prognosis of Colorectal Cancer. World J Gastroenterol. 2017;23(34):6261-72. doi: 10.3748/wjg.v23.i34.6261.

24. Jiménez D, Kopecna D, Tapson V, Briese B, Schreiber D, Lobo JL, et al. Derivation and Validation of Multimarker Prognostication for Normotensive Patients with Acute Symptomatic Pulmonary Embolism. Am J Respir Crit Care Med. 2014;189(6):718-26. doi: 10.1164/rccm.201311-2040OC.

25. Canpolat U, Özer N. Pulmoner Hipertansiyonda Ekokardiyografik Görüntülemenin Yeri. Türk Kardiyoloji Seminerleri. 2011;11(3):274-86.

26. Ozben B, Başaran Y. Echocardiography and Other Imaging Modalities in Pulmonary Arterial Hypertension. Anadolu Kardiyol Derg. 2010;10(Suppl 1):27-35. doi: 10.5152/akd.2010.116.

Association of Sympathetic Denervation, Myocardial Hypoperfusion, and Fibrosis with Ventricular Arrhythmias in Chronic Chagas Cardiomyopathy

Adriana Soares Xavier de Brito,[1] Renata Junqueira Moll-Bernardes,[1] Martha Valéria Tavares Pinheiro,[1] Gabriel Camargo,[1] Fabio Paiva Rossini Siqueira,[1] Adriana Pereira Glavam,[1] Sergio Altino Almeida,[1] Fernanda Souza Nogueira Sardinha Mendes,[2] Paulo Henrique Rosado-de-Castro,[1] Andrea Silvestre Sousa[2]

Instituto D'Or de Pesquisa e Ensino,[1] Rio de Janeiro, RJ – Brazil

Evandro Chagas National Institute of Infectious Diseases,[2] Rio de Janeiro, RJ – Brazil

Abstract

Background: Chronic Chagas cardiomyopathy (CCC) manifests as heart failure, thromboembolic events, and sudden cardiac death (SCD). Although SCD may be the presenting event, there is still no recommendation for early cardioverter/defibrillator implantation in current guidelines.

Objective: To evaluate the correlation between autonomic denervation, myocardial hypoperfusion, fibrosis, and ventricular arrhythmias in patients in the early stages of CCC.

Methods: Cross-sectional study of 29 patients with CCC and preserved left ventricular function who underwent SPECT with iodine-123-meta-iodobenzylguanidine (^{123}I-mIBG), myocardial perfusion SPECT with technetium-99m sestamibi (^{99m}Tc-MIBI), and cardiac magnetic resonance (CMR) with gadolinium, divided into two groups according to on 24h Holter findings: arrhythmia (> 6 ventricular premature complexes/hour and/or nonsustained ventricular tachycardia; n = 15) or no-arrhythmia (< 6 ventricular premature complexes/hour and no ventricular tachycardia; n = 14).

Results: Significant correlations were observed between parameters of the three cardiovascular imaging modalities and the presence of ventricular arrhythmia. Denervation on mIBG correlated moderately with diffuse fibrosis, represented by ECV on CMR (r = 0.55, P = 0.002). Hypoperfusion by MIBI-SPECT correlated with fibrosis by both LGE (r = 0.66, P = 0.005) and extracelluar volume (ECV) (r = 0.56, P = 0.002). We also observed a moderate correlation between the extent of myocardial areas with denervation and hypoperfusion (r = 0.48, P = 0.007).

Conclusion: The presence of autonomic denervation, myocardial hypoperfusion, and fibrosis was associated with ventricular arrhythmia in the early stages of CCC. A combination of these parameters can improve stratification of SCD risk in these patients.

Keywords: Chagas Disease; Sympathetic Denervation; Cardiac Arrhythmias.

Introduction

Chagas disease (CD) is among the neglected tropical diseases recognized by the World Health Organization. There are 300,000 new cases and 50,000 deaths from CD every year.[1-3] Sudden cardiac death (SCD) is the leading cause of mortality in chronic Chagas cardiomyopathy (CCC), representing the most dramatic course of CD,[4,5] and is closely associated with the presence of ventricular arrhythmia and myocardial dysfunction.[6,7] However, there is also a high incidence of SCD and malignant ventricular arrhythmia in young patients still in the early stages of the disease, when the left ventricular ejection fraction (LVEF) is normal or only slightly depressed.[8,9]

In 1916, Carlos Chagas reported: "Also quite frequent are sudden deaths in the cardiac forms of the disease. Sometimes they die still young, fully active, and in an apparently satisfactory state of health."[10]

Indeed, the clinical course of CCC is variable, and identification of patients at risk of death remains a challenge. Rassi et al. proposed a simple risk score with six independent prognostic variables used to predict death.[11] Although this tool has good applicability in clinical, many patients who experienced SCD were not classified as high risk by the score, nor did they qualify for primary prevention with an implantable cardioverter/defibrillator (ICD) according to current guidelines. Furthermore, this model disregards the role of dysautonomia, as has already been demonstrated in other studies.[12-13]

It is well known that the presence of myocardial fibrosis, associated with areas of denervation and microvascular changes, creates an arrhythmogenic substrate. However, the stage of the disease at which these changes occur is still unknown.

Mailing Address: Adriana Soares Xavier de Brito •
Instituto Nacional de Cardiologia. Rua das Laranjeiras, 374. Postal code: 22240-006. Rio de Janeiro, RJ – Brazil
E-mail: adrijsoares@hotmail.com
Manuscript received February 22,2024; revised February 23, 2024; accepted February 23, 2024
Editor responsible for the review: Marcelo Dantas Tavares de Melo

DOI: https://doi.org/10.36660/abcimg.20240008i

Central Illustration: Association of Sympathetic Denervation, Myocardial Hypoperfusion, and Fibrosis with Ventricular Arrhythmias in Chronic Chagas Cardiomyopathy

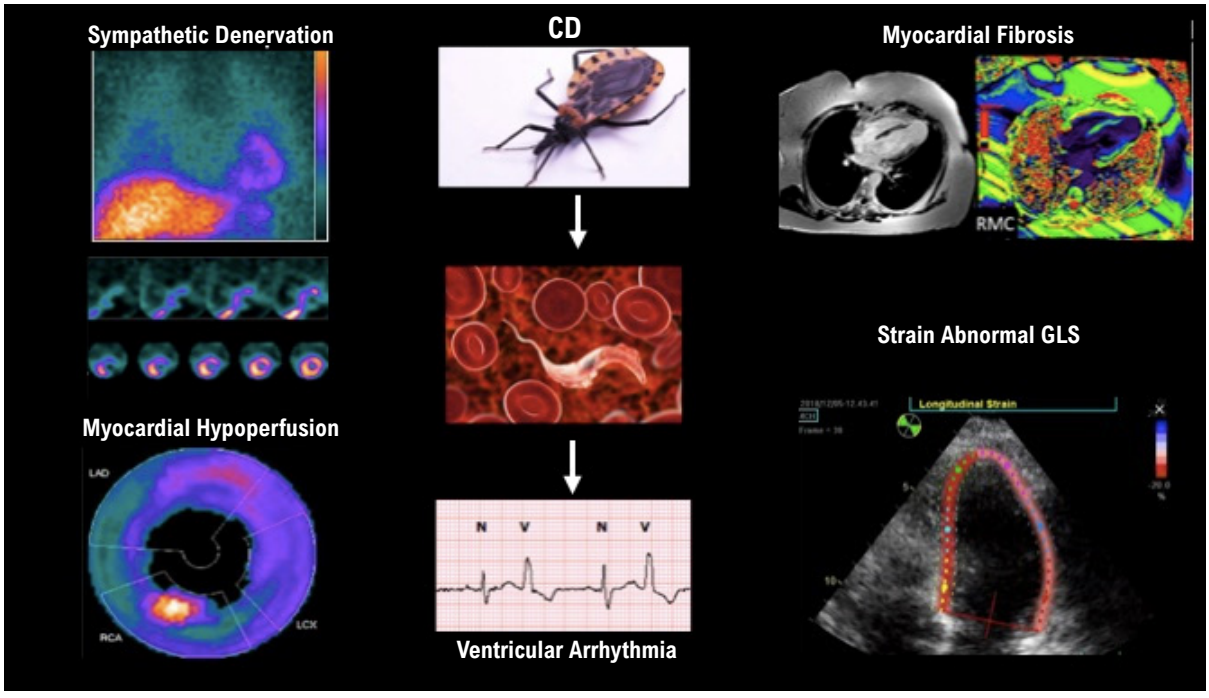

Arq Bras Cardiol: Imagem cardiovasc. 2024;37(1):e20240008

The objective of the present study was to correlate sympathetic denervation as assessed by ^{123}I-mIBG (mIBG) single photon emission computed tomography (SPECT), myocardial hypoperfusion by technetium (^{99m}Tc) sestamibi SPECT (MIBI), and fibrosis by cardiac magnetic resonance (CMR) with the incidence of ventricular arrhythmias in patients with stage A and B1 CD (Central Illustration).

Methods

Population

This prospective cross-sectional study was carried out with outpatients recruited from the CD Clinical Research Laboratory at Fundação Oswaldo Cruz (Rio de Janeiro, Brazil) who were aged ≥ 18 years, had tested positive for *T. cruzi* on two types of serology, preserved LVEF (≥ 45%), and New York Heart Association (NYHA) functional class I.

The exclusion criteria were presence of other heart disease, renal impairment, pregnancy, or breastfeeding. CD was classified according to the Brazilian consensus.[2]

Participants were divided into two groups according to the results of 24-hour Holter monitoring, based on the CAST study: those with six or more ventricular premature complexes per hour and/or nonsustained ventricular tachycardia, and those with fewer than six VPCs per hour and no ventricular tachycardia.[14]

The study was approved by the Ethics Committee of Instituto Nacional de Infectologia Evandro Chagas, Fundação Oswaldo Cruz (CAAE: 63064516.1.0000.5262).

Routine measurements

Patients underwent a 12-lead ECG, 24-hour Holter monitoring with a digital recorder (H3™; Mortara, Milwaukee, WI, USA), and two-dimensional transthoracic echocardiography (Vivid 7®, General Electric Medical Systems, Milwaukee, WI, USA).

Subsequently, they underwent CMG, mIBG scintigraphy, and a resting myocardial perfusion MIBI scan.

CMR protocol

All patients underwent CMR on a 3.0-T scanner (Magnetom Prisma; Siemens AG, Erlangen, Germany). Cine images were acquired in long- and short-axis views. Modified look-locker inversion recovery (MOLLI) T1 mapping images were obtained from short-axis views of the ventricle before and 15 minutes after contrast infusion. The MOLLI 5(3)3 sequence design was used for pre-contrast (native) T1 mapping, while the 4(1)3(1)2 design was used for post-contrast acquisition. Breath-hold late gadolinium enhancement (LGE) images were acquired 10 minutes after contrast infusion, in an inversion-recovery segmented gradient echo sequence. Myocardial fibrosis mass on LGE was characterized by semiquantitative visual scoring.

The extent of LGE was scored on a 5-point scale in each of the 17 myocardial segments on the short-axis images.[15]

MIBG and MIBI protocols

Patients received 185 MBq of mIBG by slow intravenous injection one hour after oral administration of 20 mL of a 10% potassium iodide solution. Planar images (anterior projection) and CT images were acquired with the patient supine, 15 minutes (early) and 3 hours (late) after radiotracer injection, on a SPECT/CT dual-head hybrid gamma camera (Symbia 16T; Siemens Healthineers, Germany) with a low-energy, high-resolution parallel-hole collimator. Planar images were obtained for 5 minutes. CT images were acquired with a semicircumferential orbit, in 32 projections at a rate of 60 s/projection, a 20% energy window centered at 159 keV, and a 64 × 64-pixel acquisition matrix with a pixel size of 0.6 cm. For quantitative analysis of mIBG, the early and late heart-to-mediastinum (H/M) ratios and the myocardial washout rate (%) were calculated as recommended in the current literature (Figure 1).[16,17]

Resting SPECT images were acquired 30 minutes after peripheral intravenous injection of 555 MBq of ^{99m}Tc-MIBI with the gated SPECT technique, using the same equipment and parameters described above, with a 20% energy window centered at 140 keV. All SPECT images were followed by CT images to obtain attenuation correction maps.

Processing and analysis of scintigraphic images

Perfusion and innervation images were analyzed in Syngo P software (Siemens Healthineers), aligned so as to permit simultaneous visualization of the three orthogonal planes (short, horizontal long, and vertical long axes). Two blinded, experienced observers analyzed the images visually using a 17-segment LV model. MIBI and mIBG uptake were scored semiquantitatively (0, normal; 1, mild uptake reduction; 2, moderate uptake reduction; 3, severe uptake reduction; 4, no uptake). Summed perfusion and sympathetic innervation scores were calculated to represent the extent and severity of the respective defects. MIBI total perfusion deficit (TPD) and ventricular function were automatically calculated by QPS/QGS software (Cedars Sinai Medical Center, Los Angeles, CA, USA). The innervation/perfusion mismatch, corresponding to viable but denervated myocardium, was also calculated. Segments exhibiting normal MIBI uptake and reduced mIBG uptake were considered to have innervation/perfusion mismatch.

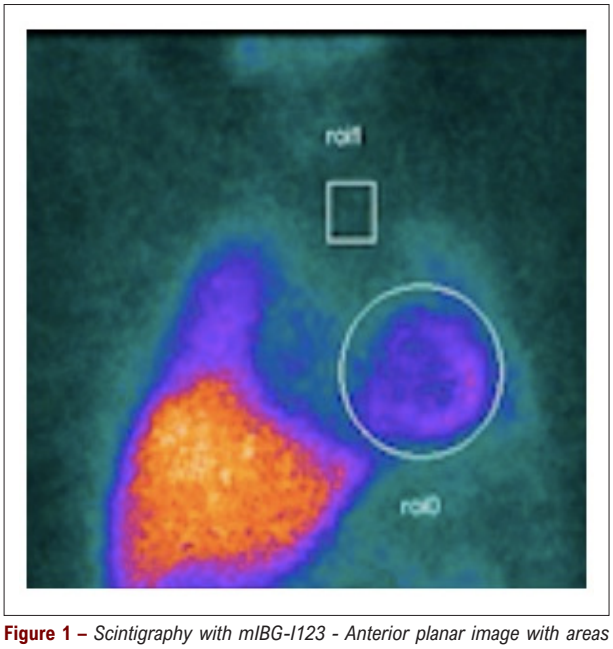

Figure 1 – *Scintigraphy with mIBG-I123 - Anterior planar image with areas of interest over the superior mediastinum (rectangular) and left ventricle (circular) to calculate the heart/mediastinum ratio.*

Statistical analysis

Continuous variables were expressed as means, medians, and standard deviations. Categorical variables were expressed as proportions. Between-group differences were analyzed by the nonparametric Mann–Whitney test.

Spearman coefficients were calculated to test for correlation between areas with sympathetic denervation, myocardial hypoperfusion, and fibrosis.

Significance was accepted at $P \leq 0.05$. All analyses were performed in the SPSS Version 24.0 software environment (IBM Corp, Armonk, NY, USA).

Results

The sample consisted of 29 patients with chronic CD, all categorized as NYHA functional class I. The mean age was 58.5 ± 9.9 years, and 18 patients (62%) were female; the sex distribution did not differ between the arrhythmia and no-arrhythmia groups.

Twenty-two patients (76%) were asymptomatic, and the only medications recorded were antihypertensives and statins. To assess functional capacity and detect myocardial ischemia, all patients underwent cardiopulmonary exercise testing (CPET), which confirmed functional class I and did not reveal any changes suggestive of exercise-induced ischemia. Clinical characteristics are described in Table 1.

Patients in the arrhythmia group had significantly greater areas of compromised cardiac sympathetic innervation, myocardial hypoperfusion, innervation/perfusion mismatch (Figure 2), and fibrosis than patients in the no-arrhythmia group. The findings obtained on cardiovascular imaging in the arrhythmia and no-arrhythmia groups are summarized in Table 2 and Figure 3.

Sympathetic denervation detected on mIBG scintigraphy correlated moderately with diffuse fibrosis, as represented by ECV on CMR images ($r = 0.55$, $P = 0.002$). Hypoperfusion on MIBI-SPECT imaging correlated with fibrosis using the LGE ($r = 0.66$, $P = 0.005$) and ECV ($r = 0.56$, $P = 0.002$) techniques. We also found a moderate correlation between the extent of denervation and the extent of hypoperfusion ($r = 0.48$, $P = 0.007$), as exemplified in Figure 4.

Global longitudinal strain (GLS) on echocardiography correlated inversely with mIBG and MIBI-SPECT scores, as well as with measures of fibrosis on CMR. Patients with GLS had more myocardial hypoperfusion ($r = –0.59$, $P = 0.001$), sympathetic denervation ($r = –0.48$, $P = 0.008$), and fibrosis as represented by LGE ($r = –0.68$; $P = 0.003$) and ECV ($r = –0.45$, $P = 0.01$).

Table 1 – Baseline profile of the study population

Clinical condition	No Arrhythmia Group (n = 14)	Group Arrhythmia (n = 15)	Total (n = 29)
Age, years – mean (± SD)	55.5 (± 10.6)	61.2 (± 8.0)	58.5 (± 9.9)
Sex, female – n (%)	9 (50)	9 (50)	18 (62)
Clinical form – n (%)			
Indeterminate	7 (64)	4 (36)	11 (38)
Stage A	3 (50)	3 (50)	6 (21)
Stage B1	4 (33)	8 (67)	12 (41)
Symptoms – n (%)			
Asymptomatic	9 (41)	13 (59)	22 (76)
Palpitations	4 (67)	2 (33)	6 (21)
Syncope	1 (50)	1 (50)	2 (7)
Medications – n (%)			
Beta-blocker	1 (33)	2 (67)	3 (10)
ACEI or ARB	5 (31)	11 (69)	16 (55)
Diuretics	2 (33)	4 (67)	6 (21)
Statins	5 (50)	5 (50)	10 (34)

SD: standard deviation; ACEI: angiotensin-converting enzyme inhibitor; ARB: angiotensin II receptor blocker.

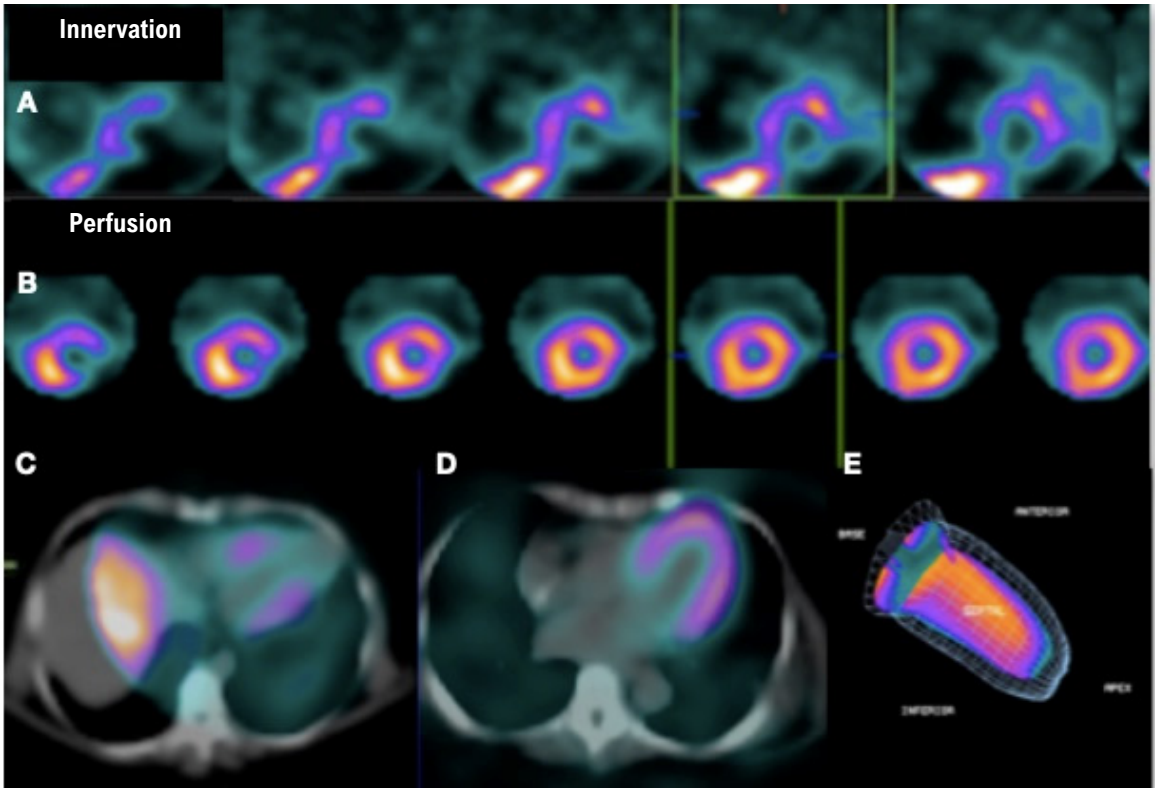

Figure 2 – *Short axes of mIBG scintigraphy and MIBI scintigraphy showing extensive myocardial sympathetic dennervation in the apical, inferior and inferolateral segments (A), with preserved myocardial perfusion (B); corresponding SPECT/CT fusion images with mIBG (C) and MIBI (D), indicating significant denervation/perfusion mismatch in a patient with chronic chagasic heart disease and ventricular arrhythmia. Three-dimensional reconstruction of the left ventricle using the gated-SPECT technique to evaluate ventricular systolic function (E).*

Table 2 – Cardiac imaging features

	No Arrhythmia Group (n = 14)		Arrhythmia Group (n = 15)		p-value[a]
	Mean	SD	Mean	SD	
Echocardiogram					
E/e' ratio	7.9	0.6	10.9	1.5	0.11
Indexed LA volume (mL/m2)	20.3	1.2	30.6	3.5	0.02
LV GLS (%)	- 20.2	0.7	- 16.3	1.0	0.04
LVEF (%)	63.9	5.2	61.3	8.3	0.31
123I-mIBG scintigraphy					
H/M ratio, early	1.81	0.18	1.72	0.21	0.20
H/M ratio, late	1.83	0.14	1.73	0.26	0.20
Washout rate (%)	25.2	7.4	27.5	1.3	0.52
Summed score	5.6	4.9	23.2	18.7	< 0.01
99mTc-MIBI scan					
Summed rest score	0.29	0.6	4.7	6.8	0.02
TPD (%)	0.43	0.6	5.9	7.6	0.01
Gated-SPECT LVEF (%)	67.5	11.0	56.8	21.7	0.10
Mismatch					
MIBG-MIBI	5.4	4.8	18.5	17.5	0.01
Cardiac Resonance (%)					
LVEF (%)	70.7	3.2	57.9	12.1	< 0.01
LGE (%)	4.0	2.9	14.3	13.5	0.04

SD: standard deviation; LA: left atrium; GLS: global longitudinal strain; LVEF: left ventricular ejection fraction; mIBG: iodine-123-metaiodobenzylguanidine; H/M: heart/mediastinum; SPECT: single photon emission computed tomography; MIBG-MIBI: innervation/perfusion mismatch; LGE: late gadolinium enhancement; CMR: cardiac magnetic resonance imaging; MIBI: technetium-99m sestamibi; TPD: total perfusion deficit; LV: left ventricle. a Mann–Whitney test.

Discussion

The present study found that, in patients with early-stage CCC and preserved ventricular function, the extent of cardiac denervation, myocardial perfusion abnormalities, and percentage of fibrosis correlated with a higher incidence of ventricular arrhythmias.

Most studies to date have analyzed patients in the more advanced stages of CCC, with impaired cardiac function and high risk of death – patients in whom ICD implantation would already be indicated for secondary prevention of SCD.[7,11] However, SCD may be the first presenting symptom of CD, affecting young individuals with normal LV function; these sudden deaths have major social and economic impact in endemic countries. Given this research gap, the present study was aimed at a subgroup considered to be at low risk within the natural history of CD, most patients being asymptomatic (76%) and having preserved LV function, but with an uncertain prognosis.

CCC is considered an arrhythmogenic cardiomyopathy. Previous studies with mIBG imaging have demonstrated that denervation can occur early in patients with normal LV function[18,19] and may also be associated with ventricular tachycardia in CCC with mild ventricular dysfunction and few or minor regional abnormalities.[20-22] In addition to confirming this finding of early denervation, the present study showed that patients with CD and ventricular arrhythmias had significantly larger areas of sympathetic denervation than those without arrhythmias, and that these areas also correlated with myocardial hypoperfusion. Several pathological processes can contribute to this phenomenon: sympathetic and parasympathetic neuronal depopulation induced by the parasite itself or by an adverse immune reaction during the acute phase of CD; circulating antibodies capable of binding to cholinergic and adrenergic receptors; and microvascular derangements.[23,24]

We also demonstrated larger areas of hypoperfusion on resting MIBI scintigraphy in the arrhythmia group, although these patients had no anginal complaints, no known CAD, and no evidence of exercise-induced ischemia on CPET. In CD, hypoperfusion has been attributed to changes in the coronary microcirculation associated with the perivascular inflammation typical of the diffuse Chagas myocarditis. Studies of patients with CCC have demonstrated that chest pain and perfusion defects on perfusion scintigraphy did not correlate with obstructive epicardial atherosclerotic disease on coronary angiography,[25-26] which strongly suggests a correlation between disturbances in the coronary

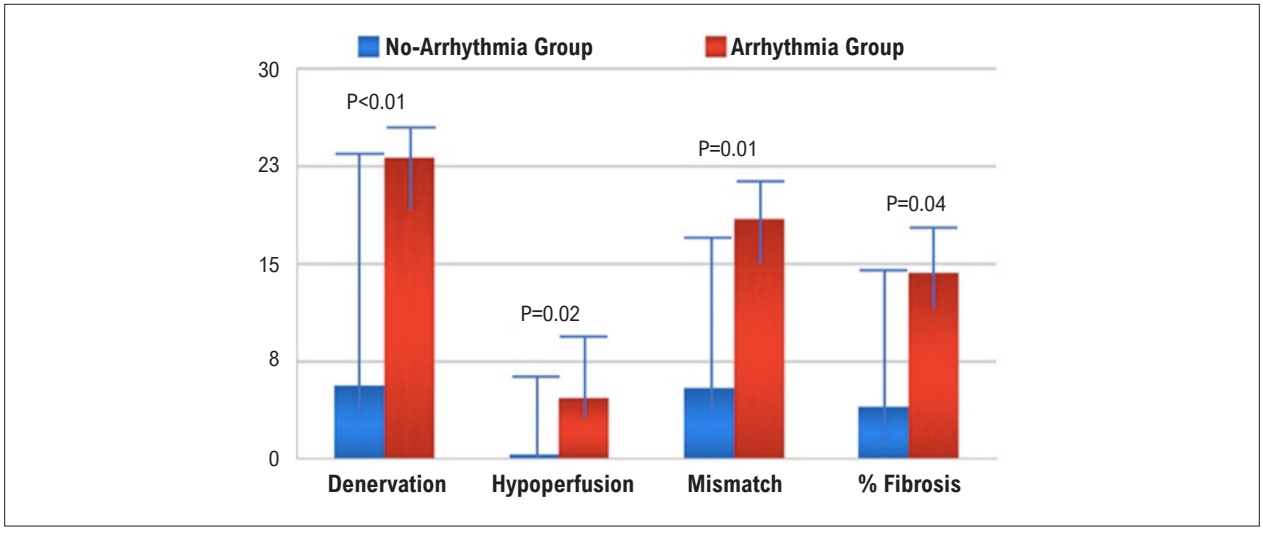

Figure 3 – *Bar graph illustrating the average hypoperfusion sympathetic denervation scores, innervation/perfusion mismatch and percentage of fibrosis between the groups of chagasic patients with and without ventricular arrhythmias.*

	mIBG-SPECT	MIBI-SPECT	GLS (ECHO)
ECV (CMR)	0.55´´	0.56´´	–0.45´
LGE (CMR)	0.48´	0.66´´	–0.68´´
GLS (ECHO)	–0.48´	–0.59´´	** P < 0.01 * P < 0.05

Figure 4 – *Correlations between cardiac sympathetic denervation (mIBG) scores, myocardial hypoperfusion (MIBI) by nuclear SPECT techniques, fibrosis by ECV and LGE techniques of CMR and GLS by transthoracic ECHO in patients with chronic chagasic heart disease and ventricular arrhythmias. ECHO: echocardiography; ECV: extracellular volume; CMR: cardiac magnetic resonance imaging; GLS: global longitudinal strain; LGE: delayed enhancement.*

microcirculation, hypoperfusion, and progression to regional fibrosis, as previously observed from experimental and human pathology evidence.[27-29] These findings support a role of regional perfusion abnormalities in the pathogenesis of myocardial damage in CCC. In the present study, these findings were replicated in patients still in the early stages of the disease.

Furthermore, we found that areas of innervation/perfusion mismatch were associated with a higher incidence of ventricular arrhythmias. It has been postulated that innervation/perfusion mismatch may predispose to fatal ventricular arrhythmias in CCC with ventricular dysfunction.[21-23,30] Although the pathophysiology is still unclear, areas so affected may be hypersensitive to catecholamines, with upregulation of β-adrenergic receptors, increased automaticity, and exaggerated responses to sympathetic activation.[31]

In our sample, fibrosis mass as estimated by CMR was also associated with ventricular arrhythmias and correlated with hypoperfusion and denervation. Regarding this finding, Gadioli et al.[21] reported a correlation of ventricular arrhythmias with the extent of cardiac sympathetic denervation, but not with fibrosis, in patients with CCC and mild ventricular dysfunction. However, it is worth noting that their study did not use CMR and considered perfusion changes on MIBI as indicative of fibrosis, which may be a limitation, as this finding may simply represent abnormalities in the microcirculation without fibrosis or scarring.

Fibrosis is a known arrhythmogenic substrate in ischemic and nonischemic LV dysfunction,[32] including CCC.[33,34] Fibrotic lesions disrupt intercellular junctions, alter the cardiac electrical potential, and form reentrant circuits for arrhythmias.[35] The extent of fibrosis as assessed by late enhancement on CMR can be used to identify high-risk patients. Recently developed techniques, such as T1 mapping and ECV assessment, can further refine this stratification, as demonstrated in a previous study by our group[36] which showed the presence of diffuse interstitial fibrosis on T1 mapping even in the undetermined form of CD, as well as an independent association between ventricular arrhythmias and ECV in CCC – which was confirmed by the current study.

Corroborating the findings of early changes in cardiac function before global and regional abnormalities develop, we observed in this study a reduction in LV GLS in the arrhythmia group as compared to the no-arrhythmia group.

This reduction in GLS in the arrhythmia group was inversely correlated with sympathetic denervation, myocardial hypoperfusion, and fibrosis, which opens fascinating avenues for further refinement of risk stratification. GLS reflects the longitudinal deformation of the myocardium in a more sensitive and reproducible way than LVEF.[37,38] Azevedo et al.[39] demonstrated a significant association between GLS and myocardial mechanical dispersion with nonsustained ventricular tachycardia in 77 patients with CCC. Recently, reductions in GLS were also observed in the undetermined form of the disease, before the onset of fibrosis.[40]

The novelty of the present study lies in our finding that, even in "low-risk" patients at the earliest stages of CCC, a significant association between ventricular arrhythmias and the various pathophysiological mechanisms involved in the genesis of SCD is already present, as demonstrated by different cardiovascular imaging methods.

Limitations

The sample size of this study was relatively small. Nevertheless, we were able to observe significant associations of fibrosis, hypoperfusion, and myocardial denervation with ventricular arrhythmias and increased risk of SCD in CCHD.

Conclusions

Sympathetic denervation (detected by mIBG), myocardial hypoperfusion (detected by MIBI), and fibrosis (represented by ECV and LGE on CMR) correlate significantly with the incidence of ventricular arrhythmias in patients with CCHD and preserved left ventricular function. These findings may aid in the development of tools to improve SCD risk stratification and identify patients who may benefit from specific therapy, such as ICD implantation.

Acknowledgments

We thank all the staff and research assistants at Instituto D'Or de Pesquisa e Ensino; Fundação Oswaldo Cruz (Fiocruz); and the patients who participated in this study.

Author Contributions

Conception and design of the research: Brito ASX, Moll-Bernardes RJ, Almeida AS, Rosado-de-Castro PH, Sousa AS; acquisition of data and analysis and interpretation of the data: Brito ASX, Moll-Bernardes RJ, Pinheiro MVT, Camargo G, Siqueira FPR, Glavam AP, Almeida AS, Mendes FSNS, Rosado-de-Castro PH, Sousa AS; statistical analysis and writing of the manuscript: Brito ASX, Moll-Bernardes RJ, Sousa AS; obtaining financing: Brito ASX, Moll-Bernardes RJ, Rosado-de-Castro PH, Sousa AS; critical revision of the manuscript for intellectual content: Brito ASX, Moll-Bernardes RJ, Pinheiro MVT, Mendes FSNS, Rosado-de-Castro PH, Sousa AS.

Potential Conflict of Interest

No potential conflict of interest relevant to this article was reported.

Sources of Funding

This study was funded by Instituto D'or de pesquisa e ensino, Instituto Nacional de Infectologia Evandro Cruz (Friocruz), Inova and CNPq.

Study Association

This article is part of the thesis of Doctoral submitted by Adriana Soares Xavier de Brito, from Instituto D'or de Pesquisa e Ensino.

Ethics Approval and Consent to Participate

This study was approved by the Ethics Committee of the Instituto Nacional de Infectologia Evandro Chagas, Fundação Oswaldo Cruz under the protocol number 63064516.1.0000.5262. All the procedures in this study were in accordance with the 1975 Helsinki Declaration, updated in 2013. Informed consent was obtained from all participants included in the study.

References

1. World Health Organization. Chagas disease (American trypanosomiasis) [Internet]. Geneva: World Health Organization; 2022 [cited 2022 Dec 4]. Available from: https://www.who.int/health-topics/chagas-disease.
2. Dias JC, Ramos AN Jr, Gontijo ED, Luquetti A, Shikanai-Yasuda MA, Coura JR, et al. 2 nd Brazilian Consensus on Chagas Disease, 2015. Rev Soc Bras Med Trop. 2016;49 (Suppl 1):3-60. doi: 10.1590/0037-8682-0505-2016.
3. Chagas Disease in Latin America: An Epidemiological Update Based on 2010 Estimates. Wkly Epidemiol Rec. 2015;90(6):33-43.
4. Manzullo EC, Chuit R. Risk of Death Due to Chronic Chagasic Cardiopathy. Mem Inst Oswaldo Cruz. 1999;94 (Suppl 1):317-20. doi: 10.1590/S0074-02761999000700060.
5. Lopes ER. Sudden Death in Patients with Chagas Disease. Mem Inst Oswaldo Cruz. 1999;94 (Suppl 1):321-4. doi: 10.1590/s0074-02761999000700061.
6. Rassi A Jr, Rassi SG, Rassi A. Sudden Death in Chagas' Disease. Arq Bras Cardiol. 2001;76(1):75-96. doi: 10.1590/s0066-782x2001000100008.
7. Souza AC, Salles G, Hasslocher-Moreno AM, Sousa AS, Brasil PEAA, Saraiva RM, et al. Development of a Risk Score to Predict Sudden Death in Patients with Chaga's Heart Disease. Int J Cardiol. 2015;187:700-4. doi: 10.1016/j.ijcard.2015.03.372.
8. Baroldi G, Oliveira SJ, Silver MD. Sudden and Unexpected Death in Clinically 'Silent' Chagas' Disease. A hypothesis. Int J Cardiol. 1997;58(3):263-8. doi: 10.1016/s0167-5273(96)02878-1.
9. Sternick EB, Martinelli M, Sampaio R, Gerken LM, Teixeira RA, Scarpelli R, et al. Sudden Cardiac Death in Patients with Chagas Heart Disease and Preserved Left Ventricular Function. J Cardiovasc Electrophysiol. 2006;17(1):113-6. doi: 10.1111/j.1540-8167.2005.00315.x.
10. Chagas C. Processos Patojenicos da Tripanozomiase Americana. Mem Inst Oswaldo Cruz. 1916;8:5-36. doi: 10.1590/S0074-02761916000200002.
11. Rassi A Jr, Rassi A, Little WC, Xavier SS, Rassi SG, Rassi AG, et al. Development and Validation of a Risk Score for Predicting Death in Chagas' Heart Disease. N Engl J Med. 2006;355(8):799-808. doi: 10.1056/NEJMoa053241.

12. Nunes MCP, Beaton A, Acquatella H, Bern C, Bolger AF, Echeverría LE, et al. Chagas Cardiomyopathy: An Update of Current Clinical Knowledge and Management: A Scientific Statement from the American Heart Association. Circulation. 2018;138(12):e169-e209. doi: 10.1161/CIR.0000000000000599.

13. Barros MV. New Predictors of Malignant Ventricular Arrhythmias in Chagas Disease: Searching for the Holy Grail. Rev Soc Bras Med Trop. 2015;48(1):1-3. doi: 10.1590/0037-8682-0059-2015.

14. Denes P, Gillis AM, Pawitan Y, Kammerling JM, Wilhelmsen L, Salerno DM. Prevalence, Characteristics and Significance of Ventricular Premature Complexes and Ventricular Tachycardia Detected by 24-Hour Continuous Electrocardiographic Recording in the Cardiac Arrhythmia Suppression Trial. CAST Investigators. Am J Cardiol. 1991;68(9):887-96. doi: 10.1016/0002-9149(91)90404-9.

15. Fine NM, Tandon S, Kim HW, Shah DJ, Thompson T, Drangova M, et al. Validation of Sub-Segmental Visual Scoring for the Quantification of Ischemic and Nonischemic Myocardial Fibrosis using Late Gadolinium Enhancement MRI. J Magn Reson Imaging. 2013;38(6):1369-76. doi: 10.1002/jmri.24116.

16. Cerqueira MD, Weissman NJ, Dilsizian V, Jacobs AK, Kaul S, Laskey WK, et al. Standardized Myocardial Segmentation and Nomenclature for Tomographic Imaging of the Heart. A Statement for Healthcare Professionals from the Cardiac Imaging Committee of the Council on Clinical Cardiology of the American Heart Association. Int J Cardiovasc Imaging. 2002;18(1):539-42.

17. Flotats A, Carrió I, Agostini D, Le Guludec D, Marcassa C, Schäfers M, et al. Proposal for Standardization of 123I-Metaiodobenzylguanidine (MIBG) Cardiac Sympathetic Imaging by the EANM Cardiovascular Committee and the European Council of Nuclear Cardiology. Eur J Nucl Med Mol Imaging. 2010;37(9):1802-12. doi: 10.1007/s00259-010-1491-4.

18. Marino VSP, Dumont SM, Mota LDG, Braga DS, Freitas SS, Moreira MDCV. Sympathetic Dysautonomia in Heart Failure by 123I-MIBG: Comparison between Chagasic, Non-Chagasic and Heart Transplant Patients. Arq Bras Cardiol. 2018;111(2):182-90. doi: 10.5935/abc.20180124.

19. Landesmann MC, Fonseca LM, Pereira BB, Nascimento EM, Castro PHR, Souza SA, et al. Iodine-123 Metaiodobenzylguanidine Cardiac Imaging as a Method to Detect Early Sympathetic Neuronal Dysfunction in Chagasic Patients with Normal or Borderline Electrocardiogram and Preserved Ventricular Function. Clin Nucl Med. 2011;36(9):757-61. doi: 10.1097/RLU.0b013e31821772a9.

20. Miranda CH, Figueiredo AB, Maciel BC, Marin-Neto JA, Simões MV. Sustained Ventricular Tachycardia is Associated with Regional Myocardial Sympathetic Denervation Assessed with 123I-Metaiodobenzylguanidine in Chronic Chagas Cardiomyopathy. J Nucl Med. 2011;52(4):504-10. doi: 10.2967/jnumed.110.082032.

21. Gadioli LP, Miranda CH, Pintya AO, Figueiredo AB, Schmidt A, Maciel BC, et al. The Severity of Ventricular Arrhythmia Correlates with the Extent of Myocardial Sympathetic Denervation, but not with Myocardial Fibrosis Extent in Chronic Chagas Cardiomyopathy: Chagas Disease, Denervation and Arrhythmia. J Nucl Cardiol. 2018;25(1):75-83. doi: 10.1007/s12350-016-0556-6.

22. Barizon GC, Simões MV, Schmidt A, Gadioli LP, Murta Junior LO. Relationship between Microvascular Changes, Autonomic Denervation, and Myocardial Fibrosis in Chagas Cardiomyopathy: Evaluation by MRI and SPECT Imaging. J Nucl Cardiol. 2020;27(2):434-44. doi: 10.1007/s12350-018-1290-z.

23. Marin-Neto JA, Simões MV, Rassi Junior A. Pathogenesis of Chronic Chagas Cardiomyopathy: the Role of Coronary Microvascular Derangements. Rev Soc Bras Med Trop. 2013;46(5):536-41. doi: 10.1590/0037-8682-0028-2013.

24. Marin-Neto JA, Cunha-Neto E, Maciel BC, Simões MV. Pathogenesis of Chronic Chagas Heart Disease. Circulation. 2007;115(9):1109-23. doi: 10.1161/CIRCULATIONAHA.106.624296.

25. Marin-Neto JA, Marzullo P, Marcassa C, Gallo Júnior L, Maciel BC, Bellina CR, et al. Myocardial Perfusion Abnormalities in Chronic Chagas' Disease as Detected by Thallium-201 Scintigraphy. Am J Cardiol. 1992;69(8):780-4. doi: 10.1016/0002-9149(92)90505-s.

26. Hiss FC, Lascala TF, Maciel BC, Marin-Neto JA, Simões MV. Changes in Myocardial Perfusion Correlate with Deterioration of Left Ventricular Systolic Function in Chronic Chagas' Cardiomyopathy. JACC Cardiovasc Imaging. 2009;2(2):164-72. doi: 10.1016/j.jcmg.2008.09.012.

27. Rossi MA, Tanowitz HB, Malvestio LM, Celes MR, Campos EC, Blefari V, et al. Coronary Microvascular Disease in Chronic Chagas Cardiomyopathy Including an Overview on History, Pathology, and Other Proposed Pathogenic Mechanisms. PLoS Negl Trop Dis. 2010;4(8):e674. doi: 10.1371/journal.pntd.0000674.

28. Ferrans VJ, Milei J, Tomita Y, Storino RA. Basement Membrane Thickening in Cardiac Myocytes and Capillaries in Chronic Chagas' Disease. Am J Cardiol. 1988;61(13):1137-40. doi: 10.1016/0002-9149(88)90148-8.

29. Rossi MA, Gonçalves S, Santos RR. Experimental Trypanosoma Cruzi Cardiomyopathy in BALB/C Mice. The Potential Role of Intravascular Platelet Aggregation in its Genesis. Am J Pathol. 1984;114(2):209-16.

30. Gadioli LP, Miranda CH, Marin-Neto JA, Volpe GJ, Filho ACLB, Filho AP, et al. Regional Myocardial Sympathetic Denervation Precedes the Development of Left Ventricular Systolic Dysfunction in Chronic Chagas' Cardiomyopathy. J Nucl Cardiol. 2022;29(6):3166-76. doi: 10.1007/s12350-021-02869-3.

31. Dae MW, O'Connell JW, Botvinick EH, Chin MC. Acute and Chronic Effects of Transient Myocardial Ischemia on Sympathetic Nerve Activity, Density, and Norepinephrine Content. Cardiovasc Res. 1995;30(2):270-80.

32. White JA, Patel MR. The Role of Cardiovascular MRI in Heart Failure and the Cardiomyopathies. Magn Reson Imaging Clin N Am. 2007;15(4):541-64, vi. doi: 10.1016/j.mric.2007.08.009.

33. Rochitte CE, Oliveira PF, Andrade JM, Ianni BM, Parga JR, Avila LF, et al. Myocardial Delayed Enhancement by Magnetic Resonance Imaging in Patients with Chagas' Disease: a Marker of Disease Severity. J Am Coll Cardiol. 2005;46(8):1553-8. doi: 10.1016/j.jacc.2005.06.067.

34. Torreão JA, Ianni BM, Mady C, Naia E, Rassi CH, Nomura C, et al. Myocardial Tissue Characterization in Chagas' Heart Disease by Cardiovascular Magnetic Resonance. J Cardiovasc Magn Reson. 2015;17:97. doi: 10.1186/s12968-015-0200-7.

35. Paola AA, Horowitz LN, Miyamoto MH, Pinheiro R, Ferreira DF, Terzian AB, et al. Angiographic and Electrophysiologic Substrates of Ventricular Tachycardia in Chronic Chagasic Myocarditis. Am J Cardiol. 1990;65(5):360-3. doi: 10.1016/0002-9149(90)90302-h.

36. Pinheiro MVT, Moll-Bernardes RJ, Camargo GC, Siqueira FP, Azevedo CF, Holanda MT, et al. Associations between Cardiac Magnetic Resonance T1 Mapping Parameters and Ventricular Arrhythmia in Patients with Chagas Disease. Am J Trop Med Hyg. 2020;103(2):745-51. doi: 10.4269/ajtmh.20-0122.

37. Belghitia H, Brette S, Lafitte S, Reant P, Picard F, Serri K, et al. Automated Function Imaging: a New Operator-Independent Strain Method for Assessing Left Ventricular Function. Arch Cardiovasc Dis. 2008;101(3):163-9. doi: 10.1016/s1875-2136(08)71798-4.

38. Cho GY, Marwick TH, Kim HS, Kim MK, Hong KS, Oh DJ. Global 2-Dimensional Strain as a New Prognosticator in Patients with Heart Failure. J Am Coll Cardiol. 2009;54(7):618-24. doi: 10.1016/j.jacc.2009.04.061.

39. Azevedo ACA, Barros MVL, Klaboe LG, Edvardsen T, Costa HS, Paixao GMM, et al. Association between Myocardial Mechanical Dispersion and Ventricular Arrhythmogenicity in Chagas Cardiomyopathy. Int J Cardiovasc Imaging. 2021;37(9):2727-34. doi: 10.1007/s10554-021-02246-8.

40. Romano MMD, Moreira HT, Marin-Neto JA, Baccelli PE, Alenezi F, Klem I, et al. Early Impairment of Myocardial Deformation Assessed by Regional Speckle-Tracking Echocardiography in the Indeterminate form of Chagas Disease without Fibrosis Detected by Cardiac Magnetic Resonance. PLoS Negl Trop Dis. 2020;14(11):e0008795. doi: 10.1371/journal.pntd.0008795.

Echocardiographic Evaluation of Right Atrial Function in Patients with Precapillary Pulmonary Hypertension

Wanessa Alves de Carvalho,[1] Andressa Alves de Carvalho,[1] Eliauria Rosa Martins,[1] Agostinho Hermes de Medeiros Neto,[1] Fernando Bacal,[2] Marcelo Dantas Tavares de Melo[1]

Universidade Federal da Paraíba,[1] João Pessoa, PB – Brazil

Universidade de Sao Paulo,[2] São Paulo, SP – Brazil

Abstract

Background: Considering that the effect of right ventricular (RV) failure on the right atrium (RA) is an essential part of the pathophysiology of pulmonary hypertension (PH), the assessment of RA function seems to have prognostic value in the course of the disease, but there are still few studies on this subject.

Objective: To evaluate myocardial strain of the RA in patients with precapillary PH.

Methods: This is an observational, longitudinal, prospective study involving 36 patients with precapillary PH, in whom two-dimensional Doppler echocardiography was performed. A control group consisting of 26 healthy individuals was used.

Results: There was a statistically significant difference in mean RA strain between the group with PH (26.3%) and the control group (40.7%). Regarding RA strain of the patients, there was a negative and moderate correlation with RA pressure, RV diameter, and RV hypokinesia; negative and weak correlation with pulmonary artery systolic pressure (PASP); negative and strong correlation with RA area; and positive and moderate correlation with, tricuspid annular plane systolic excursion (TAPSE), TAPSE/PASP, and RV strain. Patients with RA strain ≤ 23 had significantly reduced overall survival compared with patients with RA strain > 23, but this value was not a predictor of mortality.

Conclusion: It was possible to demonstrate that the analysis of myocardial strain of the RA provides more accurate information about RA function and can be used as an additional parameter in the follow-up of patients with PH, given the early evaluation of atrial dysfunction.

Keywords: Pulmonary Hypertension; Right Atrial Function; Doppler Echocardiography.

Introduction

Pulmonary hypertension (PH) is a hemodynamic condition characterized by mean pulmonary artery pressure greater than or equal to 20 mmHg at rest during right heart catheterization.[1] PH, after hypertension and coronary artery disease, is believed to be the third leading cardiovascular condition, presenting poor long-term therapeutic outcome.[2] Moreover, nonspecific clinical manifestations, the long oligosymptomatic period, and lack of knowledge about the disease lead to poor prognosis and delay in diagnosis and initiation of treatment.[3]

Patients with PH have increased afterload in the right ventricle (RV) due to increased pulmonary vascular resistance and reduced compliance.[4] Consequently, RV remodeling occurs, with increased RV end-diastolic pressure and right atrial pressure (RAP), which leads to right heart failure and a worse prognosis.[5]

Mailing Address: Marcelo Dantas Tavares de Melo •
Universidade Federal da Paraíba. Campus I, Lot. Cidade Universitária. Postal code: 58051-900. João Pessoa, PB – Brazil.
E-mail: marcelo_dtm@yahoo.com.br
Manuscript received January 18, 2024; revised January 25, 2024; accepted February 4, 2024.
Editor responsible for the review: Marcelo Dantas Tavares de Melo

DOI: https://doi.org/10.36660/abcimg.20240002i

In addition to the RV, the remodeling of the right atrium (RA), with changes in size, function, and pressure, has become a focus in PH in recent years, considering that changes in RA function are relevant prognostic markers of adverse outcomes.[6] Moreover, the evaluation of RA overload and dysfunction has important implications for assessing the severity of right heart failure in the management of patients with PH.[5]

For many years, transthoracic echocardiography has been used for the diagnosis and follow-up of PH, since it is the best noninvasive test for its screening. Thus, it allows estimating the pulmonary artery systolic pressure (PASP) through the direct measurement of the tricuspid regurgitation jet velocity and the estimation of RAP, allowing the evaluation of right and left ventricular functions.[7]

In addition to the usual linear parameters of RV function, the role of strain analysis of the RA has recently been studied as an earlier parameter and for prognostic evaluation of these patients. Strain is defined as the fractional change in the length of a myocardial segment, usually related to the length at end-diastole.[8]

Two-dimensional speckle tracking echocardiography (2D-STE) is a reliable technique for tracking, independent of the angle of myocardial strain, which allows noninvasive and quantitative assessment of global or regional myocardial function; it is, therefore, potentially able to explore RA strain during each phase of the cardiac cycle.[5]

Contents

Central Illustration: Echocardiographic Evaluation of Right Atrial Function in Patients with Precapillary Pulmonary Hypertension

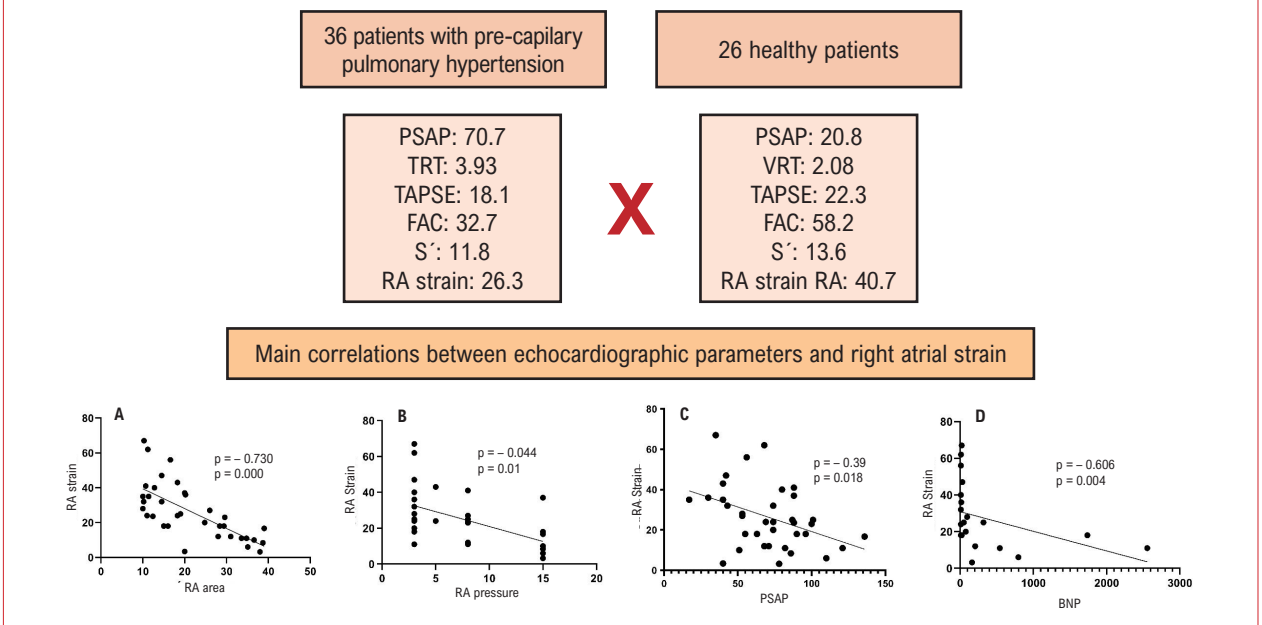

Arq Bras Cardiol: Imagem cardiovasc. 2024;37(1):e20240002

The figure summarizes the main echocardiographic parameters in patients with precapilary pulmonary hypertensio compared to healthy patients, as well as the main correlattions found in the study with right atrial deformation in the diseased group. BNP: brain natriuretic peptide; FAC: fractional area change; PASP: pulmonary artery systolic pressure; RA: right atrial; S': tricuspid annular systolic velocity; TAPSE: tricuspid annular plane systolic excursion; TRV: tricuspid regurgitation velocity.

Considering that the impact of RV insufficiency on the RA is an essential part of the pathophysiology of PH, the assessment of RA function seems essential for a better understanding of RV function in PH, considering that the importance of the RA-RV axis in PH is growing and being increasingly studied. However, despite described evidence, there are still scarce studies on the assessment of RA dysfunction in patients with precapillary PH based on the measurement of RA longitudinal strain by 2D-STE.[5]

Therefore, this study aimed to evaluate the myocardial strain of the RA in patients with precapillary PH, correlating it with echocardiographic parameters of the right heart chambers.

Methods

Study population

This is an observational, longitudinal, prospective study, conducted from May 2019 to December 2022, involving patients with PH, followed up at the pneumology outpatient clinic of a tertiary university hospital, in whom two-dimensional Doppler echocardiography was performed, and RA strain and variables related to right and left ventricular dysfunction were evaluated. Serum brain natriuretic peptide (BNP) concentration was also measured in the patients. In addition, for comparison of the RA strain values, a control group consisting of healthy people was used.

The inclusion criteria for the group of patients were: a) confirmed diagnosis of PH by echocardiographic and hemodynamic criteria; b) patients older than 18 years. The exclusion criteria were: a) patients with post-capillary PH (PH group II); b) presence, on echocardiographic examination, of hemodynamic congestion (E/E' > 14), grade 2 or 3 diastolic dysfunction, or reduced left ventricular ejection fraction; c) presence of left structural heart disease or left valvular heart disease; d) pregnant women; e) inadequate echocardiographic window. To define the control group, represented by healthy people, we included patients older than 18 years, with no comorbidities, no PH, and no cardiac alterations.

This project was approved by the Ethics Committee of the Centro de Ciências Médicas of the Universidade Federal da Paraíba, under CAAE number: 21291419.6.0000.8069.

Transthoracic echocardiography

Transthoracic echocardiography examinations were performed using the GE Vivid T8 device with a 2.5 MHz M4h-5 transducer by a single echocardiographer examiner blinded to the group participants. The images were acquired in the left lateral decubitus position, according to the recommendations of the American Society of Echocardiography.[10] Video images corresponding to 3 cardiac cycles were acquired.

The ejection fraction was estimated by Simpson's biplane method. The RAP was estimated from the inspiratory collapse of

the inferior vena cava. The evaluation of myocardial strain was performed on a workstation in the EchoPach V204 program, and the endocardial tracing was performed manually at the end of diastole, and the measurement was made after the examiner checked whether the quality of the endocardial border tracking was good. In the presence of 2 inadequate segments, the examination was excluded from the study. In the apical window, sections focused on the RV and RA were acquired. With this, the average quantification of the RV and RA free wall strain was performed.

Statistical analysis

Regarding data analysis, the continuous variables were presented as mean and standard deviation (SD) or as medians and interquartile ranges, if, respectively, they followed or did not follow normal distribution. Categorical variables, in turn, were presented as absolute and relative frequencies. The normality analysis was performed using the Kolmogorov-Smirnov test and applying the central limit theorem.

The groups of parametric continuous variables were compared using Student's t-test for independent samples; the comparison between groups of non-parametric variables was done using the Mann-Whitney U test. Three or more groups of variables with normal distribution in groups and subgroups were compared by the ANOVA test, with Tukey and Bonferroni post-hoc tests. Three or more groups of non-parametric variables were compared by the Kruskal-Wallis test, and Dunn's post hoc test was performed to assess the statistical significance between the subgroups. In addition, due to the lack of normality in the distribution of the sample, Spearman's correlation coefficient was used to assess the degree of correlation between two variables.

For data analysis, a normality cutoff point for RA strain of 25% [9] was considered, dividing into two groups: normal (> 25%) and reduced (≤ 25%). Fisher's exact test was used to assess the association between these groups and categorical variables such as mortality during patient follow-up. In addition, the receiver operating characteristic (ROC) curve was performed to assess the accuracy of RA strain for mortality, and a Kaplan-Meier survival curve was constructed.

Results

We evaluated 36 patients with PH, whose median age was 50.5 years, with a minimum value equal to 24 and a maximum of 81 years; 80.5% of the participants (29) were female. The control group was composed of 26 healthy patients, with a median age of 46.5 years. The minimum value was 22, and the maximum was 74 years. Fourteen patients were female (53.8%) (Table 1).

According to the World Health Organization functional classification, most patients with PH (55.5%) had class III;30.5% had class II; 11.1% had class IV, and only 2.7% had class I. Pericardial effusion was not observed in all patients (Table 2). Pericardial effusion was present in only 24.2% of the participants. Regarding BNP levels, the minimum value was 10, while the maximum value was equal to 2555, with a mean of 319.3 (SD ± 652.8).

The etiologies of PH, in decreasing order of prevalence, were: idiopathic (42.4%); connective tissue disease (15.2%); pulmonary thromboembolism (12.1%); chronic obstructive pulmonary disease (12.1%); HIV (3%); schistosomiasis (3%); kyphoscoliosis (3%); idiopathic pulmonary fibrosis (3%); interatrial communication (3%); and subsegmental stenosis of the left pulmonary artery suggestive of Alagille syndrome (3%).

Table 1 – Profile of patients with PH and the control group

Parameters	PH patients (n = 36)	Healthy group (n = 26)
Age (years) [a]	50.5 [37.2 – 65.7]	47 [38 – 59]
Female, n (%)	29 (80.5%)	15 (55.5%)
BMI (kg/m²) [b]	27.9 ± 8.7	25.3 ± 6.3
Functional class, n (%)		
I	1 (2.7)	
II	11 (30.5)	
III	20 (55.5)	
IV	4 (11.1)	
Number of medications in use, n (%)		
0	8 (22.2)	
1	12 (33.3)	
2	10 (27.7)	
3	6 (16.6)	
Etiology, n (%)		
Group I	27 (75)	
Group III	4 (11.1)	
Group IV	5 (13.8)	

[a] Values expressed as median and interquartile range; [b]Values expressed as mean and SD. BMI: body mass index; PH: pulmonary hypertension;

Regarding drug therapy, 78.2% of patients were using a phosphodiesterase-5 inhibitor (sildenafil); 45.4% were using some endothelin receptor antagonist (bosentan or ambrisentan), and 18.2% were using a prostacyclin analog (iloprost or selexipag). As for medication, 34.8% of patients were on monotherapy; 26% were on dual therapy; 17.4% were on triple therapy, and 21.7% were not on medication for PH. Patients who were not on optimal therapy had recently arrived for follow-up at the service.

As for the echocardiographic parameters of the right chambers of patients with PH (Table 2), the mean values of PASP, tricuspid regurgitation velocity (TRV), tricuspid annular plane systolic excursion (TAPSE), fractional area change (FAC) and S' wave were 70.7 mmHg, 3.93 m/s, 18.1 mm, 32.7%, and 11.8 cm/s, respectively. The mean strain of the RA and RV were 26.3% and 18.1%, respectively. As for RV hypokinesia, 33.3% had grade 0 (absent); 21.2% had grade 1 (mild); 15.2% had grade 2 (moderate), and 30.3% had grade 3 (severe).

In the control group, the mean values of PASP, TRV, TAPSE, FAC, and S' were 20.8 mmHg, 2.08 m/s, 22.3 mm, 58.2%, and 13.6 cm/s, respectively. The mean strains of the RA and RV were 40.7% and 26.7%, respectively. According to Table 2, there was a significant difference in the mean echocardiographic parameters of the right chambers between the groups with PH and the control group, including RA strain (p = 0.000), but there was no difference regarding the main parameters of the left chambers.

Table 2 – Echocardiographic parameters of right and left chambers of patients with PH and healthy patients

Variables	PH patients		Healthy group		p
	Mean	SD	Mean	SD	
PASP (mmHg)	70.7	26.5	20.8	4.5	0.000*
TAPSE (mm)	18.1	6.1	22.3	3.4	0.001*
TAPSE/PASP (mm/mmHg)	0.33	0.30	1.1	0.3	0.000*
VRT (m/s)	3.93	0.80	2.08	0.3	0.000*
FAC (%)	32.7	13.6	58.2	5.7	0.000*
S´ (cm/s)	11.8	3.9	13.6	2.3	0.072*
RA pressure (mmHg)	9.2	9.7	3.0	0	0.002*
RA area (cm²)	21.5	9.7	12	3.0	0.000*
RV diameter (mm)	41.7	11.2	29.4	4.2	0.000*
TAPSE/RV diameter	0.47	0.22	0.78	0.13	0.000*
RV strain/PASP	0.33	0.28	1.37	0.54	0.000*
RV strain (%)	18.1	7.7	26.7	4.0	0.000*
RA strain (%)	26.3	15.7	40.7	8.5	0.000*
RA area/RA strain	1.71	2.33	0.28	0.12	0.005*
EF (%)	68.4	6.2	65.2	5.6	0.319*
E/e´	6.7	1.7	7.3	2.1	0.376*
E/A ratio	1.1	0.7	1.3	0.4	0.167*
LVM (g)	124.9	49.8	127.7	35.7	0.816*

*E/A ratio: amplitude of the E wave of the mitral flow/amplitude of the e wave of the tissue Doppler curve in the mitral annulus; E/e': ratio between diastolic velocity E of mitral flow and diastolic velocity e' of mitral annulus; EF: ejection fraction; FAC: fractional area change; LVM: left ventricular mass; PASP: pulmonary artery systolic pressure; PH: pulmonary hypertension; RA: right atrial; RV: right ventricle; S': tricuspid annular peak systolic velocity; SD: standard deviation; TAPSE: tricuspid annular plane systolic excursion; TRV: tricuspid regurgitation velocity. * Student's t test.*

In the group with PH, there was no significant difference in mean RA strain between the female and male sexes (p = 0.8). There was no correlation of RA strain with age (p = −0.215; p = 0.208) and dyspnea grade (p = −0.314; p = 0.104), nor was there a difference in mean RA strain between dyspnea grades (p = 0.237). However, there was a statistically significant difference in mean RA strain between patients with and without pericardial effusion (p = 0.011).

A negative and moderate correlation was found between RA strain and BNP levels (p = −0.606; p = 0.004). The Kruskal-Wallis test showed that the degree of hypokinesia has an effect on RA strain (p = 0.005). In addition, Dunn's post-hoc test showed that there are differences between the groups with absent and severe grade hypokinesia (p = 0.002).

As per Table 3, regarding RA strain, there was a negative and moderate correlation with RA estimated pressure, RV diameter, and RV hypokinesia; a negative and weak correlation with PASP; and a negative and strong correlation with RA area. In addition, a positive and moderate correlation was observed between RA strain and TAPSE, TAPSE/PASP, TAPSE/RV diameter, and RV strain, as well as a positive and weak correlation with FAC and RV strain/TAPSE. Some correlations are expressed in Figure 1.

Figure 2 shows the echocardiographic representation of patients with PH who had, respectively, the highest (62%) and lowest (3.2%) RA strain in the sample evaluated. Both had the same PH etiology, but patient 2 died at the age of 24 years.

Table 3 – Spearman's correlation between RA strain and echocardiographic parameters of patients with precapillary PH

Echocardiographic variables	Correlation	
	ρ (correlation coefficient)	p value
PASP (mmHg)	−0.39	0.018
TAPSE (mm)	0.46	0.005
TAPSE/RV diameter	0.65	0.000
RV strain/PASP	0.36	0.031
RV strain (%)	0.69	0.000
RV hypokinesia	−0.61	0.000
Pericardial effusion	0.52	0.001
TAPSE/PASP	−0.27	0.108
VRT (m/s)	0.28	0.09
FAC (%)	0.12	0.45
S´ (cm/s)	−0.44	0.01
RA pressure (mmHg)	−0.73	0.000
RA area (cm²)	−0.64	0.000
RV diameter (mm)	−0.39	0.018

FAC: fractional area change; PASP: pulmonary artery systolic pressure; RA: right atrial; RV: right ventricle ; S': tricuspid annular peak systolic velocity; TAPSE: tricuspid annular plane systolic excursion; TRV: tricuspid regurgitation velocity.

During a mean follow-up period of 22.3 ± 14.9 (1 to 43) months, 6 patients died (18.2%), of whom 5 (83.3%) had RA strain < 25%. No patients were lost during follow-up. The mean RA strain of the patients who died was 15.6 (SD = 10.22), whereas, in the surviving patients, the mean was 28.4 (SD ± 15.9). There was no statistically significant difference in the means of RA strain between these two groups (p = 0.067). Furthermore, there was no association between mortality and the presence of normal or altered RA strain (p = 0.209).

The ROC curve model demonstrated that the RA strain cutoff point for which there is the highest sensitivity (83.3%) and specificity (63.3%) for association with mortality was a value ≤ 23, with the area under the ROC curve equal to 0.744 (p = 0.019) (Figure 2).

Using this cutoff point for Kaplan-Meier survival analysis, patients with RA strain ≤ 23 were found to have significantly reduced overall survival compared to patients with RA strain > 23 (log-rank p = 0.031) (Figure 2). However, Cox regression analysis did not identify RA strain ≤ 23% as a predictive factor for mortality (HR = 7.53, 95% CI = 0.87 to 65.04, p = 0.066).

Discussion

In our sample, the main echocardiographic parameters of the right chambers of patients with PH, such as PASP, TAPSE, TAPSE/PASP, TRV, and FAC (with the sole exception of S'), were significantly different compared to the parameters of the control group. RA strain, the focus of this study, also showed a significant difference between the groups.

Similarly, a group of authors[11] showed that RA longitudinal strain was reduced in patients with PH compared with controls (27.1 ± 11.6 versus 56.9 ± 12.7, adjusted p < 0.001), even after adjusting for RA area and invasive RAP. Another study[12] showed that the total longitudinal strain and total RA emptying fraction were significantly lower in patients with PH than in controls.

According to our analyses, in patients with PH, there was a strong negative correlation between RA strain and RA area. Compared with other studies, worse RA reservoir strain was also correlated with larger RA size among patients with PH (r = −0.50, p < 0.0001).[11] Furthermore, larger RA area and impaired RA function, explored by strain, were associated with worse outcomes in patients with idiopathic PH.[13]

We found a negative and weak correlation between RA strain and RAP. Previous studies[11,14,15] showed a significant negative correlation between RA strain and mean RAP, with correlation coefficients respectively equal to −0.35; r = −0.31 and −0.37 (p < 0.005).

Furthermore, we identified a negative and weak correlation between RA strain and PASP, which may be related to the fact that estimated PASP is no longer recommended as a key variable to assign

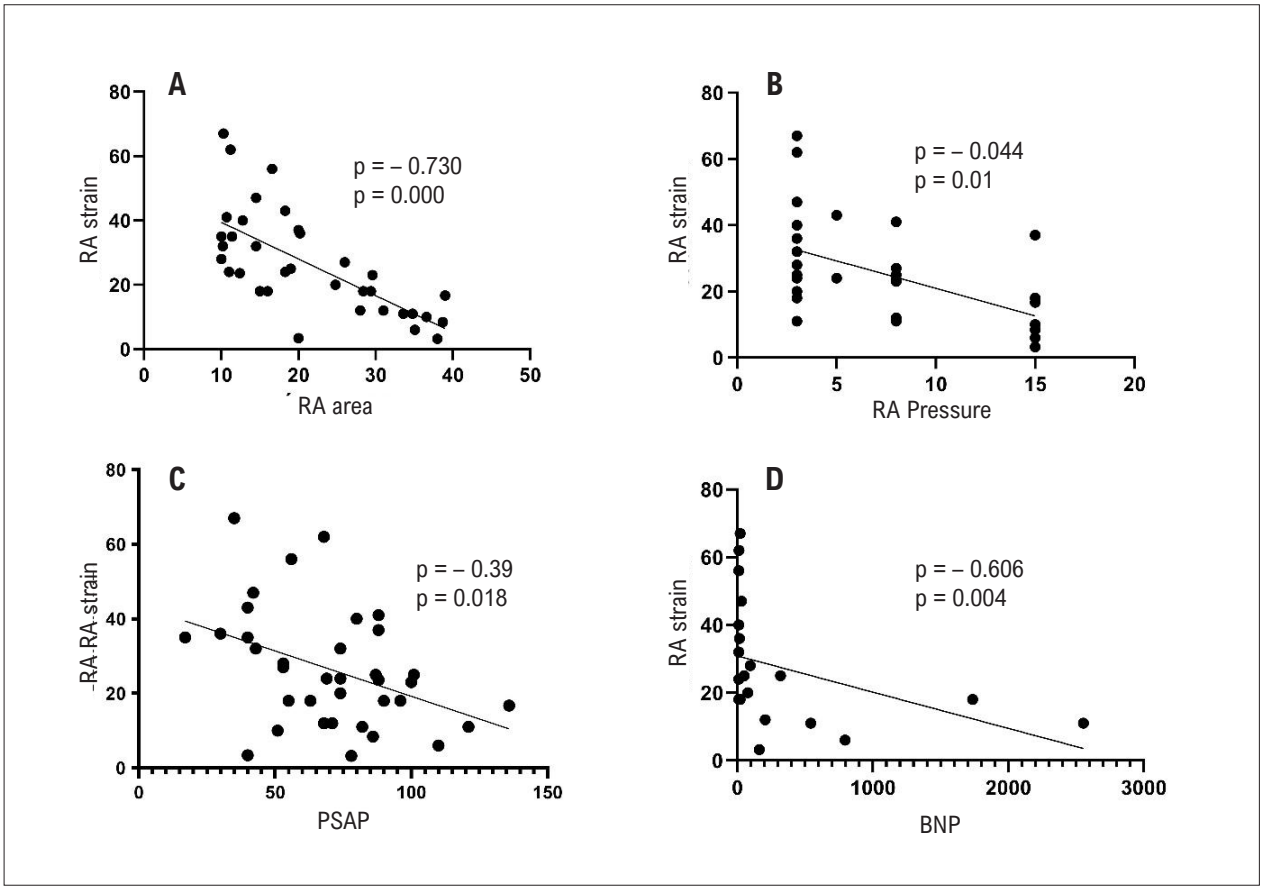

Figure 1 – *Correlation plots of RA strain with RA area, RA pressure, PASP, and BNP. BNP: brain natriuretic peptide; PASP: pulmonary artery systolic pressure; RA: right atrial.*

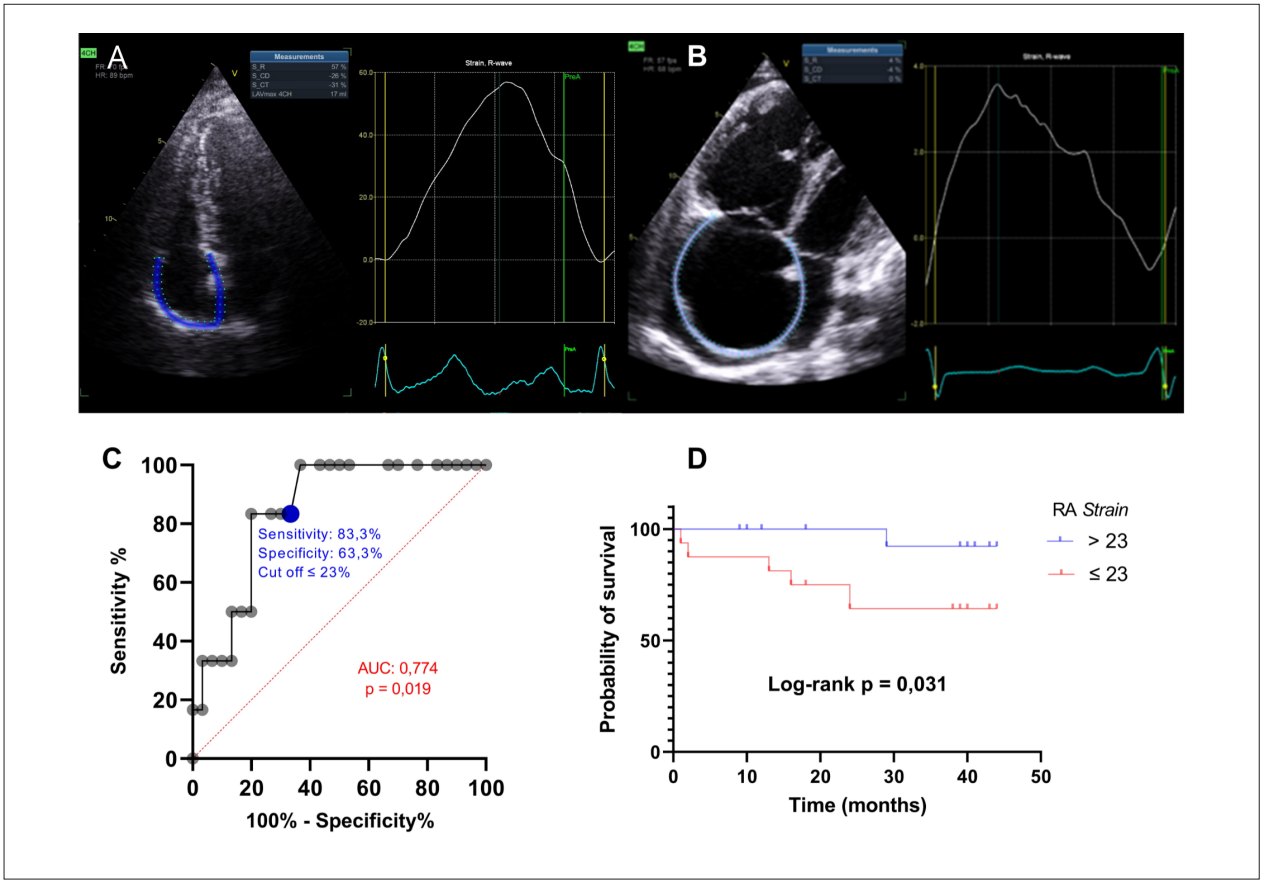

Figure 2 – *A) Echocardiographic image of the patient with the highest RA strain value (62%). PSAP: 35 mmHg; TRV: 2.86 m/s; TAPSE: 27 mm; TAPSE/PASP: 0.77 mm/mmHg; RA AREA: 10.3 cm²; Etiology: idiopathic pulmonary arterial hypertension. B) Echocardiographic image of the patient with the lowest RA strain value (3.2%). PASP: 78 mmHg; TRV: 3,98 m/s; TAPSE: 17 mm; TAPSE/PASP: 0.22 mm/mmHg; RA area: 38 cm²; Etiology: idiopathic pulmonary arterial hypertension. C) ROC curve for the relationship between right atrial strain and mortality. D) Probability of survival according to right atrial strain. PASP: pulmonary artery systolic pressure; TRV: tricuspid regurgitation velocity; TAPSE: tricuspid annular plane systolic excursion; RA: right atrial.*

the echocardiographic probability of HP,[1] given the inaccuracies in the estimation of RAP and the amplification of measurement error using derived variables.

In our study, the mean TRV value of patients with PH was outside normality, but there was no significant correlation with RA strain since the presence or absence of PH cannot be reliably determined by TRV alone, requiring other complementary parameters.[1]

In our sample, there was a positive and moderate correlation between RA strain and TAPSE/PASP. It is known that the TAPSE/PASP ratio is a noninvasive method that makes it possible to measure the RV-pulmonary artery coupling, which may help in risk stratification and prognosis of PH.[1]

We also found a significant correlation of RA strain with RV strain, RV diameter, and RV hypokinesia, confirming that assessment of RA function by strain is intrinsically related to RV dysfunction in PH.

In our study, BNP showed a significant correlation with RA strain. There was also a significant difference in the means of RA strain between BNP values stratified according to the risk of PH.[1] In some studies,[11,12] worse RA longitudinal strain also had a significant correlation with higher NT-proBNP levels, regardless of RA size, RAP, and RV dysfunction.

Finally, patients in our sample with RA strain ≤ 23 had significantly reduced overall survival compared with patients with RA strain > 23, but this value was not predictive of mortality, which may be related to the sample size, the limited number of events (only 6), and the heterogeneity of PH etiology. However, in a cohort[17] of patients with PH, it was observed that the functions of reservoir, conduit, and contraction of the RA, assessed by strain, were independent predictors of mortality and hospitalizations. A recent study[9] showed that RA strain was independently and strongly associated with 5-year mortality in patients with PH.

Conclusions

Our study demonstrated important associations between RA strain and echocardiographic parameters of RV dysfunction in PH, demonstrating that the analysis of RA myocardial strain provides more accurate information about RA function and shows potential prognostic value compared to traditional risk markers used in clinical practice. It is relevant to conduct further studies with the aim of consolidating RA strain as an earlier

parameter for evaluation of overload and dysfunction of the RA to assess the severity of right heart failure in the management of patients with PH.

Author Contributions

Conception and design of the research, acquisition of data, analysis and interpretation of the data, statistical analysis, writing of the manuscript and critical revision of the manuscript for intellectual content: Carvalho WA, Carvalho AA, Martins ER, Medeiros Neto AH, Bacal F, Tavares M.

Potential Conflict of Interest

No potential conflict of interest relevant to this article was reported.

Sources of Funding

There were no external funding sources for this study.

Study Association

This article is part of the thesis of Doctoral submitted by Eliauria Rosa Martins, from pela Universidade de São Paulo.

Ethics Approval and Consent to Participate

This study was approved by the Ethics Committee of the Centro de Ciências Médicas da Universidade Federal da Paraíba under the protocol number 21291419.6.0000.8069. All the procedures in this study were in accordance with the 1975 Helsinki Declaration, updated in 2013. Informed consent was obtained from all participants included in the study.

References

1. Humbert M, Kovacs G, Hoeper MM, Badagliacca R, Berger RMF, Brida M, et al. 2022 ESC/ERS Guidelines for the Diagnosis and Treatment of Pulmonary Hypertension. Eur Heart J. 2022;43(38):3618-731. doi: 10.1093/eurheartj/ehac237.
2. Pagnamenta A, Lador F, Azzola A, Beghetti M. Modern Invasive Hemodynamic Assessment of Pulmonary Hypertension. Respiration. 2018;95(3):201-11. doi: 10.1159/000484942.
3. Luna-López R, Martín AR, Subías PE. Pulmonary Arterial Hypertension. Med Clin. 2022;158(12):622-629. doi: 10.1016/j.medcli.2022.01.003.
4. Oishi P, Fineman JR. Pulmonary Hypertension. Pediatr Crit Care Med. 2016;17(8 Suppl 1):S140-5. doi: 10.1097/PCC.0000000000000754.
5. Sakata K, Uesugi Y, Isaka A, Minamishima T, Matsushita K, Satoh T, et al. Evaluation of Right Atrial Function using Right Atrial Speckle Tracking Analysis in Patients with Pulmonary Artery Hypertension. J Echocardiogr. 2016;14(1):30-8. doi: 10.1007/s12574-015-0270-4.
6. Richter MJ, Zedler D, Berliner D, Douschan P, Gall H, Ghofrani HA, et al. Clinical Relevance of Right Atrial Functional Response to Treatment in Pulmonary Arterial Hypertension. Front Cardiovasc Med. 2021;8:775039. doi: 10.3389/fcvm.2021.775039.
7. Calderaro D, Alves JL Jr, Fernandes CJCDS, Souza R. Pulmonary Hypertension in General Cardiology Practice. Arq Bras Cardiol. 2019;113(3):419-28. doi: 10.5935/abc.20190188.
8. Almeida ALC, Gjesdal O, Newton N, Choi EY, Teixido-Tura G, Yoneyama K, et al. Speckle Tracking Echocardiografy – Clinical Applications. Rev Bras Ecocardiogr Imagem Cardiovasc. 2013;26(1):38-49.
9. Mitchell C, Rahko PS, Blauwet LA, Canaday B, Finstuen JA, Foster MC, et al. Guidelines for Performing a Comprehensive Transthoracic Echocardiographic Examination in Adults: Recommendations from the American Society of Echocardiography. J Am Soc Echocardiogr. 2019;32(1):1-64. doi: 10.1016/j.echo.2018.06.004.
10. Hasselberg NE, Kagiyama N, Soyama Y, Sugahara M, Goda A, Ryo-Koriyama K, et al. The Prognostic Value of Right Atrial Strain Imaging in Patients with Precapillary Pulmonary Hypertension. J Am Soc Echocardiogr. 2021;34(8):851-61.e1. doi: 10.1016/j.echo.2021.03.007.
11. Roca GQ, Campbell P, Claggett B, Solomon SD, Shah AM. Right Atrial Function in Pulmonary Arterial Hypertension. Circ Cardiovasc Imaging. 2015;8(11):e003521; discussion e003521. doi: 10.1161/CIRCIMAGING.115.003521.
12. Meng X, Li Y, Li H, Wang Y, Zhu W, Lu X. Right Atrial Function in Patients with Pulmonary Hypertension: A Study with Two-Dimensional Speckle-Tracking Echocardiography. Int J Cardiol. 2018;255:200-5. doi: 10.1016/j.ijcard.2017.11.093.
13. D'Alto M, D'Andrea A, Di Salvo G, Scognamiglio G, Argiento P, Romeo E, et al. Right Atrial Function and Prognosis in Idiopathic Pulmonary Arterial Hypertension. Int J Cardiol. 2017;248:320-5. doi: 10.1016/j.ijcard.2017.08.047.
14. Fukuda Y, Tanaka H, Ryo-Koriyama K, Motoji Y, Sano H, Shimoura H, et al. Comprehensive Functional Assessment of Right-Sided Heart using Speckle Tracking Strain for Patients with Pulmonary Hypertension. Echocardiography. 2016;33(7):1001-8. doi: 10.1111/echo.13205.
15. Bhave NM, Visovatti SH, Kulick B, Kolias TJ, McLaughlin VV. Right Atrial Strain is Predictive of Clinical Outcomes and Invasive Hemodynamic Data in Group 1 Pulmonary Arterial Hypertension. Int J Cardiovasc Imaging. 2017;33(6):847-55. doi: 10.1007/s10554-017-1081-7.
16. Deschle HA, Amenabar A, Casso NA, Gantesti J, Carnevalini M, Alfie L, et al. Behavior of Right Atrial Strain in High Systolic Pulmonary Artery Pressure. Echocardiography. 2018;35(10):1557-63. doi: 10.1111/echo.14102.
17. Alenezi F, Mandawat A, Il'Giovine ZJ, Shaw LK, Siddiqui I, Tapson VF, et al. Clinical Utility and Prognostic Value of Right Atrial Function in Pulmonary Hypertension. Circ Cardiovasc Imaging. 2018;11(11):e006984. doi: 10.1161/CIRCIMAGING.117.006984.

***Supplemental Materials**

For additional information, please click here.

Left Atrial Strain: Clinical Applications and Prognostic Implications

Fernanda de Azevedo Figueiredo,[1] Admilson Lemos da Costa Filho,[1] Flávio de Azevedo Figueiredo,[1] Luz Marina Tacuri Chavez,[1] Marcia Fabrícia Almeida Teixeira,[1] William Silva Barbosa,[1] Pedro Henrique Bronzatto,[1] Priscila Rabelo Cintra,[2] Maria Carmo Pereira Nunes[1]

Universidade Federal de Minas Gerais,[1] Belo Horizonte, MG – Brazil
Universidade Federal de Lavras,[2] Lavras, MG – Brazil

Abstract

Left atrial (LA) strain, obtained using two-dimensional speckle tracking echocardiography (2DSTE), has emerged as an accurate method for evaluating LA function. Recently, it has gained prominence in clinical practice due to its significant prognostic value in various cardiovascular diseases, standing out due to its greater sensitivity compared to traditional methods of volumetric analysis and Doppler parameters.

This review article addresses the complex function of the LA and its close interdependence with left ventricular (LV) function, highlighting its relevance in cardiac performance. The LA performs three distinct functions, acting as a reservoir during ventricular systole, as a conduit in early diastole, and as a contractile chamber during the atrial contraction phase.

This review analyzes the normal patterns of LA strain and its application in various clinical conditions, such as atrial fibrillation (AF), heart failure, coronary artery disease, obesity, diabetes mellitus, hypertrophic cardiomyopathy, and cardiac amyloidosis. The crucial role of atrial strain in rheumatic mitral stenosis (MS) is highlighted due to its capacity to predict clinical outcomes.

LA function

LA function is closely interdependent with LV function, and it plays a crucial role in preserving optimal cardiac performance.[1] Assessment of LA function in both physiological and pathological states is essential to predict adverse outcomes in various cardiovascular conditions.[2] The LA performs three fundamental functions: it acts as a reservoir, functions as a conduit, and exerts a contractile function[3] (Figure 1).

1) Reservoir function: The LA functions as a reservoir receiving blood from the pulmonary veins. It begins with the closure of the mitral valve and encompasses ventricular systole, isovolumetric relaxation, and LA relaxation. This atrial function is modulated by ventricular contraction descending from the base of the LV, by right ventricular systolic pressure transmitted through pulmonary circulation, and by the properties of the LA, such as relaxation and chamber compliance.[3]

2) Conduit function: During early diastole, the LA acts as a conduit. The flow occurs passively, originating in the pulmonary veins and moving towards the LV. This function begins immediately after the opening of the mitral valve, encompassing the period of ventricular relaxation and diastasis. It ends shortly before atrial contraction, before the P wave is recorded on electrocardiogram. This function is especially modulated by LV diastolic properties in healthy individuals, considering LV relaxation and diastolic pressure.[3]

3) Contractile function: This phase occurs at the end of ventricular diastole. During atrial contraction, there is active emptying of the atrium, contributing 20% to 30% of cardiac output in the absence of heart disease. The effectiveness of this function is directly related to venous return (atrial preload), LV end-diastolic pressure (atrial afterload), and the intrinsic contractility of the atrial myocardium.[3]

Echocardiographic assessment of LA function

Non-invasive assessment of LA function has evolved considerably, surpassing volumetric analyses and Doppler parameters. Modalities such as computed tomography and magnetic resonance imaging have historically been used, but advanced echocardiographic techniques have recently gone on to provide more accurate assessment.

Analyses of atrial diameter and volume do not always reflect LA function, especially in later stages of pathological conditions, during which they may undergo changes. Thus, parameters that more accurately express LA function reveal complementary and incremental information in relation to traditional measures. [1]

The advent of advanced echocardiographic techniques has made it possible to better assess LA function. Strain measured by 2DSTE is a non-invasive method that allows automatic, frame by frame tracking of points in the myocardium throughout the cardiac cycle.[4,5]

The advantages of assessing LA function by means of strain are noteworthy. The capacity to discriminate between passive and active movement of myocardial tissue stands out. Furthermore, strain parameters are relatively independent from tethering effects and less dependent on load, making it possible to assess different phases of atrial function throughout the cardiac cycle.[6]

These advances represent a significant contribution to a more comprehensive understanding of LA function, offering valuable insights for clinical practice.

Keywords

Global Longitudinal Strain; Left Atrial Function; Atrial Fibrillation; Echocardiography.

Mailing Address: Maria do Carmo Pereira Nunes•
Universidade Federal de Minas Gerais. Professor Alfredo Balena, 190, Santa Efigênia. Postal code: 30130-100. Belo Horizonte, MG – Brazil
E-mail: mcarmo@waymail.com.br
Manuscript received January 25,2024; revised January 30, 2024; accepted February 8, 2024
Editor responsible for the review: Marcelo Dantas Tavares de Melo

DOI: https://doi.org/10.36660/abcimg.20240003i

Central Illustration: Left Atrial Strain: Clinical Applications and Prognostic Implications

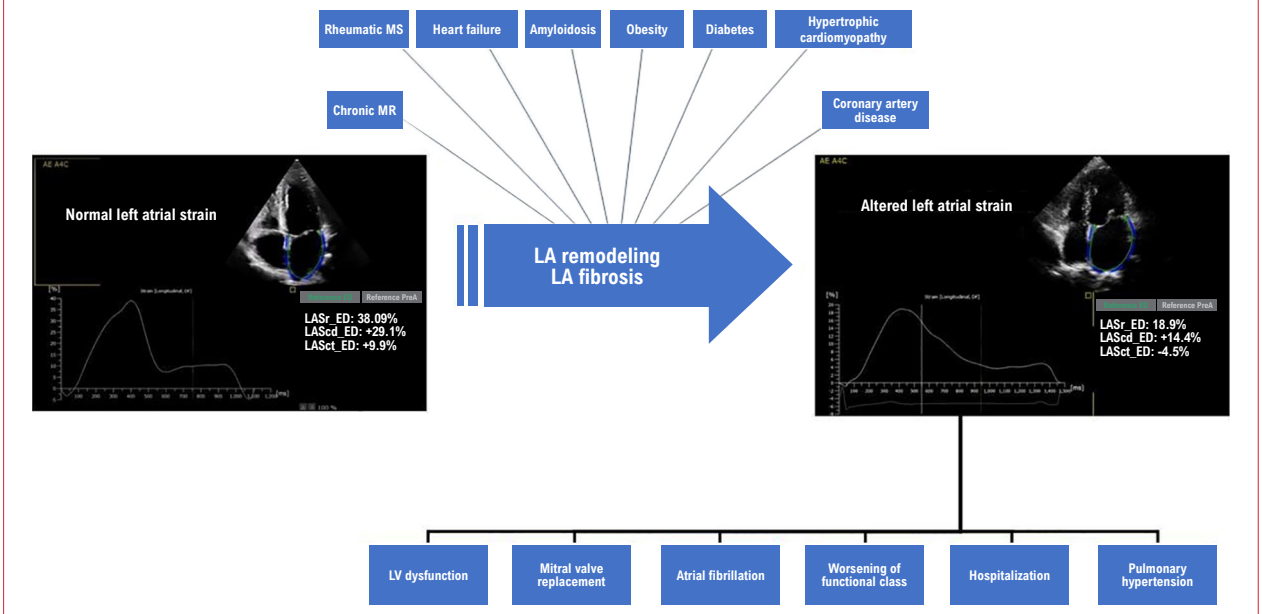

Arq Bras Cardiol: Imagem cardiovasc. 2024;37(1):e20240003

LA: left atrium; LAScd_ED: left atrial strain in the conduit phase in end diastole; LASct_ED: left atrial strain in the contractile phase in end diastole; LASr_ED: left atrial strain in the reservoir phase in end diastole; LV: left ventricle; MR: mitral regurgitation; MS: mitral stenosis.

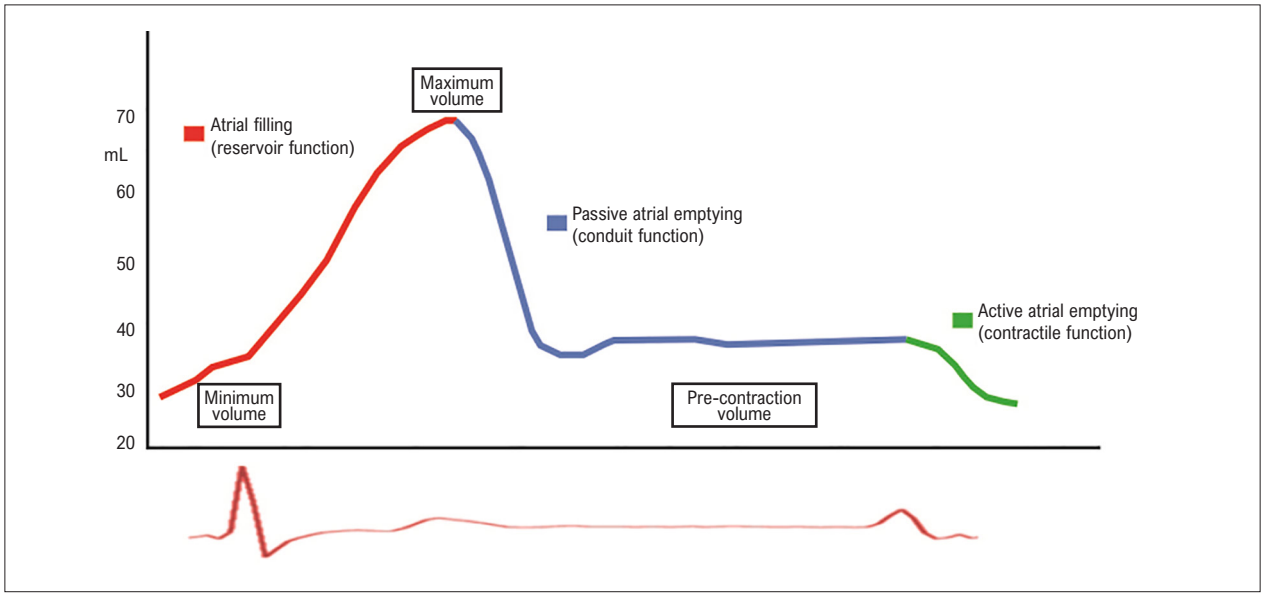

Figure 1 – *LA function: variation in LA volume during the cardiac cycle under physiological conditions.*

Assessment of atrial function by strain

During the reservoir phase, the LA expands as it fills with blood coming from the pulmonary veins. In this scenario, atrial longitudinal strain increases, reaching a positive peak at the end of atrial filling. After mitral valve opening, rapid emptying of the LA occurs, resulting in a decrease in atrial longitudinal strain, until it reaches a plateau, corresponding to the period of atrial diastasis. In the atrial contraction phase, an additional reduction in strain values is observed, due to the shortening of the wall of this chamber.[7]

The contributions of the reservoir, conduit, and contractile functions of the LA to LV filling are approximately 50%, 30%, and 20%, respectively, in healthy individuals.[2] There are differences in the nomenclature used to describe atrial strain that depend on which cycle (atrial or ventricular) is being used as a reference point, i.e., as baseline zero.[8] If the ventricular cycle is used, the QRS complex is the zero reference. Thus, the positive longitudinal peak corresponds to the atrial reservoir function (LASr), occurring during isovolumic contraction and relaxation of the LV. The periods of rapid filling and atrial contraction correspond, respectively, to the atrial conduit function (LAScd) and the pump or contraction function (LASct)[8] (Figures 2 and 3).

If the atrial cycle is used as a reference, the beginning of the P wave on electrocardiogram is the zero reference. The first negative peak represents the pump function; the positive peak corresponds to the conduit function, and their sum represents the reservoir function[8] (Figures 2 and 4).

There are some advantages to adopting end diastole as a reference point, such as the feasibility of obtaining measurements in all patients, regardless of heart rate. It is also worth emphasizing the ease of obtaining the reservoir strain measurement, which is clinically relevant, as it represents the parameter of atrial strain with most supporting evidence regarding its prognostic usefulness.[9,10]

Regarding normal LA strain values, a meta-analysis comprising 40 studies, including 2,542 healthy individuals, established the following reference values:[4] LASr: 39% (95% confidence interval: 38% to 41%), LAScd: 23% (95% confidence interval: 21% to 25%), and LASct: 17% (95% confidence interval: 16% to 19%).

LA strain in the clinical context

LA strain as a predictor of AF

Atrial dysfunction is associated with the presence of fibrosis, especially in cases of AF.[7,11] Although nuclear magnetic resonance is considered the gold standard for evaluating atrial fibrosis, its cost and availability limitations have led to a search for alternatives. The measurement of LA strain by 2DSTE has revealed an inverse correlation with the extent of fibrosis, presenting itself as a viable alternative.[12] Correlations between LA strain and histological fibrosis have been established in patients with mitral valve disease, highlighting a negative relationship between strain values and extent of fibrosis.[8] A recent study also showed that LA reservoir strain was correlated with the occurrence of paroxysmal AF, preceding atrial dilation.[13]

In patients with AF undergoing catheter ablation, peak systolic LA strain has been shown to be related to recurrence of AF after the procedure. These findings highlight the potential of LA strain as a predictor of AF and its clinical usefulness in different cardiovascular contexts.[14,15]

Hauser et al.[16] conducted a prospective study with 4,466 participants with the primary objective of evaluating the incidence of AF over an average follow-up of 5 years. During this period, 154 (4.3%) participants developed AF. In univariate analyses, they observed that peak atrial longitudinal strain (PALS), peak atrial contraction strain (PACS), and strain during the conduit phase were significantly associated with the development of AF. The results of multivariate analyses indicated that both PALS and PACS remained independent predictors of AF. Furthermore, PALS and PACS maintained a significant association with the development of AF, even in participants with normal LA size and preserved LV systolic function. Patients with atrial strain below 23% had a 6.8 times greater risk of developing AF compared to those with strain of 23% or greater.

In another study, Candan et al.[17] included 53 patients with significant mitral regurgitation in sinus rhythm who underwent mitral valve surgery. During the postoperative period, 15 patients (28.3%) developed AF. The results

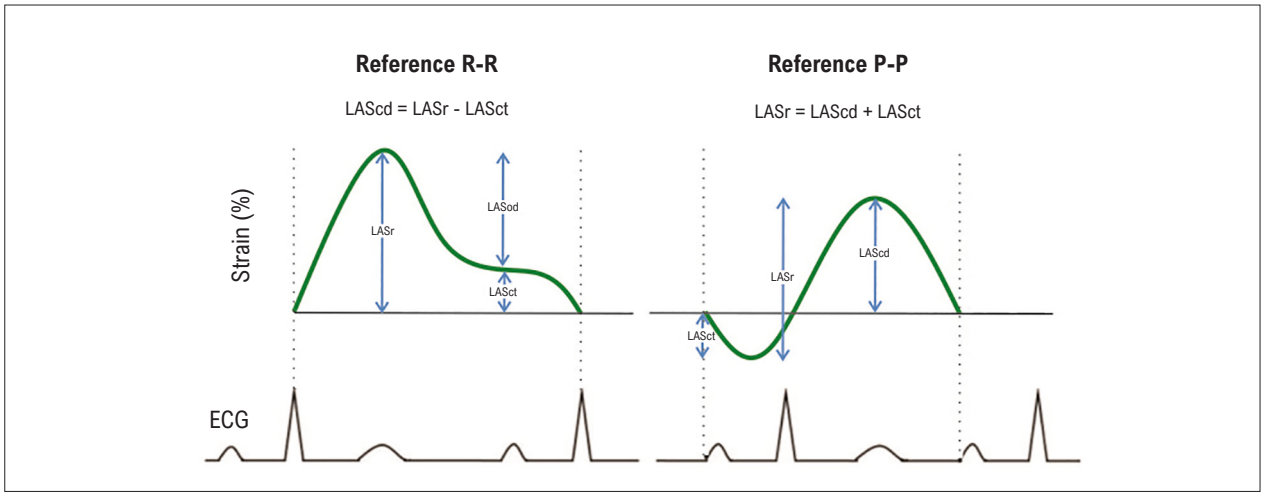

Figure 2 – *Nomenclature of strain based on the choice of the zero reference point. ECG: electrocardiogram; LAScd: left atrial strain in the conduit phase; LASct: left atrial strain in the contractile phase; LASr: left atrial strain in the reservoir phase.*

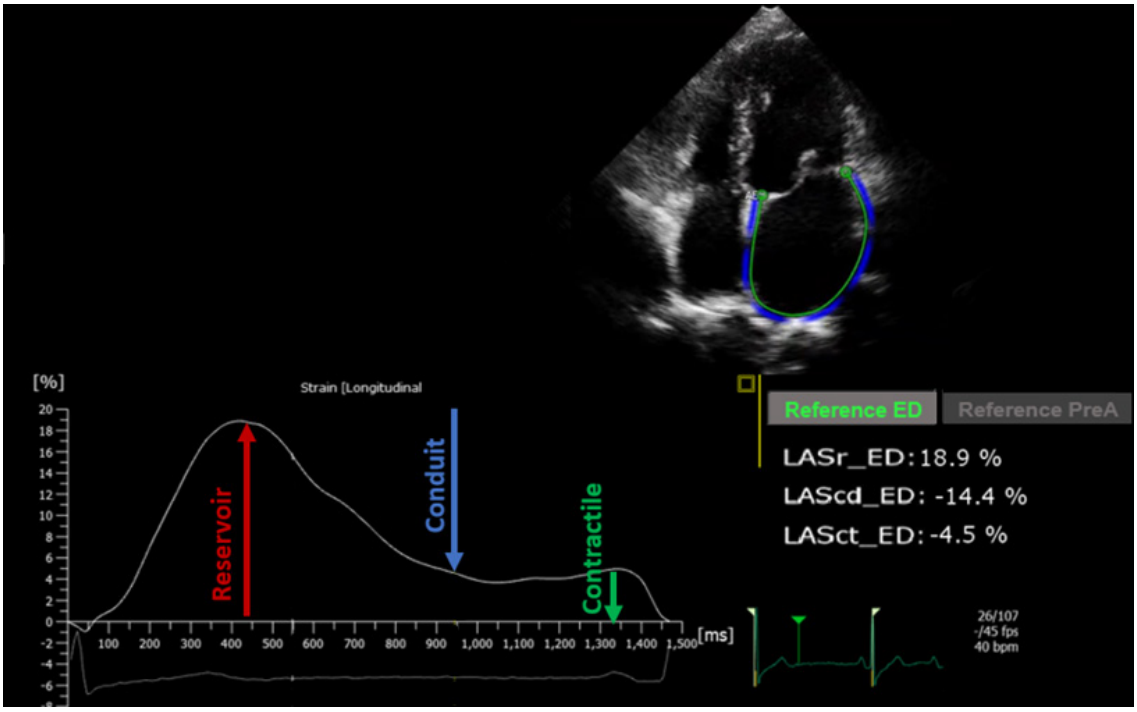

Figure 3 – *Analysis of LA strain using the QRS as a reference. Conduit: conduit phase; Contractile: contractile or pump phase; LAScd_ED: left atrial strain in the conduit phase _ end diastole; LASct_ED: left atrial strain in the contractile phase _ end diastole; LASr_ED: left atrial strain in the reservoir phase _ end diastole; Reservoir: reservoir phase.*

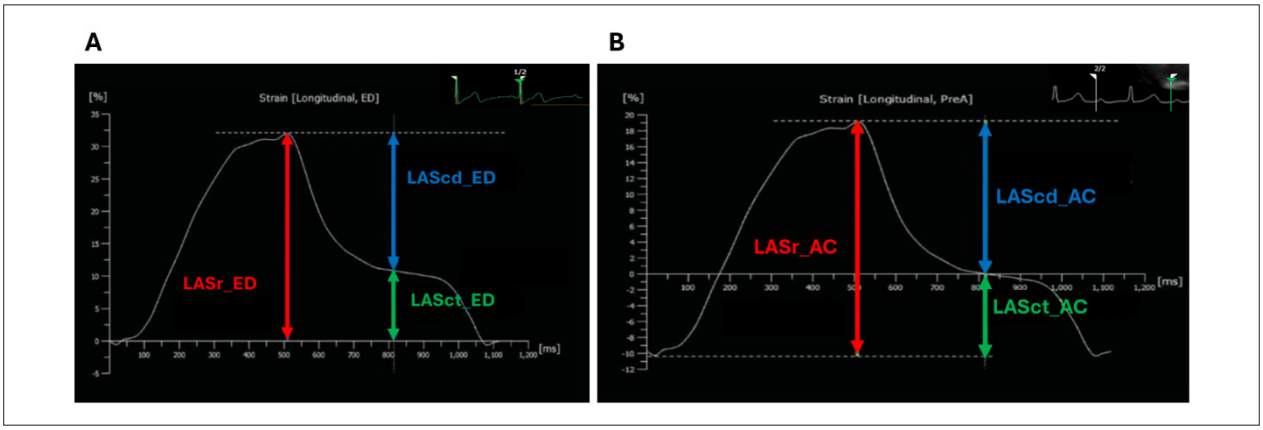

Figura 4 – *LA strain measurements using the QRS as a reference; B) LA strain measurements using the P wave as a reference. LAScd_AC: left atrial strain in the conduit phase _ pre-atrial contraction; LAScd_ED: left atrial strain in the conduit phase _ end diastole; LASct_AC: left atrial strain in the contractile phase _ pre-atrial contraction; LASct_ED: left atrial strain in the contractile phase _ end diastole; LASr_AC: left atrial strain in the reservoir phase _ pre-atrial contraction; LASr_ED: left atrial strain in the reservoir phase _ end diastole.*

revealed that both PACS and PALS were significantly lower in the group of patients who developed AF.

In a study conducted by Park et al.,[18] which analyzed 2,461 patients with acute heart failure over 5 years of follow-up, 397 patients (16.1%) developed new-onset AF. The incidence of AF was significantly higher in patients with reduced LA longitudinal strain values compared to those with normal strain values. These findings suggest an association between atrial dysfunction, measured by strain, and the development of AF in patients with acute heart failure.

In the evaluation of cryptogenic ischemic stroke, Pathan et al.[19] included 538 patients who underwent transthoracic echocardiography with LA strain. During follow-up, 61 (11%) developed AF. These patients had significantly lower

atrial strain values compared to those who did not develop AF during follow-up.

Strain indices, especially LASr with a cutoff of ≤ 21.4% and LASct with a cutoff of > 10.4%, have been identified as high-risk markers. The isolated analysis of these indices revealed a subgroup of patients at considerably higher risk, making them candidates for empirical anticoagulation. This is due to the incremental and independent value of atrial strain in predicting the risk of thromboembolic events, superior to the CHA2DS2-VASc score.[20]

LA strain in rheumatic MS

LA function plays a crucial role in rheumatic MS, influencing blood flow through the stenosed valve.[21,22]

In MS, the reservoir function of the LA, which is essential for ventricular filling during diastole, is impaired due to the compensatory elevation in atrial pressure, fibrosis, and dilation. The conduit function, which is responsible for passive filling of the LV, is also affected due to reduced duration of ventricular diastole. In patients with MS, an initial increase is observed in the contractile function of the LA as a compensatory response; however, this function decreases with the progression of the disease.[23] Studies have shown that, even in mild MS, the LA reservoir and conduit strain may be reduced.[24-26]

LA strain assessment has shown to be valuable in predicting adverse events in patients with MS, such as hospitalizations, AF, thromboembolism, symptoms of heart failure, and the need for mitral valve intervention.[26] LASr has emerged as a significant prognostic indicator, which is reduced even in early stages of mild MS.[26] In follow-up studies, LASr was shown to be a consistent predictor of AF and other adverse outcomes.[27]

Table 1 displays an overview of the main studies that have used LA strain to evaluate rheumatic MS, highlighting its role in risk stratification and prognosis of these patients.

LA strain in heart failure

Increased filling pressures represent a crucial condition in the pathophysiology of heart failure. In this context, LA strain can be used as a diagnostic and prognostic tool, especially in heart failure with reduced ejection fraction.[33]

Reduced LASr (LA strain in the reservoir phase) is associated with increased LV systolic dysfunction, as well as right ventricular systolic and diastolic dysfunction, risk of AF, elevated levels of brain natriuretic peptide, and worsening of NYHA functional class. It is also an important predictor of death and hospitalization due to heart failure.[33-35]

In addition to these prognostic associations, LA strain can be used to evaluate therapeutic response. Optimized therapy reduces pre- and afterload, in addition to reducing the metabolic demand of the myocyte, reducing myocardial work. These effects lead to reduced LA overload, improving strain parameters.[2]

LA strain has also shown to be a promising prognostic marker in heart failure with preserved ejection fraction. Patients with heart failure with preserved ejection fraction have reduced LASr and LASct values, which are strongly associated with increased pressure and resistance in the pulmonary artery, reduced cardiac output, and low exercise tolerance.[36]

Despite the aforementioned evidence, the value of LA strain as a predictor of hospitalization and death in HF, regardless of LV strain, remains uncertain.[37,38]

LA strain in various cardiovascular conditions

LA dysfunction in the context of coronary artery disease, despite initially being mild, can be identified through analysis of LA strain.[39] Atrial strain in the reservoir phase (LASr) has been observed to be is significantly reduced in patients with involvement of the anterior descending artery, and reduced values are correlated with greater severity of the coronary lesion. This evidence supports the view that LA strain not only plays a diagnostic role, but also provides crucial prognostic information. Therefore, when weighing between conservative and interventional treatment approaches, the inclusion of LA strain analysis can contribute to clinical decision-making.[40]

Obesity leads to increased cardiac output and stroke volume, increased afterload, systemic inflammation (with myopathic effect), in addition to the paracrine effect of epicardial fat. These factors are associated with the occurrence of atrial remodeling, which can be detected early by analyzing LA strain.[41-44] In a study carried out by Chirinos et al.,[43] involving 1,531 patients, increased body mass index was associated with reduced LASr and LASct (atrial strain in the reservoir and conduit phases), and a compensatory increase in contractile strain (LASct), when adjusted for age and sex. The authors also observed that, as body mass index increases, there is a decrease in this atrial compensatory contractile function, which increases the likelihood of developing heart failure.

Diabetes mellitus is an important cardiovascular risk factor, and its prevalence is growing significantly.[45] Long-standing diabetes mellitus is associated with LV diastolic dysfunction, LA dilation, and greater predisposition to heart failure.[46] Previous studies have shown reduced LA strain in the reservoir and conduit phases (LASr and LASct) in patients with diabetes,[47] even in the absence of systemic arterial hypertension and LV hypertrophy.[48] The impact of diabetes mellitus on atrial remodeling contributes to a greater risk of developing AF in patients with diabetes.[49]

Hypertrophic cardiomyopathy induces progressive LV diastolic dysfunction, with a consequent increase in filling pressures, which are transmitted to the LA, culminating in the remodeling and progressive dilation of this chamber. As a clinical manifestation, patients present heart failure, AF, ventricular arrhythmias, and sudden death.[50] Previous studies have shown that hypertrophic cardiomyopathy leads to a progressive stiffening of the LA myocardium with reduced reservoir function in this chamber.[51] A study with 76 patients with hypertrophic cardiomyopathy provided evidence of an association between this condition and reduced indices of LA conduit and contractile strain (LAScd and LASct).[52] This study also found that lower LASct values correlated with a significant increase in the rates of hospitalization for heart failure and AF.

Cardiac amyloidosis leads to progressive thickening of the LV myocardium with consequent diastolic dysfunction and elevated filling pressures.[53] This increase in LV filling

Table 1 – Main studies using atrial strain in the context of rheumatic MS

Study	Population	Objectives	Main findings
Ancona et al., 2013 [27]	101 asymptomatic patients with MS 70 controls	Assess the function of the LA in MS using LA strain and its value in predicting AF at 4 years of follow-up.	LA dimensions, volumes, and PASP were significantly increased, and LA strain was significantly decreased in patients with MS. Patients who progressed to AF (20%) were older, with no difference in LA dimensions or volumes. The best predictor of AF at 4 years of follow-up was LA peak systolic strain, with a cutoff value of 17.4%.
Pourafkari et al., 2015 [28]	603 patients with MS (33% with AF)	Establish a mathematical model for predicting the risk of AF in patients with MS.	The factors independently associated with AF were LA strain, right atrial pressure, age, and ejection fraction.
Chien et al., 2018 [29]	69 stable patients with MS	Identify the determinants of NYHA functional class in patients with MS and assess the relationship between atrial strain and HF symptoms.	In multivariate analyses, adjusted for the use of diuretics, LASr was an independent predictor of NYHA functional class.
Mahfouz et al., 2020 [24]	75 patients with mild MS in sinus rhythm 40 healthy controls	Assess atrial strain in patients with mild MS and correlate it with exercise tolerance.	Patients with mild MS had significantly lower LASr and LAScd values. Patients with exercise intolerance (MET < 8) had lower LASr, LAScd, and LASct values. LASr ≤ 26.5% was an independent predictor of low exercise capacity in patients with mild MS.
Vriz et al., 2021[30]	101 patients with severe MS	Determine the correlation between atrial strain, PASP, and other parameters of RV function Verify whether atrial strain is a predictor of development of AF.	With the increase in LASr there was a decrease in PASP and PVR. RV function increased significantly with the increase in LASr. LASr was one of the best predictors of AF.
Kaur V et al., 2021 [31]	83 patients with MS undergoing PTMC	Assess the association between LA-RAs and increased PVR measured by hemodynamics.	Low LA-RAs correlated with more severe MS, higher mean pulmonary artery pressure, and pulmonary capillary wedge pressure, when compared with patients with high LA-RAs. LA-RAs showed a strong correlation with PH. LA-RAs increased significantly after PTMC.
Stassen et al., 2022 [32]	125 patients with MS, with no history of AF	Assess the association of atrial strain with the development of AF in the follow-up of patients with MS.	During a mean follow-up period of 32 months, 41 patients (32.8%) developed new-onset AF. Patients who developed AF had significantly more impaired LASr than those who remained in sinus rhythm. LASr < 21% was independently associated with the development of AF during follow-up.
Mehta et al., 2022 [25]	80 patients with severe MS in sinus rhythm 40 controls	Assess LA function using strain and its correlation with NYHA functional class and echocardiographic parameters in patients with severe MS and PH, compared with the control group.	The mean LASr, LAScd, and LASct values in patients with MS were significantly lower than in controls.

LA: left atrium; AF: atrial fibrillation; HF: heart failure; MS: mitral stenosis; LA-RAs: left atrial to right atrial strain ratio; LAScd: left atrial strain during the conduit phase; LASct: left atrial strain during the contractile phase; LASr: left atrial strain during the reservoir phase; NYHA: New York Heart Association; PASP: pulmonary artery systolic pressure; PH: pulmonary hypertension; PTMC: percutaneous mitral commissurotomy; PVR: pulmonary vascular resistance; RV: right ventricle.

pressures, associated with the deposition of amyloid proteins in the atrial myocardium, causes progressive LA dysfunction and dilation.[54] Mohty et al.,[55] in a study with 77 patients with cardiac amyloidosis (type AL, light chain amyloidosis), showed reduced LA reservoir strain values (LASr), with significantly lower 2-year survival in patients with LASr < 14%. Another study conducted by Nochioka et al.,[56] found reduced values of atrial strain in the reservoir, conduit, and contractile phases in individuals with cardiac amyloidosis, regardless of the subtype.

Mitral regurgitation causes progressive dilation and dysfunction of the LA, leading to an increased risk of developing AF.[57] In a study conducted by Yang et al.,[58] involving patients with severe primary mitral regurgitation, the reduction in LA strain in the reservoir phase was associated with higher mortality rates and need for mitral valve replacement surgery or repair after a follow-up period of 13.2 months. In another study, Ring et al.[59] evaluated 192 patients with mitral prolapse and regurgitation, observing that LA strain values in the reservoir and contractile phases were independent predictors

of the need for mitral valve replacement. Although small, these studies show the relevance of atrial strain measurements for risk stratification and possible optimization of the ideal time to perform surgical interventions in this group of patients.

Challenges in current clinical applications of LA strain

The routine, widespread application of LA strain as a prognostic marker in different cardiovascular conditions is still limited. Comprehensive assessment of LA function requires joint analysis of both atrial pressure and volume. In the absence of modalities for direct assessment of LA pressure, estimates are made indirectly, which can be influenced both by LV dysfunction and by primary abnormalities in the LA.[2] Furthermore, it is worth highlighting the variation in LA strain values obtained by different software platforms.

Conclusions and future perspectives

LA strain has emerged as a promising tool in the assessment of various cardiovascular conditions, offering valuable insights for risk stratification and for monitoring the progression of heart diseases.

Notwithstanding its potential, it is crucial to recognize the need for prospective multicenter studies, in addition to the standardization of techniques and the development of specific guidelines on the interpretation and clinical application of atrial strain.

The establishment of specific guidelines will guarantee consistency and reliability in the interpretation of LA strain, leading to its widespread use in clinical practice.

Author Contributions

Conception and design of the research: Figueiredo Fernanda A, Figueiredo Flávio A, Chavez LMT, Teixeira MFA, Nunes MC; acquisition of data: Barbosa WS, Bronzatto PH, Nunes MC; analysis and interpretation of the data: Figueiredo Fernanda A, Nunes MC; obtaining financing: Nunes MC; writing of the manuscript: Figueiredo Fernanda A, Costa Filho AL, Figueiredo Flávio A, Chavez LMT, Cintra PR, Nunes MC; critical revision of the manuscript for intellectual content: Figueiredo Fernanda A, Figueiredo Flávio A, Nunes MC.

Potential Conflict of Interest

No potential conflict of interest relevant to this article was reported.

Sources of Funding

This study was partially funded by CNPq. Maria do Carmo P Nunes has a scientific productivity grant (PQ-1A) - CNPq Notice No. 09/2020.

Study Association

This article is part of the thesis of master submitted by Fernanda de Azevedo Figueiredo, from Universidade Federal de Minas Gerais.

Ethics Approval and Consent to Participate

This article does not contain any studies with human participants or animals performed by any of the authors.

References

1. Gan GCH, Ferkh A, Boyd A, Thomas L. Left Atrial Function: Evaluation by Strain Analysis. Cardiovasc Diagn Ther. 2018;8(1):29-46. doi: 10.21037/cdt.2017.06.08.
2. Jain V, Ghosh R, Gupta M, Saijo Y, Bansal A, Farwati M, et al. Contemporary Narrative Review on Left Atrial Strain Mechanics in Echocardiography: Cardiomyopathy, Valvular Heart Disease and Beyond. Cardiovasc Diagn Ther. 2021;11(3):924-38. doi: 10.21037/cdt-20-461.
3. Rosca M, Lancellotti P, Popescu BA, Piérard LA. Left Atrial Function: Pathophysiology, Echocardiographic Assessment, and Clinical Applications. Heart. 2011;97(23):1982-9. doi: 10.1136/heartjnl-2011-300069.
4. Pathan F, D'Elia N, Nolan MT, Marwick TH, Negishi K. Normal Ranges of Left Atrial Strain by Speckle-Tracking Echocardiography: A Systematic Review and Meta-Analysis. J Am Soc Echocardiogr. 2017;30(1):59-70.e8. doi: 10.1016/j.echo.2016.09.007.
5. Roediger V. AutoStrain VE/VD/AE - Medições Automatizadas da Deformação Longitudinal. Amesterdam: Koninklijke Philips; 2019.
6. Saraiva RM, Demirkol S, Buakhamsri A, Greenberg N, Popović ZB, Thomas JD, et al. Left Atrial Strain Measured by Two-Dimensional Speckle Tracking Represents a New Tool to Evaluate Left Atrial Function. J Am Soc Echocardiogr. 2010;23(2):172-80. doi: 10.1016/j.echo.2009.11.003.
7. Thomas L, Abhayaratna WP. Left Atrial Reverse Remodeling: Mechanisms, Evaluation, and Clinical Significance. JACC Cardiovasc Imaging. 2017;10(1):65-77. doi: 10.1016/j.jcmg.2016.11.003.
8. Cameli M, Lisi M, Righini FM, Massoni A, Natali BM, Focardi M, et al. Usefulness of Atrial Deformation Analysis to Predict Left Atrial Fibrosis and Endocardial Thickness in Patients Undergoing Mitral Valve Operations for Severe Mitral Regurgitation Secondary to Mitral Valve Prolapse. Am J Cardiol. 2013;111(4):595-601. doi: 10.1016/j.amjcard.2012.10.049.
9. Vieira MJ, Teixeira R, Gonçalves L, Gersh BJ. Left Atrial Mechanics: Echocardiographic Assessment and Clinical Implications. J Am Soc Echocardiogr. 2014;27(5):463-78. doi: 10.1016/j.echo.2014.01.021.
10. Donal E, Lip GY, Galderisi M, Goette A, Shah D, Marwan M, et al. EACVI/EHRA Expert Consensus Document on the Role of Multi-Modality Imaging for the Evaluation of Patients with Atrial Fibrillation. Eur Heart J Cardiovasc Imaging. 2016;17(4):355-83. doi: 10.1093/ehjci/jev354.
11. Boldt A, Wetzel U, Lauschke J, Weigl J, Gummert J, Hindricks G, et al. Fibrosis in Left Atrial Tissue of Patients with Atrial Fibrillation with and without Underlying Mitral Valve Disease. Heart. 2004;90(4):400-5. doi: 10.1136/hrt.2003.015347.
12. Kuppahally SS, Akoum N, Burgon NS, Badger TJ, Kholmovski EG, Vijayakumar S, et al. Left Atrial Strain and Strain Rate in Patients with Paroxysmal and Persistent Atrial Fibrillation: Relationship to Left Atrial Structural Remodeling Detected by Delayed-Enhancement MRI. Circ Cardiovasc Imaging. 2010;3(3):231-9. doi: 10.1161/CIRCIMAGING.109.865683.
13. Kojima T, Kawasaki M, Tanaka R, Ono K, Hirose T, Iwama M, et al. Left Atrial Global and Regional Function in Patients with Paroxysmal Atrial Fibrillation has Already Been Impaired Before Enlargement of Left Atrium: Velocity Vector Imaging Echocardiography Study. Eur Heart J Cardiovasc Imaging. 2012;13(3):227-34. doi: 10.1093/ejechocard/jer281.

14. Hwang HJ, Choi EY, Rhee SJ, Joung B, Lee BH, Lee SH, et al. Left Atrial Strain as Predictor of Successful Outcomes in Catheter Ablation for Atrial Fibrillation: a Two-Dimensional Myocardial Imaging Study. J Interv Card Electrophysiol. 2009;26(2):127-32. doi: 10.1007/s10840-009-9410-y.

15. Yasuda R, Murata M, Roberts R, Tokuda H, Minakata Y, Suzuki K, et al. Left Atrial Strain is a Powerful Predictor of Atrial Fibrillation Recurrence after Catheter Ablation: Study of a Heterogeneous Population with Sinus Rhythm or Atrial Fibrillation. Eur Heart J Cardiovasc Imaging. 2015;16(9):1008-14. doi: 10.1093/ehjci/jev028.

16. Hauser R, Nielsen AB, Skaarup KG, Lassen MCH, Duus LS, Johansen ND, et al. Left Atrial Strain Predicts Incident Atrial Fibrillation in the General Population: the Copenhagen City Heart Study. Eur Heart J Cardiovasc Imaging. 2021;23(1):52-60. doi: 10.1093/ehjci/jeab202.

17. Candan O, Ozdemir N, Aung SM, Dogan C, Karabay CY, Gecmen C, et al. Left Atrial Longitudinal Strain Parameters Predict Postoperative Persistent Atrial Fibrillation Following Mitral Valve Surgery: a Speckle Tracking Echocardiography Study. Echocardiography. 2013;30(9):1061-8. doi: 10.1111/echo.12222.

18. Park JJ, Park JH, Hwang IC, Park JB, Cho GY, Marwick TH. Left Atrial Strain as a Predictor of New-Onset Atrial Fibrillation in Patients with Heart Failure. JACC Cardiovasc Imaging. 2020;13(10):2071-81. doi: 10.1016/j.jcmg.2020.04.031.

19. Pathan F, Sivaraj E, Negishi K, Rafiudeen R, Pathan S, D'Elia N, et al. Use of Atrial Strain to Predict Atrial Fibrillation after Cerebral Ischemia. JACC Cardiovasc Imaging. 2018;11(11):1557-65. doi: 10.1016/j.jcmg.2017.07.027.

20. Obokata M, Negishi K, Kurosawa K, Tateno R, Tange S, Arai M, et al. Left Atrial Strain Provides Incremental Value for Embolism Risk Stratification Over CHA_2DS_2-Vasc Score and Indicates Prognostic Impact in Patients with Atrial Fibrillation. J Am Soc Echocardiogr. 2014;27(7):709-16.e4. doi: 10.1016/j.echo.2014.03.010.

21. Demirkol S, Kucuk U, Baysan O, Balta S, Celik T, Kurt IH, et al. The Impact of Mitral Stenosis on Left Atrial Function Assessed by Two-Dimensional Speckle Tracking Echocardiography. Echocardiography. 2012;29(9):1064-70. doi: 10.1111/j.1540-8175.2012.01751.x.

22. Nikitin NP, Witte KK, Thackray SD, Goodge LJ, Clark AL, Cleland JG. Effect of Age and Sex on Left Atrial Morphology and Function. Eur J Echocardiogr. 2003;4(1):36-42. doi: 10.1053/euje.2002.0611.

23. Dernellis JM, Stefanadis CI, Zacharoulis AA, Toutouzas PK. Left Atrial Mechanical Adaptation to Long-Standing Hemodynamic Loads Based on Pressure-Volume Relations. Am J Cardiol. 1998;81(9):1138-43. doi: 10.1016/s0002-9149(98)00134-9.

24. Mahfouz RA, Gouda M, Abdelhamed M. Relation between Left Atrial Strain and Exercise Tolerance in Patients with Mild Mitral Stenosis: an Insight from 2D Speckle-Tracking Echocardiography. Echocardiography. 2020;37(9):1406-12. doi: 10.1111/echo.14818.

25. Mehta V, Chaudhari D, Mehra P, Mahajan S, Yusuf J, Gupta MD, et al. Left Atrial Function by Two-Dimensional Speckle Tracking Echocardiography in Patients with Severe Rheumatic Mitral Stenosis and Pulmonary Hypertension. Indian Heart J. 2022;74(1):63-5. doi: 10.1016/j.ihj.2021.12.011.

26. Caso P, Ancona R, Di Salvo G, Comenale Pinto S, Macrino M, Di Palma V, et al. Atrial Reservoir Function by Strain Rate Imaging in Asymptomatic Mitral Stenosis: Prognostic Value at 3 Year Follow-Up. Eur J Echocardiogr. 2009;10(6):753-9. doi: 10.1093/ejechocard/jep058.

27. Ancona R, Comenale Pinto S, Caso P, Di Salvo G, Severino S, et al. Two-Dimensional Atrial Systolic Strain Imaging Predicts Atrial Fibrillation at 4-Year Follow-Up in Asymptomatic Rheumatic Mitral Stenosis. J Am Soc Echocardiogr. 2013;26(3):270-7. doi: 10.1016/j.echo.2012.11.016.

28. Pourafkari L, Ghaffari S, Bancroft GR, Tajlil A, Nader ND. Factors Associated with Atrial Fibrillation in Rheumatic Mitral Stenosis. Asian Cardiovasc Thorac Ann. 2015;23(1):17-23. doi: 10.1177/0218492314530134.

29. Chien CY, Chen CW, Lin TK, Lin Y, Lin JW, Li YD, et al. Atrial Deformation Correlated with Functional Capacity in Mitral Stenosis Patients. Echocardiography. 2018;35(2):190-5. doi: 10.1111/echo.13770.

30. Vriz O, Blassy B, Almozel A, Almohammadi SM, Galzerano D, Alfehaid A, *et al*. Left Atrial Strain can Predict Right Ventricular Impairment and Developement of Atrial Fibrilation in Patients with Severe Mitral Stenosis Better than Transmitral Gradients. Eur Heart Cardiovasc Imag. 2021;22(Suppl 10):i79. doi: 10.1093/ehjci/jeaa356.060.

31. Kaur V, Manouras A, Venkateshvaran A. Association of Atrial Strain Ratio with Invasive Pulmonary Hemodynamics in Rheumatic Mitral Stenosis. Echocardiography: Valve Disease. Eur Heart Cardiovasc Imag. 2021;22(Suppl 10):i72.

32. Stassen J, Butcher SC, Namazi F, Ajmone Marsan N, Bax JJ, Delgado V. Left Atrial Deformation Imaging and Atrial Fibrillation in Patients with Rheumatic Mitral Stenosis. J Am Soc Echocardiogr. 2022;35(5):486-94.e2. doi: 10.1016/j.echo.2021.12.010.

33. Carluccio E, Biagioli P, Mengoni A, Cerasa MF, Lauciello R, Zuchi C, et al. Left Atrial Reservoir Function and Outcome in Heart Failure with Reduced Ejection Fraction. Circ Cardiovasc Imaging. 2018;11(11):e007696. doi: 10.1161/CIRCIMAGING.118.007696.

34. Kurt M, Tanboga IH, Aksakal E, Kaya A, Isik T, Ekinci M, et al. Relation of Left Ventricular End-Diastolic Pressure and N-Terminal Pro-Brain Natriuretic Peptide Level with Left Atrial Deformation Parameters. Eur Heart J Cardiovasc Imaging. 2012;13(6):524-30. doi: 10.1093/ejechocard/jer283.

35. Malagoli A, Rossi L, Bursi F, Zanni A, Sticozzi C, Piepoli MF, et al. Left Atrial Function Predicts Cardiovascular Events in Patients with Chronic Heart Failure with Reduced Ejection Fraction. J Am Soc Echocardiogr. 2019;32(2):248-56. doi: 10.1016/j.echo.2018.08.012.

36. Telles F, Nanayakkara S, Evans S, Patel HC, Mariani JA, Vizi D, et al. Impaired Left Atrial Strain Predicts Abnormal Exercise Haemodynamics in Heart Failure with Preserved Ejection Fraction. Eur J Heart Fail. 2019;21(4):495-505. doi: 10.1002/ejhf.1399.

37. Freed BH, Daruwalla V, Cheng JY, Aguilar FG, Beussink L, Choi A, et al. Prognostic Utility and Clinical Significance of Cardiac Mechanics in Heart Failure with Preserved Ejection Fraction: Importance of Left Atrial Strain. Circ Cardiovasc Imaging. 2016;9(3):e003754. doi: 10.1161/CIRCIMAGING.115.003754.

38. Santos AB, Roca GQ, Claggett B, Sweitzer NK, Shah SJ, Anand IS, et al. Prognostic Relevance of Left Atrial Dysfunction in Heart Failure with Preserved Ejection Fraction. Circ Heart Fail. 2016;9(4):e002763. doi: 10.1161/CIRCHEARTFAILURE.115.002763.

39. Yan P, Sun B, Shi H, Zhu W, Zhou Q, Jiang Y, et al. Left Atrial and Right Atrial Deformation in Patients with Coronary Artery Disease: a Velocity Vector Imaging-Based Study. PLoS One. 2012;7(12):e51204. doi: 10.1371/journal.pone.0051204.

40. Said KM, Nassar AI, Fouad A, Ramzy AA, Abd Allah MFF. Left Atrial Deformation Analysis as a Predictor of Severity of Coronary Artery Disease. Egypt Heart J. 2018;70(4):353-9. doi: 10.1016/j.ehj.2018.09.004.

41. Ayer JG, Sholler GF, Celermajer DS. Left Atrial Size Increases with Body Mass Index in Children. Int J Cardiol. 2010;141(1):61-7. doi: 10.1016/j.ijcard.2008.11.157.

42. Oliver W, Matthews G, Ayers CR, Garg S, Gupta S, Neeland IJ, et al. Factors Associated with Left Atrial Remodeling in the General Population. Circ Cardiovasc Imaging. 2017;10(2):e005047. doi: 10.1161/CIRCIMAGING.116.005047.

43. Chirinos JA, Rietzschel ER, De Buyzere ML, De Bacquer D, Gillebert TC, Gupta AK, et al. Arterial Load and Ventricular-Arterial Coupling: Physiologic Relations with Body Size and Effect of Obesity. Hypertension. 2009;54(3):558-66. doi: 10.1161/HYPERTENSIONAHA.109.131870.

44. Mahabadi AA, Lehmann N, Kälsch H, Bauer M, Dykun I, Kara K, et al. Association of Epicardial Adipose Tissue and Left Atrial Size on Non-Contrast CT with Atrial Fibrillation: the Heinz Nixdorf Recall Study. Eur Heart J Cardiovasc Imaging. 2014;15(8):863-9. doi: 10.1093/ehjci/jeu006.

45. Shaw JE, Sicree RA, Zimmet PZ. Global Estimates of the Prevalence of Diabetes for 2010 and 2030. Diabetes Res Clin Pract. 2010;87(1):4-14. doi: 10.1016/j.diabres.2009.10.007.

46. Nichols GA, Hillier TA, Erbey JR, Brown JB. Congestive Heart Failure in Type 2 Diabetes: Prevalence, Incidence, and Risk Factors. Diabetes Care. 2001;24(9):1614-9. doi: 10.2337/diacare.24.9.1614.

47. Ernande L, Rietzschel ER, Bergerot C, De Buyzere ML, Schnell F, Groisne L, et al. Impaired Myocardial Radial Function in Asymptomatic Patients with Type 2 Diabetes Mellitus: a Speckle-Tracking Imaging Study. J Am Soc Echocardiogr. 2010;23(12):1266-72. doi: 10.1016/j.echo.2010.09.007.

48. Tadic M, Vukomanovic V, Cuspidi C, Suzic-Lazic J, Stanisavljevic D, Celic V. Left Atrial Phasic Function and Heart Rate Variability in Asymptomatic Diabetic Patients. Acta Diabetol. 2017;54(3):301-8. doi: 10.1007/s00592-016-0962-x.

49. Tadic M, Cuspidi C. Type 2 Diabetes Mellitus and Atrial Fibrillation: from Mechanisms to Clinical Practice. Arch Cardiovasc Dis. 2015;108(4):269-76. doi: 10.1016/j.acvd.2015.01.009.

50. Siontis KC, Geske JB, Ong K, Nishimura RA, Ommen SR, Gersh BJ. Atrial Fibrillation in Hypertrophic Cardiomyopathy: Prevalence, Clinical Correlations, and Mortality in a Large High-Risk Population. J Am Heart Assoc. 2014;3(3):e001002. doi: 10.1161/JAHA.114.001002.

51. Sanada H, Shimizu M, Sugihara N, Shimizu K, Ino H, Takeda R. Increased Left Atrial Chamber Stiffness in Hypertrophic Cardiomyopathy. Br Heart J. 1993;69(1):31-5. doi: 10.1136/hrt.69.1.31.

52. Fujimoto K, Inoue K, Saito M, Higashi H, Kono T, Uetani T, et al. Incremental Value of Left Atrial Active Function Measured by Speckle Tracking Echocardiography in Patients with Hypertrophic Cardiomyopathy. Echocardiography. 2018;35(8):1138-48. doi: 10.1111/echo.13886.

53. Klein AL, Hatle LK, Taliercio CP, Oh JK, Kyle RA, Gertz MA, et al. Prognostic Significance of Doppler Measures of Diastolic Function in Cardiac Amyloidosis. A Doppler echocardiography study. Circulation. 1991;83(3):808-16. doi: 10.1161/01.cir.83.3.808.

54. Mohty D, Pibarot P, Dumesnil JG, Darodes N, Lavergne D, Echahidi N, et al. Left Atrial Size is an Independent Predictor of Overall Survival in Patients with Primary Systemic Amyloidosis. Arch Cardiovasc Dis. 2011;104(12):611-8. doi: 10.1016/j.acvd.2011.10.004.

55. Mohty D, Petitalot V, Magne J, Fadel BM, Boulogne C, Rouabhia D, et al. Left Atrial Function in Patients with Light Chain Amyloidosis: a Transthoracic 3D Speckle Tracking Imaging Study. J Cardiol. 2018;71(4):419-27. doi: 10.1016/j.jjcc.2017.10.007.

56. Nochioka K, Quarta CC, Claggett B, Roca GQ, Rapezzi C, Falk RH, et al. Left Atrial Structure and Function in Cardiac Amyloidosis. Eur Heart J Cardiovasc Imaging. 2017;18(10):1128-37. doi: 10.1093/ehjci/jex097.

57. Nishimura RA, Otto CM, Bonow RO, Carabello BA, Erwin JP 3rd, Fleisher LA, et al. 2017 AHA/ACC Focused Update of the 2014 AHA/ACC Guideline for the Management of Patients with Valvular Heart Disease: a Report of the American College of Cardiology/American Heart Association Task Force on Clinical Practice Guidelines. Circulation. 2017;135(25):e1159-95. doi: 10.1161/CIR.0000000000000503.

58. Yang LT, Liu YW, Shih JY, Li YH, Tsai LM, Luo CY, et al. Predictive Value of Left Atrial Deformation on Prognosis in Severe Primary Mitral Regurgitation. J Am Soc Echocardiogr. 2015;28(11):1309-17.e4. doi: 10.1016/j.echo.2015.07.004.

59. Ring L, Rana BS, Wells FC, Kydd AC, Dutka DP. Atrial Function as a Guide to Timing of Intervention in Mitral Valve Prolapse with Mitral Regurgitation. JACC Cardiovasc Imaging. 2014;7(3):225-32. doi: 10.1016/j.jcmg.2013.12.009.

The Indiscriminate Use Of Androgenic Anabolic Steroids: The Contribution of Cardiovascular Imaging

Irving Gabriel Araújo Bispo,[1] *Isabella Montanher Zago*[2]
UNIFESP, Cardiologia,[1] *São Paulo, SP – Brazil*
Universidade Municipal de São Caetano do Sul,[2] *São Caetano do Sul, SP – Brazil*

Abstract

Anabolic androgenic steroids (AAS) are natural or synthetic compounds similar to the male hormone testosterone. The literature also describes cases of AAS abuse, such as in bodybuilding, cosmetics, recreational use, and aesthetic enhancement. It was discovered that AAS alone directly induce myocardial injury, with the main pathological finding in autopsied hearts being left ventricle (LV) hypertrophy in frequent association with myocyte hypertrophy, increased collagen deposition in the matrix, increased activity of the cardiac angiotensin, and myocardial fibrosis.

Patients who used illicit AAS present decreased LV systolic function. In athletes who self-administer AAS, LV hypertrophy and elevated sympathetic modulation were observed, as well as elevated blood pressure (BP). High doses of AAS can cause the user to have ventricular arrhythmias and sudden death. Furthermore, AAS users demonstrated greater coronary artery plaque volume than non-users. The objective of this review is to revisit the main effects of the use of AAS on cardiac changes through cardiovascular imaging as well as to establish a difference in relation to athletic heart syndrome.

Introduction

Anabolic androgenic steroids (AAS) are natural or synthetic compounds that mimic the effects of the male hormone testosterone. Alterations to their molecular structure are made to modify their bioactivity, delay absorption into the bloodstream, minimize androgenic effects, and maximize anabolic effects. While testosterone replacement therapy is the current standard treatment for pathological hypogonadism in men, the increasing and indiscriminate use of AAS for aesthetic and competitive purposes lacks support in the literature.

The misuse of anabolic steroids is also reported in bodybuilding, cosmetics, recreational use, and aesthetic enhancement.[1]

Keywords

Steroids; Global Longitudinal Strain; Doppler Echocardiography; Tomography.

Mailings Addess: Irving Gabriel Araújo Bispo •
UNIFESP, Cardiologia. Rua Napoleão de Barros, 715. Postal code: 04021-001. Vila Clementino, São Paulo, SP – Brazil
E-mail: irvingbispo@yahoo.com.br
Manuscript received December 8,2023; revised January 31, 2024; accepted February 4, 2024.
Editor responsible for the review: Marcelo Dantas Tavares de Melo

DOI: https://doi.org/10.36660/abcimg.20230113i

Illicit AAS use has been linked to decreased left ventricular (LV) systolic function. Long-term AAS use has been associated with LV impairment, while recent use has been linked to decreased LV ejection fraction, myocardial hypertrophy, and diastolic dysfunction.[1,2]

Independent studies have found associations between increased plasma total testosterone levels and decreased LV ejection fraction and LV myocardial hypertrophy. Cardiac hypertrophy resulting from AAS abuse is frequently associated with sudden death and arrhythmias in athletes.[1,3]

Bowman et al. studied autopsies of athletes who used AAS. Their main findings were cardiomegaly (33%) and hypertrophy (30%). The most frequently reported histological changes were foci of fibrosis (79%) and necrosis (52%) of myocardial tissue.

The increased dimensions of the cavities, wall thickness, and LV mass are typical consequences of high-intensity physical training and are included in the physiological cardiac remodeling of athletic heart syndrome, which can be a confusing factor regarding the use of AAS.[4,5]

The objective of this review is to assess the primary effects of AAS use on cardiac changes using cardiovascular imaging and to distinguish these effects from those of athletic heart syndrome.

Main changes of anabolic steroids in the cardiovascular system

Metabolic changes

One well-documented factor related to the effects of AAS on the cardiovascular system is its action on plasma lipids. Studies show that users of these drugs had increased low density liprotein (LDL) and decreased high density liprotein (HDL).[6,7] Their actions may be related to the increased activity of the enzyme hepatic triglyceride lipase (HTGL), responsible for regulating lipids and lipoprotein levels, stimulating the formation of atherosclerotic plaques with consequent plaque increase.[8,9] Such changes increase the risk of coronary disease three to six times.[10]

Coronary artery disease (CAD)

AAS use may also be associated with acute myocardial infarction and sudden death in younger people. In a case study, a 20-year-old man using AAS experienced sudden cardiac death (SCD) accompanied by pulmonary hemorrhage.[6] Similar findings were reported in another case involving a 31-year-old bodybuilder who had been using AAS for ten years and presented with chest pain due to an

Contents

Central Illustration: The Indiscriminate Use Of Androgenic Anabolic Steroids: The Contribution of Cardiovascular Imaging

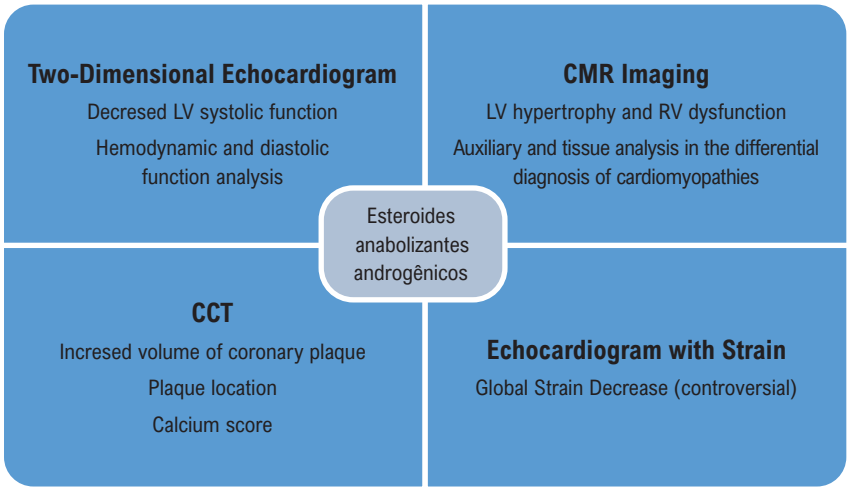

Arq Bras Cardiol: Imagem cardiovasc. 2024;37(1):e20230113

CCT: Coronary Tomography; CMR: Cardiac Magnetic Resonance

acute myocardial infarction, which resulted from occlusion of the right coronary artery.[11]

Some studies have shown beneficial effects on the coronary arteries of patients using AAS, through the release of nitric oxide and the inhibition of smooth muscle contraction. However, animal studies have shown that the misuse of AAS, such as nandrolone in high doses, can cause a vasoconstriction response and lead to side effects.[12-14]

Arterial hypertension

Another widely discussed topic in the literature is the impact of AAS on blood pressure (BP). Studies indicate that AAS use among athletes leads to an increase in BP, which may persist even after discontinuation of the drug. For instance, one study showed that systolic BP remained approximately 6 mmHg higher at rest in AAS users compared to non-users, even after five months of cessation.[15]

This increased BP could be attributed to greater sodium and water retention, as the structure of AAS is similar to aldosterone, potentially leading to increased blood volume and BP.[12] Another hypothesis suggests that AAS may affect the sympathetic nervous system. In spontaneously hypertensive rats, blocking the androgen receptor was effective in reducing BP in the early stages, indicating the significant role of testosterone in the initial phase of hypertension. Additionally, changes in endothelium-dependent vasodilatory responses or alterations in baroreflex control could also contribute to increased BP.[15]

On the other hand, some authors have not observed an increase in BP associated with AAS use. Nottin *et al*. found no differences in BP between bodybuilders using AAS and non-users. Similarly, a study with weight-lifters did not observe increased BP at rest or during exercise in AAS users.[7,16] Similar findings were reported in previous studies, where rats treated with AAS and trained by swimming did not exhibit significant changes in BP. The discrepancies in the literature regarding the effects of AAS on BP may be attributed to variations in study methodologies.[11,17]

Ventricular remodeling

Hypertrophy may be related to the increased afterload of isometric exercise.[18] Possible associations between AAS and LV hypertrophy can be explained as secondary to hypertension or as a direct effect on the myocardium. Notably, studies on isolated myocytes have shown that AAS bind to androgen receptors and can directly cause hypertrophy, potentially due to tissue regulation of the renin-angiotensin system.[19-21]

In fact, clinical studies suggest a distinct form of LV hypertrophy in AAS users, as evidenced by echocardiographic changes in the myocardium before the onset of visible hypertrophy.[22]

Arrhythmias

Animal experiments suggest that AAS abuse may lead to cardiac ischemia during peak exercise, possibly due to accelerated atherosclerosis caused by lipoprotein abnormalities over years of abuse.[23] Additionally, AAS can increase platelet aggregation and thrombus formation through various mechanisms, including increasing

platelet production of thromboxane A2 (a potent platelet aggregator), reducing prostacyclin production (a platelet aggregation inhibitor), and raising fibrinogen levels.[24]

The relative clinical contributions of these mechanisms are uncertain. Still, their combined effects could plausibly explain instances of acute infarction or ventricular arrhythmias in young athletes without traditional cardiac risk factors.[25]

Revisiting the concept of athletic heart syndrome

The physiological hypertrophy of athletic heart syndrome is characterized by homogeneously distributed symmetrical parietal thickening involving all cardiac cavities. The chamber thickening induced by exercise is proportional to the type of physical activity performed and its load (mainly combined power and resistance disciplines). It is reversible after temporary detraining, generally after three (3) months.[26]

A physiological enlargement of both ventricles is usually observed (mainly with endurance athletes), along with proportional atrial dilation. Despite hypertrophy and enlargement of cardiac chambers, cardiac systolic function is not compromised in athletes, with no significant differences compared to non-athlete individuals. Likewise, LV diastolic function is normal, and an increased contribution of early filling velocity can be seen at rest with pulsed Doppler E/A > 2. Aortic root diameters are generally normal in athletes.[6]

The human heart feels the demand and adapts in both the short and long terms. Assessing cardiac remodeling in athletes presents several challenges, including the impact of training load — particularly in amateur athletes — and the difficulty in establishing sport- and sex-specific reference ranges. Additionally, factors such as race and the use of performance-enhancing substances, like AAS, further complicate the assessment.[27]

The morphology of the LV in the athlete's heart is typically studied using echocardiography, revealing a distinct pattern of LV dilation and hypertrophy. Current recommendations from the European Association of Preventive Cardiology (EAPC) and the European Association of Cardiovascular Imaging (EACVI) suggest echocardiography as a secondary investigative tool to differentiate between an athlete's physiological heart adaptations and underlying cardiac conditions. However, contrary to these guidelines, echocardiography is often used as a primary screening tool in the cardiovascular assessment of both professional and amateur athletes, even when clinical and electrocardiographic assessments are normal.[28,29]

For endurance athletes exhibiting LV and/or right ventricular (RV) dilation with mildly reduced ejection fraction at rest, stress echocardiography can be used to evaluate contractile reserve during exercise. A significant improvement in contractility during exercise indicates physiological cardiac remodeling, whereas a lack of improvement or subnormal response suggests a pathological condition (e.g., dilated cardiomyopathy, non-compacted LV, arrhythmogenic cardiomyopathy). Likewise, exercise-induced ventricular arrhythmias also support the hypothesis of underlying heart disease.[30]

Cardiac magnetic resonance (CMR) can more accurately assess cardiac structure and function, as well as characterize the myocardium, detecting relevant changes, including the quantification of myocardial fibrosis. CMR also enables the assessment of myocardial tissue characteristics, including fat and water content, fibrosis, and cardiomyocyte mass.[31,32]

While the vast majority of athletes have suitable echo windows, it is important to note that echocardiography is not used as the gold standard for measuring cavity, mass, and intracavitary volumes. Instead, its routine use in suspected athletic heart syndrome is primarily due to its ability, within a coherent clinical context, for tissue characterization. Therefore, CMR is useful for assessing athletic heart syndrome, as the precision of the measurements is superior to echocardiography.

Given the complex structure of RV morphological assessment, CMR is more reproducible than echocardiography. Increases in RV mass, end-diastolic volumes, and stroke volumes relative to non-athletes have been described. The relationship between LV and RV size was maintained, leading to the conclusion that athlete's heart syndrome involves balanced remodeling of both ventricles' diameter.[32]

Anabolic androgen steroids and changes in the echocardiogram

AAS use resulted in impaired LV systolic function, as assessed by left ventricular ejection fraction (LVEF) and longitudinal strain, and demonstrated in a study by Baggish *et al*. This finding was driven almost entirely by AAS users who were under the influence of drugs at the time of the study, suggesting that LV dysfunction may be dynamically related to AAS use.[33]

In subsequent analyses examining the association of outcomes with duration and use of AAS: 41 (71%) of the 58 AAS users had an LVEF below the limit of 52% calculated by the Simpson method. In contrast, non-users had a largely normal LVEF.[33]

In another analysis, the primary outcome variables LVEF and E', AAS users showed significant deficits compared to non-users, therefore compromising the parameters of systolic and diastolic function in parallel.

Regarding ventricular remodeling, AAS users exhibited higher LV mass index, thicker LV walls, and more concentric LV geometry than non-users.[34]

AAS users also showed impaired diastolic function, both in relation to non-users and also as defined by current diagnostic criteria according to the American Society of Echocardiography. Twenty-nine (50%) drug users had values below the normal E´ threshold of 8.5 cm/s. Similar associations with AAS use have been found in other studies.[35]

No association was found between the duration of AAS use and the primary outcome variables (for every additional

10 years of AAS exposure, the estimated mean change [95% CI] in LVEF was −3.3% [−8.3% to 1.6%], p = 0.19; and the estimated mean change in E´ was 0.1 cm/s [-1.0 to 1.2cm/s], p = 0 ,90).[35]

When assessing the associations separately for AAS users and non-users, there was a significant association between increased LV mass index and decreased LVEF among AAS users (estimated mean change [95% CI] in LVEF for each increase of 10 g in LV mass index -1.6% [-2.4 to -0.8%], p < 0.001). In contrast, no significant association between LV mass index and LVEF was seen in non-users (estimated mean change in LVEF for each 10 g increase in LV mass index –0.2% [–1.5 to 1.2%], p = 0.80).[35,36]

The Speckle-Tracking Echocardiography (STE) is another advanced echocardiographic strain imaging technique that provides new insights into the characterization of myocardial properties in athletes, detecting subclinical ventricular systolic function in early-stage heart disease when LVEF is still normal.[37]

The LV global longitudinal strain (GLS) obtained by STE is the most used parameter in clinical practice, but there is controversy in the literature, whose studies show differences. Therefore, a reduction in longitudinal deformation in athletes should be considered a subclinical sign of LV contractile dysfunction and should raise the suspicion of myocardial disease, particularly in the presence of hypertrophy or equivocal LV dilation.[37]

Data regarding the interpretation of parameters derived from VR and STE in athletes are still controversial. Chronic, strenuous physical training appears to have a detrimental effect on RV function, with reduced RV strain immediately after endurance running, followed by complete recovery. Finally, RV deformation imaging can help differentiate between physiological and pathological conditions by identifying regional wall motion abnormalities in patients with arrhythmogenic cardiomyopathy.[37]

Myocardial work is a novel echocardiographic index of LV contractile function, being less dependent on load and adjusting parameters derived from STE for afterload. Increased afterload in various physiological and pathological conditions can result in impaired effort. This is particularly relevant for athletes whose BP and loading conditions may vary between exams and different phases of their training programs, and it may also be beneficial for monitoring AAS users.[38]

The use of coronary tomography (CCT) in users of anabolic androgen steroids

Recent technological advances have expanded the role of CCT beyond the evaluation of coronary arteries and large vessels. LV morphological and functional assessment is performed using an ECG-controlled retrospective scanning protocol. The assessment of LV volumes, systolic volume, ejection fraction, and mass showed excellent correlation with the CMR assessment.[39]

LV functional assessment by CCT is particularly useful in claustrophobic patients, as they are unable to perform CMR, or if there are any contraindications to CMR (although rare among athlete patients). Otherwise, CCT cannot be recommended as a first-line imaging technique for LV functional assessment in athletes, given the greater radiation exposure required. The use of iodinated contrast media allows the assessment of the LV and myocardial fibrosis (with analysis of late iodine enhancement) by CCT, even if not routinely used in clinical practice, with good agreement with the same assessments performed by contrast-enhanced CMR.

All athletes with ambiguous anomalous coronary artery anatomy, suspected following echocardiography, should undergo CCT based on institutional preferences and knowledge. In cases of suspected coronary atherosclerotic disease, CCT is valuable for coronary artery calcium scoring and non-invasive coronary angiography. When dilation of the aortic root or ascending aorta is suspected or confirmed, a comprehensive tomographic evaluation of the aorta is recommended.

While regular aerobic exercise is known to be beneficial for the primary and secondary prevention of cardiovascular diseases, the impact of lifelong resistance exercise on the heart has only recently been studied. In a minority of susceptible veteran athletes, exercise can trigger adverse events such as SCD, often attributable to silent CAD. Several studies have demonstrated a higher-than-expected prevalence of CAD in veteran athletes, and failure to detect those at risk using routine cardiovascular screenings such as exercise testing has potentially devastating consequences. CCT, including calcium scoring, has revealed CAD in 25-53% of veteran athletes and offers prognostic benefits by determining plaque morphology and total atherosclerotic burden.[40]

AAS use has been linked to increased coronary atherosclerosis, with disease severity strongly associated with the cumulative duration of AAS use over a lifetime. Taken together, our findings suggest that prolonged AAS use is associated with adverse cardiovascular phenotypes characterized by both myocardial disease and CAD.[41]

AAS users had significantly greater coronary plaque volume than non-users. When investigating the relationship between ATT measurements and the duration of AAS use, we observed strong associations between lifetime use time and all angiographic measures of coronary pathology (table 1). However, there was no significant change in the association between AAS use and plaque volume (estimated mean difference between users with and without drugs in classifications: -0.07 SD units [-0.56 to 0.41]; p = 0.76). It is noteworthy that three AAS users had experienced prior myocardial infarctions due to atherosclerotic disease, as documented by cardiac catheterization. These events occurred at ages 38 (ST-segment myocardial infarction with complete occlusion of the left anterior descending artery), 43 (Myocardial infarction without ST-segment elevation with 99% occlusion of both the right coronary and left circumflex coronary arteries), and 46 (ST-segment elevation myocardial infarction with complete occlusion of an obtuse 2nd marginal artery), after 17, 11, and 5 years of accumulated exposure to AAS over their lifetime, respectively.[42]

Table 1 – Main changes in cardiovascular imaging methods with the use of AAS

Method	Finding
Echocardiogram	Decreased LV systolic function Hemodynamic and diastolic function analysis Reduction of cardiac mechanics (strain), (controversial)
CCT	Increased volume of coronary plaque Plaque location Calcium score
CMR Imaging	LV hypertrophy and RV dysfunction Auxiliary and tissue analysis in the differential diagnosis of cardiomyopathies

LF: Left Ventricle; RV: Right Ventricle; CCT: Coronary Tomography; CMR: Cardiac Magnetic Resonance

CMR in AAS users

CMR is the most valuable imaging method for the differential diagnosis between physiology and pathology in athletes, aiding in the discrimination of diseases where the echocardiography does not provide clarification.[43]

CMR is the gold standard for defining myocardial morphology, assessing parietal mobility, size of cardiac chambers, and tissue definition. It provides a precise and reproducible assessment of the volume and mass of the heart chambers, as well as the global and regional contractile function. This method is the preferred choice for accurately assessing the morphology and function of the RV.[12]

CMR represents the superior method for identifying myocardial fibrosis and its distribution pattern through the assessment of late gadolinium enhancement, native T1, and extracellular volume (ECV) mapping. Furthermore, CMR can identify edema and fat in the myocardial walls.[22]

In particular, the identification of myocardial fibrosis can differentiate between athletic heart syndrome and pathological LV hypertrophy (Figure 1), as fibrosis often accompanies cardiac remodeling due to pathology.[44]

In hypertrophic cardiomyopathy, midwall fibrosis is typically found in areas of extreme hypertrophy, although it can also occur in non-hypertrophied segments.[36]

Myocardial fibrosis has been observed in athletes with a higher prevalence than in healthy non-athlete populations. In healthy athletes, myocardial fibrosis involves less than 3% of the myocardium. It varies greatly in quantity, location and pattern, but is generally found in the RV or interventricular septum. The prevalence of myocardial fibrosis in individuals with athletic heart syndrome appears to increase with a longer history of resistance training. However, the prognostic significance of myocardial fibrosis in individuals with athletic heart syndrome is unknown.[45] Regarding diffuse interstitial fibrosis, studies comparing ECV in athletes and controls reported similar or lower ECV values in athletes.[45]

Stress CMR, usually with exercise, can be used to identify reduced functional reserve and early-stage cardiomyopathy when resting functional assessment is mildly abnormal. However, further studies are needed to evaluate the cost-effectiveness of stress CMR imaging in this setting.[45]

A cross-sectional cohort design was used with 21 strength-trained participants who underwent heart CMR imaging and STE. Thirteen participants (30 ± 5 years) who had been taking AAS for at least two years and were currently on a "use" cycle were compared with age- and training-matched controls (n = 8; 29 ± 6 years) who had never taken AAS.[23]

AAS users had a significantly greater absolute LV mass (220 ± 45 g) compared to non-users (163 ± 27 g; $p < 0.05$), but this difference was removed when indexed to fat-free mass. AAS users also had a reduced RV ejection fraction (AS 51 ± 4% vs. NAS 59 ± 5%; $p < 0.05$) and a significantly lower myocardial tissue velocity ratio E' by LV tissue Doppler (AAS 0.99[0.54] vs. non-AAS users 1.78[0.46]; $p < 0.05$). Maximum LV longitudinal strain was lower in AAS users (−14.2 ± 2.7% vs. −16.6 ± 1.9%; $p < 0.05$). There was no evidence of focal fibrosis in any participant. AAS use was associated with significant LV hypertrophy, although in line with greater fat-free mass, reduced LV strain, diastolic function, and reduced RV ejection fraction in male bodybuilders. There was, however, no evidence of focal fibrosis in any AAS user.[23]

Conclusions

The indiscriminate use of AAS among athletes has been on the rise and is linked to LV hypertrophy and dysfunction. Cardiologists must be vigilant about this public health concern and should assess its impact on users early on using cardiovascular imaging.

Author Contributions

Conception and design of the research: Bispo I, Zago IM; acquisition of data, analysis and interpretation of the data: Zago IM; writing of the manuscript and critical revision of the manuscript for intellectual content: Bispo I.

Potential Conflict of Interest

No potential conflict of interest relevant to this article was reported.

Sources of Funding

There were no external funding sources for this study.

Study Association

This study is not associated with any thesis or dissertation work.

Ethics Approval and Consent to Participate

This article does not contain any studies with human participants or animals performed by any of the authors.

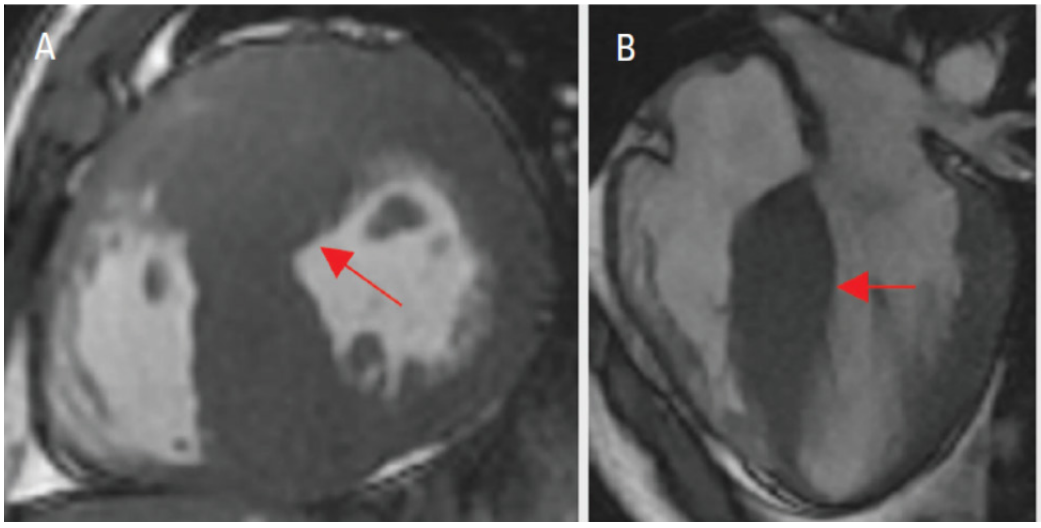

Figure 1 – *CMR Imaging for the differential diagnosis of cardiomyopathy Hypertrophic x Athlete's Heart*

References

1. Rasmussen JJ, Schou M, Madsen PL, Selmer C, Johansen ML, Ulriksen PS, et al. Cardiac Systolic Dysfunction in Past Illicit Users of Anabolic Androgenic Steroids. Am Heart J. 2018;203:49-56. doi: 10.1016/j.ahj.2018.06.010.
2. Barbosa O Neto, Mota GR, De Sordi CC, Resende EAMR, Resende LAPR, Silva MAV, et al. Long-Term Anabolic Steroids in Male Bodybuilders Induce Cardiovascular Structural and Autonomic Abnormalities. Clin Auton Res. 2018;28(2):231-44. doi: 10.1007/s10286-017-0470-2.
3. Zhang Q, Shan KS, Raza A, Manda N, Nace T. A Rare Case Report and Literature Review of Anabolic-Androgenic Steroids (AAS)-Induced Acute Myocardial Infarction. Cureus. 2020;12(5):e8332. doi: 10.7759/cureus.8332.
4. Torrisi M, Pennisi G, Russo I, Amico F, Esposito M, Liberto A, et al. Sudden Cardiac Death in Anabolic-Androgenic Steroid Users: a Literature Review. Medicina. 2020;56(11):587. doi: 10.3390/medicina56110587.
5. Bowman S. Anabolic Steroids and Infarction. BMJ. 1990;300(6726):750. doi: 10.1136/bmj.300.6726.750-c.
6. McNutt RA, Ferenchick GS, Kirlin PC, Hamlin NJ. Acute Myocardial Infarction in a 22-Year-Old World Class Weight Lifter using Anabolic Steroids. Am J Cardiol. 1988;62(1):164. doi: 10.1016/0002-9149(88)91390-2.
7. Nottin S, Nguyen LD, Terbah M, Obert P. Cardiovascular Effects of Androgenic Anabolic Steroids in Male Bodybuilders Determined by Tissue Doppler Imaging. Am J Cardiol. 2006;97(6):912-5. doi: 10.1016/j.amjcard.2005.10.026.
8. Norton GR, Trifunovic B, Woodiwiss AJ. Attenuated Beta-Adrenoceptor-Mediated Cardiac Contractile Responses Following Androgenic Steroid Administration to Sedentary Rats. Eur J Appl Physiol. 2000;81(4):310-6. doi: 10.1007/s004210050048.
9. Krieg A, Scharhag J, Albers T, Kindermann W, Urhausen A. Cardiac Tissue Doppler in Steroid Users. Int J Sports Med. 2007;28(8):638-43. doi: 10.1055/s-2007-964848.
10. Lenders JW, Demacker PN, Vos JA, Jansen PL, Hoitsma AJ, van ,t Laar A, et al. Deleterious Effects of Anabolic Steroids on Serum Lipoproteins, Blood Pressure, and Liver Function in Amateur Body Builders. Int J Sports Med. 1988;9(1):19-23. doi: 10.1055/s-2007-1024972.
11. Lang RM, Badano LP, Mor-Avi V, Afilalo J, Armstrong A, Ernande L, et al. Recommendations for Cardiac Chamber Quantification by Echocardiography in Adults: an Update from the American Society of Echocardiography and the European Association of Cardiovascular Imaging. J Am Soc Echocardiogr. 2015;28(1):1-39.e14. doi: 10.1016/j.echo.2014.10.003.
12. Angell PJ, Ismail TF, Jabbour A, Smith G, Dahl A, Wage R, et al. Ventricular Structure, Function, and Focal Fibrosis in Anabolic Steroid Users: a CMR Study. Eur J Appl Physiol. 2014;114(5):921-8. doi: 10.1007/s00421-014-2820-2.
13. Wynne FL, Khalil RA. Testosterone and Coronary Vascular Tone: Implications in Coronary Artery Disease. J Endocrinol Invest. 2003;26(2):181-6. doi: 10.1007/BF03345150.
14. Ferrer M, Encabo A, Marín J, Balfagón G. Chronic Treatment with the Anabolic Steroid, Nandrolone, Inhibits Vasodilator Responses in Rabbit Aorta. Eur J Pharmacol. 1994;252(2):233-41. doi: 10.1016/0014-2999(94)90602-5.
15. Thompson PD, Cullinane EM, Sady SP, Chenevert C, Saritelli AL, Sady MA, et al. Contrasting Effects of Testosterone and Stanozolol on Serum Lipoprotein Levels. JAMA. 1989;261(8):1165-8.
16. Angell PJ, Ismail TF, Jabbour A, Smith G, Dahl A, Wage R, et al. Ventricular Structure, Function, and Focal Fibrosis in Anabolic Steroid Users: A CMR Study. Eur J Appl Physiol. 2014;114(5):921-8. doi: 10.1007/s00421-014-2820-2.
17. Maurovich-Horvat P, Ferencik M, Bamberg F, Hoffmann U. Methods of Plaque Quantification and Characterization by Cardiac Computed Tomography. J Cardiovasc Comput Tomogr. 2009;3 (Suppl 2):S91-8. doi: 10.1016/j.jcct.2009.10.012.
18. Hoffmann MH, Shi H, Schmitz BL, Schmid FT, Lieberknecht M, Schulze R, et al. Noninvasive Coronary Angiography with Multislice Computed Tomography. JAMA. 2005;293(20):2471-8. doi: 10.1001/jama.293.20.2471.
19. Bates G, Begley E, Tod D, Jones L, Leavey C, McVeigh J. A Systematic Review Investigating the Behaviour Change Strategies in Interventions to Prevent Misuse of Anabolic Steroids. J Health Psychol. 2019;24(11):1595-612. doi: 10.1177/1359105317737607.

20. Vanberg P, Atar D. Androgenic Anabolic Steroid Abuse and the Cardiovascular System. Handb Exp Pharmacol. 2010;(195):411-57. doi: 10.1007/978-3-540-79088-4_18.

21. Baggish AL, Weiner RB, Kanayama G, Hudson JI, Lu MT, Hoffmann U, et al. Cardiovascular Toxicity of Illicit Anabolic-Androgenic Steroid Use. Circulation. 2017;135(21):1991-2002. doi: 10.1161/CIRCULATIONAHA.116.026945.

22. Kuhn CM. Anabolic Steroids. Recent Prog Horm Res. 2002;57:411-34. doi: 10.1210/rp.57.1.411.

23. Hassan NA, Salem MF, Sayed MA. Doping and Effects of Anabolic Androgenic Steroids on the Heart: Histological, Ultrastructural, and Echocardiographic Assessment in Strength Athletes. Hum Exp Toxicol. 2009;28(5):273-83. doi: 10.1177/0960327109104821.

24. Liu PY, Death AK, Handelsman DJ. Androgens and Cardiovascular Disease. Endocr Rev. 2003;24(3):313-40. doi: 10.1210/er.2003-0005.

25. Payne JR, Kotwinski PJ, Montgomery HE. Cardiac Effects of Anabolic Steroids. Heart. 2004;90(5):473-5. doi: 10.1136/hrt.2003.025783.

26. Di Bello V, Giorgi D, Bianchi M, Bertini A, Caputo MT, Valenti G, et al. Effects of Anabolic-Androgenic Steroids on Weight-Lifters' Myocardium: an Ultrasonic Videodensitometric Study. Med Sci Sports Exerc. 1999;31(4):514-21. doi: 10.1097/00005768-199904000-00004.

27. Fineschi V, Riezzo I, Centini F, Silingardi E, Licata M, Beduschi G, et al. Sudden Cardiac Death During Anabolic Steroid Abuse: Morphologic and Toxicologic Findings in Two Fatal Cases of Bodybuilders. Int J Legal Med. 2007;121(1):48-53. doi: 10.1007/s00414-005-0055-9.

28. Sharma S. Athlete's Heart--Effect of Age, Sex, Ethnicity and Sporting Discipline. Exp Physiol. 2003;88(5):665-9. doi: 10.1113/eph8802624.

29. Ferenchick GS. Anabolic/Androgenic Steroid Abuse and Thrombosis: is There a Connection? Med Hypotheses. 1991;35(1):27-31. doi: 10.1016/0306-9877(91)90079-e.

30. Christou GA, Christou KA, Nikas DN, Goudevenos JA. Acute Myocardial Infarction in a Young Bodybuilder Taking Anabolic Androgenic Steroids: a Case Report and Critical Review of the Literature. Eur J Prev Cardiol. 2016;23(16):1785-96. doi: 10.1177/2047487316651341.

31. Pelliccia A, Caselli S, Sharma S, Basso C, Bax JJ, Corrado D, et al. European Association of Preventive Cardiology (EAPC) and European Association of Cardiovascular Imaging (EACVI) Joint Position Statement: Recommendations for the Indication and Interpretation of Cardiovascular Imaging in the Evaluation of the Athlete's Heart. Eur Heart J. 2018;39(21):1949-69. doi: 10.1093/eurheartj/ehx532.

32. D'Ascenzi F, Anselmi F, Mondillo S, Finocchiaro G, Caselli S, Garza MS, et al. The use of Cardiac Imaging in the Evaluation of Athletes in the Clinical Practice: a Survey by the Sports Cardiology and Exercise Section of the European Association of Preventive Cardiology and University of Siena, in Collaboration with the European Association of Cardiovascular Imaging, the European Heart Rhythm Association and the ESC Working Group on Myocardial and Pericardial Diseases. Eur J Prev Cardiol. 2021;28(10):1071-7. doi: 10.1177/2047487320932018.

33. Androulakis E, Swoboda PP. The Role of Cardiovascular Magnetic Resonance in Sports Cardiology; Current Utility and Future Perspectives. Curr Treat Options Cardiovasc Med. 2018;20(10):86. doi: 10.1007/s11936-018-0679-y.

34. Maestrini V, Torlasco C, Hughes R, Moon JC. Cardiovascular Magnetic Resonance and Sport Cardiology: a Growing Role in Clinical Dilemmas. J Cardiovasc Transl Res. 2020;13(3):296-305. doi: 10.1007/s12265-020-10022-7.

35. Baggish AL, Weiner RB, Kanayama G, Hudson JI, Lu MT, Hoffmann U, et al. Cardiovascular Toxicity of Illicit Anabolic-Androgenic Steroid use. Circulation. 2017;135(21):1991-2002. doi: 10.1161/CIRCULATIONAHA.116.026945.

36. Stergiopoulos K, Brennan JJ, Mathews R, Setaro JF, Kort S. Anabolic Steroids, Acute Myocardial Infarction and Polycythemia: a Case Report and Review of the Literature. Vasc Health Risk Manag. 2008;4(6):1475-80. doi: 10.2147/vhrm.s4261.

37. Baggish AL, Weiner RB, Kanayama G, Hudson JI, Picard MH, Hutter AM Jr, et al. Long-Term Anabolic-Androgenic Steroid use is Associated with Left Ventricular Dysfunction. Circ Heart Fail. 2010;3(4):472-6. doi: 10.1161/CIRCHEARTFAILURE.109.931063.

38. D'Andrea A, Caso P, Salerno G, Scarafile R, De Corato G, Mita C, et al. Left Ventricular Early Myocardial Dysfunction after Chronic Misuse of Anabolic Androgenic Steroids: A Doppler Myocardial and Strain Imaging Analysis. Br J Sports Med. 2007;41(3):149-55. doi: 10.1136/bjsm.2006.030171.

39. Hassan NA, Salem MF, Sayed MA. Doping and Effects of Anabolic Androgenic Steroids on the Heart: Histological, Ultrastructural, and Echocardiographic Assessment in Strength Athletes. Hum Exp Toxicol. 2009;28(5):273-83. doi: 10.1177/0960327109104821.

40. Urhausen A, Albers T, Kindermann W. Are the Cardiac Effects of Anabolic Steroid Abuse in Strength Athletes Reversible?. Heart. 2004;90(5):496-501. doi: 10.1136/hrt.2003.015719.

41. Sader MA, Griffiths KA, McCredie RJ, Handelsman DJ, Celermajer DS. Androgenic Anabolic Steroids and Arterial Structure and Function in Male Bodybuilders. J Am Coll Cardiol. 2001;37(1):224-30. doi: 10.1016/s0735-1097(00)01083-4.

42. McCrohon JA, Death AK, Nakhla S, Jessup W, Handelsman DJ, Stanley KK, et al. Androgen Receptor Expression is Greater in Macrophages from Male than from Female Donors. A Sex Difference with Implications for Atherogenesis. Circulation. 2000;101(3):224-6. doi: 10.1161/01.cir.101.3.224.

43. Tagarakis CV, Bloch W, Hartmann G, Hollmann W, Addicks K. Anabolic Steroids Impair the Exercise-Induced Growth of the Cardiac Capillary Bed. Int J Sports Med. 2000;21(6):412-8. doi: 10.1055/s-2000-3835.

44. Kanayama G, Hudson JI, Pope HG Jr. Features of Men with Anabolic-Androgenic Steroid Dependence: a Comparison with Nondependent AAS Users and with AAS Nonusers. Drug Alcohol Depend. 2009;102(1-3):130-7. doi: 10.1016/j.drugalcdep.2009.02.008.

45. Santora LJ, Marin J, Vangrow J, Minegar C, Robinson M, Mora J, et al. Coronary Calcification in Body Builders using Anabolic Steroids. Prev Cardiol. 2006;9(4):198-201. doi: 10.1111/j.1559-4564.2006.05210.x.

Atrial Functional Mitral Regurgitation

Alexsander da Silva Pretto[1]
ImagemCor,[1] *Tenente Portela, RS – Brazil*

Abstract

Secondary mitral insufficiency (MI) in the setting of ventricular disease has always been a topic at conferences and has achieved extensive pathophysiological knowledge over the years. More recently, with the increasing incidence of atrial fibrillation (AF) and heart failure with preserved ejection fraction (HFpEF), a new phenotype that had been little discussed has come to light: atrial functional mitral regurgitation. In this entity, special attention should be addressed to the left atrium and the mitral annulus because, in early stages, they present normal left ventricular dimensions and function.

Introduction

Mitral Insufficiency (MI) is one of the most common valvulopathies in the world[1]. New knowledge about its physiopathology, diagnosis and treatment are arising. In this sense, Atrial Fibrillation (AF) is the disorder of the rhythm more usually observed in the general population[2]. The estimation is that the prevalence of MI in the USA in 2030 will be higher than 4 million cases, and FA will reach 12.1 million[3]. Data indicate that, until 2050, the population aged more than 80 years will triple[4].

The "epidemic" growth of the incidence of AF, with approximately 5 million new cases per year around the world[5], and heart failure with preserved ejection fraction (HFpEF), responsible for 37 to 53% of the cases of Congestive Heart Failure (CHF) in the different series make us get to know this subgroup of patients better[6]. Besides, one to two thirds of the patients with HFpEF will experience AF at the time of diagnosis or at some point of the condition[7].

The identification of the MI mechanism is the key for the treatment sequence. The Carpentier classification is the starting point for better understanding, which, in this author's opinion, should be part of all reports of patients with moderate or severe MI (Figure 1). Additionally, MI is classified as primary or organic (PMI) when leaflets and the subvalvular apparatus are normal and it is caused by functional abnormalities in the left heart. It occurs due to the imbalance between the increased tethering forces (resulting exclusively from the global or regional remodeling of the left ventricle (LV), promoting the apical-lateral displacement of papillary muscles (leaflet tethering) and the reduction of closing forces (reduced contractility and dyssynchrony)[8]. This model, which was known until then, began to be called ventricular functional mitral regurgitation (VFMR), and a new concept appeared: atrial functional mitral regurgitation (AFMR).

Historically, AFMR is only owed to mitral annular dilation, but recent evidence showed that this is only one piece of the puzzle, and new mechanisms were added. Its early recognition seems to be extremely important because studies demonstrate that a successful ablation and the maintenance of sinus rhythm reduce its severity[9].

The data about its real incidence and prevalence lack variable diagnostic criteria. Kagiyama et al. revised the prevalence of AFMR in nine studies and identified, initially, very different rates (between 2.8 and 66.7%). After excluding studies that used qualitative methods to classify the MI, and another one that included hospitalized patients, they reached a prevance rate of 3 to 15%[10]. Moonen et al. Studied 140,014 adults in 25 centers of Australia, only including patients with severe FMR, and found VFMR in 60% of the cases, and AFMR in 40% of the cases. Patients with AFMR were older (mean of 78 +- 11 years), with higher proportion of women (58%)[11].

Mesi et al., in a study with 283 patients, compared PMI with AFMR and identified that the latter presented more comorbidities, such as systemic arterial hypertension (SAH), Type 2 Diabetes Mellitus, permanent AF, previous non-mitral cardiac surgery and pacemaker insertion[12].

A group from the Mayo Clinic published a study, led by Dziadzko, which analyzed 727 inhabitants of the Olmsted County, in Minnesota, referred to echocardiogram due to a diagnosis of moderate or severe MI, and reported FMI in 65% of the cases; organic, in 32%; and mixed, in 3%. Among the cases of FMI (65%), VFMR was found in 38% of the cases, and AFMR, in 27%.

Physiopathology

The best proposal to understand the genesis of this entity was described by Silbiger[14,21]. He described that left atrial dysfunction and the augmented pressure inside it lead this chamber and the mitral annulus to dilate, thus generating the consequent displacement of the posterior mitral annulus to the ridge in the LV input pathway. The progressive growth of the LA in the posterior direction leads to other findings.

At first, we believed this situation happened only and exclusively because of annular dilation; however, other studies added new mechanisms to the process.

Keywords

Atrial Fibrillation; Heart Failure; Echocardiography; Mitral Valve Insufficiency.

Mailing Address: Alexsander da Silva Pretto •
Clínica ImagemCor, Rua Tibiriçá, 155. Postal code: 98500-000. Tenente Portela, RS – Brazil.
E-mail: axspretto@gmail.com
Manuscript received November 1, 2023; revised November 9, 2023; accepted November 10, 2023
Editor responsible for the review: Daniela do Carmo Rassi Frota

DOI: https://doi.org/10.36660/abcimg.20230097i

Contents

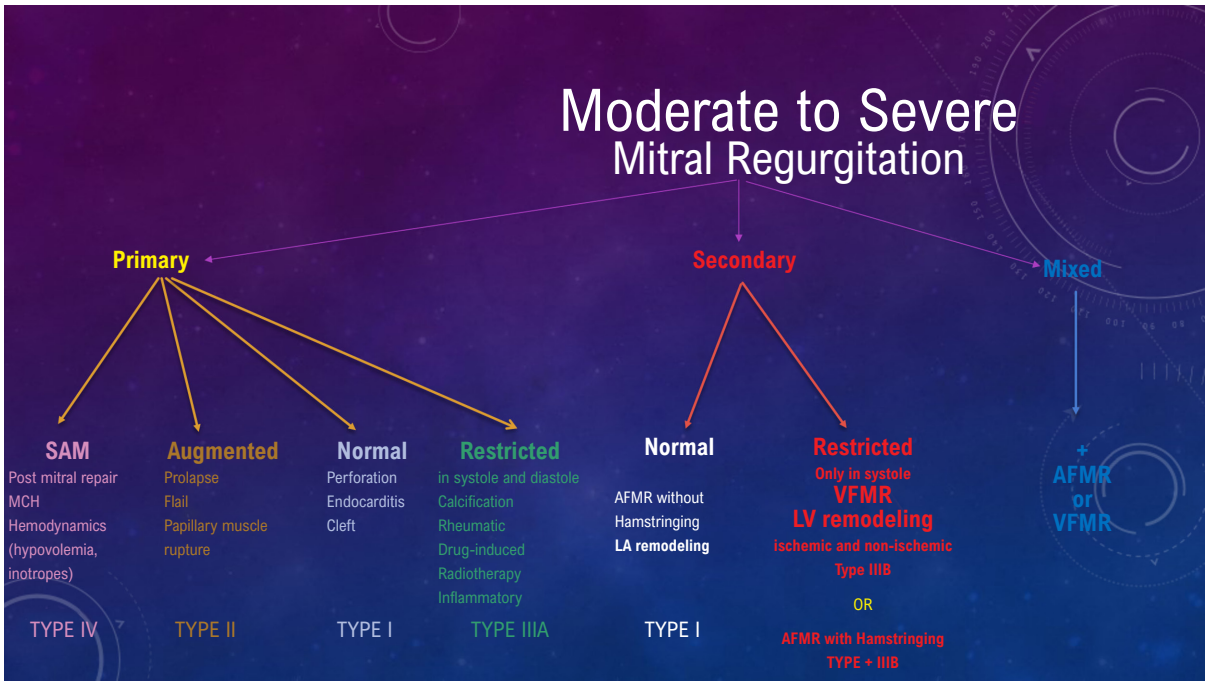

Figure 1 – *Carpentier Classification. AFMR: atrial functional mitral regurgitation; VFMR: ventricular functional mitral regurgitation; MCH: hypertrophic cardiomyopathy; SAM: systolic anterior motion; LV: left ventricle.*

1. ISOLATED MITRAL ANNULAR DILATION: in a retrospective study, Gertz et al.[15], when analyzing 53 patients referred to first AF ablation, who presented with moderate to severe MI, type I, and Ejection Fraction (EF) >50%, demonstrated that the dimension of the mitral annulus was the most important factor for MI in patients with FA (odds ratio 8.39; p= 0.004). Besides, they detected major MI in 82% of the patients with recurrene of FA, and in only 24% of patients with effective ablation. Another study that included 170 patients with AF, structurally normal mitral valve, normal function and dimensions of the LV, who underwent multidetector CT before the ablation, showed that patients with moderate to severe MI presented larger perimeter, annular area and intercommissural and anteroposterior diameters in comparison to patients without MI[16].

2. INSUFFICIENT LEAFLET REMODELING: heart valves are capable of presenting the compensatory growth of leaflets secondary to annular dilation and heart dimensions. This happens thanks to endothelial-mesenchymal cells. Kagiyama et al.[17] found that the leaflet area was significantly larger in all patients with FA. Regarding the total leaflet area (TLA) to mitral annular area (MAA), it was significantly smaller in the MI group when compared to the group without MI and controls. In most patients with significant MI, the TLA/MMA ratio was lower than 1.4. This shows that when the mitral annulus is significantly dilated, leaflet growth does not follow and reaches a plateau, and this insufficient adaptation contributes with the onset of MI.

3. CHANGES IN ANNULAR CONTRACTILITY AND SADDLE SHAPE: the mitral annulus is primarily composed of fibrous and fat tissue. It does not contract actively, but it moves passively with the contraction of the LA and the LV. Annular contraction begins in late diastole and continues through mesosystole, resulting in a reduction of approximately 25% of its area. About 60% of this reduction takes place in late diastole. Anatomic studies by Silbiger and Bazaz[19,20] suggest that, during late diastole, the mitral annulus becomes narrow due to the contraction of circumferential fibers that outlines the base of the LA (atriogenic annular contraction), whereas in systole, annular narrowing is facilitated by the superficial oblique fibers of the LV input pathway = basal twist (ventricular annular contraction). In FA, it is possible to identify the flattening of the mitral annulus and loss of annular movement. The flattening of the mitral annulus increases valvular stress, leading to fibrosis, thickening and calcification;

4. ATRIOGENIC *TETHERING* OF THE LEAFLETS: the anterior portion of the mitral annulus is connected to the aorta, at a more fixed and stable position of the heart. The posterior mitral annulus is anchored between the LA and the ridge in the LV input pathway. With the growth of the LA, it is pushed towards the epicardial surface of the posterior basal wall. The posterior leaflet follows this movement and increases annulo-papillary distance, causing a more abrupt angle and larger curvature towards the LV = atriogenic asymmetric posterior tethering[21].

5. ATRIAL DYSFUNCTION AND CHANGES IN HEART RATE: there is probably a bidirectional relation between AFMR and atrial myopathy. Further studies are required to answer this question.

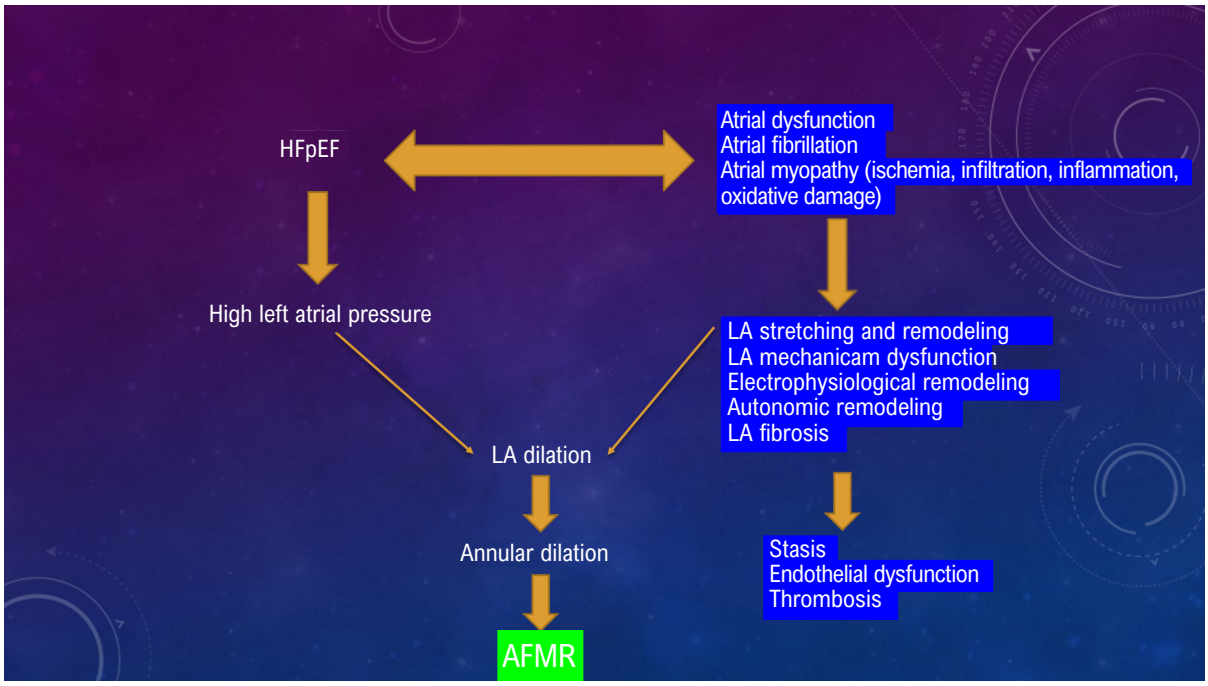

Figure 2 – *Physiopathology of AFMR. AFMR: atrial functional mitral regurgitation; VFMR: ventricular functional mitral regurgitation; LA: left atrium.*

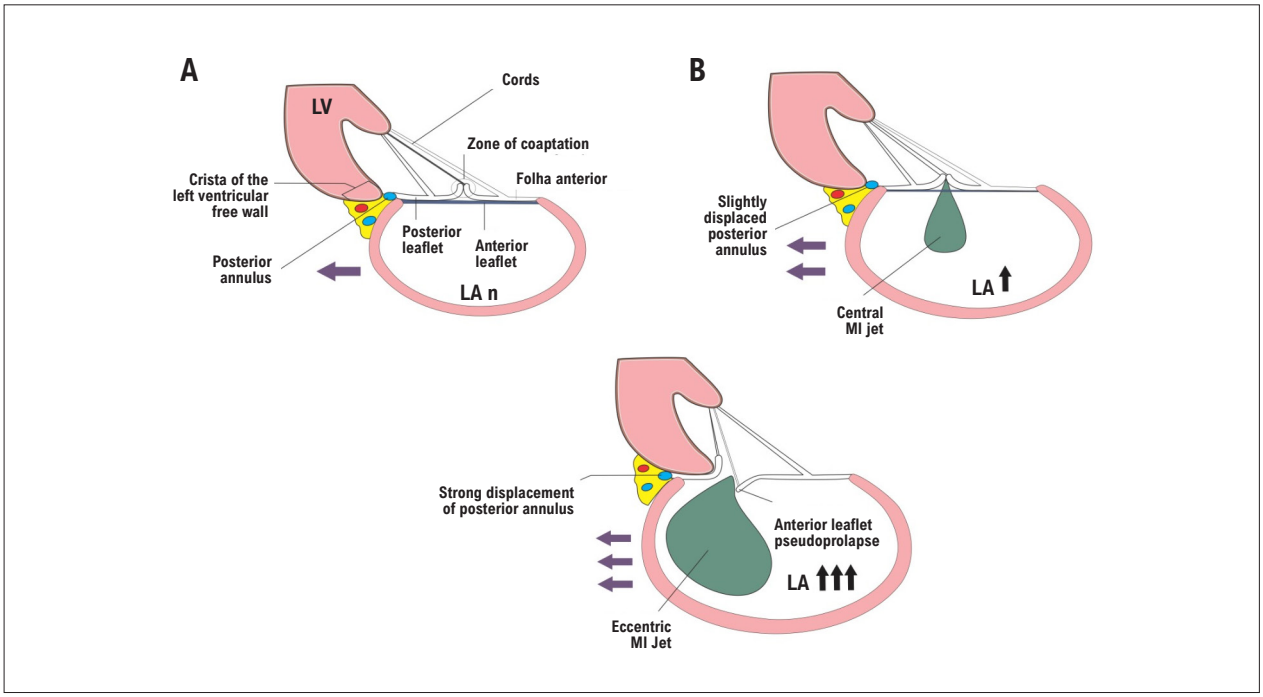

Figure 3 – *Demonstrative model of pathological Evolution. Acknowledge to Kátia Debus for creating this artwork.*

Echocardiographic findings

This item presents findings that are not commonly known, and the approach about the subject is necessary:

Hamstringing: it is identified as a blocked movement of the posterior leaflet, which is practically paralyzed, favoring eccentric jets[12].

1. Bending: it is characterized as a fold or arching of the posterior leaflet, forming an angle between the posterior

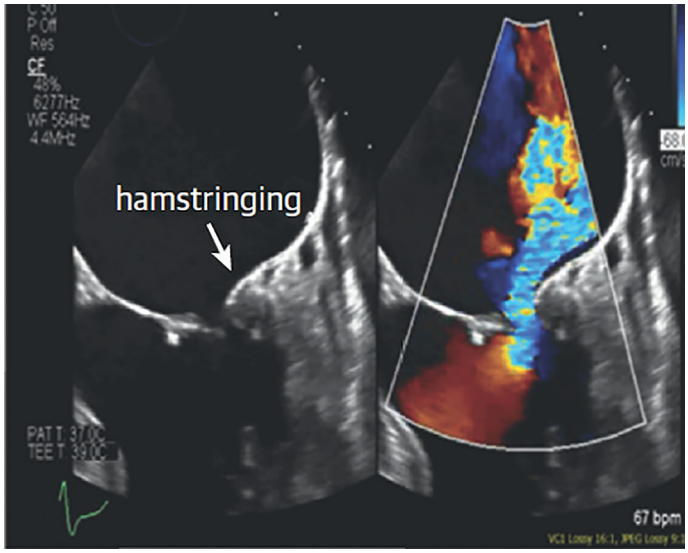

Figure 4 – *Hamstringing. Kindly reproduced with permission from Serge Harb. Image taken from Mesi et al.[12]*

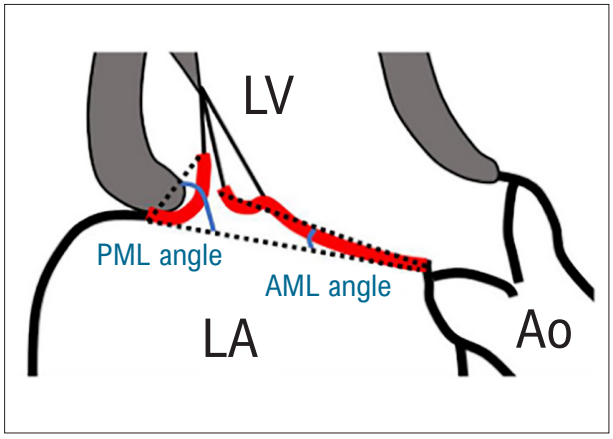

Figure 5 – *Bending. Kindly reproduced with permission from Makoto Miyake. Image taken from Okamoto et al.[22]*

and the anterior leaflet. In a retrospective study, Okamoto et al.[22] examined 118 patients with AFMR and EF > 50%, and compared 24 patients with bending and 94 patients without bending. For that, they defined bending as a relation between the angle of the posterior leaflet and the angle of the anterior leaflet as higher than or equal to 3.1. Survival rate after 36 months of follow-up was significantly lower in the group with bending of the posterior leaflet (63 x 78%, p= 0.047).

2. Anterior leaflet pseudoprolapse: the free border of the anterior leaflet does not meet the border of the posterior leaflet, which is pulled, leading to flawed coaptation and the false impression of a prolapse[21]**.**

The Table 1[1,23] provides data that allow the comparison of aspects for the differential diagnosis between AFMR and VFMR.

Conclusion

This review aimed to approach several current aspects of AFMR. However, new studies are required to bring more information, adjusting the diagnostic criteria of this entity.

Acknowledgments

To the colleagues in the Echocardiography Department of Rio Grande do Sul, who encouraged me to study the theme and speak at our annual event, especially Dr. Michel Cadore. To Dr. Daniela Rassi and DIC, I am grateful for the opportunity.

Author Contributions

Conception and design of the research, acquisition of data, analysis and interpretation of the data, writing of the manuscript, critical revision of the manuscript for intellectual content: Pretto AS.

Potential Conflict of Interest

No potential conflict of interest relevant to this article was reported.

Sources of Funding

There were no external funding sources for this study.

Study Association

This study is not associated with any thesis or dissertation work.

Ethics Approval and Consent to Participate

This article does not contain any studies with human participants or animals performed by any of the authors.

Table 1 - Differential diagnosis between AMIF and CMIF.

PARAMETERS	AFMR	VFMR
LV size and geometry	= Normal by definition (Volume < 78 ml/m2 for women and < 85 ml/m2 for men) with preservation of usual morphology. = Absence of papillary displacement. = Preserved geometry. = In late stages of major AFMR, the LV can dilate and the papillary can be displaced due to volume overload.	= Often dilated (but not necessarily). = Asymmetrical displacement of the papillary muscle (common Acute inferior / dorsal Myocardial Infarction) or symmetrical displacement in Dilated Cardiomyopathy. = Sphericity index (SI) often increased
Wall thickness	= At early stages, usually normal. May present concentric hypertrophy due to associated comorbidities. = Eccentric hypertrophy only at advanced stages.	= Normal thickness, fibrotic of eccentric hypertrophy.
EF	= Preserved regional and global function (EF > 50%) = slightly reduced EF at advanced stages.	= EF usually < 50% with global systolic dysfunction, or up to > 50% with segmental abnormalities = May present intraventricular dyssynchrony
Global Longitudinal Strain	= Usually preserved (> 18%) or borderline (between 16-18%). = Depending on the stage, might be slightly reduced.	= Typically reduced (< 16%).
LA size	= Dilated by definition. Usually, moderated (42-28 ml/m2) or marked (> 48 ml/m2) growth is found in volume	= Often dilated.
Annular size	= Dilated by definition. Systolic Antero-posterior diameter > 35 mm in PLAX or > 36 mm in 4 chambers or indexed annular area > 7 cm2/m2 in 3D in mesosystole; = Relation periphery artery disease /diastolic length of anterior leaflet > 1.3. = Annular flattening.	= Often dilated in response to LA dilatation.
Leaflet morphology	= Normal macroscopic appearance. = Most presents mild thickening.	= Normal macroscopic appearance. = Different levels of thickening.
Leaflet mobility	Usually normal (Carpentier I), but can be classified as III b when Hamstringing is identified.	Restricted (Carpentier III b).
Point of leaflet coaptation	At the annulus level or slightly apically displaced	Apically displaced (subvalvular tethering).
Tenting height	Reduced. Usually between 3.5 +- 1.5 mm	Augmented. Usually between 8.1+- 2.4 mm.
Jet direction	Usually central, but can be eccentric in case of Hamstringing, or with shorter length of the posterior leaflet .	It is usually central in cases of symmetrical displacement of papillary muscles and eccentric in cases of asymmetrical displacement.
Associated RA dilation	More common	Less common
Moderate / severe RV systolic dysfunction	Less common, but if present, prognosis is worse.	More common
Prognosis	Better prognosis in relation to VFMR[24]. However, its prognosis is worse in comparison to PMI.	It is the worst prognosis. VFMR > AFMR > PMI

EF: ejection fraction; AFMR: atrial functional mitral regurgitation; VFMR: ventricular functional mitral regurgitation; LV: left ventricle.

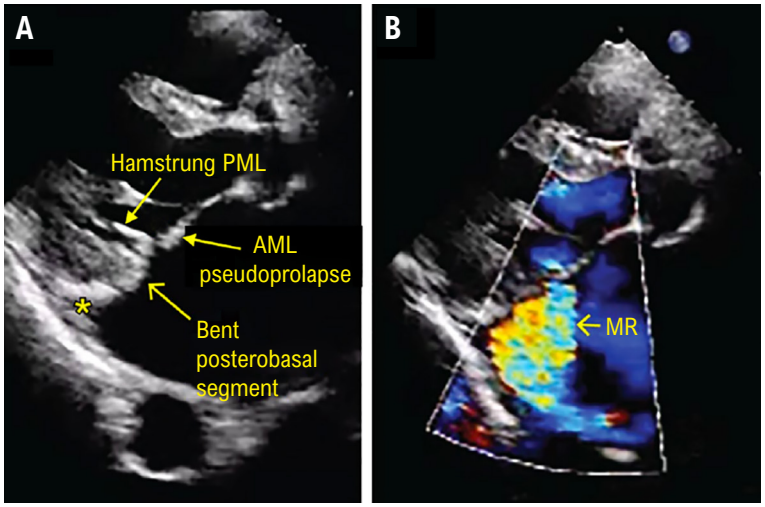

Figura 6 – *Anterior leaflet prolapse and eccentric jet (posteriorly driven). Reproduced with permission from Silbiger.*[19]

Reference

1. Deferm S, Bertrand PB, Verbrugge FH, Verhaert D, Rega F, Thomas JD, et al. Atrial Functional Mitral Regurgitation: JACC Review Topic of the Week. J Am Coll Cardiol. 2019;73(19):2465-76. doi: 10.1016/j.jacc.2019.02.061.
2. Abe Y, Takahashi Y, Shibata T. Functional Mitral Regurgitation, Updated: Ventricular or Atrial?. J Echocardiogr. 2020;18(1):1-8. doi: 10.1007/s12574-019-00453-w.
3. Benjamin EJ, Blaha MJ, Chiuve SE, Cushman M, Das SR, Deo R, et al. Heart Disease and Stroke Statistics-2017 Update: a Report from the American Heart Association. Circulation. 2017;135(10):e146-603. doi: 10.1161/CIR.0000000000000485.
4. Kodali SK, Velagapudi P, Hahn RT, Abbott D, Leon MB. Valvular Heart Disease in Patients ≥80 Years of Age. J Am Coll Cardiol. 2018;71(18):2058-72. doi: 10.1016/j.jacc.2018.03.459.
5. Chugh SS, Havmoeller R, Narayanan K, Singh D, Rienstra M, Benjamin EJ, et al. Worldwide Epidemiology of Atrial Fibrillation: a Global Burden of Disease 2010 Study. Circulation. 2014;129(8):837-47. doi: 10.1161/CIRCULATIONAHA.113.005119.
6. Dunlay SM, Roger VL, Redfield MM. Epidemiology of Heart Failure with Preserved Ejection Fraction. Nat Rev Cardiol. 2017;14(10):591-602. doi: 10.1038/nrcardio.2017.65.
7. Zakeri R, Chamberlain AM, Roger VL, Redfield MM. Temporal Relationship and Prognostic Significance of Atrial Fibrillation in Heart Failure Patients with Preserved Ejection Fraction: a Community-Based Study. Circulation. 2013;128(10):1085-93. doi: 10.1161/CIRCULATIONAHA.113.001475.
8. Delgado V, Bax JJ. Atrial Functional Mitral Regurgitation: from Mitral Annulus Dilatation to Insufficient Leaflet Remodeling. Circ Cardiovasc Imaging. 2017;10(3):e006239. doi: 10.1161/CIRCIMAGING.117.006239.
9. Gertz ZM, Raina A, Mountantonakis SE, Zado ES, Callans DJ, Marchlinski FE, et al. The Impact of Mitral Regurgitation on Patients Undergoing Catheter Ablation of Atrial Fibrillation. Europace. 2011;13(8):1127-32. doi: 10.1093/europace/eur098.
10. Kagiyama N, Mondillo S, Yoshida K, Mandoli GE, Cameli M. Subtypes of Atrial Functional Mitral Regurgitation: Imaging Insights Into Their Mechanisms and Therapeutic Implications. JACC Cardiovasc Imaging. 2020;13(3):820-35. doi: 10.1016/j.jcmg.2019.01.040.
11. Moonen A, Ng MKC, Playford D, Strange G, Scalia GM, Celermajer DS. Atrial Functional Mitral Regurgitation: Prevalence, Characteristics and Outcomes from the National Echo Database of Australia. Open Heart. 2023;10(1):e002180. doi: 10.1136/openhrt-2022-002180.
12. Mesi O, Gad MM, Crane AD, Ramchand J, Puri R, Layoun H, et al. Severe Atrial Functional Mitral Regurgitation: Clinical and Echocardiographic Characteristics, Management and Outcomes. JACC Cardiovasc Imaging. 2021;14(4):797-808. doi: 10.1016/j.jcmg.2021.02.008.
13. Dziadzko V, Dziadzko M, Medina-Inojosa JR, Benfari G, Michelena HI, Crestanello JA, et al. Causes and Mechanisms of Isolated Mitral Regurgitation in the Community: Clinical Context and Outcome. Eur Heart J. 2019;40(27):2194-202. doi: 10.1093/eurheartj/ehz314.
14. Silbiger JJ. Does Left Atrial Enlargement Contribute to Mitral Leaflet Tethering in Patients with Functional Mitral Regurgitation? Proposed Role of Atriogenic Leaflet Tethering. Echocardiography. 2014;31(10):1310-1. doi: 10.1111/echo.12629.
15. Gertz ZM, Raina A, Saghy L, Zado ES, Callans DJ, Marchlinski FE, et al. Evidence of Atrial Functional Mitral Regurgitation Due to Atrial Fibrillation: Reversal with Arrhythmia Control. J Am Coll Cardiol. 2011;58(14):1474-81. doi: 10.1016/j.jacc.2011.06.032.
16. van Rosendael PJ, Katsanos S, Kamperidis V, Roos CJ, Scholte AJ, Schalij MJ, et al. New Insights on Carpentier I Mitral Regurgitation from Multidetector Row Computed Tomography. Am J Cardiol. 2014;114(5):763-8. doi: 10.1016/j.amjcard.2014.06.005.
17. Kagiyama N, Hayashida A, Toki M, Fukuda S, Ohara M, Hirohata A, et al. Insufficient Leaflet Remodeling in Patients with Atrial Fibrillation: Association with the Severity of Mitral Regurgitation. Circ Cardiovasc Imaging. 2017;10(3):e005451. doi: 10.1161/CIRCIMAGING.116.005451.
18. Kim DH, Heo R, Handschumacher MD, Lee S, Choi YS, Kim KR,et al. Mitral Valve Adaptation to Isolated Annular Dilation: Insights Into the Mechanism of Atrial Functional Mitral Regurgitation. JACC Cardiovasc Imaging. 2019;12(4):665-77. doi: 10.1016/j.jcmg.2017.09.013.
19. Silbiger JJ. Mechanistic Insights Into Atrial Functional Mitral Regurgitation: Far More Complicated than Just Left Atrial Remodeling. Echocardiography. 2019;36(1):164-9. doi: 10.1111/echo.14249.

20. Silbiger JJ, Bazaz R. The Anatomic Substrate of Mitral Annular Contraction. Int J Cardiol. 2020;306:158-61. doi: 10.1016/j.ijcard.2019.11.129.

21. Farhan S, Silbiger JJ, Halperin JL, Zhang L, Dukkipati SR, Vogel B, et al. Pathophysiology, Echocardiographic Diagnosis, and Treatment of Atrial Functional Mitral Regurgitation: JACC State-of-the-Art Review. J Am Coll Cardiol. 2022;80(24):2314-30. doi: 10.1016/j.jacc.2022.09.046.

22. Okamoto H, Miyake M, Hayashi A, Matsutani H, Tamura T, Nakagawa Y. Differences in Clinical and Echocardiographic Features and Outcomes Between Atrial Functional Mitral Regurgitation Patients with and without Posterior Mitral Leaflet Bending. J Cardiol. 2023;82(1):22-8. doi: 10.1016/j.jjcc.2023.02.001.

23. Zoghbi WA, Levine RA, Flachskampf F, Grayburn P, Gillam L, Leipsic J, et al. Atrial Functional Mitral Regurgitation: a JACC: Cardiovascular Imaging Expert Panel Viewpoint. JACC Cardiovasc Imaging. 2022;15(11):1870-82. doi: 10.1016/j.jcmg.2022.08.016.

24. Okamoto C, Okada A, Nishimura K, Moriuchi K, Amano M, Takahama H, et al. Prognostic Comparison of Atrial and Ventricular Functional Mitral Regurgitation. Open Heart. 2021;8(1):e001574. doi: 10.1136/openhrt-2021-001574.

Review Article

Cardiac Sarcoidosis: The Chameleon of Cardiology

Diego Moraes De Moura,[1] *Aluísio José De Oliveira Monteiro Neto,*[2] *Marcelo Dantas Tavares de Melo,*[2] *Fábio Fernandes*[1]

Universidade de São Paulo, Instituto do Coração,[1] *São Paulo, SP – Brasil*
Universidade Federal da Paraíba,[2] *João Pessoa, PB – Brasil*

Abstract

Sarcoidosis is a multisystemic granulomatous disease of unknown etiology, characterized by the formation of non-caseating granulomas in multiple organs. Cardiac involvement, an important cause of morbidity and mortality in these patients, has been generating interest in cardiology, because it is a cause of heart failure, atrioventricular blocks, and ventricular arrhythmias with unfavorable prognosis; however, there are specific treatments with the potential to change the natural history of this condition. The main challenge of cardiac sarcoidosis (CS) is diagnosis, given that the gold standard method of endomyocardial biopsy has limited sensitivity due to the focal nature of the pathology.

Accordingly, cardiovascular imaging methods play the role of guiding most diagnoses of CS. In this scenario, knowledge about these methods, their main findings, and their rational use are essential to the diagnosis of this disease with such diverse presentations.

Electrocardiogram and echocardiography are practical and widely available exams; however, they provide greater diagnostic capacity in patients with clinically manifest disease. On the other hand, to identify incipient forms, which are often silent, it is necessary to use advanced imaging methods, such as positron emission tomography with 18F-fluorodeoxyglucose and cardiac magnetic resonance, which primarily identify signs of active inflammatory activity and fibrosis, respectively. Despite the advances in these imaging methods, due to the lack of studies comparing them with the gold standard (endomyocardial biopsy), the diagnosis of CS currently remains a major challenge.

Introduction

Sarcoidosis is a multisystemic granulomatous disease of unknown etiology, characterized by the accumulation of T lymphocytes and mononuclear phagocytes with the formation of non-caseating granulomas in various organs. Its genesis is believed to be the consequence of an immune-mediated response from antigenic triggers, which are not yet well understood, in people who are genetically predisposed.[1]

Its prevalence varies worldwide, with particularities related to regions, ethnic groups, and sex, and descriptions range from 10 to 60 cases per 100,000 individuals.[2]

Systemic sarcoidosis generally manifests with lung and intrathoracic lymph node involvement, in more than 90% of cases; however, the disease can affect virtually any organ, such as the skin, eyes, heart, nervous system, musculoskeletal system, renal system, and endocrine system.[1]

The importance of myocardial involvement in cardiac sarcoidosis (CS) is mainly due to its prognostic implications, associated with the fact that there are targeted treatments that are potentially capable of preventing severe complications.

CS is a known cause of ventricular dysfunction, conduction disturbances, and ventricular arrhythmias, which eventually present in the form of sudden death.[3]

In several samples, CS appears as one of the main causes of death in individuals with sarcoidosis, accounting for approximately 50% of deaths in a North American sample and up to 85% in an Asian population.[3,4]

Despite the severity, the identification of these patients still poses a challenge, since the majority of them have subclinical cardiac involvement. Thus, the prevalence of myocardial involvement described in the literature varies from 5% (considering patients with clinically evident cardiac involvement) to approximately 54%, when advanced imaging methods are used, identifying asymptomatic patients, who are known as subclinical.[5]

The gold standard for diagnosis is the presentation of a suggestive clinical picture associated with histological evaluation of myocardial tissue showing evidence of a non-caseating granulomatous process, after excluding other potential causes of granuloma formation (especially infectious and neoplastic causes). However, due to the focal nature of the disease (involvement beginning with the formation of granulomas), endomyocardial biopsy has low sensitivity, revealing the presence of non-caseating granulomas in less than 25% of patients who undergo the procedure.[6]

Therefore, the main guidelines have established an alternative route that is not dependent on myocardial histopathology to diagnose CS. In the case of patients with a histopathological diagnosis of extracardiac sarcoidosis, with myocardial structural changes compatible with the disease that cannot be explained by other etiologies, myocardial involvement due to sarcoidosis is inferred.[7,8]

Keywords

Sarcoidosis; Electrocardiography; Echocardiography; Positron Emission Tomography Computed Tomography; X-Ray Computed Tomography.

Mailing Address: Diego Moraes De Moura •
Universidade de São Paulo, Instituto do Coração, Unidade de miocardiopatias e doenças da aorta; Av. Dr. Enéas Carvalho de Aguiar, 44. Postal code: 05403-900. Cerqueira César, São Paulo, SP – Brazil
E-mail: moraesdemouradiego@gmail.com
Manuscript received February 14, 2024; revised February 22, 2024; accepted February 23, 2024
Editor responsible for the review: Marcelo Dantas Tavares de Melo

DOI: https://doi.org/10.36660/abcimg.20240007i

Central Illustration: Cardiac Sarcoidosis: The Chameleon of Cardiology

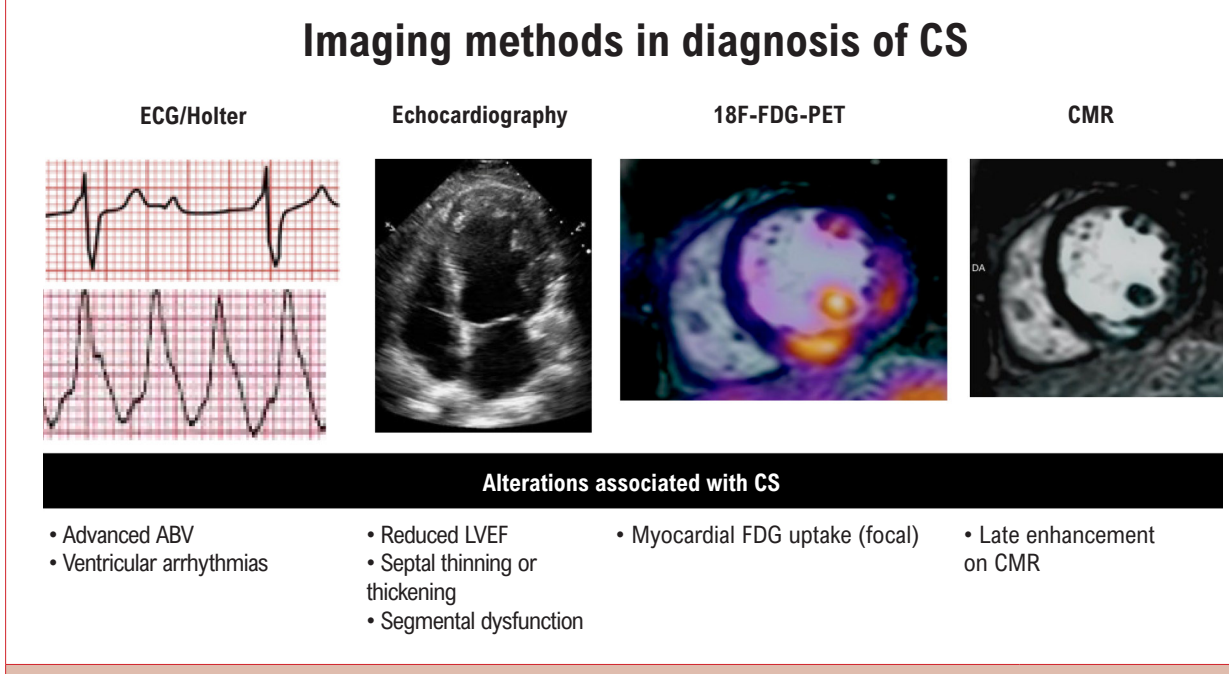

Arq Bras Cardiol: Imagem cardiovasc. 2024;37(1):e20240007

18F-FDG-PET: positron emission tomography with 18F-fluorodeoxyglucose; ABV: atrioventricular block; CMR: cardiac magnetic resonance imaging; ECG: electrocardiography; LVEF: left ventricular ejection fraction; CS: cardiac sarcoidosis.

Accordingly, the diagnosis of CS, except for cases in which endomyocardial biopsy presents compatible histopathology, depends on the presence of specific cardiac changes observed in complementary exams such as electrocardiogram (ECG), echocardiogram, cardiac magnetic resonance (CMR), and nuclear medicine exams, with emphasis on positron emission tomography (PET) with ^{18}F-fluorodeoxyglucose (18FDG) combined with computed tomography (CT) (Central Illustration).

The objective of this article is to conduct a review about the non-invasive analysis of cardiac involvement due to sarcoidosis, emphasizing the importance of advanced imaging methods in the clinical evaluation of this highly challenging disease.

Diagnostic criteria for CS

The first international guideline on the diagnosis of CS was published in 2014, by experts appointed by the Heart Rhythm Society (HRS), with representatives from several other societies.[8] Previously, the diagnostic criteria of the Japanese Ministry of Health and Welfare (JMHW) had been published in 2006.[9] They did not include FDG-PET, and they attributed less importance to late gadolinium enhancement (LGE) on CMR, consequently offering less ability to identify these patients. Subsequently, the Japanese Circulation Society (JCS)[7] published a new guideline, with recommendations very close to those put forth by the HRS (highlighting the importance of FDG-PET and CMR), while admitting the possibility of diagnosing CS without histopathological documentation of sarcoidosis (Table 1).

Currently, the most used diagnostic criteria are those developed by the HRS and JCS. Although both include the same complementary exams in their approaches, such as ECG/Holter, echocardiogram, FDG-PET, and CMR, there appears to be low concordance between these criteria.[10] Faced with this diagnostic difficulty, some centers have created multidisciplinary teams to evaluate suspected cases, using the aforementioned criteria as a guide, without being limited to them.[11] This type of approach requires experience on the part of the team and a high degree of familiarity with the main alterations in cardiovascular imaging methods associated with CS.

Cardiovascular imaging in the assessment of CS

Among the complementary exams used in the assessment of patients with suspected CS, CMR and FDG-PET/CT stand out, due to the possibility of identifying changes still in the initial phase of the disease, with minimal or absent cardiovascular manifestations,[8] which is known as the silent form of CS. ECG and echocardiography, although they are less accurate, can also suggest diagnosis of CS in a probable clinical context, with the advantage of being widely available.[7,8]

Role of electrocardiography

ECG can assist in the diagnosis of CS, both as a screening tool for cardiac involvement, in patients with a previous diagnosis of non-CS, and by raising the suspicion of sarcoidosis as the etiology of specific cardiac alterations.[8]

Table 1 – Diagnostic guidelines for CS

HRS 2014 Expert Consensus	JCS 2016 Guidelines
1. Histological diagnosis of myocardial tissue	1. Histological diagnosis group
CS is diagnosed in the presence of non-caseating granuloma on histological examination of myocardial tissue with no alternative cause identified (including negative organismal stains, if applicable)	CS is diagnosed histologically when endomyocardial biopsy or surgical specimens demonstrate non-caseating epithelioid granulomas, and granulomas due to other causes and local sarcoid reactions can be ruled out
2. Clinical diagnosis based on invasive and non-invasive exams	2. Clinical diagnosis group (negative myocardial biopsy findings or patients not undergoing myocardial biopsy)
a) There is diagnosis of extracardiac sarcoidosis b) One or more of the following are present: • Steroid +/ immunosuppressant responsive cardiomyopathy or heart block • Unexplained decrease in LVEF (40%) • Unexplained sustained VT (spontaneous or induced) • Mobitz type II second-degree heart block or third-degree heart block • Irregular uptake on dedicated cardiac PET (in a pattern consistent with CS) • Late gadolinium enhancement on CMR (in a pattern consistent with CS) • Positive gallium uptake (in a pattern consistent with CS)	1. When epithelioid granulomas are found in organs other than the heart, and clinical findings strongly suggestive of cardiac involvement are present 2. When the patient presents clinical findings strongly suggestive of pulmonary or ophthalmic sarcoidosis, and at least 2 of the following 5 laboratory findings characteristic of sarcoidosis: • Bilateral hilar lymphadenopathy • Elevated serum angiotensin-converting enzyme activity or elevated serum lysozyme levels • Elevated serum soluble interleukin-2 receptor levels • Significant tracer accumulation in gallium-67 citrate scintigraphy or 18F-FDG-PET • A high percentage of lymphocytes with a CD4/CD8 ratio of > 3.5 in BAL fluid

18F-FDG-PET: positron emission tomography with 18F-fluorodeoxyglucose; CMR: cardiac magnetic resonance imaging; CS: cardiac sarcoidosis; HRS: Heart Rhythm Society; JCS: Japanese Circulation Society; LVEF: left ventricular ejection fraction; PET: positron emission tomography; TV: ventricular tachycardia. Adapted from Shrivastav et al.[9]

Several electrocardiographic changes have already been described in patients with CS. Nonspecific changes, when present in individuals with prior diagnosis of sarcoidosis, should raise the suspicion of myocardial involvement. These changes may vary from ventricular or atrial arrhythmias, varying degrees of atrioventricular block (AVB), bundle branch blocks, hemiblocks, QRS fragmentation, and T wave changes, such as inversion, alternation, and increased amplitude.[12]

Another role of ECG in this pathology is due to the fact that CS is an important cause of advanced AVB and sustained ventricular tachycardia, initially seen as idiopathic in middle-aged adults. In some samples, CS was responsible for up to 30% of idiopathic cases of AVB and sustained ventricular tachycardia in this age group (< 60 years).[13,14] It is worth highlighting that the identification of CS as the cause of AVB has prognostic importance, since immunosuppressive treatment has the potential to reverse the block.[15]

Another change already described in individuals with CS is the epsilon wave. This change is classically observed in individuals with arrhythmogenic right ventricular cardiomyopathy. There are case reports of patients who met the criteria for arrhythmogenic right ventricular cardiomyopathy according to the task force criteria, but who were subsequently diagnosed with CS after endomyocardial biopsy.[16,17] Signs such as advanced AVB, important left ventricular dysfunction, septal LGE, absence of family history, and mediastinal lymphadenopathy should raise the suspicion of CS.[18]

In general, patients with CS and cardiovascular symptoms present some degree of electrocardiographic alteration. Nonetheless, a normal ECG does not rule out myocardial involvement, but it reduces the likelihood, especially in patients without cardiovascular symptoms.[19]

Role of echocardiography

Echocardiography, as it is practical and easily accessible, is generally the first imaging test to be requested when screening for CS. It is usually altered in symptomatic patients, but frequently normal in patients with the silent form.[20]

Its findings vary, including increased ventricular wall thickness (resulting from focal areas of edema or granulomatous infiltration) or, in more advanced phases of the disease, thinning (most commonly septal, in the basal portion), akinesia, dyskinesia, or even aneurysms.[21] The most commonly affected regions are the left ventricular free wall and the interventricular septum. The ejection fraction may be reduced or preserved, with varying degrees of diastolic dysfunction. However, unlike reduced ejection fraction, changes in diastolic function have not yet been included in the diagnostic criteria for CS.[21]

Echocardiography has limited sensitivity when compared to advanced imaging exams such as CMR and F-FDG-PET. In a study including 321 patients with a histopathological diagnosis of sarcoidosis, echocardiography showed a sensitivity of less than 30%.[22] Therefore, in patients with extracardiac sarcoidosis and cardiovascular symptoms, even with a normal echocardiogram, clinical investigation with advanced imaging methods is recommended.[8]

More recently, the use of techniques such as speckle tracking appears to have improved the sensitivity of echocardiography in identifying myocardial injury due to sarcoidosis, with some studies showing reduced global longitudinal strain in patients with sarcoidosis, normal ejection fraction, and evidence of myocardial injury on FDG-PET/CT and CMR.[23] In the evaluation of 23 patients with CS (compared to controls), the global longitudinal strain was −15.9% ± 2.5% versus −18.2%

± 2.7%. Worsening of this parameter was also associated with the development of heart failure and hospital admission.

Furthermore, echocardiography is also a valuable tool for assessing cardiovascular alterations secondary to severe lung disease caused by sarcoidosis, such as pulmonary artery pressure and changes in the right ventricle. These cardiological alterations should not be confused with cardiac involvement caused by the granulomatous infiltration of sarcoidosis.[24]

Papel do 18F-FDG-PET/CT

18F-FDG is a glucose analogue labeled with radioactive fluorine, which remains inside the cell, contributing to the generation of the PET image. It is frequently used in association with CT for attenuation correction and anatomical correlation.

The rationale behind this method lies in the fact that the inflammatory cells involved in sarcoidosis granuloma have avidity for uptake of glucose and glucose analogues, thus making it possible to identify regions with active inflammation.[25]

The usual pattern of the image generated by FDG in CS is focal and irregular, which can appear as areas of hyper-uptake in a myocardium with physiological uptake completely suppressed or merely reduced; in the latter case, it generates a pattern of focal hyper-uptake in a myocardium with diffuse uptake (focal on diffuse) (Figure 1).

Generally, cardiac PET is associated with whole-body PET, assisting in the identification of areas suggestive of extracardiac involvement.[26]

One of the challenges of this method is that the myocyte is also usually avid for glucose (and consequently FDG) uptake. Therefore, for the exam to be interpretable, preparation must be carried out in order to suppress this physiological uptake of the radiotracer by the myocardium. Protocols may vary between services, but, in general, a high-fat diet restricted in carbohydrates is recommended during the 24 hours preceding the exam, associated with 12 hours of fasting.[27] However, in spite of this, in up to approximately 25% of cases, adequate suppression of myocardial FDG uptake does not occur, making it impossible to interpret the exam.[28] In some centers, it is also common to administer unfractionated heparin with the aim of increasing the circulation of free fatty acids, which could potentially contribute to suppressing myocyte avidity for glucose.[27]

It is important to remember that myocardial FDG uptake is not synonymous with CS. Other conditions can also generate myocardial uptake of FDG, such as physiological uptake itself (which will normally appear as diffuse uptake), different etiologies of myocarditis, cardiac involvement due to rheumatological diseases, hibernating myocardium, and even some genetic cardiomyopathies.[29] Therefore, the exam needs to be interpreted within the clinical context, seeking to rule out differential diagnoses, especially ischemic disease. The presence of extracardiac uptake appears to significantly increase the specificity of CS.[29]

Given that F-FDG-PET assesses active inflammation, a normal exam does not rule out the presence of CS; it only indicates that there is no inflammatory process active in the myocardium at that time.[27] The intensity of uptake is quantified using the standardized uptake value (SUV), whose calculation considers the concentration of radioactivity in the region of interest, the dose injected, and the patient's weight.

The sensitivity and specificity described in the literature are approximately a little over 80%. Kim et al., in a meta-analysis with 891 patients from 17 studies, observed a sensitivity of 84% and specificity of 83%.[30] An important limitation of these data is that they did not use histopathology as a reference method, but rather the JMHW criteria, published in 2006.

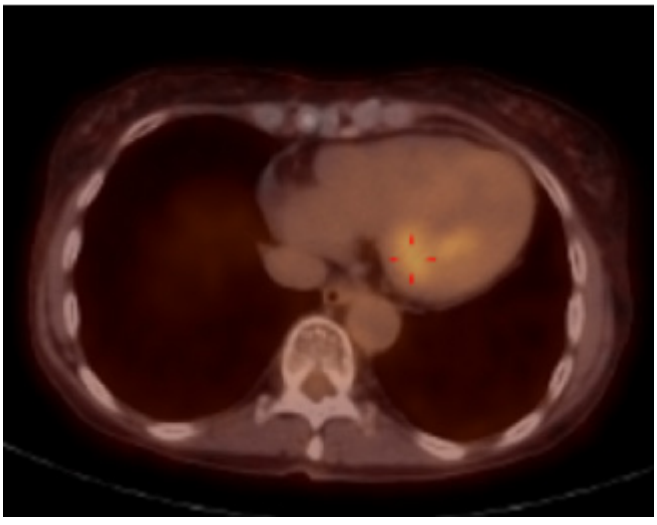

Figure 1 – *Cardiac 18F-FDG-PET/CT with heterogeneous distribution of FDG in the left ventricular walls, showing focal areas with greater uptake in the inferior wall (middle and basal segment) in a 46-year-old female patient, with endomyocardial biopsy suggestive of CS. Author's data. 18F-FDG-PET/CT: positron emission tomography with 18F-fluorodeoxyglucose combined with computed tomography.*

In addition to the great usefulness of F-FDG-PET in the diagnostic evaluation of CS, the test also has therapeutic and prognostic implications.

The main guidelines on this topic (HRS and JCS) recommend immunosuppression in patients with clinical manifestations attributed to CS when there are signs of inflammation detected by PET-FDG.[7,8] Reduced FDG uptake after immunosuppression seems to be a predictor of improved ejection fraction; thus, this method has also been used as a parameter to evaluate therapeutic response.[31,32]

The persistence of FDG uptake in serial exams is strongly associated with worse prognosis, increasing the risk of major cardiovascular events by up to 20-fold in patients who do not respond to immunosuppression.[33]

Another important predictor of worse prognosis is FDG uptake in the right ventricle, associated with increased mortality, ventricular arrhythmias, and a decline in left ventricular ejection fraction.[34,35]

Perfusion study, when associated with PET-FDG, also adds prognostic information; thus, patients with myocardial FDG uptake associated with perfusion alterations in these regions (which would be a mismatch) appear to have worse prognosis than those with myocardial inflammation but normal perfusion.[36] Perfusion studies can be performed by means of PET/CT using radiotracers such as ammonia labeled with nitrogen-13 and rubidium-82, which are rarely used due to their high cost, or with perfusion scintigraphy.[37]

For the future, we expect the use of radiotracers that are not usually captured by the normal myocardium, consequently making dietary preparations unnecessary, for example somatostatin analogues.[27]

Role of cardiac magnetic resonance imaging

CMR is an indispensable exam in the assessment of patients with suspected CS. In addition to assessing morphological and functional details of the right and left ventricles with high accuracy, it also makes it possible to identify signs of inflammation, mainly necrosis and fibrosis.[38]

CMR has the advantage of not using radiation and of using gadolinium, which is a contrast material with a low risk of adverse events.

One of the main resources of CMR is LGE analysis, detecting the expansion of the extracellular matrix, which suggests, especially in the more advanced phase of the disease, the presence of fibrosis (Figure 2).

Although there are no pathognomonic findings, the LGE patterns most commonly observed in CS are focal, mesocardial or subepicardial in basal regions of the septum and lateral wall.[11] These patterns are not specific and can be found in several other conditions of myocardial injury, especially inflammatory ones. However, even transmural patterns can occur.[39]

An LGE pattern was recently described that initially appeared to be specific to CS, namely, the hug sign. This is characterized by LGE that extends from the interventricular septum towards the right ventricle, observed in cases of isolated CS with histopathological diagnosis.[40] Nonetheless, this pattern has already been observed in giant cell myocarditis.[41]

CMR can also suggest the presence of myocardial inflammation through the presence of T2 hypersignal, which indicates excess fluid in the myocardium. However, the absence of this alteration does not rule out the presence of inflammation when compared to PET.[42] In CMR, it is also possible to estimate diffuse interstitial fibrosis through T1 and T2 maps, suggesting subclinical sarcoidosis, although the clinical usefulness of this parameter is still uncertain.[43]

The real accuracy, sensitivity, and specificity of imaging tests in CS are still quite debatable, because, in most studies, these methods were not compared with the gold standard of endomyocardial biopsy, but rather with diagnostic criteria, generally those proposed by the HRS[8] and the JMHW.[9] These studies describe sensitivities ranging from 75% to 100% and specificities ranging from 77% to 85%.[44]

Thus, in individuals with extracardiac sarcoidosis, the presence of LGE is indicative of probable CS; however, a negative test cannot rule out the presence of heart disease, for instance, still in the initial phase.

To date, no large prospective study has been designed with the objective of comparing the accuracy of CMR and PET in diagnosing CS. Some services, when there is a strong suspicion of CS, suggest that CMR investigation should be started before PET, for some reasons; for example, it does not depend on preparation, and it provides good structural and tissue characterization of the heart. However, the current impression is that these are exams that offer complementary information; PET shows signs of inflammatory activity, and CMR shows fibrosis[45] (Table 2).

In addition to its diagnostic usefulness, several studies have observed an important prognostic role. A meta-analysis with 694 patients observed higher cardiovascular mortality, all-cause mortality, and ventricular arrhythmias in patients with CS and LGE.[46] Specific LGE patterns, such as involvement of the right ventricle and multifocal pattern, also seem to be associated with worse prognosis.[47]

Regarding the limitations of this exam, we highlight the at least relative contraindication in patients with glomerular filtration rate < 30 mL/min/1.73 m^2 and the difficulties in image interpretation (due to the presence of artifacts) in patients with cardiac devices, such as pacemakers and implantable cardioverter defibrillators, even though they are compatible with magnetic resonance devices.[48]

Integrating imaging exams in the assessment of patients with suspected CS

When discussing the ideal diagnostic approach for individuals with suspected CS, it is essential to distinguish at least two main scenarios: patients who already have a previous diagnosis of extracardiac sarcoidosis and those who do not.[44]

In the former case, any cardiovascular symptom or alteration on ECG/echocardiography increases the probability that the myocardium is also affected by sarcoidosis, indicating further investigation with CMR, generally followed by FDG-PET, and, in exceptional cases, endomyocardial biopsy[8] (Figure 3).

The main diagnostic challenge is the second scenario, regarding patients with cardiovascular alterations such as heart

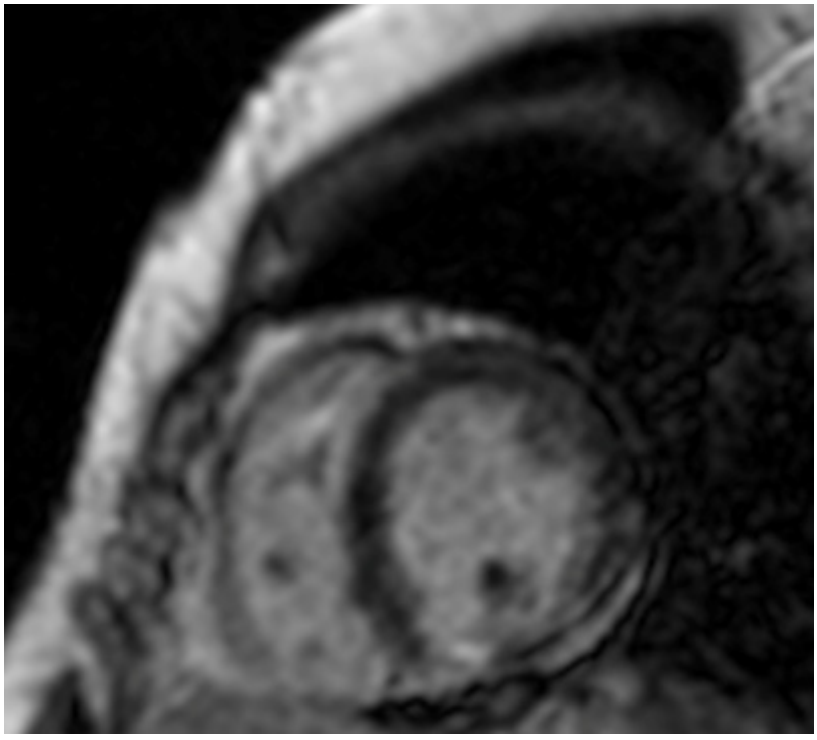

Figure 2 – *CMR showing the presence of mesocardial late enhancement in the inferior wall of a 38-year-old male patient diagnosed with CS. Author's data. CMR: cardiac magnetic resonance imaging.*

Table 2 – Diagnostic interpretation of combined data from CMR with 18F-FDG-PET

Interpretation	CMR findings	18F-FDG-PET findings
Active disease with the presence of scarring and inflammation	Presence of LGE	18F-FDG uptake observed
Scarring without active inflammation (inactive)	Presence of LGE	No 18F-FDG uptake observed
Normal (no disease)	Presence of LGE	Lack of 18F-FDG uptake
Early disease/false positive	Presence of LGE	18F-FDG uptake observed

18F-FDG-PET: positron emission tomography with 18F-fluorodeoxyglucose; CMR: cardiac magnetic resonance imaging; LGE: late gadolinium enhancement. Adapted from Shrivastav et al.[9]

failure, advanced AVB, or ventricular arrhythmias, without previous diagnosis of any systemic condition, in which the range of etiologies is immense, and CS is just one among dozens of possibilities. In these cases, the suspicion of CS should be raised mainly in cases of advanced AVB or ventricular tachycardia of unexplained cause in patients under 60 years of age, or even in patients with heart failure not justified by the most prevalent etiologies, especially with the presence of thinning of the basal septum and thinning or thickening of the ventricular wall.[7,31] For these patients, the investigation must include both the characterization of the pattern of myocardial injury, with CMR and cardiac FDG-PET, searching for signs that may suggest CS, as well as whole-body FDG-PET, with the aim of identifying possible signs of extracardiac sarcoidosis. The search for signs of extracardiac sarcoidosis can be refined with ophthalmological, dermatological, and pulmonary evaluation. In selected cases, endomyocardial biopsy will also be recommended.[7]

Take-home messages

- CS is a complex disease to diagnose.
- Generally, diagnosis is made without confirmation of myocardial histology, based on alterations in imaging tests.
- Most alterations observed in these tests are nonspecific findings that need to be interpreted in the patient's clinical context.
- The lack of studies that compare the accuracy of these tests with the gold standard (histopathology) makes it

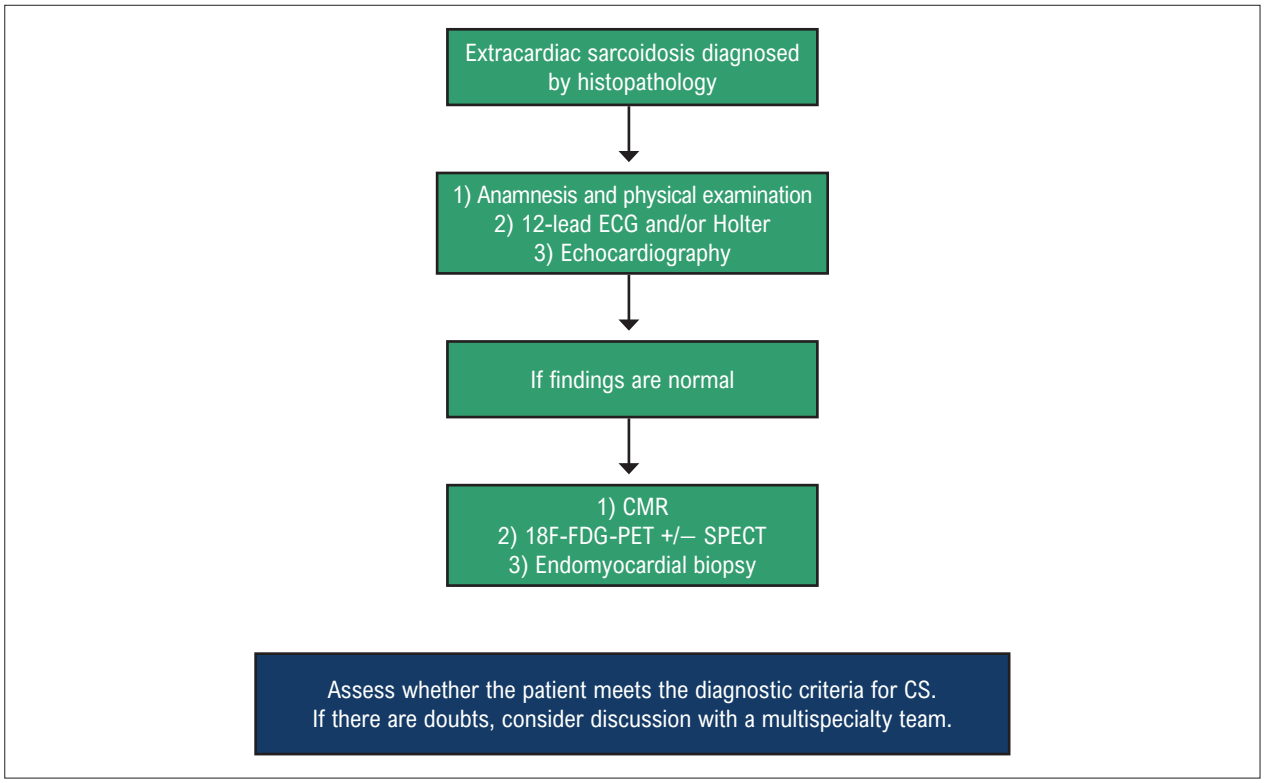

Figura 3 – *Diagnostic investigation flowchart for CS in patients diagnosed with extracardiac sarcoidosis. 18F-FDG-PET: positron emission tomography with 18F-fluorodeoxyglucose; CMR: cardiac magnetic resonance imaging; ECG: electrocardiography; SPECT: single-photon emission computerized tomography. Adapted from Montera et al.*[49]

difficult to understand the real diagnostic capacity of each method, reinforcing the importance of using multimodal imaging in the investigation of suspected cases.

- CMR and PET appear to be the imaging tests with the greatest accuracy, providing complementary information regarding the presence and extent of fibrosis and inflammation, respectively.
- CS should always be suspected in the presence of significant rhythm disturbances or heart failure of unexplained cause, especially in middle-aged patients.

Conclusion

CS is a disease whose etiology is still little understood. Its diagnosis is challenging, with most diagnoses made without confirmation of myocardial histology, based on alterations in imaging tests. Despite the low prevalence, its identification is of fundamental importance due to its unfavorable prognosis, in addition to the fact that there are treatments with the potential to modify the natural history of this disease. Fortunately, in recent years there has been a major advance in cardiovascular imaging methods, allowing greater understanding of diagnostic and prognostic aspects. Nonetheless, it is still necessary to conduct further studies that involve direct comparison between imaging tests and histopathological findings of myocardia affected by sarcoidosis, in order to usher in a new era of more accurate diagnoses.

Author Contributions

Conception and design of the research and critical revision of the manuscript for intellectual content: Moura DM, Melo MDT, Fernandes F;

Acquisition of data and writing of the manuscript: Moura DM, Monteiro Neto AJO, Melo MDT, Fernandes F; image editing: Monteiro Neto AJO; article lead: Fernandes F.

Potential Conflict of Interest

No potential conflict of interest relevant to this article was reported.

Sources of Funding

There were no external funding sources for this study.

Study Association

This article is part of the thesis of Doctoral submitted by Diego Moraes de Moura, from Universidade de São Paulo.

Ethics Approval and Consent to Participate

This article does not contain any studies with human participants or animals performed by any of the authors.

References

1. Iannuzzi MC, Fontana JR. Sarcoidosis: Clinical Presentation, Immunopathogenesis, and Therapeutics. JAMA. 2011;305(4):391-9. doi: 10.1001/jama.2011.10.
2. Milman N, Selroos O. Pulmonary Sarcoidosis in the Nordic Countries 1950-1982. Epidemiology and Clinical Picture. Sarcoidosis. 1990;7(1):50-7.
3. Doughan AR, Williams BR. Cardiac Sarcoidosis. Heart. 2006;92(2):282-8. doi: 10.1136/hrt.2005.080481.
4. Silverman KJ, Hutchins GM, Bulkley BH. Cardiac sarcoid: A Clinicopathologic Study of 84 Unselected Patients with Systemic Sarcoidosis. Circulation. 1978;58(6):1204-11. doi: 10.1161/01.cir.58.6.1204.
5. Tan JL, Fong HK, Birati EY, Han Y. Cardiac Sarcoidosis. Am J Cardiol. 2019;123(3):513-22. doi: 10.1016/j.amjcard.2018.10.021.
6. Bennett MK, Gilotra NA, Harrington C, Rao S, Dunn JM, Freitag TB, et al. Evaluation of the Role of Endomyocardial Biopsy in 851 Patients with Unexplained Heart Failure from 2000-2009. Circ Heart Fail. 2013;6(4):676-84. doi: 10.1161/CIRCHEARTFAILURE.112.000087.
7. Terasaki F, Azuma A, Anzai T, Ishizaka N, Ishida Y, Isobe M, et al. JCS 2016 Guideline on Diagnosis and Treatment of Cardiac Sarcoidosis - Digest Version. Circ J. 2019;83(11):2329-88. doi: 10.1253/circj.CJ-19-0508.
8. Birnie DH, Sauer WH, Bogun F, Cooper JM, Culver DA, Duvernoy CS, et al. HRS Expert Consensus Statement on the Diagnosis and Management of Arrhythmias Associated with Cardiac Sarcoidosis. Heart Rhythm. 2014;11(7):1305-23. doi: 10.1016/j.hrthm.2014.03.043.
9. Diagnostic Guideline and Criteria for Sarcoidosis--2006. Nippon Ganka Gakkai Zasshi. 2007;111(2):117-21.
10. Ribeiro Neto ML, Jellis C, Hachamovitch R, Wimer A, Highland KB, Sahoo D, et al. Performance of Diagnostic Criteria in Patients Clinically Judged to Have Cardiac Sarcoidosis: Is it Time to Regroup? Am Heart J. 2020;223:106-9. doi: 10.1016/j.ahj.2020.02.008.
11. Kouranos V, Sharma R. Cardiac Sarcoidosis: State-of-the-Art Review. Heart. 2021;107(19):1591-9. doi: 10.1136/heartjnl-2019-316442.
12. Willy K, Dechering DG, Reinke F, Bögeholz N, Frommeyer G, Eckardt L. The ECG in Sarcoidosis - a Marker of Cardiac Involvement? Current Evidence and Clinical Implications. J Cardiol. 2021;77(2):154-9. doi: 10.1016/j.jjcc.2020.07.006.
13. Nery PB, McArdle BA, Redpath CJ, Leung E, Lemery R, Dekemp R, et al. Prevalence of Cardiac Sarcoidosis in Patients Presenting with Monomorphic Ventricular Tachycardia. Pacing Clin Electrophysiol. 2014;37(3):364-74. doi: 10.1111/pace.12277.
14. Nery PB, Beanlands RS, Nair GM, Green M, Yang J, McArdle BA, et al. Atrioventricular Block as the Initial Manifestation of Cardiac Sarcoidosis in Middle-aged Adults. J Cardiovasc Electrophysiol. 2014;25(8):875-81. doi: 10.1111/jce.12401.
15. Sadek MM, Yung D, Birnie DH, Beanlands RS, Nery PB. Corticosteroid Therapy for Cardiac Sarcoidosis: A Systematic Review. Can J Cardiol. 2013;29(9):1034-41. doi: 10.1016/j.cjca.2013.02.004.
16. Khaji A, Zhang L, Kowey P, Martinez-Lage M, Kocovic D. Mega-epsilon Waves on 12-lead ECG--just Another Case of Arrhythmogenic Right Ventricular Dysplasia/Cardiomyopathy? J Electrocardiol. 2013;46(6):524-7. doi: 10.1016/j.jelectrocard.2013.08.007.
17. Waki H, Eguchi K, Toriumi S, Ikemoto T, Suzuki T, Fukushima N, et al. Isolated Cardiac Sarcoidosis Mimicking Arrhythmogenic Right Ventricular Cardiomyopathy. Intern Med. 2018;57(6):835-9. doi: 10.2169/internalmedicine.9395-17
18. Philips B, Madhavan S, James CA, te Riele AS, Murray B, Tichnell C, et al. Arrhythmogenic Right Ventricular Dysplasia/Cardiomyopathy and Cardiac Sarcoidosis: Distinguishing Features When the Diagnosis is Unclear. Circ Arrhythm Electrophysiol. 2014;7(2):230-6. doi: 10.1161/CIRCEP.113.000932.
19. Willy K, Dechering DG, Reinke F, Bögeholz N, Frommeyer G, Eckardt L. The ECG in Sarcoidosis - A Marker of Cardiac Involvement? Current Evidence and Clinical Implications. J Cardiol. 2021;77(2):154-9. doi: 10.1016/j.jjcc.2020.07.006.
20. Mehta D, Lubitz SA, Frankel Z, Wisnivesky JP, Einstein AJ, Goldman M, et al. Cardiac Involvement in Patients with Sarcoidosis: Diagnostic and Prognostic Value of Outpatient Testing. Chest. 2008;133(6):1426-35. doi: 10.1378/chest.07-2784.
21. Kurmann R, Mankad SV, Mankad R. Echocardiography in Sarcoidosis. Curr Cardiol Rep. 2018;20(11):118. doi: 10.1007/s11886-018-1065-9.
22. Kouranos V, Tzelepis GE, Rapti A, Mavrogeni S, Aggeli K, Douskou M, et al. Complementary Role of CMR to Conventional Screening in the Diagnosis and Prognosis of Cardiac Sarcoidosis. JACC Cardiovasc Imaging. 2017;10(12):1437-47. doi: 10.1016/j.jcmg.2016.11.019.
23. Murtagh G, Laffin LJ, Patel KV, Patel AV, Bonham CA, Yu Z, et al. Improved Detection of Myocardial Damage in Sarcoidosis Using Longitudinal Strain in Patients with Preserved Left Ventricular Ejection Fraction. Echocardiography. 2016;33(9):1344-52. doi: 10.1111/echo.13281.
24. Crouser ED, Maier LA, Wilson KC, Bonham CA, Morgenthau AS, Patterson KC, et al. Diagnosis and Detection of Sarcoidosis. An Official American Thoracic Society Clinical Practice Guideline. Am J Respir Crit Care Med. 2020;201(8):26-51. doi: 10.1164/rccm.202002-0251ST.
25. Koiwa H, Tsujino I, Ohira H, Yoshinaga K, Otsuka N, Nishimura M. Images in Cardiovascular Medicine: Imaging of Cardiac Sarcoid Lesions Using Fasting Cardiac 18F-fluorodeoxyglucose Positron Emission Tomography: An Autopsy Case. Circulation. 2010;122(5):535-6. doi: 10.1161/CIRCULATIONAHA.110.952184.
26. Slart RHJA, Glaudemans AWJM, Lancellotti P, Hyafil F, Blankstein R, Schwartz RG, et al. A Joint Procedural Position Statement on Imaging in Cardiac Sarcoidosis: From the Cardiovascular and Inflammation & Infection Committees of the European Association of Nuclear Medicine, the European Association of Cardiovascular Imaging, and the American Society of Nuclear Cardiology. J Nucl Cardiol. 2018;25(1):298-319. doi: 10.1007/s12350-017-1043-4.
27. Chareonthaitawee P, Beanlands RS, Chen W, Dorbala S, Miller EJ, Murthy VL, et al. Joint SNMMI-ASNC Expert Consensus Document on the Role of 18F-FDG PET/CT in Cardiac Sarcoid Detection and Therapy Monitoring. J Nucl Med. 2017;58(8):1341-53. doi: 10.2967/jnumed.117.196287.
28. Osborne MT, Hulten EA, Murthy VL, Skali H, Taqueti VR, Dorbala S, et al. Patient Preparation for Cardiac Fluorine-18 Fluorodeoxyglucose Positron Emission Tomography Imaging of Inflammation. J Nucl Cardiol. 2017;24(1):86-99. doi: 10.1007/s12350-016-0502-7.
29. Divakaran S, Stewart GC, Lakdawala NK, Padera RF, Zhou W, Desai AS, et al. Diagnostic Accuracy of Advanced Imaging in Cardiac Sarcoidosis. Circ Cardiovasc Imaging. 2019;12(6):1-17. doi: 10.1161/CIRCIMAGING.118.008975.
30. Kim SJ, Pak K, Kim K. Diagnostic Performance of F-18 FDG PET for Detection of Cardiac Sarcoidosis; A Systematic Review and Meta-analysis. J Nucl Cardiol. 2020;27(6):2103-15. doi: 10.1007/s12350-018-01582-y.
31. Giblin GT, Murphy L, Stewart GC, Desai AS, Di Carli MF, Blankstein R, et al. Cardiac Sarcoidosis: When and How to Treat Inflammation. Card Fail Rev. 2021;7:1-10. doi: 10.15420/cfr.2021.16.
32. Osborne MT, Hulten EA, Singh A, Waller AH, Bittencourt MS, Stewart GC, et al. Reduction in ^{1}□F-fluorodeoxyglucose Uptake on Serial Cardiac Positron Emission Tomography is Associated with Improved Left Ventricular Ejection Fraction in Patients with Cardiac Sarcoidosis. J Nucl Cardiol. 2014 Feb;21(1):166-74. doi: 10.1007/s12350-013-9828-6.
33. Muser D, Santangeli P, Castro SA, Liang JJ, Enriquez A, Werner TJ, et al. Prognostic Role of Serial Quantitative Evaluation of 18F-fluorodeoxyglucose Uptake by PET/CT in Patients with Cardiac Sarcoidosis Presenting with Ventricular Tachycardia. Eur J Nucl Med Mol Imaging. 2018;45(8):1394-404. doi: 10.1007/s00259-018-4001-8.

34. Bekki M, Tahara N, Tahara A, Sugiyama Y, Maeda-Ogata S, Honda A, et al. Localization of Myocardial FDG Uptake for Prognostic Risk Stratification in Corticosteroid-naïve Cardiac Sarcoidosis. J Nucl Cardiol. 2022;29(5):2132-44. doi: 10.1007/s12350-021-02684-w.

35. Tuominen H, Haarala A, Tikkakoski A, Kähönen M, Nikus K, Sipilä K. FDG-PET in Possible Cardiac Sarcoidosis: Right Ventricular Uptake and High Total Cardiac Metabolic Activity Predict Cardiovascular Events. J Nucl Cardiol. 2021;28(1):199-205. doi: 10.1007/s12350-019-01659-2.

36. Blankstein R, Osborne M, Naya M, Waller A, Kim CK, Murthy VL, et al. Cardiac Positron Emission Tomography Enhances Prognostic Assessments of Patients with Suspected Cardiac Sarcoidosis. J Am Coll Cardiol. 2014;63(4):329-36. doi: 10.1016/j.jacc.2013.09.022.

37. Writing group. A Joint Procedural Position Statement on Imaging in Cardiac Sarcoidosis: From the Cardiovascular and Inflammation & Infection Committees of the European Association of Nuclear Medicine, the European Association of Cardiovascular Imaging, and the American Society of Nuclear Cardiology. Eur Heart J Cardiovasc Imaging. 2017;18(10):1073-89. doi: 10.1093/ehjci/jex146.

38. Smedema JP, Snoep G, van Kroonenburgh MP, van Geuns RJ, Dassen WR, Gorgels AP, et al. Evaluation of the Accuracy of Gadolinium-enhanced Cardiovascular Magnetic Resonance in the Diagnosis of Cardiac Sarcoidosis. J Am Coll Cardiol. 2005;45(10):1683-90. doi: 10.1016/j.jacc.2005.01.047.

39. Patel MR, Cawley PJ, Heitner JF, Klem I, Parker MA, Jaroudi WA, et al. Detection of Myocardial Damage in Patients with Sarcoidosis. Circulation. 2009;120(20):1969-77. doi: 10.1161/CIRCULATIONAHA.109.851352.

40. Trivieri MG, Spagnolo P, Birnie D, Liu P, Drake W, Kovacic JC, et al. Challenges in Cardiac and Pulmonary Sarcoidosis: JACC State-of-the-Art Review. J Am Coll Cardiol. 2020;76(16):1878-901. doi: 10.1016/j.jacc.2020.08.042.

41. Yang S, Chen X, Li J, Sun Y, Song J, Wang H, et al. Late Gadolinium Enhancement Characteristics in Giant Cell Myocarditis. ESC Heart Fail. 2021;8(3):2320-7. doi: 10.1002/ehf2.13276.

42. Cain MA, Metzl MD, Patel AR, Addetia K, Spencer KT, Sweiss NJ, et al. Cardiac Sarcoidosis Detected by Late Gadolinium Enhancement and Prevalence of Atrial Arrhythmias. Am J Cardiol. 2014;113(9):1556-60. doi: 10.1016/j.amjcard.2014.01.434.

43. Puntmann VO, Isted A, Hinojar R, Foote L, Carr-White G, Nagel E. T1 and T2 Mapping in Recognition of Early Cardiac Involvement in Systemic Sarcoidosis. Radiology. 2017;285(1):63-72. doi: 10.1148/radiol.2017162732.

44. Lehtonen J, Uusitalo V, Pöyhönen P, Mäyränpää MI, Kupari M. Cardiac Sarcoidosis: Phenotypes, Diagnosis, Treatment, and Prognosis. Eur Heart J. 2023;44(17):1495-510. doi: 10.1093/eurheartj/ehad067.

45. Vita T, Okada DR, Veillet-Chowdhury M, Bravo PE, Mullins E, Hulten E, et al. Complementary Value of Cardiac Magnetic Resonance Imaging and Positron Emission Tomography/Computed Tomography in the Assessment of Cardiac Sarcoidosis. Circ Cardiovasc Imaging. 2018;11(1):1-26. doi: 10.1161/CIRCIMAGING.117.007030.

46. Hulten E, Agarwal V, Cahill M, Cole G, Vita T, Parrish S, et al. Presence of Late Gadolinium Enhancement by Cardiac Magnetic Resonance Among Patients With Suspected Cardiac Sarcoidosis Is Associated With Adverse Cardiovascular Prognosis: A Systematic Review and Meta-Analysis. Circ Cardiovasc Imaging. 2016;9(9):1-21. doi: 10.1161/CIRCIMAGING.116.005001.

47. Kalra R, Malik S, Chen KA, Ogugua F, Athwal PSS, Elton AC, et al. Sex Differences in Patients With Suspected Cardiac Sarcoidosis Assessed by Cardiovascular Magnetic Resonance Imaging. Circ Arrhythm Electrophysiol. 2021;14(9):1-21. doi: 10.1161/CIRCEP.121.009966.

48. Shrivastav R, Hajra A, Krishnan S, Bandyopadhyay D, Ranjan P, Fuisz A. Evaluation and Management of Cardiac Sarcoidosis with Advanced Imaging. Heart Fail Clin. 2023;19(4):475-89. doi: 10.1016/j.hfc.2023.06.002.

How Do I Diagnose and Classify Endomyocardial Fibrosis in Under-Resourced Settings

Ana Mocumbi[1,2]
Universidade Eduardo Mondlane,[1] *Maputo – Mozambique*
Instituto Nacional de Saúde,[2] *Marracuene – Mozambique*

Central Illustration: Echocardiographic Characteristics of EMF

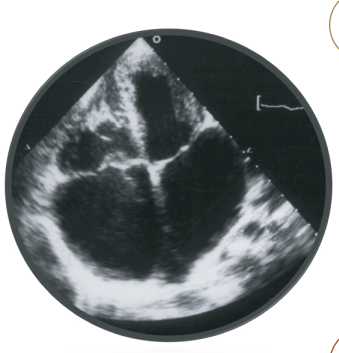

- Enlarged atrium with normal-size ventricle
- Pericardial hemorrhage – abundant in advanced forms and predominantly in right-side EMF
- Single ventricular thrombi (predominantly apical) or multiple ventricular thrombi without severe ventricular dysfunction
  Atrial thrombi and/or spontaneous contrast and aneurysmal atria
- RV apical retraction
  In severe cases, apical notch between RV and LV
- Endomyocardial plaques affecting the ventricular wall, predominantly at the apex, sometimes with calcification
  Obliteration of the apex of the RV or LV
- Restrictive flow pattern across mitral or tricuspid valves
  Low regurgitation velocity in severe right EMF without valve coaptation because of extreme atrial dilatation
- AV valve thickening, habitually throughout the valve and with mild involvement of tendinous cords
  AV valve dysfunction caused by adhesion of the valvular apparatus to the ventricular wall.

Arq Bras Cardiol: Imagem cardiovasc. 2024;37(1):e20230107

EMF: Endomyocardial fibrosis; RV: right ventricle; LV: left ventricle.

Abstract

Endomyocardial fibrosis (EMF) is a disease of unclear etiology and pathogenesis that is characterized by fibrosis in the ventricular cavities and mainly affects children and adolescents from tropical regions of Africa, South America, and Asia. It is classified as a restrictive cardiomyopathy, with pathophysiology of restriction to diastolic filling associated with valve abnormalities, both caused by endocardial fibrosis. Typical echocardiographic features of this condition are endocardial thickening, severe atrioventricular (AV) valve regurgitation, aneurysmal atria, and heart distortion.

In endemic areas of Africa, in the absence of advanced imaging techniques, EMF diagnosis and management relies on transthoracic echocardiography for careful assessment of structural and hemodynamic abnormalities, aiming at planning medical or surgical management. This review highlights the key echocardiographic aspects of diagnosis and classification of EMF, as used in under-resourced settings in Africa. This is a standardized approach to screening populations with known occurrence of the disease and for informing medical and surgical management.

Keywords

Endomyocardial Fibrosis; Echocardiography; Diagnosis

Mailing Address: Ana Mocumbi •
Universidade Eduardo Mondlane. Av Julius Nyerere Maputo, Campus Universitário 3453 1102, Maputo – Mozambique
E-mail: amocumbi@gmail.com
Manuscript received December 4,2023; revised December 6, 2023; accepted December 6, 2023
Editor responsible for the review: Daniela do Carmo Rassi Frota

DOI: https://doi.org/10.36660/abcimg.20230107i

Contents

Introduction

Endomyocardial fibrosis (EMF) is a progressive disease of unclear etiology and pathogenesis that, when established, is characterized by fibrosis in the ventricular cavities, particularly affecting the apex and the subvalvular regions. It is a restrictive cardiomyopathy that affects mainly children and adolescents, predominantly from certain rural settings in Africa.[1] The pathophysiology of EMF associates restricted diastolic filling with major changes in the valve apparatus caused by endocardial fibrosis, resulting in severe atrioventricular (AV) valve regurgitation, aneurysmal atria, and heart distortion. Advanced forms of EMF have high morbidity and mortality, with death occurring due to progression to chronic heart failure or as a result of arrhythmia and thromboembolism.[2] Although there is no specific treatment for EMF, surgery should be considered to correct some structural and functional abnormalities in symptomatic individuals. Surgical techniques have been progressing,[3] but outcomes are yet to be fully understood.[4]

In endemic areas of Africa, in the absence of advanced imaging techniques such as magnetic resonance imaging, EMF diagnosis and management often relies on detailed transthoracic echocardiography. Transesophageal and three-dimensional echocardiography are rarely used, magnetic resonance imaging is also rarely available, and catheterization is often contraindicated because the risks outweigh the benefit - due to presence of thrombi and because of the difficulty of obtaining endomyocardial tissue in advanced disease. Detailed echocardiographic characterization and classification of EMF has been shown to provide reliable information on the key structural and hemodynamic abnormalities that are confirmed in surgery.[5] This review highlights the key echocardiographic aspects of diagnosis and classification of EMF in under-resourced settings in Africa.

Echocardiographic Criteria for Diagnosis of EMF

The echocardiographic criteria for diagnosis of EMF were described in a highly endemic population from Mozambique.[6] Using these echocardiographic features, cardiac abnormalities in patients with EMF were divided into "major" or "minor", according to their clinical relevance, uniqueness to the diagnosis, influence on management decision, and prognostic importance. (Table 1)

Major criteria are distinctive or pathognomonic features of EMF, which usually have a major impact on management. Each feature is attributed an individual score according to its relevance to determination of structural and hemodynamic changes. The following are considered major criteria for diagnosis of EMF: i) Endocardial plaque of at least 5mm in width or endocardial thickening greater than 1mm; ii) Patchy endocardial thickening in two or more ventricular walls; iii) Obliteration of ventricular apices or valve recesses; iv) Ventricular thrombi or spontaneous contrast in the absence of ventricular dysfunction; v) Reduction of the right ventricle (RV) cavity volume due to exclusion of the trabecular portion vi) Restriction of AV valve leaflet movements due to adherence to the ventricular walls.

For screening, endocardial plaques or endocardial thickening of more than 5mm in width and thicker than 1mm are considered a major criterion for diagnosis of EMF. The term "large plaque" is used when endocardial thickening exceeds 10 mm in width.

Minor criteria are not specific for EMF but may suggest the disease. Although commonly found in patients with EMF, these features are not exclusive to this condition and do not define the condition when found in isolation. They are considered to have less influence on management and prognosis, when compared to the major criteria previously described. The features that are considered minor criteria for the diagnosis of EMF are: i) Patchy endomyocardial thickening localized to one ventricular wall; ii) Restrictive ventricular filling pattern; iii) Diffuse thickening of the AV valve leaflets; iv) Enhanced density of the moderator band or intraventricular trabeculae; v) Abnormal M-movement of the interventricular septum and/or posterior left ventricle (LV) wall; vi) Enlarged atrium with normal-sized homolateral ventricle; and vii) Presence of thickened "false tendon" of the LV.

In asymptomatic individuals, patchy endocardial thickening corresponds to small areas of endocardium with enhanced density, less than 1mm in depth and evenly distributed in the ventricular walls.

Table 1 – Criteria for Diagnosis and Assessment of the Severity of FEM*[6]

Criterion	Score
Major criteria	
Endomyocardial plaques > 2 mm in thickness	2
Thin (≤ 1 mm) endomyocardial patches affecting more than one ventricular wall	3
Obliteration of the right ventricular or left ventricular apex	4
Thrombi or spontaneous contrast without severe ventricular dysfunction	4
Retraction of the right ventricular apex (right ventricular apical notch)	4
AV-valve dysfunction due to adhesion of the valvular apparatus to the ventricular wall	1-4†
Minor criteria	
Thin endomyocardial patches localized to one ventricular wall	1
Restrictive flow pattern across mitral or tricuspid valves	2
Pulmonary-valve diastolic opening	2
Diffuse thickening of the anterior mitral leaflet	1
Enlarged atrium with normal-size ventricle	2
M-movement of the interventricular septum and flat posterior wall‡	1
Enhanced density of the moderator or other intraventricular bands	1

**A definite diagnosis of EMF was made in the presence of two major criteria or one major criterion associated with two minor criteria. A total score of less than 8 indicates mild EMF, 8 to 15 moderate disease, and more than 15 severe disease. † The score is assigned according to the severity of AV regurgitation. ‡ M-movement of the interventricular septum refers to a pattern of movement observed on M-mode echocardiography that is thought to be due to obliteration or restriction of the left ventricular apex combined with mitral regurgitation. EMF: Endomyocardial Fibrosis; AV: atrioventricular; LV: left ventricle*

Classification of EMF

The echocardiographic appearance of EMF varies both in terms of the distribution and of the severity of the structural lesions and hemodynamic abnormalities. The criteria described above are used to assess the presence of lesions in each side of the heart, and the scoring system is applied to each ventricle separately. According to the distribution of lesions (affecting exclusively or predominantly one or both sides of the heart) we classified the disease as Right EMF, Left EMF, or Bilateral EMF (Figure 1).

Severity of EMF

The severity of EMF is assessed by quantifying structural and hemodynamic lesions. Four progressive degrees of severity are defined, supporting management decisions and informing on prognosis (Table 2):

- *Grade I (or Mild EMF)*: Endocardial plaque or patchy thickening associated with thickening of the AV valve leaflets, with no other structural or hemodynamic abnormalities.
- *Grade II (or Moderate EMF)*: Large endocardial plaques, apical/valve recess, ventricular obliteration, and mild to moderate AV valve regurgitation. There is mild to moderate atrial dilatation, mild ventricular cavity reduction, and preserved myocardial function.
- *Grade III (or Severe EMF)*: Large endocardial plaques, moderate reduction of ventricular cavity dimensions, marked atrial dilatation, and severe AV valve dysfunction. Myocardium is visible underneath the endocardial thickening and ventricular function is nearly normal.
- *Grade IV (or Advanced EMF)*: Presence of large endocardial plaques associated with severe reduction of ventricular size and compression of the contralateral cavities by the severely dilated atrium. Endocardial calcification, poor ventricular contractility, and large persistent effusions (pericardial, peritoneal, and/or pleural) are other features of advanced EMF.

The different stages of EMF are exemplified in Figure 2.

Staging and Mode of Progression

Staging and characterization of the mode of progression of EMF aims to distinguish active from latent disease, particularly in clinical settings, and is used to support management and to indicate prognosis. In a patient with an echocardiographic diagnosis of EMF, activity was defined as a finding of two or more of the following signs: i) unexplained fever, recurrent facial edema, urticaria or asthma-like episodes; ii) severe hypereosinophilia (absolute eosinophil count > 1.5 x 109/L); iii) ventricular thrombi not attributable to severe myocardial dysfunction; iv) evidence of pancarditis with acute heart failure; and, v) increased C-Reactive Protein and/or erythrocyte sedimentation rate. The persistence of these signs and the speed of progression of structural and/or functional abnormalities in the six months following the diagnosis are used to define three distinct stages of the disease: active with remission, active persistent, and rapidly progressive.

Active EMF with remission refers to patients who had signs of activity at diagnosis that regressed during the first six months of follow up, while *Active persistent disease* signified persistence of signs of activity for 6 months or more. Finally, we use the expression *Active rapidly progressive* to define patients with persistence of signs of activity after the initial episode of heart failure, who progress to a higher degree of severity or death in less than six months. Depending on the occurrence of disease recrudescence during the first six months of follow up, patients are classified as having quiescent or recurrent disease. Patients who develop recrudescence of active disease in the course of follow up, going back to a quiescent stage thereafter, are considered to have chronic recurrent disease.

Signs of activity are frequent in patients from the clinical registries, who present laboratory signs of active disease, hypereosinophilia, and facial edema. Rapidly progressive disease and death may be associated with intraventricular thrombi and myocardial dysfunction.

Patients are also classified according to the duration of symptoms; if these are present for less than 6 months, they are considered to have acute disease. Chronic disease is defined by the presence of signs and symptoms attributable to EMF for more than six months with echocardiographic features of established EMF.

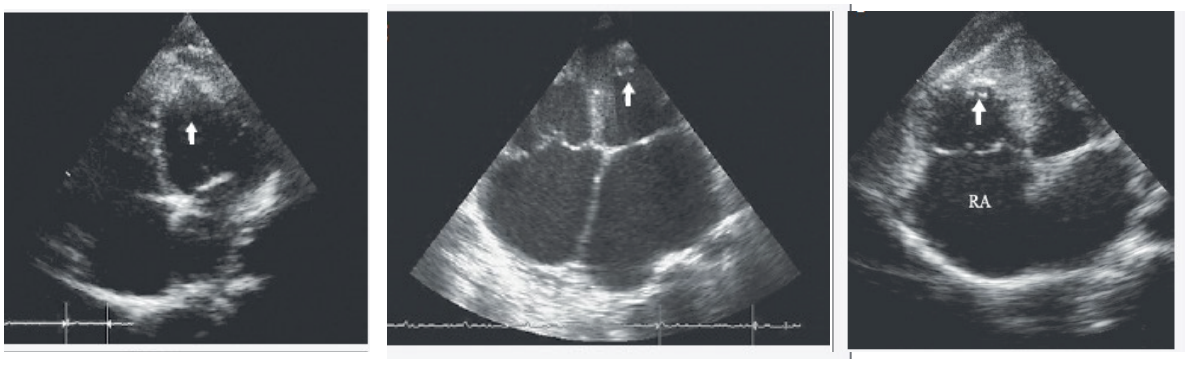

Figure 1 – *Progression of EMF from occupation of the apex with thrombi (left), to ventricular cavity reduction and atrial dilatation (centre); and large plaque of fibrosis and ventricular retraction (right).*

Experience from Community- and Hospital-Based Studies

The information used to develop the criteria results from careful evaluation of transthoracic echocardiography and follow-up of 1534 individuals (1063 individuals of all ages randomly selected from the community, 296 school children, and 175 patients with established disease cared for in hospitals). On clinical grounds, the clinical features, biological profile, findings during open heart surgery, and pathological features of tissue obtained in vivo were used to complement the studies.[6,7] Of the 413 individuals with EMF (mean age at diagnosis 15 years, with no gender differences), 52 patients (12,1%) recalled having any complaints before diagnosis, confirming the high occurrence of clinical-echocardiographic dissociation in EMF.[8] The most common features seen on echocardiography are summarized in Table 3.

Table 2 – Main features in EMF of different degrees of severity

Grade	FEATURES
I MILD	Patchy fibrosis of any ventricle, diffuse thickening of the leaflets and restrictive pattern of ventricular filling, without any other structural changes
II MODERATE	Hyperdense lesions on the mural and valvular endocardium, obliteration of the ventricular apex, ventricular thrombi, and/or AV valvular dysfunction, in the absence of cavity deformation/reduction or myocardial dysfunction
III SEVERE	Extensive fibrosis and/or calcification with functioning myocardium visible underneath it, reduction of ventricular size, severe atrial dilatation, and AV valvular dysfunction
IV ADVANCED	Heart distortion and cavity deformation due to extensive fibrosis or calcification that affects the contractility of the myocardium and leads to free AV regurgitation

AV: atrioventricular.

Abnormalities of the Left Side of the Heart

Early left EMF is often detected in asymptomatic individuals in the community and may be characterized by fibrosis of the *false tendons*, thickening of the mitral leaflets (Figure 2a), apical thrombus, and/or obliteration of the apex or the recess between the posterior leaflet and the posterior wall. Thrombi in the subvalvular apparatus involve the free edges of both papillary muscles. Flow across the mitral valve shows early diastolic filling.

In established left EMF, thickening of the endocardium is prominent in the apex and posterior wall behind the recess of the posterior leaflet of the mitral valve. The ventricle assumes a spherical shape (Figure 2b), being hypercontractile in its basal portion. At this stage, most cases may have a competent mitral valve, but in some cases the movement of the posterior leaflet is restricted, leading to an eccentric mitral regurgitation and passive pulmonary hypertension. A common finding in left EMF is the so-called M-movement of the interventricular septum on M-mode.

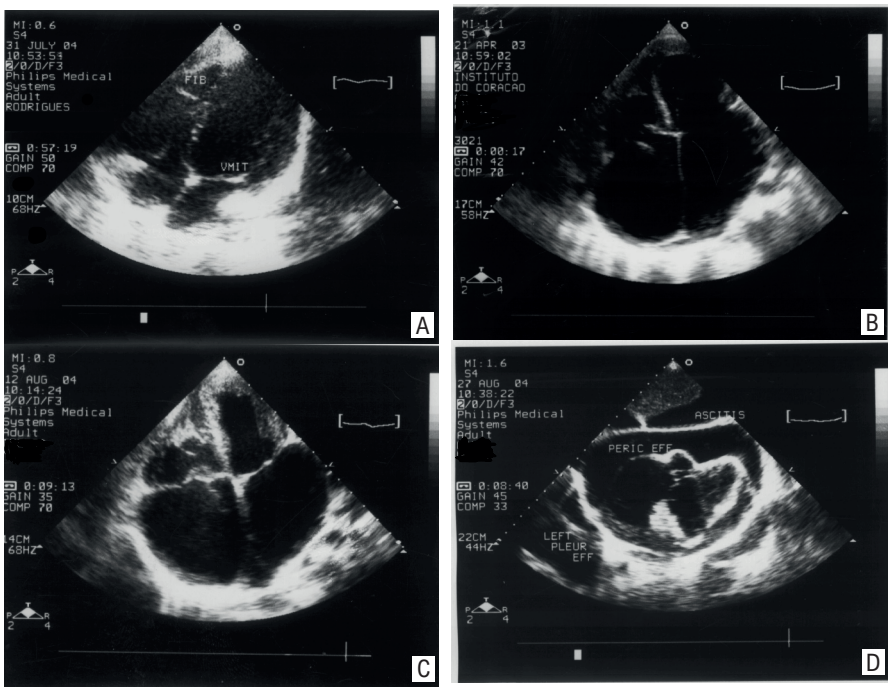

Figure 2 – *The classification of EMF captures the diversity in location and severity of structural abnormalities detected on echocardiography. A) Grade I predominantly right; B) Grade II bilateral; C) Grade III bilateral with obliteration of the right ventricle; D) Grade IV with severe retraction of the right ventricle, heart distortion and pericardial effusion.*

Table 3 – Frequency of echocardiographic features on the left side of the heart in 411 EMF patients in clinical and community studies performed in Mozambique

Echocardiographic features	Community Studies	Clinical Registry
Thickening of the AML	121 (51.3%)	148 (84.5%)
Thickening of the PML	117 (49.6%)	102 (58.3%)
Endocardial thickening of the septal wall	106 (44.9%)	140 (80.0%)
Restrictive filling pattern	81 (34.3%)	57 (24.2%)
Enhanced density of the papillary muscles	78 (33.1%)	130 (74.3%)
Apical endocardial thickening	55 (23.3%)	57 (32.6%)
Thickening of the false tendon	47 (19.9%)	11 (6.29%)
Obliteration of the recess behind the PML	27 (11.4%)	30 (17.1%)
Mitral regurgitation	26 (11.0%)	107 (61.1%)
Severe dilatation of the left atrium	13 (5.5%)	87 (49.7%)
Apical thrombus/obliteration	4 (1.7%)	13 (7.4%)
Non-apical intraventricular thrombus	1 (0.4%)	5 (2.9%)
Left atrial thrombus	0 (0%)	7 (4.0%)
Total	**236**	**175**

PML: posterior mitral leaflet; AML: anterior mitral leaflet

The most characteristic features of advanced left EMF are septal and apical fibrosis, severe eccentric mitral regurgitation, due to fusion of posterior leaflet to the wall, disproportionally small LV, aneurysmal left atrium, and severe pulmonary hypertension (Table 4). Even in patients with extensive endocardial thickening, retraction of the LV apex does not occur.(Figure 2c)

Abnormalities of the Right Side of the Heart

In early right EMF disease, the longitudinal view of the RV (using the short axis view of the LV at the level of the aorta) shows a stretched moderator band separating the inflow and outflow tracts from the trabecular portion. (Figure 2a) There may be turbulent blood flow inside the trabecular portion of the ventricle. Right ventricular obliteration (disappearance of the trabecular portion of the RV) is usually associated with mild to moderate tricuspid regurgitation caused by restriction to the movement of the tricuspid anterior and septal leaflets. (Figure 2b) The leaflets may be attached to the wall leading to an echocardiographic picture similar to the "Ebstein Malformation", with dilatation of the tricuspid annulus and tricuspid regurgitation jet originating inside the RV.

Severe right EMF is characterized by retraction of the RV (Figure 2c, 2d), severe tricuspid regurgitation with almost no turbulence, restriction of leaflet motion caused by involvement of the papillary muscles in the fibrotic process, and dilatation of the tricuspid annulus, related to severe right atrial dilatation. Spontaneous contrast images are common inside the right atrium, extending both to the right ventricular inflow tract and to the inferior vena cava and dilated supra-hepatic veins; these do not usually show the normal respiratory changes, indicating increased systemic venous pressure.

In patients with advanced right EMF , the reduction of the right ventricular cavity size is partially compensated for by dilation of the outflow tract and free tricuspid regurgitation occurs due to an aneurysmal right atrium. There are usually dynamic intracavitary echoes or large thrombi. There may be equalization of pressure between the atrium, the ventricle, and the pulmonary artery, as well as diastolic opening of the pulmonary valve. The aneurysmal right atrium causes heart distortion and compression of the left cavities, hampering evaluation of the mitral valve. Abundant pericardial effusion is common in advanced right EMF (Table 4).

Bilateral EMF

In established bilateral EMF, the heart has a peculiar aspect of enlarged atria with small ventricles - the "Mickey mouse" heart in the four chambers view - coexistence of mitral and tricuspid regurgitation (Figures 2b & 2c). The reduced right ventricular output and pulmonary perfusion partially reduces the effects of the pulmonary venous hypertension caused by left ventricular disease, favoring a better outcome compared to that of pure left EMF.

Discussion

The echocardiographic criteria for diagnosis of EMF can be employed for screening, follow-up, and management of EMF in endemic areas. We hypothesize that serial evaluations of early EMF using these criteria would provide better understanding of its natural history. However, epidemiological studies to validate these criteria in follow up studies are difficult to implement in endemic areas.[7] The classification has been used to assess geographic variation in clinical presentations of EMF in India.[9]

The hallmark of established EMF is endocardial thickening in large plaques or patchy distribution, interfering with diastolic function and reducing cardiac output. Ventricular thrombosis or "spontaneous contrast" are frequently seen: in left EMF, ventricular thrombi are mostly apical and may involve the subvalvular apparatus, while the trabecular portion is more affected in right EMF. In this classification, thrombi are attributed a high score because they pose an enormous risk to life and are a major determinant of management and prognosis.[10]

Heart distortion is a characteristic feature of EMF due to the aneurysmal atria and partial or complete exclusion of the right ventricular trabecular portion from the circulation, in cases of ventricular retraction with the characteristic "apical notch" – a distinctive feature of advanced right EMF (Figure 2d).

The criteria discussed in this paper do not include the conventional measures for assessment of left ventricular systolic function because these are difficult to apply in severe and advanced EMF due to marked heart cavity distortion. Evaluation of myocardial function is hampered by the presence

Table 4 – Echocardiographic characteristics of EMF that allow classification as left, right and bilateral

RIGHT EMF	LEFT EMF
• Enhancement of endocardial echo	• Enhancement of endocardial echo
• Tricuspid Valve apparatus adherent to the mural fibrosis	• Plastered down post mitral leaflet
• Obliteration or retraction of RV trabecular portion; apical notch or shrunken RV cavity	• Obliterated LV apex, reduction of the longitudinal diameter, with oval or globular shape
• Features of Tricuspid Regurgitation	• Features of Mitral Regurgitation
• Endocardial calcification on the RV	• Calcificação endocárdica no VE
• Dilated and hyperdynamic RV outflow tract; paradoxical movement of the IVS	• M movement of IVS/PW; dilated and hyperdynamic basal portion of the LV
• Restrictive pattern of RV filling	• Restrictive pattern of LV filling
• Dilated right atrium	• Dilatation of the left atrium
• Variable pericardial effusion	• Features of Pulmonary Hypertension
• Dynamic intracavitary echoes or thrombi	• Dynamic intracavitary echoes or thrombi
• Dilatation of the IVC and IHV	
• Pulmonary Valve diastolic opening	

EMF: Endomyocardial fibrosis; LV: left ventricle; RV: right ventricle; IVC: inferior vena cava; IHV: intra-hepatic veins; IVS: interventricular septum; PW: posterior wall

of endocardial fibrosis restricting the underlying myocardial contractility. Visual semi-quantitative scales are used to assess systolic ventricular function.[11] Regarding right ventricular assessment, the ventricular outflow tract shortening fraction (a simple and noninvasive measure of systolic function)[12] does not seem adequate, due to the presence of compensatory dilatation and hypercontractility of the outflow tract, as a result of trabecular cavity obliteration or retraction.

Due to the geometric changes associated with EMF, the sphericity index has been suggested as a good tool to describe abnormalities in ventricular shape and volume. This index is used to assess changes occurring in non-ischemic cardiomyopathy and seems to be a good tool to quantify the abnormal geometric changes that accompany heart failure in dilated failing LVs,[13] but it needs to be validated.

Importantly, the standardized criteria for diagnosis and classification of EMF identify patients who can benefit from surgery and allow for risk stratification, defining patients with mild EMF who do not benefit from surgery and those who are unsuitable for surgery. Extensive endocardial thickening with disappearance of the AV valve apparatus, thick endocardium without visible myocardium underneath it, extensive calcification, and/or severe myocardial dysfunction are signs used to define contraindication to surgery. This classification also allows stratification of operative risk, planning of tailored surgical techniques, and post-operative follow up.

Limitations

We acknowledge the limitations of transthoracic echocardiography to accurately assess structural and hemodynamic abnormalities in adult patients with advanced EMF, particularly when calcification or major distortion of the heart cavities are present. Three-dimensional echocardiography allows better characterization of EMF, but is not widely used in endemic settings. Magnetic resonance imaging and myocardial contrast echocardiography provide more detailed anatomical and functional information, including the location and size of endocardial fibrosis and thrombi and are the techniques of choice for pre- and post-surgery evaluation, particularly for detecting recurrence.[14-16]

In areas endemic for both EMF and rheumatic heart disease, differentiation between left EMF and rheumatic heart valve disease may be challenging; while diffuse irregular AV valve leaflet thickening with thin chordae is suggestive of EMF, prominent thickening of the free borders of the leaflets extending to the chordae is typical of rheumatic valve disease.[17]

Conclusions

The use of echocardiography allows a confident non-invasive diagnosis of EMF, is essential for indication of surgery and choice of operative techniques, and has the potential to be used to define prognosis. EMF presents great phenotypic variability with lesions varying from patchy endocardial thickening without any hemodynamic changes, to extensive mural and AV valve endocardial fibrosis with resulting structural and hemodynamic changes.

Because the assumptions made to calculate parameters for assessment of systolic and diastolic function of both ventricles are not present in a considerable number of individuals with moderate, severe, and advanced EMF, non-conventional measurements and indices have been used to evaluate ventricular function. The standardized criteria for diagnosis and classification of EMF may support better understanding of its pathogenesis and natural history, and allow comparison of affected individuals in different endemic areas.

Author Contributions

Conception and design of the research, acquisition of data, analysis and interpretation of the data, writing of the manuscript, critical revision of the manuscript for intellectual content: Mocumbi A.

Potential Conflict of Interest

No potential conflict of interest relevant to this article was reported.

Sources of Funding

There were no external funding sources for this study.

Study Association

This study is not associated with any thesis or dissertation work.

Ethics Approval and Consent to Participate

This article does not contain any studies with human participants or animals performed by any of the authors.

References

1. Mocumbi AO, Falase AO. Recent Advances in the Epidemiology, Diagnosis and Treatment of Endomyocardial Fibrosis in Africa. Heart. 2013;99(20):1481-7. doi: 10.1136/heartjnl-2012-303193.
2. Lachaud M, Lachaud C, Sidi D, Menete A, Jouven X, Marijon E, et al. Tropical Endomyocardial Fibrosis: Perspectives. Ann Cardiol Angeiol (Paris). 2018;67(2):74-81. doi: 10.1016/j.ancard.2018.01.001.
3. Mocumbi AO, Sidi D, Vouhe P, Yacoub M. An Innovative Technique for Tte Relief of Right Ventricular Trabecular Cavity Obliteration in Endomyocardial Fibrosis. J Thorac Cardiovasc Surg. 2007;134(4):1070-2. doi: 10.1016/j.jtcvs.2007.04.062.
4. Fiore A, Grande AM, Pellegrini C, Viganò M, Massetti M. Long-Term Survival Following Surgery for Endomyocardial Fibrosis. J Card Surg. 2013;28(6):675-7. doi: 10.1111/jocs.12159.
5. Mocumbi AO, Carrilho C, Sarathchandra P, Ferreira MB, Yacoub M, Burke M. Echocardiography Accurately Assesses the Pathological Abnormalities of Chronic Endomyocardial Fibrosis. Int J Cardiovasc Imaging. 2011;27(7):955-64. doi: 10.1007/s10554-010-9753-6.
6. Mocumbi AO, Ferreira MB, Sidi D, Yacoub MH. A Population Study of Endomyocardial Fibrosis in a Rural Area of Mozambique. N Engl J Med. 2008;359(1):43-9. doi: 10.1056/NEJMoa0708629.
7. Mbanze J, Cumbane B, Jive R, Mocumbi A. Challenges in Addressing the Knowledge Gap on Endomyocardial Fibrosis Through Community-Based Studies. Cardiovasc Diagn Ther. 2020;10(2):279-88. doi: 10.21037/cdt.2019.08.07.
8. Salemi VM, Rochitte CE, Barbosa MM, Mady C. Images in Cardiology. Clinical and Echocardiographic Dissociation in a Patient with Right Ventricular Endomyocardial Fibrosis. Heart. 2005;91(11):1399. doi: 10.1136/hrt.2005.063610.
9. Gupta PN, Kunju SM, Rajan B, Koshy AG, Vishwanathan S, George PS, et al. Geographical Variation in the Clinical Presentation of Endomyocardial Fibrosis in India? Indian Heart J. 2018;70(1):56-65. doi: 10.1016/j.ihj.2016.12.015.
10. Lungu ND, Dujawara A. Complications of Endomyocardial Fibrosis and Their Physiological Compromise: a Review. Curr Probl Cardiol. 2023;48(8):101730. doi: 10.1016/j.cpcardiol.2023.101730.
11. Berdnikov A, Roifman I, Tang E, Muhtaseb O, Chenkin J. Structured Cardiac Assessment Outperforms Visual Estimation in Novice Ultrasound Users: a Randomized Controlled Trial. J Emerg Med. 2023;65(6):e563-7. doi: 10.1016/j.jemermed.2023.05.018.
12. Alsoos F, Almobarak M, Shebli H. Right Ventricular Outflow Tract Systolic Excursion: a Useful Method for Determining Right Ventricular Systolic Function. J Echocardiogr. 2014;12(4):151-8. doi: 10.1007/s12574-014-0229-x.
13. Krittayaphong R, Boonyasirinant T, Saiviroonporn P, Thanapiboonpol P, Nakyen S, Udompunturak S. Correlation Between NT-Pro BNP Levels and Left Ventricular Wall Stress, Sphericity Index and Extent of Myocardial Damage: a Magnetic Resonance Imaging Study. J Card Fail. 2008;14(8):687-94. doi: 10.1016/j.cardfail.2008.05.002.
14. Grimaldi A, Mocumbi AO, Freers J, Lachaud M, Mirabel M, Ferreira B, et al. Tropical Endomyocardial Fibrosis: Natural History, Challenges, and Perspectives. Circulation. 2016;133(24):2503-15. doi: 10.1161/CIRCULATIONAHA.115.021178.
15. Moraes F, Lapa C, Hazin S, Tenorio E, Gomes C, Moraes CR. Surgery for Endomyocardial Fibrosis Revisited. Eur J Cardiothorac Surg. 1999;15(3):309-12. doi: 10.1016/s1010-7940(99)00027-5.
16. Oh J, Kim SH, Youn JC, Choi BW, Kang SM. Endomyocardial Fibrosis: Evaluation with Myocardial Contrast Echocardiography and Magnetic Resonance Imaging. Can J Cardiol. 2012;28(5):612.e11-2. doi: 10.1016/j.cjca.2012.03.004.
17. Hassan WM, Fawzy ME, Al Helaly S, Hegazy H, Malik S. Pitfalls in Diagnosis and Clinical, Echocardiographic, and Hemodynamic Findings in Endomyocardial Fibrosis: a 25-Year Experience. Chest. 2005;128(6):3985-92. doi: 10.1378/chest.128.6.3985.

My Approach to Patent Foramen Ovale Closure

Fernando Melo Netto,[1,2] *Maria Estefânia Bosco Otto*[1,3]
Hospital DF Star, Rede D'Or São Luiz,[1] *Brasília, DF – Brazil*
Hospital Sírio-Libanês,[2] *Brasília, DF – Brazil*
Instituto de Cardiologia e Transplante do Distrito Federal,[3] *Brasília, DF – Brazl*

Central Illustration: Echocardiographic Analysis for Diagnosis, Risk Stratification, and Planning of Percutaneous PFO Closure

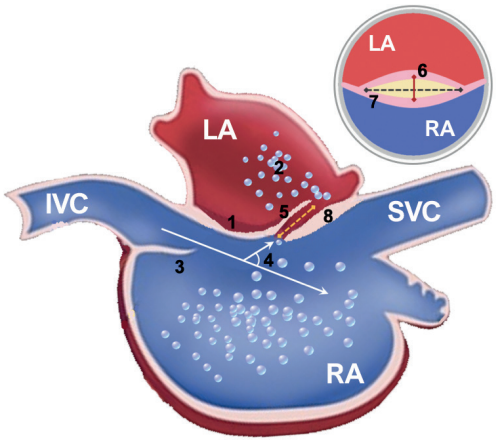

1. Aneurysm/hypermobility of the interatrial septum
2. Magnitude of the right-to-left shunt
3. Eustachian valve
4. Angle between the IVC and the PFO tunnel
5. Tunnel length
6. Tunnel height
7. Tunnel width
8. Thickness of the septum secundum

Arq Bras Cardiol: Imagem cardiovasc. 2024;37(1):e20230103

Schematic representation of the bicaval echocardiographic projection (lower figure on the left) and "en face" view of the PFO (upper figure on the right). IVC: inferior vena cava; LA: left atrium; PFO: patent foramen ovale; RA: right atrium; SVC: superior vena cava. White lines: angle between the IVC and the PFO tunnel. Yellow line: PFO tunnel length. Red line: PFO tunnel height. Black line: PFO tunnel width.

Abstract

The patent foramen ovale (PFO), a relatively common and generally benign finding, has been associated with paradoxical embolisms. The closure of PFO, performed in patients with cryptogenic stroke, has been shown to reduce the recurrence rates of ischemic events, as evidenced by recent clinical trials. In this article, the authors synthesize the crucial role played by echocardiography in this context, from diagnosis and risk stratification to planning and monitoring of percutaneous intervention.

Introduction

Patent foramen ovale (PFO), a remnant of fetal circulation, is prevalent in 25% of the population.[1] The presence of PFO has often been associated with paradoxical embolism or local thrombus formation, with consequent embolic ischemic stroke.[1] However, due to the high prevalence of PFO in the population, the cause-effect correlation with ischemic stroke remains controversial.

Older randomized studies with PFO closure did not show benefits compared to antiplatelet or anticoagulation therapy in the prevalence of ischemic stroke.[2-4] Recently, new studies[5-7] and reevaluation of the RESPECT[8] study concluded that percutaneous PFO closure is beneficial for reducing cryptogenic ischemic stroke, without increasing the risk of serious complications (Table 1). Thaler et al. identified an improvement in the characterization of ischemic stroke related to PFO using a clinical risk score, named RoPE (Risk of Paradoxical Embolism), which takes into account age; presence of risk factors such as diabetes, hypertension, and smoking; and type of image found on skull tomography (Table 2), where scores greater than 7 indicate the ischemic stroke-PFO association.[9]

Combined with the RoPE score, the high-risk anatomical characteristics of PFO must be evaluated.[10,11] In a meta-analysis of 6 studies, the RoPE score was associated with the anatomical-clinical risk classification named PASCAL (PFO-Associated Stroke Causal Likelihood) (Table 3). The application of this classification system, proposed by Kent et al.,[12] has the potential to guide individualized decision-

Keywords

Brain Ischemia; Foramen Ovale

Mailing Address: Fernando Melo Netto •
Hospital Sirio-Libanês Brasília. SGAS 613, s/n 94, Via L2 Sul. Postal code: 70200-730. Brasília, DF – Brazil
E-mail: fermnetto@gmail.com
Manuscript received November 14,2023; revised November 17, 2023; accepted November 17, 2023.
Editor responsible for the review: Daniela do Carmo Rassi Frota

DOI: https://doi.org/10.36660/abcimg.20230103i

Contents

Table 1 – Summary of the results of multicenter studies on percutaneous PFO closure compared to medical treatment

	Number of patients	Result	High-risk PFO (%)	Relative risk 95% CI	P	NNT/years
Closure I (2012)[2]	909	Negative	42.7	1.48 (0.36 to 6.14)	0.53	----
PC (2013)[3]	414	Negative	37.2	0.59 (0.06 to 6.15)	0.558	----
RESPECT (2017)[8]	980	Positive	63.2	0.29 (0.13 to 0.69)	0.002	43/5
REDUCE (2017)[6]	664	Positive	41.1	0.08 (0.01 to 0.52)	<0.001	33/3
CLOSE (2017)[5]	653	Positive	100	0.05 (0.00 to 0.88)	0.002	20/5.3
DEFENSE PFO (2018)[7]	120	Positive	100	0.07 (0.00 to 0.26)	0.13	10/2.1

Closure I: Evaluation of the STARFlex Septal Closure System in Patients With a Stroke and/or Transient Ischemic Attack to Presumed Paradoxical Embolism Through a Patent Foramen Ovale; PC: Clinical Trial Comparing Percutaneous Closure of PFO Using the Amplatzer PFO Occluder With Medical Treatment in Patients With Cryptogenic Embolism; RESPECT: Randomized Evaluation of Recurrent Stroke Comparing PFO Closure to Establish Current Standard of Care Treatment; REDUCE: PFO closure with the Gore Septal Occluder ; CLOSE, Patent Foramen Ovale Closure or Anticoagulants Versus Antiplatelet Therapy to Prevent Stroke Recurrence; DEFENSE-PFO, Device Closure Versus Medical Therapy for Cryptogenic Stroke Patients with High-Risk Patent Foramen Ovale. CI: confidence interval; NNT: number needed to treat; PFO: patent foramen ovale. Adapted from Song, 2023.[15]

making. Despite these relevant clinical and structural data, which make it possible to expand percutaneous treatment, the indication for PFO closure according to the neurology guidelines[13] is restricted to patients with proven embolic ischemic stroke, between 18 and 60 years of age, with high-risk anatomical and functional characteristics. More recently, the Society for Cardiovascular Angiography and Interventions guidelines[14] expanded the recommendation of PFO closure to proven hypoxemia in platypnea-orthodeoxia syndrome, patients with systemic embolism and PFO without another cause, and patients over 60 years of age with proven embolic ischemic stroke without other causes. However, these last recommendations have a low level of evidence.

Echocardiography is fundamental for diagnosis, risk stratification, and monitoring of PFO closure. The anatomical characteristics of PFO will be described, with the main criteria for high anatomical risk and recommendations for adequate monitoring of percutaneous closure.

Diagnosis

Transthoracic echocardiography

Diagnosis of PFO by transthoracic echocardiography must be carried out while injecting agitated saline solution and performing the Valsalva maneuver. Color Doppler alone, even at low speeds, has low sensitivity because pressure equalization may occur between the atria with the absence of shunt at the time of the examination. Blood flow through the inferior vena cava favors the passage of macrobubbles through the PFO. In this sense, lower limb venipuncture may be useful if the suspicion of PFO is high and the passage of macrobubbles does not occur with conventional puncture in the arm. The preparation of macrobubbles must be adequate; the Valsalva maneuver must be effective, and multiple infusions of agitated saline solution are recommended to make the diagnosis more sensitive.[15] Nonetheless, transthoracic echocardiography with agitated saline infusion is an indirect diagnostic method that is not capable of describing the anatomy of the septum and the PFO.

Table 2 – RoPE score

Characteristic	Points
No history of	
Hypertension	1
DM	1
Stroke or TIA	1
Non-smoker	1
Proven cortical infarct	1
Age (years)	
18-29	5
30-39	4
40-49	3
50-59	2
60-69	1
>70	0

DM: diabetes mellitus; TIA: transient ischemic attack. A sum above 7 points indicates greater likelihood of cerebral ischemia due to PFO. Adapted from Thaler et al.9

Transesophageal echocardiogram

Transesophageal echocardiography offers excellent visualization of the interatrial septum, identifying the separation of the laminae of the septum primum and secundum and septal thickness. Using color Doppler at low speeds in the region of the foramen ovale, it is possible, in some cases, to identify the right-to-left flow. Even so, it is necessary to infuse agitated saline as in the transthoracic echocardiogram and to perform the Valsalva maneuver to separate the laminae of the interatrial septum, thus identifying the shunt. Adequate filling of the right atrium with macrobubbles and identification of movement of the septum towards the left atrium, with increased intra-abdominal pressure, determine the appropriate technique. The flow of macrobubbles must be monitored in the pulmonary veins to rule out extracardiac shunts (in which case the macrobubbles take more than 5 beats to opacify the left atrium and are visualized in the pulmonary veins).[15]

PFO risk stratification: essential measures and findings for defining high risk

- PFO height[10,11] (Figure 1A): greater separation of the laminae of the septum primum and secundum > 2 mm.
- Tunnel length[10,11] (Figure 1A): tunnel extension ≥ 10 mm.
- Angle between the inferior vena cava and the PFO[10] (Figure 1B): angle ≤ 10°.
- Mobility of the interatrial septum:[10,11] definition of an aneurysm, when the septal excursion is ≥ 10 mm from the septal plane or ≥ 15 mm in both directions (Video 1A).
- Prominent Chiari network and redundant Eustachian valve measuring ≥ 10 mm.
- Number of macrobubbles that pass into the left atrium (Video 1B): ≥ 20 macrobubbles.[12]

Nakayama et al.[10] described a risk score based on the parameters described above and displayed in Table 4, where a score greater than or equal to 2 points is associated with a significant risk of ischemic stroke. This assists in therapeutic decision-making, in addition to alerting to possible complications during the procedure.

Monitoring the procedure: planning and choice of prosthesis

Percutaneous PFO closure is performed with the implantation of a double-disc device in the interatrial septum. Two versions of specific prostheses exist: one with discs with different diameters, where the right disc has a larger diameter (Figure 2D), and another version with discs of equal diameters, similar to cribriform prostheses for multi-fenestrated atrial septal defect. In both versions, the waist is extremely thin, in order to avoid deformation of the PFO tunnel.

Transesophageal echocardiographic monitoring is recommended for safety, efficacy, and evaluation of the final result of the procedure.[16] In conjunction with fluoroscopy, transesophageal echocardiography allows visualization of catheters, guidewires, and the prosthesis. The use of the 3-dimensional modality better details the position of the device and its spatial relationship with adjacent cardiac structures. The guidance and information provided by

Table 3 – PASCAL score (the extended PFO-Associated Casual Likelihood Classification System)

Risk	Characteristics	Casual likelihood	
		Low RoPE score (<7)	High RoPE score (≥7)
Very high	Thrombus extending through the PFO	Definitive	Definitive
High	– PFO with aneurysm or large shunt – Pulmonary embolism or DVT before ischemia	Likely	Highly likely
Medium	– PFO + aneurysm – Large shunt through the PFO	Possible	Likely
Low	– Small shunt – Absence of aneurysm	Unlikely	Possible

DVT: deep vein thrombosis; PFO: patent foramen ovale; RoPE: risk of paradoxical embolism. Adapted from Thaler et al.[9]

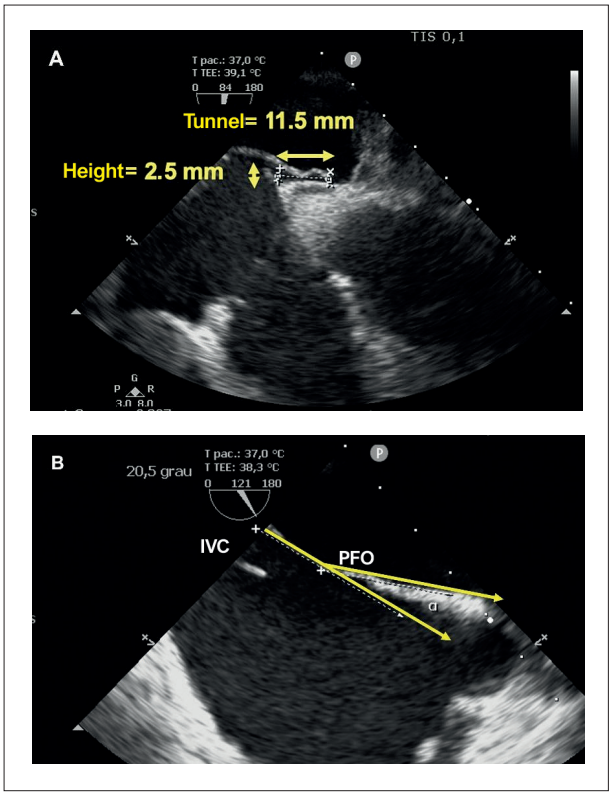

Figure 1 – *Main measurements for risk assessment of PFO: A) PFO height and tunnel length. B) Angle between the inferior vena cava (IVC) and the PFO. Figures produced by Maria Estefânia Bosco Otto using Echonova's company image bank. IVC: inferior vena cava; PFO: patent foramen ovale.*

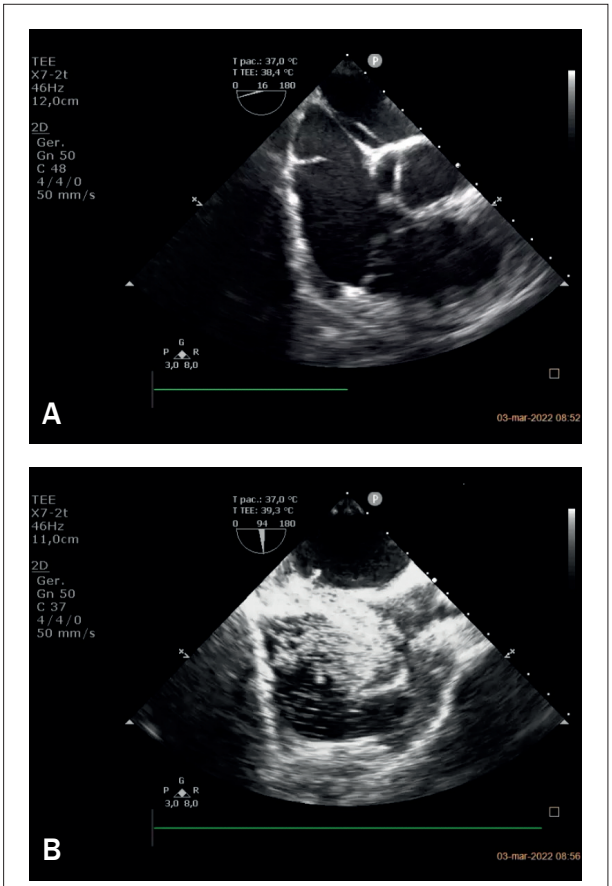

Video 1 – *Septal mobility and passage of macrobubbles. A) Septal mobility before macrobubble infusion. B) Passage of more than 20 bubbles from the right atrium to the left atrium. Video edited by Maria Estefânia Bosco Otto using Echonova's company image bank. Links: http://abcimaging.org/supplementary-material/2024/3701/2023-0103_AR_video1A.mp4 and http://abcimaging.org/supplementary-material/2024/3701/2023-0103_AR_video1B.mp4.*

Table 4 – PFO risk score

Variable	Points
Long tunnel ≥ 10 mm	1
Hypermobility of the interatrial septum	1
Prominent Chiari network or Eustachian valve	1
Large shunt with Valsalva maneuver (≥ 20 bubbles)	1
Angle between the IVC and PFO ≤ 10°	1

Score ≥ 2 considered high risk. IVC: inferior vena cava; PFO: patent foramen ovale. Adapted from Nakayama, 2019.[10]

transesophageal echocardiography are crucial for the various steps of the procedure (Figure 2; Video 2), which include the following:[17,18]

I. Crossing the PFO with a multipurpose catheter (Figure 2A).
II. Introduction of the sheath into the left atrium through the PFO, using a rigid guidewire positioned in the left superior pulmonary vein.
III. Loading and advancing the occluder prosthesis. Exposure and opening of the left disc (Figure 2B), which is retracted until it is seated on the left side of the interatrial septum. This is followed by the opening of the right disc in the right atrium (Figure 2C). The correct positioning of the device is checked, ensuring parallelism between the two discs, which must be visualized surrounding the septum. Systematic assessment of the device edges rules out interference with adjacent structures, such as the mitral valve, coronary sinus, aorta, and posterior wall of the atria. Color Doppler allows verification of possible persistence of a residual shunt on the edges of the device or inside it.
IV. The "wiggle maneuver," carried out by a careful movement, pushing and pulling the device, which is still connected to the delivery cable, to guarantee that the right disc and left disc do not shift into the contralateral chamber.[19]
V. Prosthesis release (Figure 2D).

For the treatment to be successful, in the hemodynamics laboratory, adequate interaction and communication are indispensable between the interventionist and the echocardiographer, who must provide accurate information on the anatomy of the interatrial septum and the dimensions of the PFO. Nonetheless, standardization is still lacking to determine the appropriate size of the occluder device.[20] Furthermore, the nomenclature to describe the size of the PFO is still not uniform, and it is often based solely on 2-dimensional images.[21,22] Recently, Datta and et al.[23] proposed a standardization of terminologies for PFO dimensions, as follows:

- **Tunnel length** (Figure 1A): distance between the opening of the foramen ovale in the right atrium and the left atrium.
- **Tunnel height** (Figure 1A): separation between the septum primum and septum secundum (minor axis of the oval opening).
- **Tunnel width** (Figure 3): size of the openings in the right atrium and left atrium, seen when viewing the PFO *en face* (major axis of the oval opening).

The width of the PFO tunnel is a crucial indicator, most appropriately assessed with 3-dimensional images. *En face* visualization of the PFO by 3-dimensional transesophageal echocardiography makes accurate assessment of the dimensions possible, and it may be particularly useful in cases of variant anatomy, such as double-orifice tunnels.

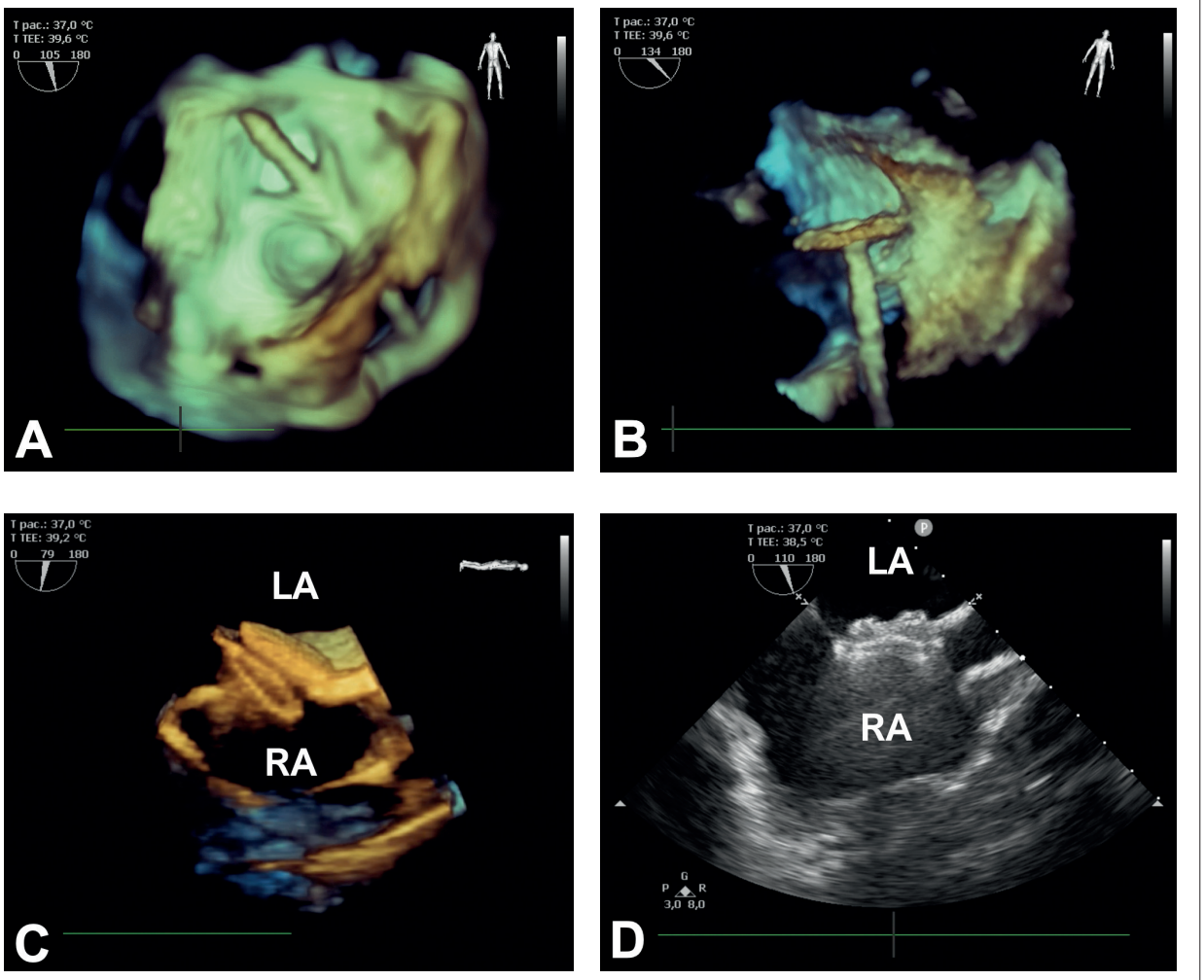

Figure 2 – *Monitoring of percutaneous closure (Video 2): A) Introduction of a catheter into the left atrium (LA) through the PFO. B) Opening of the left disc of the prosthesis in the LA. C) Opening of the right disc in the right atrium (RA), with delivery cable connected to the prosthesis. D) Final appearance after releasing the double-disc prosthesis appropriate for PFO closure (right disc larger than the left disc). Figures produced by Fernando Melo Netto using Echonova's company image bank. LA: left atrium; RA: right atrium.*

For device selection, some operators and manufacturers recommend balloon sizing, which aims to transform the elliptical shape of the PFO into a circular defect, where the diameter of the balloon waist approximates the width of the tunnel as assessed by 3-dimensional transesophageal echocardiography;[20] however, it is essential to avoid excessively stretching the PFO or damaging the interatrial septum with balloon inflation.[24] Recent instructions for the most widely used occluder (Amplatzer-PFO)[25] recommend the choice of larger prostheses according to the length of the tunnel, the presence of aneurysm, and thickness of the septum secundum (Table 5). Nonetheless, in the experience of several authors,[22,23,26] the width of the PFO tunnel is the best parameter to guide selection of device size. In this approach, it is important for the diameter of the right disc of the prosthesis to exceed the width of the tunnel in the right atrium. If the diameter of the disc is

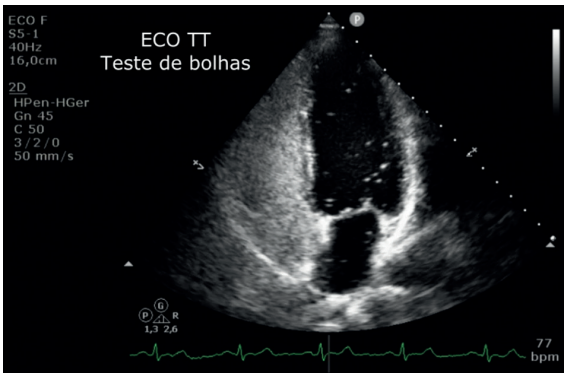

Video 2 – *PFO, from diagnosis to closure. Case of a young patient with cerebral ischemia. Video edited by Fernando Melo Netto using Echonova's company image bank. L. O. C., female 38 years old 2 episodes of stroke Link: http://abcimaging.org/supplementary-material/2024/3701/2023-0103_AR_video2.mp4*

smaller, there is a risk of thrombi penetrating through the margins of the device.

In addition to the PFO dimensions, it is essential to measure the anteroposterior diameter of the interatrial septum (midesophageal view of approximately 45°), in order to ensure that the disk can be adequately accommodated without impinging on surrounding cardiac structures, especially the posterior atrial wall or the aortic sinuses.[23]

In situations where visualization of the tunnel is difficult due to the absence of separation between the septum primum and secundum, measurements must be performed during the percutaneous procedure, after the introduction of a guidewire or catheter through the tunnel, inducing mechanical separation of the septa and allowing a more precise assessment of PFO dimensions[26] (Figure 3).

Intracardiac echocardiography is an alternative to transesophageal echocardiography during the procedure. Nonetheless, it has limitations, such as the cost of disposable probes, the need for specific training, potential risks related to femoral puncture, and the impossibility of multiplanar or 3-dimensional assessments, which impairs the measurement of the width of the PFO tunnel.

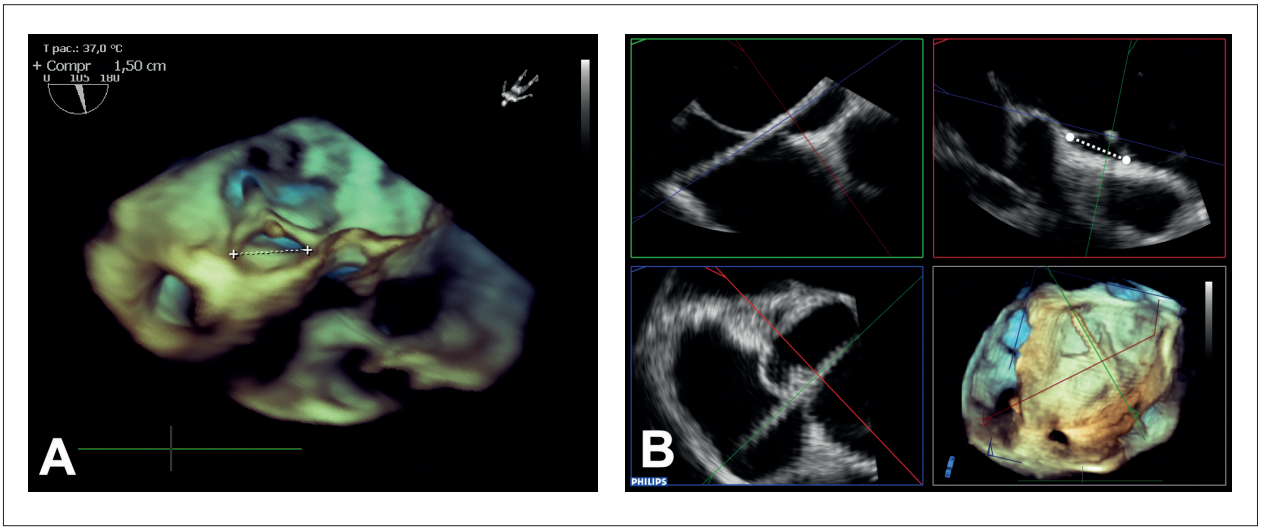

Figure 3 – *Measurement of the width of the PFO tunnel using 3-dimensional transesophageal echocardiography: A) En face view of the PFO tunnel from the left atrium, after introduction of the catheter. The width of the tunnel corresponds to the dotted white line. B) Multiplanar reconstruction of the same image block to obtain PFO width. Figures produced by Fernando Melo Netto using Echonova's company image bank.*

Table 5 – Recommendations for device dimensions

PFO morphology	Anatomical characteristics	Suggested Amplatzer™ Talisman™ occluder size
Simple PFO or PFO without prominent ASA PFO in which a secure device position and effective closure can be achieved when using the 25-mm device	1. Absence of ASA, long tunnel, and thickening of the septum secundum 2. Non-prominent ASA (total excursion < 20 mm) without long tunnel (≥ 10 mm in length), and without thickening of the septum secundum (≥ 10 mm in thickness)	25
Complex PFO PFO with one or more anatomical features that may complicate the ability to achieve safe device position and effective PFO closure when using the 25-mm device	1. ASA (excursion ≥ 10 mm) with a long tunnel (≥ 10 mm long) 2. ASA (excursion ≥ 10 mm) with thickening of the septum secundum (thickness ≥ 10 mm) 3. Prominent ASA with excessive mobility (total excursion ≥ 20 mm) 4. Lipomatous hypertrophy of the septum secundum (≥ 15 mm thick)	30 or 35
PFO with small anatomy Anatomy that is not appropriate for 25-mm device due to interference with adjacent cardiac structures	Septum primum length < 20 mm	18

ASA: atrial septal aneurysm; PFO: patent foramen ovale. Adapted from Abbott Laboratories. Amplatzer Talisman PFO Occluder Instructions for Use.[25]

In most cases, the PFO has a typical anatomy that allows for effective and uncomplicated closure. Occasionally, specific characteristics of the septum make the procedure more complex and may increase the failure rate, for example: interatrial septal aneurysm; presence of multiple accessory fenestrations; long, rigid tunnel; lipomatous and hypertrophic septum secundum; prominent Eustachian valve and/or Chiari network; or misalignment of the interatrial septum ("spiral septum" or "double septum").[17]

In cases of aneurysm and/or hypermobility where there is significant separation (above 8 mm) between the septum primum and secundum, it is necessary to use a balloon to measure the stretched diameter of the tunnel. If it is equal to or greater than 13 mm, self-centering devices (with wide waists, for occlusion of interatrial communication) are preferable to non-self-centering devices (with a thin waist), due to the lower risk of residual shunt.[27,28]

The presence of multiple fenestrations may require the implantation of several devices.[29] When there is no predominant defect, the preferred approach aims to cross the central defect and implant a thin-waisted device (cribriform prosthesis) to cover the peripheral fenestrations, depending on the distance between them and adjacent cardiac structures.

Suspicion of an excessively rigid and long septum primum (over 8 mm) arises when the tunnel opens less than 4 mm after the introduction of a guidewire or catheter, in which case the device may not seat properly. The frequently used technique is the implantation of the prosthesis through a transseptal puncture close to the tunnel opening, allowing adequate compression and positioning of the discs.[30]

A septum secundum thicker than 7 mm is classified as hypertrophic. Mild hypertrophies do not usually complicate the procedure. However, if the thickness is greater than 15 mm, the risk of failure increases significantly. The use of a ventricular septal defect occluder prosthesis can obtain success.[31]

A prominent Eustachian valve, which interferes with the compression of the right disc against the interatrial septum, can be displaced with a pigtail catheter to help accommodate the device.[32]

Complications

The use of transesophageal echocardiography is fundamental in assisting diagnosis, in therapeutic monitoring, and also in preventing and detecting immediate complications, including the following: assessment of mitral valve competence and patency of the coronary sinus, formation of intracardiac thrombi, early device embolization, and positioning of wires and catheters, thus avoiding perforation of the left atrial appendage, pericardial effusion, and cardiac tamponade.[17,33-35]

The frequency and appropriate timing for echocardiographic monitoring still generate uncertainty. As most devices are endothelialized in approximately 6 months, a bubble study may be considered at the end of this period, when the success rate is approximately 95%.[35] The results support the feasibility and safety of percutaneous closure, with no evidence of an increase in serious adverse events. Late complications, although rare, include device thrombosis, erosion of adjacent structures, prosthesis embolization, and endocarditis.[36,37]

Arrhythmic complications, such as atrial fibrillation and flutter, have an incidence of approximately 3%. This can be attributed, in part, to manipulation of the catheter, passage of wires into the left atrium, and stretching of the atrial wall with the device. Atrial fibrillation generally manifests within the first 45 days after implantation, and it is a transient phenomenon in 76% of cases.[38]

Conclusions

Percutaneous PFO closure has evolved with remarkable advances, driven by recent studies that support its benefits in preventing cryptogenic ischemic stroke. Risk stratification, considering clinical and anatomical aspects, together with the evolution of echocardiography, plays a crucial role in adequate patient selection and device choice. The need for strict monitoring, comprehension of potential complications, and careful assessment of individual characteristics are essential to optimize long-term outcomes. Ultimately, close collaboration between neurologists and cardiologists (clinicians, echocardiographers, and interventionalists) is fundamental to the success of the procedure and patient safety.

Author Contribution

Writing of the manuscript; critical revision of the manuscript for intellectual content; acquisition of images and video: Netto FM; Otto MEB.

Potential Conflict of Interest

No potential conflict of interest relevant to this article was reported.

Sources of Funding

There were no external funding sources for this study.

Study Association

This study is not associated with any thesis or dissertation work.

Ethics Approval and Consent to Participate

This article does not contain any studies with human participants or animals performed by any of the authors.

References

1. Koutroulou I, Tsivgoulis G, Tsalikakis D, Karacostas D, Grigoriadis N, Karapanayiotides T. Epidemiology of Patent Foramen Ovale in General Population and in Stroke Patients: a Narrative Review. Front Neurol. 2020;11:281. doi: 10.3389/fneur.2020.00281.
2. Furlan AJ, Reisman M, Massaro J, Mauri L, Adams H, Albers GW, et al. Closure or Medical Therapy for Cryptogenic Stroke with Patent Foramen Ovale. N Engl J Med. 2012;366(11):991-9. doi: 10.1056/NEJMoa1009639.
3. Meier B, Kalesan B, Mattle HP, Khattab AA, Hildick-Smith D, Dudek D, et al. Percutaneous Closure of Patent Foramen Ovale in Cryptogenic Embolism. N Engl J Med. 2013;368(12):1083-91. doi: 10.1056/NEJMoa1211716.
4. Carroll JD, Saver JL, Thaler DE, Smalling RW, Berry S, MacDonald LA, et al. Closure of Patent Foramen Ovale Versus Medical Therapy after Cryptogenic Stroke. N Engl J Med. 2013;368(12):1092-100. doi: 10.1056/NEJMoa1301440.
5. Mas JL, Derumeaux G, Guillon B, Massardier E, Hosseini H, Mechtouff L, et al. Patent Foramen Ovale Closure or Anticoagulation vs. Antiplatelets after Stroke. N Engl J Med. 2017;377(11):1011-21. doi: 10.1056/NEJMoa1705915.
6. Søndergaard L, Kasner SE, Rhodes JF, Andersen G, Iversen HK, Nielsen-Kudsk JE, et al. Patent Foramen Ovale Closure or Antiplatelet Therapy for Cryptogenic Stroke. N Engl J Med. 2017;377(11):1033-42. doi: 10.1056/NEJMoa1707404.
7. Lee PH, Song JK, Kim JS, Heo R, Lee S, Kim DH, et al. Cryptogenic Stroke and High-Risk Patent Foramen Ovale: the DEFENSE-PFO Trial. J Am Coll Cardiol. 2018;71(20):2335-42. doi: 10.1016/j.jacc.2018.02.046.
8. Saver JL, Carroll JD, Thaler DE, Smalling RW, MacDonald LA, Marks DS, et al. Long-Term Outcomes of Patent Foramen Ovale Closure or Medical Therapy after Stroke. N Engl J Med. 2017;377(11):1022-32. doi: 10.1056/NEJMoa1610057.
9. Thaler DE, Di Angelantonio E, Di Tullio MR, Donovan JS, Griffith J, Homma S, et al. The Risk of Paradoxical Embolism (Rope) Study: Initial Description of the Completed Database. Int J Stroke. 2013;8(8):612-9. doi: 10.1111/j.1747-4949.2012.00843.x.
10. Nakayama R, Takaya Y, Akagi T, Watanabe N, Ikeda M, Nakagawa K, et al. Identification of High-Risk Patent Foramen Ovale Associated with Cryptogenic Stroke: Development of a Scoring System. J Am Soc Echocardiogr. 2019;32(7):811-6. doi: 10.1016/j.echo.2019.03.021.
11. Hołda MK, Krawczyk-Ożóg A, Koziej M, Kołodziejczyk J, Sorysz D, Szczepanek E, et al. Patent Foramen Ovale Channel Morphometric Characteristics Associated with Cryptogenic Stroke: the MorPFO Score. J Am Soc Echocardiogr. 2021;34(12):1285-93. doi: 10.1016/j.echo.2021.07.016.
12. Kent DM, Saver JL, Kasner SE, Nelson J, Carroll JD, Chatellier G, et al. Heterogeneity of Treatment Effects in an Analysis of Pooled Individual Patient Data from Randomized Trials of Device Closure of Patent Foramen Ovale After Stroke. JAMA. 2021;326(22):2277-86. doi: 10.1001/jama.2021.20956.
13. Messé SR, Gronseth GS, Kent DM, Kizer JR, Homma S, Rosterman L, et al. Practice Advisory Update Summary: Patent Foramen Ovale and Secondary Stroke Prevention: Report of the Guideline Subcommittee of the American Academy of Neurology. Neurology. 2020;94(20):876-85. doi: 10.1212/WNL.0000000000009443.
14. Kavinsky CJ, Szerlip M, Goldsweig AM, Falck-Ytter Y, Babatunde I, Morgan RL. SCAI Guidelines for the Management of Patent Foramen Ovale. JSCAI. 2022;1(4):1-15. doi: 10.1016/j.jscai.2022.100039.
15. Song JK. Pearls and Pitfalls in the Transesophageal Echocardiographic Diagnosis of Patent Foramen Ovale. J Am Soc Echocardiogr. 2023;36(9):895-905.e3. doi: 10.1016/j.echo.2023.05.004.
16. Davison P, Clift PF, Steeds RP. The Role of Echocardiography in Diagnosis, Monitoring Closure and Post-Procedural Assessment of Patent Foramen Ovale. Eur J Echocardiogr. 2010;11(10):i27-34. doi: 10.1093/ejechocard/jeq120.
17. Sperlongano S, Giordano M, Ciccarelli G, Bassi G, D'Aquino MMC, Del Giudice C, et al. Advances in Percutaneous Patent Foramen Ovale Closure: from the Procedure to the Echocardiographic Guidance. J Clin Med. 2022;11(14):4001. doi: 10.3390/jcm11144001.
18. Agricola E, Meucci F, Ancona F, Sanz AP, Zamorano JL. Echocardiographic Guidance in Transcatheter Structural Cardiac Interventions. EuroIntervention. 2022;17(15):1205-26. doi: 10.4244/EIJ-D-21-00582.
19. Vitarelli A. Patent Foramen Ovale: Pivotal Role of Transesophageal Echocardiography in the Indications for Closure, Assessment of Varying Anatomies and Post-procedure Follow-up. Ultrasound Med Biol. 2019;45(8):1882-95. doi: 10.1016/j.ultrasmedbio.2019.04.015.
20. Kumar P, Rusheen J, Tobis JM. A Comparison of Methods to Determine Patent Foramen Ovale Size. Catheter Cardiovasc Interv. 2020;96(6):E621-9. doi: 10.1002/ccd.28665.
21. Rana BS, Shapiro LM, McCarthy KP, Ho SY. Three-Dimensional Imaging of the Atrial Septum and Patent Foramen Ovale Anatomy: Defining the Morphological Phenotypes of Patent Foramen Ovale. Eur J Echocardiogr. 2010;11(10):i19-25. doi: 10.1093/ejechocard/jeq122.
22. Tanaka J, Izumo M, Fukuoka Y, Saitoh T, Harada K, Harada K, et al. Comparison of Two-Dimensional Versus Real-Time Three-Dimensional Transesophageal Echocardiography for Evaluation of Patent Foramen Ovale Morphology. Am J Cardiol. 2013;111(7):1052-6. doi: 10.1016/j.amjcard.2012.12.024.
23. Datta T, Ruggiero N, Peters A, Pender A, Vishnevsky A, Mehrotra P. Three-dimensional Transesophageal Echocardiography for Transcatheter Patent Foramen Ovale Closure: Standardizing Anatomic Nomenclature and Novel Sizing Concepts. CASE (Phila). 2022;7(1):14-20. doi: 10.1016/j.case.2022.10.007.
24. Collado FMS, Poulin MF, Murphy JJ, Jneid H, Kavinsky CJ. Patent Foramen Ovale Closure for Stroke Prevention and Other Disorders. J Am Heart Assoc. 2018;7(12):e007146. doi: 10.1161/JAHA.117.007146.
25. Abbott Laboratories. Amplatzer Talisman PFO Occluder Instructions for Use [Internet]. Chicago: Abbott Laboratories; 2023 [cited 2023 Nov 11]. Available from: https://www.cardiovascular.abbott/int/en/hcp/products/structural-heart/structural-interventions/amplatzer-talisman.html.
26. Demulier L, Paelinck BP, Coomans I, Hemelsoet D, De Backer J, Campens L, et al. A New Dimension in Patent Foramen Ovale Size Estimation. Echocardiography. 2020;37(7):1049-55. doi: 10.1111/echo.14696.
27. Giordano M, Gaio G, Santoro G, Palladino MT, Sarubbi B, Golino P, et al. Patent Foramen Ovale with Complex Anatomy: Comparison of Two Different Devices (Amplatzer Septal Occluder Device and Amplatzer PFO Occluder Device 30/35). Int J Cardiol. 2019;279:47-50. doi: 10.1016/j.ijcard.2018.10.053.
28. Matsumura K, Gevorgyan R, Mangels D, Masoomi R, Mojadidi MK, Tobis J. Comparison of Residual Shunt Rates in Five Devices used to Treat Patent Foramen Ovale. Catheter Cardiovasc Interv. 2014;84(3):455-63. doi: 10.1002/ccd.25453.
29. Awad SM, Garay FF, Cao QL, Hijazi ZM. Multiple Amplatzer Septal Occluder Devices for Multiple Atrial Communications: Immediate and Long-Term Follow-Up Results. Catheter Cardiovasc Interv. 2007;70(2):265-73. doi: 10.1002/ccd.21145.
30. Thompson AJ, Hagler DJ, Taggart NW. Transseptal Puncture to Facilitate Device Closure of "Long-Tunnel" Patent Foramen Ovale. Catheter Cardiovasc Interv. 2015;85(6):1053-7. doi: 10.1002/ccd.25723.
31. Lin CH, Balzer DT, Lasala JM. Defect Closure in the Lipomatous Hypertrophied Atrial Septum with the Amplatzer Muscular Ventricular Septal Defect Closure Device: a Case Series. Catheter Cardiovasc Interv. 2011;78(1):102-7. doi: 10.1002/ccd.22858.

32. Magraner EM, López AD, Domingo EB, Pardeiro CA, Recalde ÁS, Aguado FGL. Incomplete Cor Triatriatum Dexter: an Unsettling Guest in the Percutaneous Closure of Atrial Septal Defects. Rev Esp Cardiol (Engl Ed). 2019;72(7):582-3. doi: 10.1016/j.rec.2018.05.036.

33. Vettukattil JJ, Ahmed Z, Salmon AP, Mohun T, Anderson RH. Defects in the Oval Fossa: Morphologic Variations and Impact on Transcatheter Closure. J Am Soc Echocardiogr. 2013;26(2):192-9. doi: 10.1016/j.echo.2012.10.019.

34. Vitarelli A, Mangieri E, Capotosto L, Tanzilli G, D'Angeli I, Toni D, et al. Echocardiographic Findings in Simple and Complex Patent Foramen Ovale before and after Transcatheter Closure. Eur Heart J Cardiovasc Imaging. 2014;15(12):1377-85. doi: 10.1093/ehjci/jeu143.

35. Giblett JP, Williams LK, Kyranis S, Shapiro LM, Calvert PA. Patent Foramen Ovale Closure: State of the Art. Interv Cardiol. 2020;15:e15. doi: 10.15420/icr.2019.27.

36. Abaci A, Unlu S, Alsancak Y, Kaya U, Sezenoz B. Short and Long Term Complications of Device Closure of Atrial Septal Defect and Patent Foramen Ovale: Meta-Analysis of 28,142 Patients from 203 Studies. Catheter Cardiovasc Interv. 2013;82(7):1123-38. doi: 10.1002/ccd.24875.

37. Krantz SB, Lawton JS. Subacute Endocarditis of an Atrial Septal Closure Device in a Patient with a Patent Foramen Ovale. Ann Thorac Surg. 2014;98(5):1821-3. doi: 10.1016/j.athoracsur.2013.12.079.

38. Elgendy AY, Elgendy IY, Mojadidi MK, Mahmoud AN, Barry JS, Jneid H, et al. New-Onset Atrial Fibrillation Following Percutaneous Patent Foramen Ovale Closure: a Systematic Review and Meta-Analysis of Randomised Trials. EuroIntervention. 2019;14(17):1788-90. doi: 10.4244/EIJ-D-18-00767.

My Approach to 3D Echocardiography in Mitral Valve Insufficiency: How and When

Fábio Cañellas[1]

Irmandade da Santa Casa de Misericórdia de Porto Alegre,[1] *Porto Alegre, RS – Brazil*

Central Illustration: My Approach to 3D Echocardiography in Mitral Valve Insufficiency: How and When

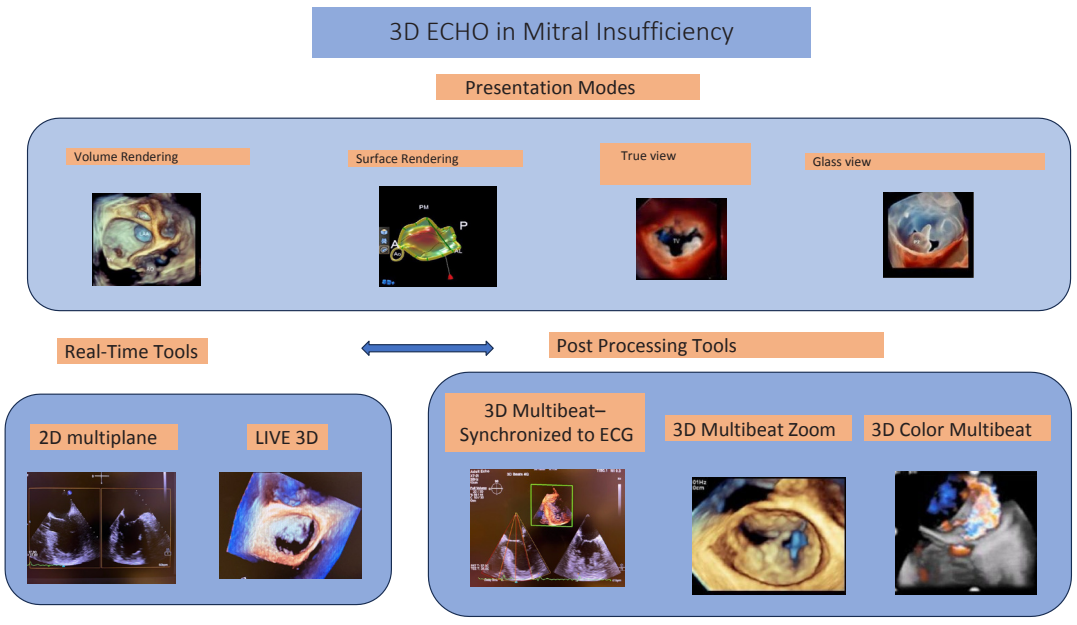

Arq Bras Cardiol: Imagem cardiovasc. 2024;37(1):e20230105

Abstract

3D Echocardiogram is an indispensable tool in all stages of mitral valve disease, from its diagnosis to the moment of treatment, playing a fundamental role mainly in the decision for surgical plasty or percutaneous correction. In this article, we sought to present very important basic concepts in the use of the technique, from obtaining a 2D image, through the main tools for obtaining 3D images, to new solutions brought by manufacturers for presenting images and for post-processing software. This knowledge is fundamental and contributes to the demystification of 3D Echo, often labeled as difficult to perform and still little incorporated into our clinical practice.

Keywords

Three-Dimensional Echocardiography; Mitral Valve Insufficiency Diagnosis

Correspondência: Fábio Cañellas •
Irmandade da Santa Casa de Misericórdia de Porto Alegre. Praca Anes Dias, S/N. Postal code: 90020-090. Porto Alegre, RS – Brazil
E-mail: canellasecocardio@gmail.com
Manuscript received November 16,2023; revised December 1, 2023; accepted December 1, 2023
Editor responsible for the review: Daniela do Carmo Rassi Frota

DOI: https://doi.org/10.36660/abcimg.20230105i

Introduction

Mitral regurgitation is the most common valvulopathy in developed countries, accounting for 2 to 3% of the population.[1] When it comes to correcting mitral insufficiency, whether surgical or percutaneous, 3D Echocardiography is the method of choice, whether to confirm the degree of reflux, or to confirm the possibility of preferential plasty treatment or, in cases where the procedure Percutaneous surgery is recommended to assess the feasibility of the procedure and assist the team during surgery.

This occurs because the 3D transesophageal method allows a perpendicular angulation between the emitted pyramidal beam and the mitral leaflets, an ideal proximity, allowing the use of high frequency, better temporal and spatial resolution, in

Contents

addition to allowing visualization of the entire valve apparatus of various angles and perspectives.

However, 3D echocardiography is no magic trick. Simply pressing a button to capture an image is not enough. The secret of 3D imaging is in an excellent capture of the two-dimensional (2D) image. There is no quality 3D exam without a good 2D echocardiographic window. Furthermore, adjustments made on a case-by-case basis are very important for obtaining excellent images and 3D data sets that can be properly manipulated offline, such as computed tomography (CT) and magnetic resonance imaging (MRI) images.

My approach to

Knowing the basic principles of 3D that influence image acquisition is essential, especially in valvular heart diseases whose regurgitant flow velocities are quite high.

Fortunately, electronic advances and miniaturization have allowed modern transesophageal probes to have approximately 2,500 piezoelectric crystals that can be activated simultaneously for imaging. This significant number of crystals allows the transducer to emit a wide beam and receive multiple smaller beams that will form the received volumes.[2] Obviously, the greater the number of beams received, the greater the chance of deterioration in image quality (signal to noise), or of a drop in temporal resolution with the appearance of stitches.

Therefore, the 2D image must always be optimized primarily. Poor 2D images result in even worse 3D images. I usually set an intermediate gain, up to 60, with intermediate compression.

As a rule, we try to optimize the 2D image and then activate the 2D multiplane mode, where the system receives the command to activate two or three lines of orthogonal crystals, which despite not presenting a 3D image, generate the simultaneous visualization of two orthogonal planes. Initially, we use the image at 0 degrees, positioning the rotation line, under which we will make the other orthogonal cuts at the level of the anterior mitral leaflet (Figure 1) (Video 1). One can then activate color Doppler, which can give us a perspective on the extent of a possible regurgitant jet.

The wide and rapid mobility of the mitral valve leaflets, often associated with the presence of structures with even greater mobility, such as vegetation, require the use of a 3D technique of high spatial and temporal resolution.

Initially, we activate, through a dedicated button (normally identified on the display as a 3D key), the analysis modality in real time, beat by beat — Real Time Single Beat or Live 3D —, capturing a volume that encompasses the entire mitral apparatus, the atrial appendage and the aortic valve, normally from a 2D section of 120°.[3] Once 3D is activated, the "in face" view is obtained, similar to the surgeon's view, with the aortic valve at 12 o'clock on the display, the appendix

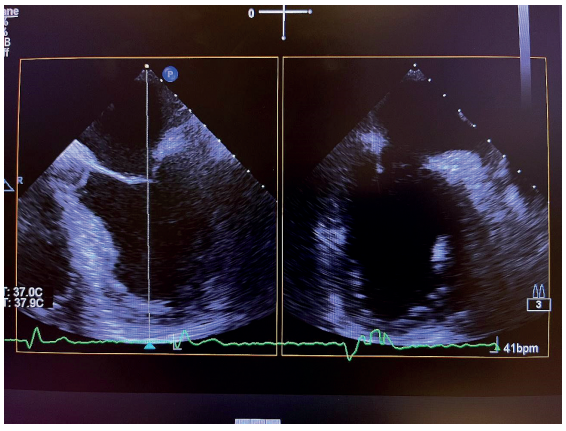

Figure 1 – *Activation of 2D Multiplane mode, with the display showing, simultaneously, 2 orthogonal planes of four and two chambers. The image can be rotated at the cursor line axis.*

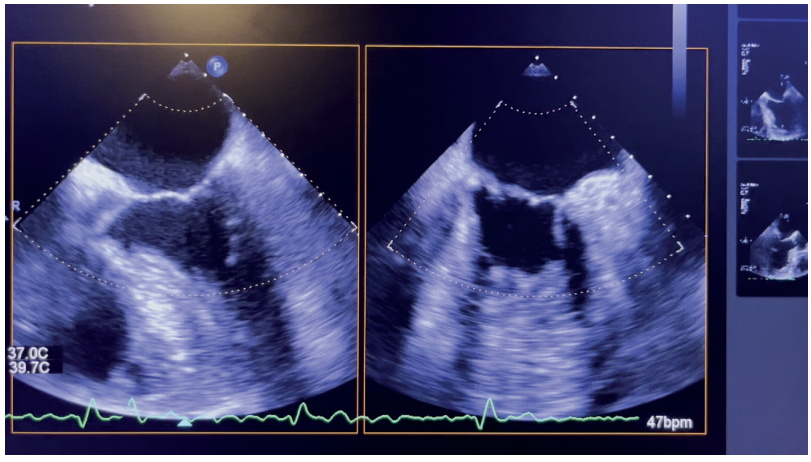

Video 1 – *2D multiplane mode activated, showing two orthogonal planes simultaneously. Link: http://abcimaging.org/supplementary-material/2024/3701/2023-0105_AR_video1_1.mp4*

at 9 o'clock and the interatrial septum at 15 o'clock (Video 2A). With this module activated, it is possible to move the 3D pyramidal block containing the mitral valve in several directions, allowing accurate anatomical visualization. You can also change the dimensions of the volumetric pyramid obtained, improving spatial and temporal resolution. Normally the acquired volume appears as a pyramidal block of 30 x 60°, which can be adjusted up to 90 x 90° (Figure 2). At this point, tangential and angled cuts allow us to accurately identify prolapses and flails, mainly.

This modality enables excellent spatial resolution, being the preferred method of analysis in patients with rhythm disturbances, mainly atrial fibrillation, very common in mitral insufficiency. It is also the method used to monitor structural procedures, as it does not present the Stitching artifact (image fragmentation).

We then use acquisition synchronized to the electrocardiogram (ECG-gated), with multi-beat acquisition, essential for offline analyses and measurements.[4,5]

This mode of acquisition requires a regular rhythm and collaboration from the patient, with breath holding. If the heart rate is too high, an IV B-blocker can be used to maintain it at approximately 80 bpm, optimizing the volume rate achieved.

The acquired pyramid is built from the fusion of up to six subvolumes obtained, which allows the final image to have the same volume rate and smaller density of lines, with the same high temporal and spatial resolution, allowing an excellent image for later analysis (post-processing). However, the disadvantage of this method is that it does not happen in real time, which makes it difficult to use during structural procedures (Figure 3).

Alternatively, one can choose to directly use the ECG-gated 3D Zoom multi-beat modality, which presents the highest temporal resolution, with more than 100 volumes/s and excellent spatial resolution, since the zoom will be used to capture a smaller block focused only on the mitral valve (Vídeo 2B).

After using the above modalities for morphological analysis of the valve, we normally begin to evaluate the mitral regurgitant jet and its relationship with the leaflets. This is carried out by means of the 3D color Doppler modality, both multi-beat and single-beat. Obviously, if the regurgitation jet has a wide base, along the corners, the multi-beat method is preferred, providing us with better temporal resolution. In narrow base jets, most of the time the single-beat is sufficient to evaluate reflux and quantitative measurements (PISA), even with lower volume rates (Figure 4) (Video 2C).

Post processing of obtained volumes

Every echocardiographer debuting in the 3D world searches for literature and guidelines on ideal gain adjustments, smoothing, and compression to optimize 3D images, but this data is scarce.[6]

As a rule, we must remember that when compression is reduced, one is actually producing more contrasted images, which facilitate the evaluation of fine or delicate structures.

When Smoothing is increased, one can falsely make a surface less irregular (for example, in AAE assessment).

By increasing the Gain, one is actually increasing or amplifying the echoes that return to the transducer, which can create artifacts and static echoes within the cavity that are mistaken for spontaneous contrast (Figures 5A and 5B).

By reducing the gain too much, there is a risk of producing Dropout artifacts, which are the absence of echoes mainly in the mitral leaflets, which in turn can be confused with leaks or perforations.

Therefore, optimal gain must be sought on a case-by-case basis, depending on the depth, thickness, location, and orientation of the structure of interest in relation to the ultrasound beam. In most cases, optimal gain is achieved by reducing echoes (static echoes) from inside the atrial cavity (Figures 5A and B).

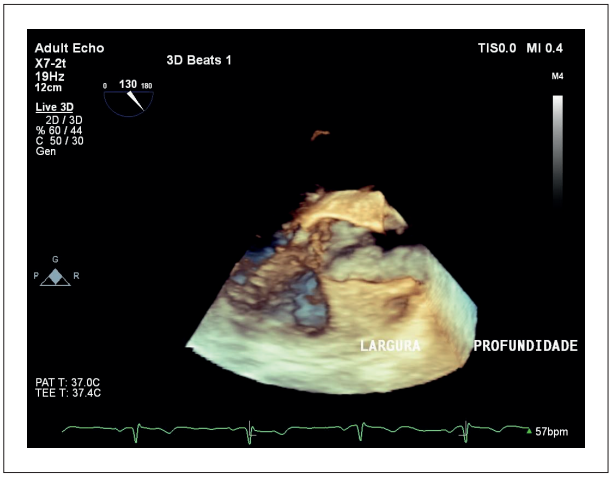

Figure 2 – *Live 3D zoom mode, preferably obtained from a 2D slice at 120 degrees, encompassing the aortic valve, the left ventricle outflow tract (LVOT), and the mitral valve. One can adjust both the width (A) and the height of the pyramidal volume.*

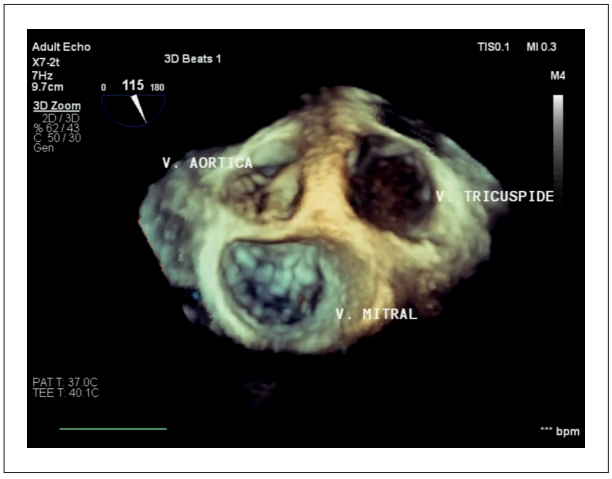

Video 2A – *In-face view of the mitral valve obtained from a 2D section at 120°. When obtaining this volume, the Left Atrial Appendage (LAA) must always be included with the volume, in addition to the LVOT and the aortic valve. Link: http://abcimaging.org/supplementary-material/2024/3701/2023-0105_AR_video2A_1.mp4*

Using the tools for cropping the obtained volumes

Once the appropriate volumes have been captured, we move on to using the tools that will allow us to evaluate the valve in three dimensions.[7-9]

One can use the cropping tool, initially on the fixed axes (x,y,z).

Obviously, fixed cuts do not always offer us ideal images and in some situations, such as flails and prolapses, the free cropping plane tool must be used, which allows us adjustable and angled cuts, revealing images not possible with fixed cuts and in 2D (Figures 6A and B) (Videos 3A and 3B).

Another important tool is focused cropping, which allows to evaluate smaller volumes in real time, resulting in better image definition, often eliminating structures that are not of interest (Video 4).

Finally, in cases of doubt regarding the severity of the reflux, we can use color Doppler associated with 3D to calculate the area of the *vena contracta* and the regurgitant volume. The method was validated against 2D and MRI methods, with a value greater than 0.41 cm^2 presenting a sensitivity of 97% and a specificity of 82% to differentiate moderate and severe MI. The color box must be as small as possible to allow the highest possible frame rate, due to the high speed of the regurgitant jet. Cropping must be done orthogonally to the plane of the jet and planimetry must be done at the point of its greatest speed (Video 4) (Figure 7).

The 3D image presentation/display process

In recent years, the process of demonstrating and presenting images on the 3D ultrasound screen has undergone profound transformations.

Today, depending on the manufacturer, there are different ways of presenting the 3D image on the equipment's display/screen. Each of them has its own characteristics that

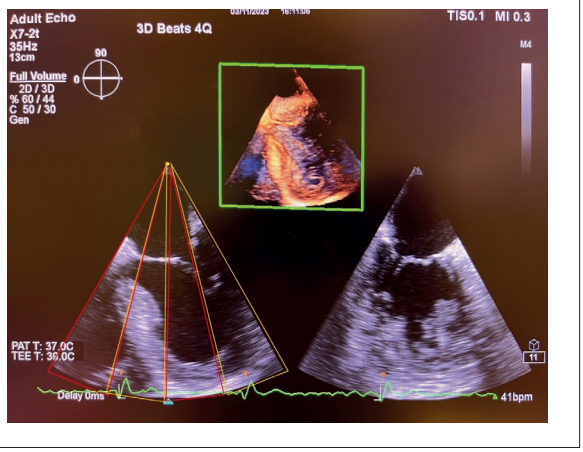

Figure 3 – *Full volume section at 0°, mid-esophageal, with 3D image formation from subvolumes obtained by synchronized electro capture, obtaining the same spatial and temporal resolution of the subvolumes.*

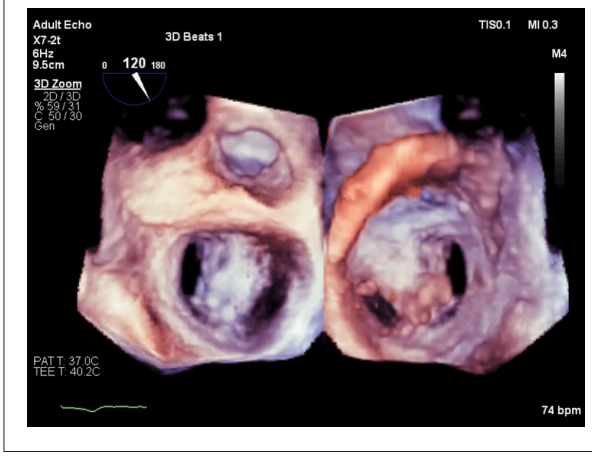

Video 2B – *The result of a miter-clip can be seen, a procedure in which the 3D modality is fundamental. Link: http://abcimaging.org/supplementary-material/2024/3701/2023-0105_AR_video2B_1.mp4*

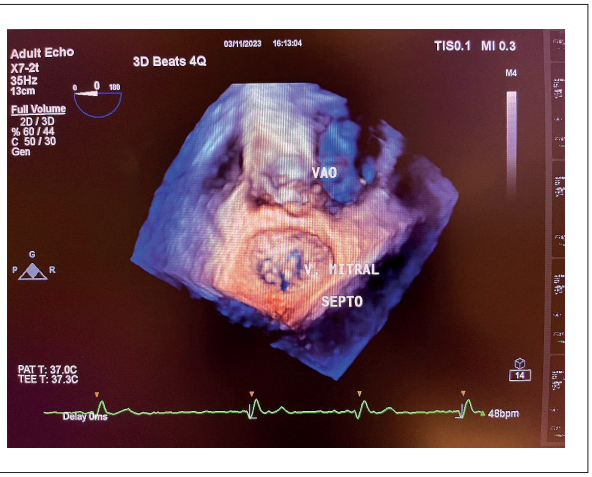

Figure 4 – *3D zoom color multi-beat, a modality that presents excellent temporal resolution of the mitral regurgitation jet along the entire edge of the leaflets.* VAO: aortic valve.

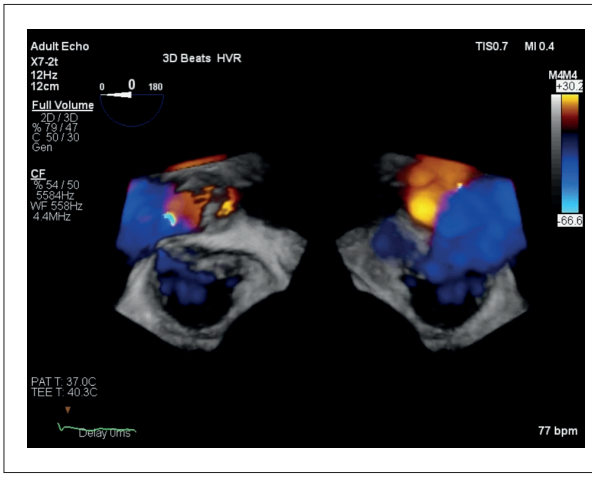

Video 2C – *The use of 3D color is essential to study the relationship and extent of the reflux jet along the edges of the leaflets. Link: http://abcimaging.org/supplementary-material/2024/3701/2023-0105_AR_video2C_1.mp4*

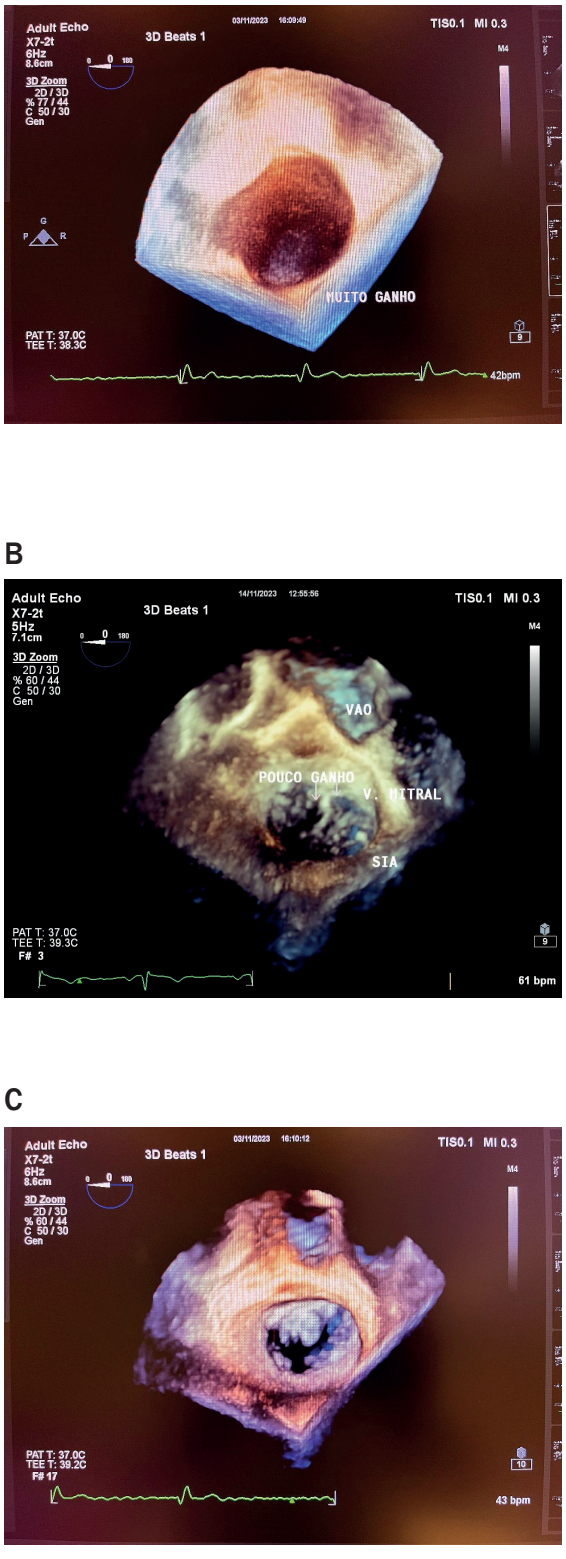

Figure 5 – *(A) excess gain in the 2D image preventing visualization of the mitral V. in the in face section; (B) little gain from the appearance of artifacts that simulate perforations or leaks in the leaflets and base of the LA; (C) ideal gain.*

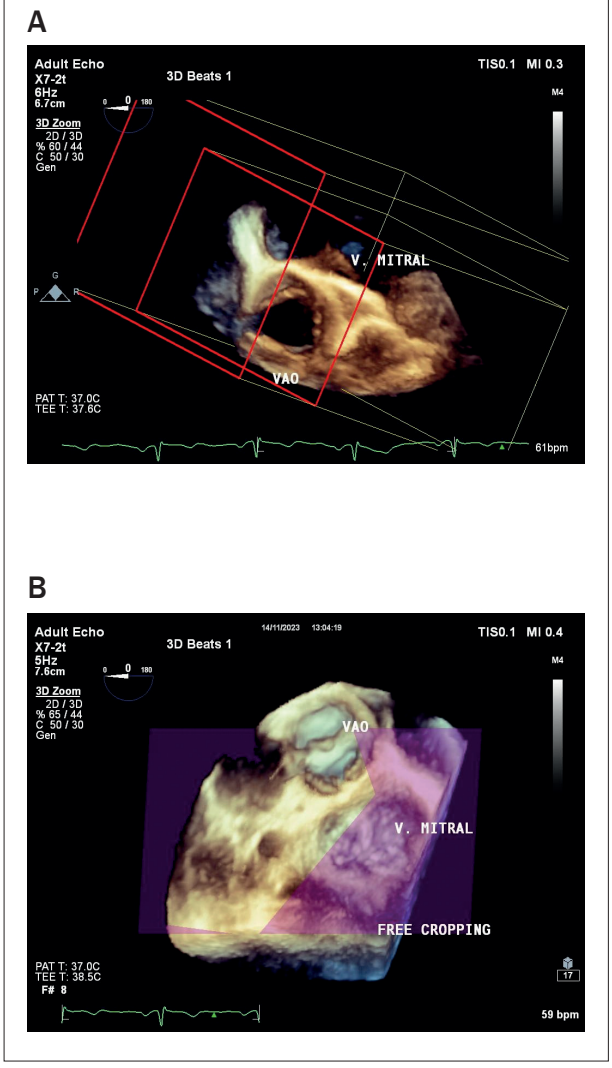

Figure 6 – *(A) activation of the cropping tool in depth for better visualization of the aortic valve; (B) free cropping tool, very useful for evaluating valve prolapses and flails.*

can contribute to better image definition and diagnostic accuracy. This is done through computerized texturing or shading of the image, creating the visual perception of a three-dimensional image.

In mitral valve disease, the first mode of presentation of the 3D image was volume rendering, and to this day it is the most used in most machines, where the software uses different modalities of blue and bronze in combination, to give us the perception of the third dimension. Typically, softwares use lighter colors like yellow and bronze to define superficial structures and darker colors like blue and brown to define deep structures (Figure 8A).

Some devices also have surface rendering for the mitral valve, where the machine uses automatic algorithms or artificial intelligence (AI) to identify pre-defined anatomical points or not (in the case of AI), allowing the creation of

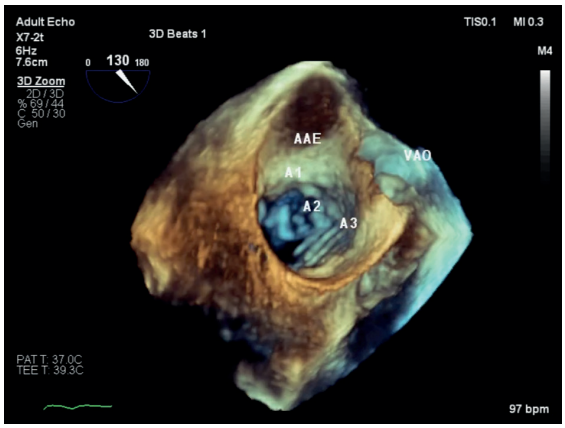

Video 3A – *Isolated prolapse of A3 identified mainly in an angled section, cutting out the interatrial septum using the cropping tool. Link: http://abcimaging.org/supplementary-material/2024/3701/2023-0105_AR_video3A_1.mp4*

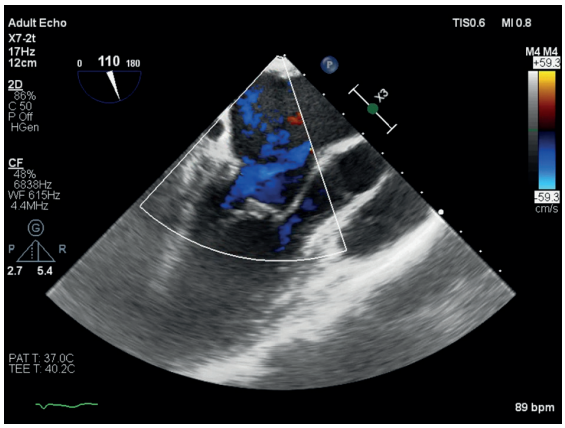

Video 3B – *2D image where the identification of the bocellation responsible for the prolapse is quite imprecise. Em: http://abcimaging.org/supplementary-material/2024/3701/2023-0105_AR_video3B_1.mp4*

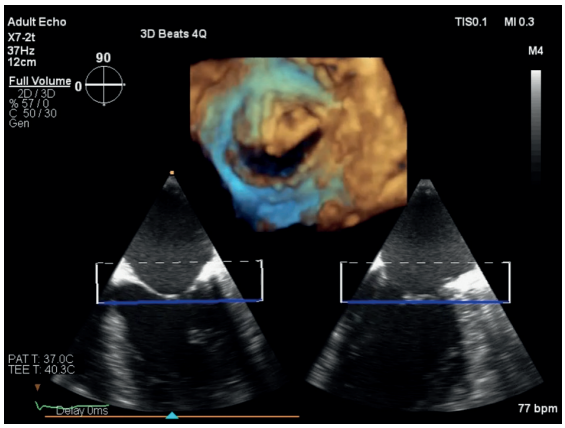

Vídeo 4 – *Focused cropping tool allowing an impressive improvement in temporal resolution. Link: http://abcimaging.org/supplementary-material/2024/3701/2023-0105_AR_video4_1.mp4*

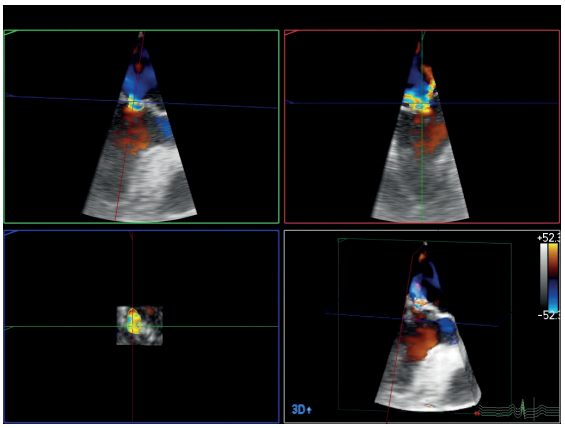

Figure 7 – *Moving the planes perpendicularly to the edges of the mitral valve, the area of the regurgitant orifice is identified.*

anatomical models of the valve and its apparatus, very useful for taking measurements on the ring and leaflets (Figure 8B).

More recently, new and creative ways of presenting and texturing images have emerged.

In the case of the photorealistic vision software, it is possible to use a virtual light focus, as if it were a flashlight, which creates shading of the structure and the sensation of depth. The operator manipulates the focus in any direction, generating a transillumination effect that, in the case of the mitral valve, delimits the valve orifice. Furthermore, this technique can define areas of greater valve thickening and calcification, as the light does not cross these structures (Figure 8C).

Another software available is Glass View, which allows to adjust degrees of transparency of the valve and neighboring structures, but honestly I do not fathom additional advantages in terms of diagnostics and accuracy in relation to its use. However, associated with color Doppler, it often favors the exact location of the regurgitant jet.

So... What about 3D transesophageal echo in mitral insufficiency?

In cases of mitral prolapse where plasty is planned, 3D certainly plays a fundamental role, as even the most common P2 prolapses have different anatomies. In some cases of P3 or anterior leaflet prolapse, 2D diagnosis is quite limited.

Other situations in which the use of 3D is essential are cases of suspected congenital clefts and in the study of posterior leaflet indentations, especially those that can be confused with clefts.

There is no doubt that 3D echocardiography, especially transesophageal echocardiography, will be increasingly

Figura 8 – *3D image presentation modes. (A) volume rendering; (B) used to measure mitral valve structures, such as annulus area, diameters, angles between the mitral and aortic valves, leaflet volumes, prolapse height, etc.; (C): photorealistic view.*

used in mitral anatomical assessment, morphological quantification, through reconstruction and surface rendering softwares, which are increasingly automated, as well as in reflux quantification. 2D assessment remains a mainstay in diagnosing the severity of mitral insufficiency. But once we enter the scenario of searching for the best treatment and during percutaneous procedures, 3D is essential.

Author Contributions

Conception and design of the research and writing of the manuscript: Cañellas F.

Potential Conflict of Interest

No potential conflict of interest relevant to this article was reported.

Sources of Funding

There were no external funding sources for this study.

Study Association

This study is not associated with any thesis or dissertation work.

Ethics Approval and Consent to Participate

This article does not contain any studies with human participants or animals performed by any of the authors.

References

1. Iung B, Vahanian A. Epidemiology of Valvular Heart Disease in the Adult. Nat Rev Cardiol. 2011;8(3):162-72. doi: 10.1038/nrcardio.2010.202.
2. Yang HS, Bansal RC, Mookadam F, Khandheria BK, Tajik AJ, Chandrasekaran K. Practical Guide for Three-Dimensional Transthoracic Echocardiography using a Fully Sampled Matrix Array Transducer. J Am Soc Echocardiogr. 2008;21(9):979-89. doi: 10.1016/j.echo.2008.06.011.
3. Scali MC, Basso M, Gandolfo A, Bombardini T, Bellotti P, Sicari R. Real Time 3D Echocardiography (RT3D) for Assessment of Ventricular and Vascular Function in Hypertensive and Heart Failure Patients. Cardiovasc Ultrasound. 2012;10:27. doi: 10.1186/1476-7120-10-27.
4. Lang RM, Badano LP, Tsang W, Adams DH, Agricola E, Buck T, et al. EAE/ASE Recommendations for Image Acquisition and Display using Three-Dimensional Echocardiography. Eur Heart J Cardiovasc Imaging. 2012;13(1):1-46. doi: 10.1093/ehjci/jer316.
5. Faletra FF, Agricola E, Flachskampf FA, Hahn R, Pepi M, Marsan NA, et al. Three-Dimensional Transoesophageal Echocardiography: How to use and When to use-a Clinical Consensus Statement from the European Association of Cardiovascular Imaging of the European Society of Cardiology. Eur Heart J Cardiovasc Imaging. 2023;24(8):e119-97. doi: 10.1093/ehjci/jead090.
6. Pino PG, Madeo A, Lucà F, Ceravolo R, di Fusco SA, Benedetto FA, et al. Clinical Utility of Three-Dimensional Echocardiography in the Evaluation of Mitral Valve Disease: Tips and Tricks. J Clin Med. 2023;12(7):2522. doi: 10.3390/jcm12072522.
7. Mantegazza V, Gripari P, Tamborini G, Muratori M, Fusini L, Ali SG, et al. 3D Echocardiography in Mitral Valve Prolapse. Front Cardiovasc Med. 2023;9:1050476. doi: 10.3389/fcvm.2022.1050476.
8. Yosefy C, Hung J, Chua S, Vaturi M, Ton-Nu TT, Handschumacher MD, et al. Direct Measurement of Vena Contracta Area by Real-Time 3-Dimensional Echocardiography for Assessing Severity of Mitral Regurgitation. Am J Cardiol. 2009;104(7):978-83. doi: 10.1016/j.amjcard.2009.05.043.
9. Pastore MC, Mandoli GE, Sannino A, Dokollari A, Bisleri G, D'Ascenzi F, et al. Two and Three-Dimensional Echocardiography in Primary Mitral Regurgitation: Practical Hints to Optimize the Surgical Planning. Front Cardiovasc Med. 2021;8:706165. doi: 10.3389/fcvm.2021.706165.

My Approach to Nuclear Medicine in the Assessment of Microvascular Disease in Women

Lara Cristiane Terra Ferreira Carreira,[1] Lívia Carreira,[2] Adriana Soares Xavier de Brito[3,4]

Cardiologia Nuclear de Curitiba (CNC),[1] Curitiba, PR – Brazil
PUC Paraná,[2] Curitiba, PR – Brazil
Instituto Nacional de Cardiologia,[3] Rio de Janeiro, RJ – Brazil
Instituto D'Or de Pesquisa e Ensino,[4] Rio de Janeiro, RJ – Brazil

Abstract

Coronary microvascular dysfunction (CMD) is a condition that has been increasingly recognized as a cause of angina, with prognostic importance in multiple cardiovascular processes, especially in women. It results from abnormalities in the structure and/or function of the coronary microcirculation. Even in the absence of obstructive coronary artery disease (CAD), CMD is associated with worse prognosis, greater morbidity, impaired quality of life, and recurrent hospitalizations due to angina and heart failure, posing a challenge for diagnosis and treatment. In this article, we briefly review CMD and how nuclear medicine can assist in its assessment.

Introduction

Coronary microvascular dysfunction (CMD) results from abnormalities in the structure and/or function of the coronary microcirculation that occur in a variety of cardiovascular conditions (Central Figure). It has been increasingly recognized as a cause of angina, with prognostic importance in multiple cardiovascular disease processes, including its association with adverse outcomes in patients with signs and symptoms of ischemia with non-obstructive coronary arteries (INOCA).[1]

Although the diagnostic and therapeutic focus in patients with suspected ischemic heart disease (IHD) has traditionally been on obstructive atherosclerosis in the epicardial coronary arteries, there is currently a greater understanding of the impact of disorders affecting the microcirculation.

This condition has been increasingly diagnosed, especially in women, accounting for almost 60% to 70% of women and 30% of men undergoing coronary angiography.[2] This population presents greater morbidity, impaired quality of life, and recurrent hospitalizations due to angina and heart failure, with repeated non-invasive tests and coronary angiograms, posing a challenge for diagnosis and treatment. The majority of women with CMD also have cardiovascular risk factors such as diabetes, hypertension, hyperlipidemia, or family history of premature coronary artery disease (CAD), and evidence of non-obstructive coronary atherosclerosis. CMD is an important factor in the observation of similar or worse outcomes of atherosclerosis in women, notwithstanding a lower rate of obstructive epicardial CAD.[1]

Pathophysiological mechanisms of CMD

Notably, the epicardial arteries represent only 10% of the volume of coronary circulation, while the microcirculation accounts for the remaining 90%, and it is the site responsible for most of the resistance to coronary blood flow and its regulation.[1]

In INOCA, mismatch between blood supply and myocardial oxygen demands may be caused by CMD and/or epicardial coronary artery spasm, typically in the context of non-obstructive coronary atherosclerosis. Ischemia can be caused by transient or sustained impairments in myocardial perfusion that can be structural and/or functional, involving the epicardial coronary arteries and/or their microcirculation.[3]

Structural factors implicated in CMD include decreased capillary density, luminal narrowing of arterioles/capillaries related to edematous endothelial cells, proliferated smooth muscle cells, and external compression.

Functional mechanisms include endothelial and/or smooth muscle cell dysfunction, mainly at the arteriolar level. Endothelial dysfunction leads to an attenuated response to typical triggers for microvascular dilation, such as exercise or acetylcholine exposure. Furthermore, endothelial dysfunction can even lead to a vasoconstrictor response to these triggers, thus resulting in vasospasm. In addition to the endothelium, the myogenic response of the microvasculature is abnormal in CMD. This can be observed in the attenuated response to vasodilators, such as adenosine, which directly target smooth muscle cells.[1]

There are also myocardial factors, such as left ventricular hypertrophy, diastolic dysfunction associated with interstitial and perivascular fibrosis, and increased intramyocardial and intracavitary pressure that substantially contribute to microvascular dysfunction (Figure 1).[4]

Keywords

Microvascular Angina; Myocardial Ischemia; Nuclear Medicine.

Mailing Address: Lara Cristiane Terra Ferreira Carreira •
Cardiologia Nuclear de Curitiba (CNC). Rua Desembargador Hugo Simas, 322 A. Postal code: 80520-250. Curitiba, PR – Brazil
E-mail: lara_carreira@yahoo.com.br
Manuscript received February 23, 2024; revised February 23, 2024; accepted February 23, 2024
Editor responsible for the review: Marcelo Dantas Tavares de Melo

DOI: https://doi.org/10.36660/abcimg.20240015i

Central Illustration: My Approach to Nuclear Medicine in the Assessment of Microvascular Disease in Women

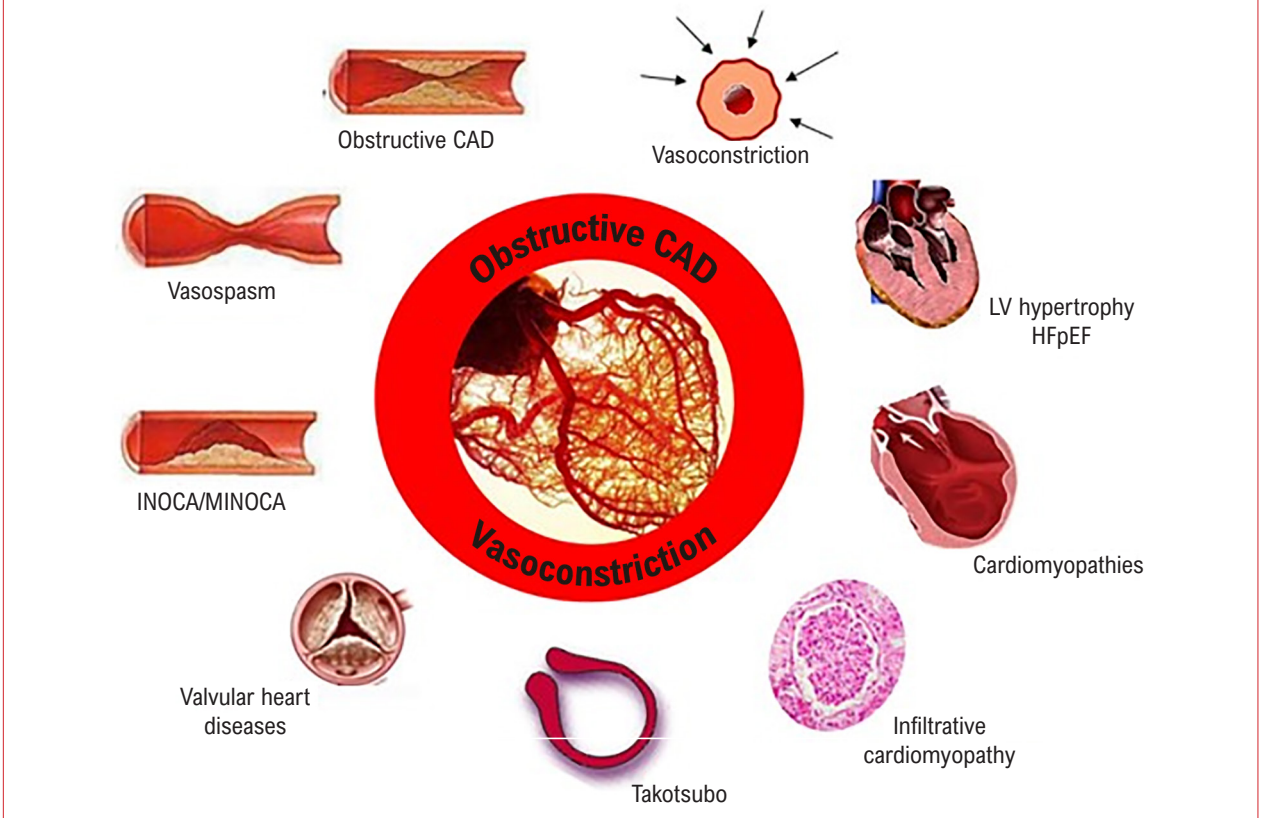

Arq Bras Cardiol: Imagem cardiovasc. 2024;37(1):e20240015

Role of coronary microvascular dysfunction in different cardiovascular diseases .CAD: coronary artery disease; HFpEF: heart failure with preserved ejection fraction; INOCA: ischemia with non-obstructive coronary arteries; LV: left ventricular; MINOCA: myocardial infarction with non-obstructive coronary arteries: CMD: Coronary microvascular dysfunction. Source: Authors' archives.

Patients with CMD present a spectrum of symptoms, similar to patients with obstructive epicardial CAD, including typical angina pectoris, atypical chest pain, and anginal equivalent symptoms, such as dyspnea on exertion. Compared to patients with angina due to obstructive CAD, patients with microvascular angina tend to respond less to nitrates.

Diagnosis of CMD

Diagnosis of CMD should be suspected, and additional tests should be considered when there are symptoms of angina and/or objective signs of ischemia on non-invasive testing, without explanatory obstructive epicardial CAD.

The Coronary Vasomotor Disorders International Study (COVADIS) Group was established in 2012 to develop international standards for the diagnostic criteria for microvascular and vasospastic angina (Table 1).[6]

In the initial evaluation, these patients often present electrocardiographic alterations on the exercise test, although there may or may not be hypoperfusion in traditional myocardial perfusion imaging methods (Clinical Case 1).

Historically, the methods available for assessment of CMD were based on the quantification of coronary blood flow in response to vasoactive stimuli and the angiographic assessment of myocardial blush, such as invasive tests that measure coronary flow reserve (CFR) in response to adenosine and acetylcholine using a flow catheter with intracoronary Doppler or thermodilution.[7]

However, invasive assessment of coronary function is rarely performed as a routine procedure. The advent of non-invasive techniques such as positron emission tomography (PET), myocardial perfusion scintigraphy (MPS), cardiac magnetic resonance imaging, and stress echocardiography have increased the feasibility of diagnosing reduced myocardial flow reserve indicative of CMD.[8,9]

Nuclear imaging is able to evaluate the entire spectrum of IHD, from ischemia resulting from obstruction of the epicardial arteries to CMD. National and international

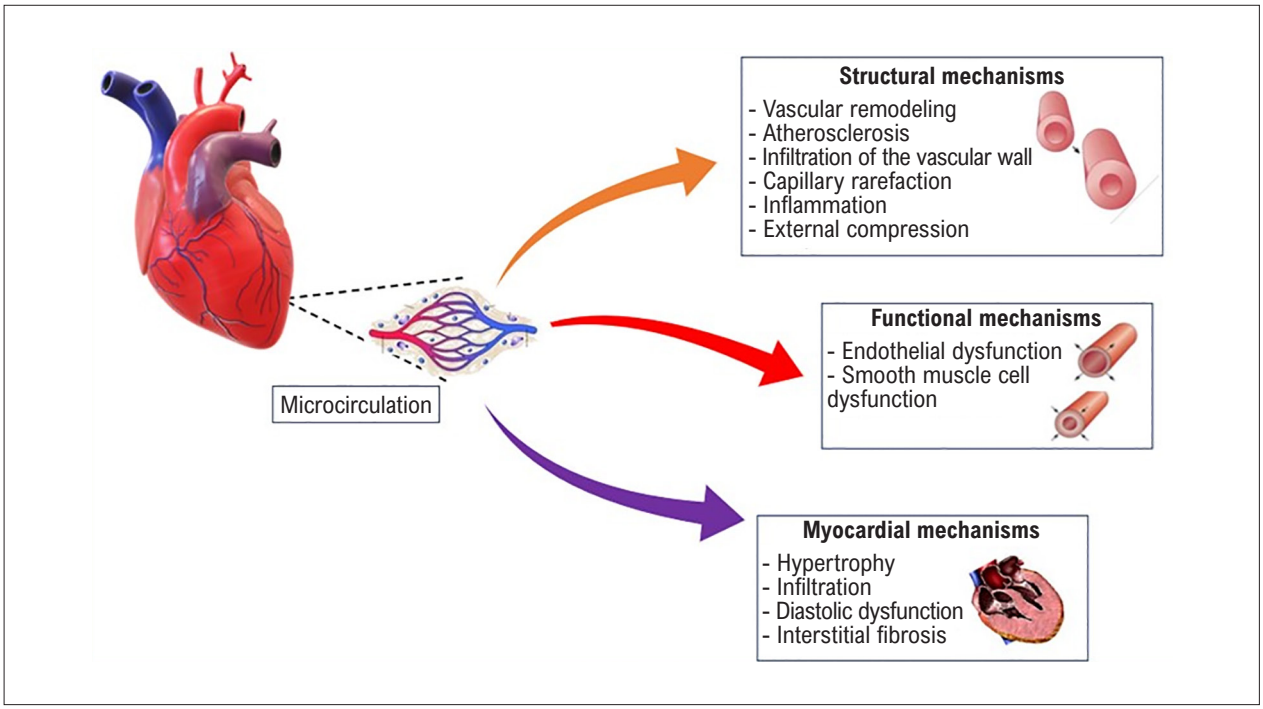

Figure 1 – *Mecanismos da disfunção da microcirculação (adaptado de Rehan et al.).*[5]

guidelines emphasize, when evaluating IHD, the use of MPS, which can be performed on all patients, regardless of renal function, presence of arrhythmias, obesity, or intracardiac devices.[10] The techniques used are SPECT and PET. For more than three decades, MPS using SPECT has been used extensively in clinical practice due to its wide availability and to the extensive literature supporting its value in the diagnosis and risk stratification of IHD. It is the most commonly used non-invasive imaging study in the evaluation of women at intermediate to high risk of IHD with stable ischemic symptoms.

Patients who present altered perfusion, whether using SPECT or PET, have a greater risk of cardiovascular events. However, in CMD, perfusion defects may not be evident, or they may not have a typical regional distribution corresponding to an epicardial artery. Contractile abnormalities are not normally observed.

The difficulty in observing myocardial ischemia using traditional imaging methods may be related to a non-uniform distribution of microvasculature dysfunction.[1]

Definitive non-invasive clinical diagnosis of CMD depends on the identification of impaired CFR in the absence of flow-limiting CAD. Impaired CFR, calculated as the ratio of hyperemic coronary blood flow to resting coronary blood flow, reflects flow abnormalities in the epicardial coronary arteries and microvasculature.

Cardiac PET examination is currently considered the gold standard for non-invasive assessment of myocardial blood flow (MBF), both at rest and in hyperemia, and it represents a crucial tool for evaluating CFR, reflecting microvascular dysfunction, with a significant prognostic value. Murphy et al. demonstrated that CFR < 2.0 was associated with an annual rate of major adverse cardiac events of 7.8% and 5.6% among symptomatic men and women without obstructive CAD versus 3.3% and 1.7%, respectively, for those with RFC ≥ 2.0.[11]

Despite the enormous known advantages in terms of diagnosis and risk stratification (Figure 2), cardiac PET cannot yet be integrated into the clinical routine in Brazil, due to the unavailability of PET perfusion tracers in our country.

In the last decade, nuclear cardiology has witnessed a major advance, due to the introduction of cameras with solid-state cadmium-zinc-telluride (CZT) detectors, which allow the assessment of MBF and CFR using SPECT. In view of its advantages in spatial, temporal, and energy resolution over standard gamma camera systems, MBF quantification is feasible, and it has good consistency with coronary flow values based on PET/CT.[13]

Another benefit of dynamic SPECT-CZT is the wide availability of tracers labeled with technetium-99m. It has also demonstrated good reliability in the diagnostic and prognostic assessment of patients with suspected or known CAD, with a potential role in identifying CMD.[14]

Although very promising, it is important to highlight that most studies to date are from single centers, and they have small samples. However, this technology arouses a great deal of interest on the part of the scientific community, since the radiopharmaceuticals used are widely available, and the equipment has a lower cost when compared to PET/CT.

Table 1 – COVADIS (Coronary Vasomotor Disorders International Study) diagnostic criteria for microvascular angina and vasospastic angina in patients with INOCA

Criteria	Microvascular angina	Vasospastic angina
1 Symptoms of myocardial ischemia	Angina at rest or during exertion	1. Nitrate-responsive angina during spontaneous episode, with at least 1 of the following: A. Resting angina, especially between night and early morning B. Marked diurnal variation in exercise tolerance, reduced in the morning C. Hyperventilation can precipitate an episode D. Calcium channel blockers suppress episodes
2 Absence of obstructive CAD (< 50% diameter reduction or FFR > 0.80)	Coronary CT angiography Invasive coronary angiography	Coronary CT angiography Invasive coronary angiography
3 Objective evidence of myocardial ischemia	Presence of reversible defect, abnormalities in flow reserve on functional imaging tests	Transient ischemic ECG changes during spontaneous episode, including any of the following in at least 2 contiguous leads: A. ST segment elevation ≥ 0.1 mV B. ST segment depression ≥ 0.1 mV C. New negative U waves
4 Evidence of coronary dysfunction	Coronary flow reserve decreased (≤2.0 or ≤2.5 depending on the methodology used), determined invasively or non-determinant. Microvascular coronary spasm, defined as reproduction of symptoms, changes ischemic on ECG but without epicardial spasm during acetylcholine test. Coronary microvascular resistance index decreased (e.g. IMR ≥ 25) Slow coronary flow phenomenon, defined with TIMI > 25.	Coronary artery spasm defined as total or subtotal coronary artery occlusion (> 90% constriction) with angina and ischemic ECG changes, either spontaneously or in response to provocative stimuli (typically acetylcholine, ergot, or hyperventilation)

"Definitive" diagnosis: all 4 criteria present; "Suspicious" diagnosis: criteria 1 + 2 present, but only criteria 3 or 4 present or equivocal. CAD: Coronary Artery Disease; FFR: Fractional Flow Reserve; IMR: Microcirculatory Resistance Index; TIMI: thrombolysis in myocardial infarction.

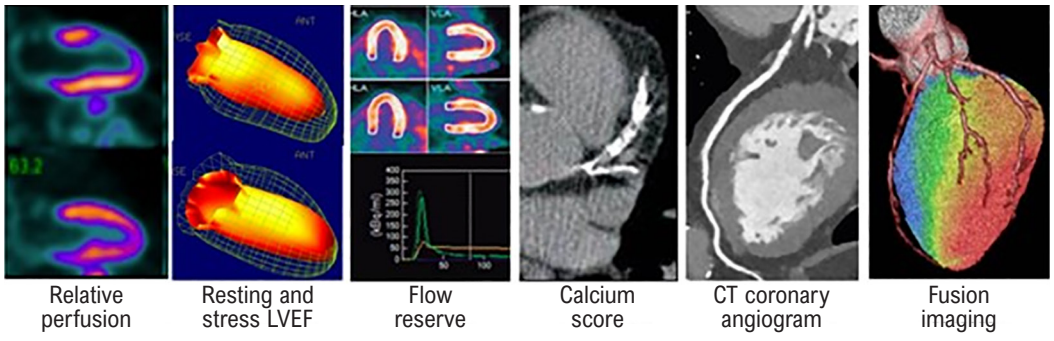

Figure 2 – *CT: computed tomography; LVEF: left ventricular ejection fraction; PET: positron emission tomography. PET/CT perfusion images – comprehensive data Adapted from Al-Mallah et al, J Nucl Cardiol 2010; 17:498-513.*[12]

My approach

Given the diagnostic and prognostic importance of coronary flow measurements obtained non-invasively in CMD, it has become vital to introduce new methods that make it possible to quantify them. Studies that standardize and validate protocols for obtaining MBF and CFR using CZT gamma cameras are necessary for the method to be widely available and reproducible in the investigation of CMD.

The exam is performed at rest and under pharmacological stress with a vasodilator (dipyridamole or adenosine), in a protocol that lasts 1 or 2 days. Patients are advised to suspend caffeine and methylxanthines for 24 hours before the exam.

Images are acquired dynamically on a CZT gamma camera, to allow the quantification of MBF and CFR in

specific commercial software, coupled to the perfusion image acquisition protocol. The protocol usually begins with the intravenous injection of 0.5 to 1 mCi of sestamibi-^{99m}Tc to position the heart in the field of view of the gamma camera, through a rapid acquisition of 60 seconds.

The resting phase involves the acquisition of dynamic images, simultaneous with the beginning of intravenous administration of the radiotracer sestamibi-^{99m}Tc, immediately followed by perfusion imaging. With the patient still positioned in field of view of the gamma camera, the pharmacological stress phase is carried out with intravenous injection of dipyridamole at a dose of 0.56 mg/kg or adenosine at 140 mcg/kg/min for 4 or 6 minutes. At peak stress, a second dose of sestamibi-^{99m}Tc is administered, with triple the activity value of the dose injected at rest. Both stages are acquired coupled with electrocardiogram monitoring to evaluate the function and volumes of the left ventricle using gated SPECT.[15,16]

The dynamic data from acquisitions are processed using a dedicated workstation, with specific commercial software.

Clinical cases from clinical practice

Clinical case 1: Woman, 73 years old, sedentary, with grade III obesity, systemic arterial hypertension, glucose intolerance, and dyslipidemia, complaining of palpitations, oppressive chest discomfort associated with fatigue on minor exertion, and hypertensive peaks. MPS (SPECT) at rest and under pharmacological stress with a vasodilator demonstrated a significant area of reversible hypoperfusion compatible with ischemia in the anterior, anteroseptal, and inferior apical walls (Figure 3A).

Coronary angiography revealed coronary arteries without obstructive lesions. She became asymptomatic after 10 months of treatment, with changes in lifestyle habits, supervised exercise, a low-calorie diet, and optimization of medications. MPS was repeated, which demonstrated a significant reduction in the area of radiotracer hypoperfusion, without evidence of ischemia, and improved left ventricular function (Figure 3B).

Clinical Case 2: Woman, 62 years old, former smoker, with hypertension and dyslipidemia, complaining of recent onset of fatigue. History of breast cancer and mastectomy 7 years prior, with recurrence of the disease 2 years prior, undergoing radiotherapy and chemotherapy. She experienced a transient reduction in left ventricular ejection fraction while taking trastuzumab. Coronary CT angiography showed no obstructive lesions. She was referred for MPS at rest and under pharmacological stress with vasodilator and analysis of coronary flow reserve (SPECT-CZT) to investigate CMD, which demonstrated preserved myocardial perfusion (Figure 4A), but with significant changes in coronary flow reserve in the territory of the 3 coronary arteries (Figure 4B).

Conclusion

CMD has a high prevalence and significant clinical implications in daily practice, especially in women. Functional and/or structural microcirculation abnormalities can lead to ischemia in the absence of significant epicardial stenosis or worsen concomitant atherosclerotic CAD.

The recognition of microvascular angina reinforces the importance of functional nuclear techniques, as well as the fact that assessment of IHD should be more comprehensive, beyond the detection of obstructive epicardial CAD.

Cardiac PET is currently the gold standard for assessing MBF and CFR. Nonetheless, the method's low availability and high costs make widespread use difficult. The development of new technologies, such as CZT gamma camera equipment, with good accuracy and agreement with PET in evaluating CFR, has been promising in this context, making diagnosis of CMD possible. However, standardization of acquisition and post-processing protocols, as well as updates to available software, are necessary to reduce variability between centers and increase the clinical robustness of SPECT-CZT results, with improved risk stratification, better therapeutic approach, and consequent changes in the prognosis of CMD.

Acknowledgments

We would like to thank Dr. Renata Christian Martins Félix, nuclear medicine physician and cardiologist at the Villela Pedras Clinic and the National Cancer Institute, for kindly providing the clinical case and images for example 2.

Author Contributions

Conception and design of the research, acquisition of data, analysis and interpretation of the data, statistical analysis, writing of the manuscript, critical revision of the manuscript for intellectual content: Carreira LCTF, Carreira L, Brito ASX.

Potential Conflict of Interest

No potential conflict of interest relevant to this article was reported.

Sources of Funding

There were no external funding sources for this study.

Study Association

This study is not associated with any thesis or dissertation work.

Ethics Approval and Consent to Participate

This article does not contain any studies with human participants or animals performed by any of the authors.

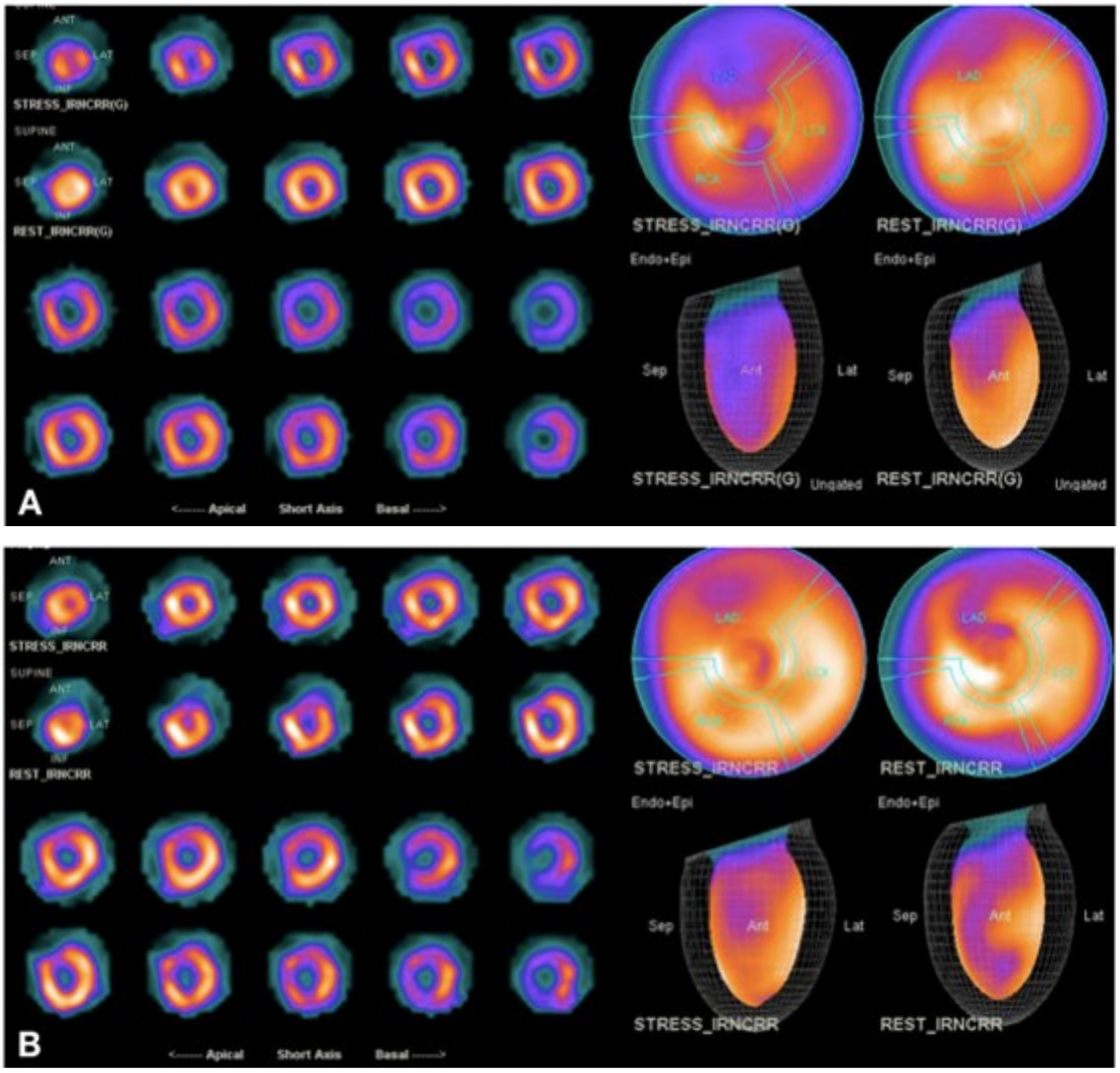

Figure 3 – *A) CPM (SPECT) with 99mTc-Sestamibi: moderate hypoperfusion of the radiopharmaceutical is observed in the anterior wall, anteroseptal region, and inferior apical region of the left ventricle in the stress images (lines a and c), which normalize in the rest images (lines b and d). B) CPM (SPECT) with 99mTc-Sestamibi: normal distribution of the radiopharmaceutical is observed in the walls of the left ventricle, with no evidence of ischemia.*

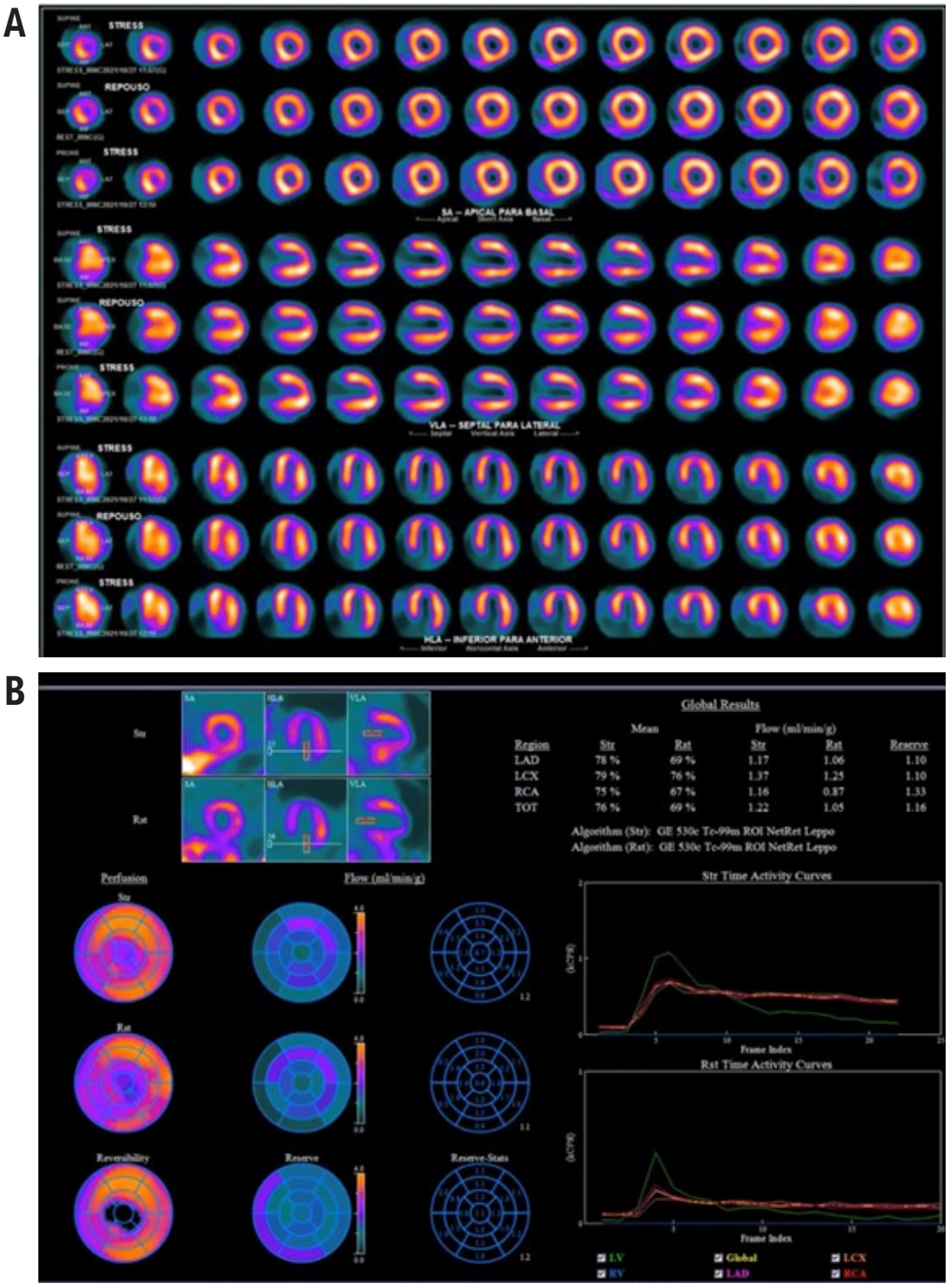

Figure 4 – *A) CPM (SPECT-CZT) with 99mTc-Sestamibi at rest and pharmacological stress: homogeneous distribution of the radiopharmaceutical is observed in the walls of the left ventricle. B) CPM (SPECT-CZT) with 99mTc-Sestamibi at rest and pharmacological stress: significant reduction in myocardial perfusion in the territory of the three coronary arteries is observed.*

References

1. Marano P, Wei J, Merz CNB. Coronary Microvascular Dysfunction: What Clinicians and Investigators Should Know. Curr Atheroscler Rep. 2023;25(8):435-46. doi: 10.1007/s11883-023-01116-z.
2. Jespersen L, Hvelplund A, Abildstrøm SZ, Pedersen F, Galatius S, Madsen JK, et al. Stable Angina Pectoris with no Obstructive Coronary Artery Disease is Associated with Increased Risks of Major Adverse Cardiovascular Events. Eur Heart J. 2012;33(6):734-44. doi: 10.1093/eurheartj/ehr331.
3. Kunadian V, Chieffo A, Camici PG, Berry C, Escaned J, Maas AHEM, et al. An EAPCI Expert Consensus Document on Ischaemia with Non-Obstructive Coronary Arteries in Collaboration with European Society of Cardiology Working Group on Coronary Pathophysiology & Microcirculation Endorsed by Coronary Vasomotor Disorders International Study Group. Eur Heart J. 2020;41(37):3504-20. doi: 10.1093/eurheartj/ehaa503.
4. Schindler TH, Fearon WF, Pelletier-Galarneau M, Ambrosio G, Sechtem U, Ruddy TD, et al. Myocardial Perfusion PET for the Detection and Reporting of Coronary Microvascular Dysfunction: A JACC: Cardiovascular Imaging Expert Panel Statement. JACC Cardiovasc Imaging. 2023;16(4):536-48. doi: 10.1016/j.jcmg.2022.12.015.
5. Rehan R, Yong A, Ng M, Weaver J, Puranik R. Coronary Microvascular Dysfunction: A Review of Recent Progress and Clinical Implications. Front Cardiovasc Med. 2023;10:1111721. doi: 10.3389/fcvm.2023.1111721.
6. Ong P, Camici PG, Beltrame JF, Crea F, Shimokawa H, Sechtem U, et al. International Standardization of Diagnostic Criteria for Microvascular Angina. Int J Cardiol. 2018;250:16-20. doi: 10.1016/j.ijcard.2017.08.068.
7. Ford TJ, Berry C. How to Diagnose and Manage Angina Without Obstructive Coronary Artery Disease: Lessons from the British Heart Foundation CorMicA Trial. Interv Cardiol. 2019;14(2):76-82. doi: 10.15420/icr.2019.04.R1.
8. Liu A, Wijesurendra RS, Liu JM, Forfar JC, Channon KM, Jerosch-Herold M, et al. Diagnosis of Microvascular Angina Using Cardiac Magnetic Resonance. J Am Coll Cardiol. 2018;71(9):969-79. doi: 10.1016/j.jacc.2017.12.046.
9. Taqueti VR, Di Carli MF. Coronary Microvascular Disease Pathogenic Mechanisms and Therapeutic Options: JACC State-of-the-Art Review. J Am Coll Cardiol. 2018;72(21):2625-41. doi: 10.1016/j.jacc.2018.09.042.
10. Oliveira GMM, Almeida MCC, Rassi DDC, Bragança ÉOV, Moura LZ, Arrais M, et al. Position Statement on Ischemic Heart Disease - Women-Centered Health Care - 2023. Arq Bras Cardiol. 2023;120(7):e20230303. doi: 10.36660/abc.20230303.
11. Murthy VL, Naya M, Taqueti VR, Foster CR, Gaber M, Hainer J, et al. Effects of Sex on Coronary Microvascular Dysfunction and Cardiac Outcomes. Circulation. 2014;129(24):2518-27. doi: 10.1161/CIRCULATIONAHA.113.008507.
12. Al-Mallah MH, Sitek A, Moore SC, Di Carli M, Dorbala S. Assessment of Myocardial Perfusion and Function with PET and PET/CT. J Nucl Cardiol. 2010;17(3):498-513. doi: 10.1007/s12350-010-9223-5.
13. Acampa W, Zampella E, Assante R, Genova A, De Simini G, Mannarino T, et al. Quantification of Myocardial Perfusion Reserve by CZT-SPECT: A Head to Head Comparison with 82Rubidium PET Imaging. J Nucl Cardiol. 2021;28(6):2827-39. doi: 10.1007/s12350-020-02129-w.
14. D'Antonio A, Mannarino T. Exploring Coronary Microvascular Function by Quantitative CZT-SPECT: A Small Step or Giant Leap for INOCA Patients? Eur J Nucl Med Mol Imaging. 2023;50(13):3806-8. doi: 10.1007/s00259-023-06358-2.
15. Dorbala S, Ananthasubramaniam K, Armstrong IS, Chareonthaitawee P, DePuey EG, Einstein AJ, et al. Single Photon Emission Computed Tomography (SPECT) Myocardial Perfusion Imaging Guidelines: Instrumentation, Acquisition, Processing, and Interpretation. J Nucl Cardiol. 2018;25(5):1784-846. doi: 10.1007/s12350-018-1283-y.
16. Souza ACDAH, Gonçalves BKD, Tedeschi AL, Lima RSL. Quantification of Myocardial Flow Reserve Using a Gamma Camera with Solid-state Cadmium-zinc-telluride Detectors: Relation to Angiographic Coronary Artery Disease. J Nucl Cardiol. 2021;28(3):876-84. doi: 10.1007/s12350-019-01775-z

Como Eu Faço a Avaliação da Atividade Simpática Cardíaca

My Approach to Assess Cardiac Sympathetic Activity

Adriana Soares Xavier de Brito,[1,2] Jessica Costa Leite,[3] Simone Cristina Soares Brandão[4]

Instituto Nacional de Cardiologia,[1] Rio de Janeiro, RJ – Brasil
Instituto D'Or de Pesquisa e Ensino,[2] Rio de Janeiro, RJ – Brasil
Faculdade de Ciencias Medicas da Paraiba,[3] Joao Pessoa, PB – Brasil
Universidade Federal de Pernambuco,[4] Recife, PB – Brasil

Resumo

A inervação simpática desempenha um papel crucial na regulação do fluxo sanguíneo, cronotropismo, dromotropismo, lusitropismo e inotropismo miocárdico. Em várias doenças cardíacas e neurodegenerativas, observam-se alterações no sistema nervoso autonômico. A imagem neuronal cardíaca pode ajudar no entendimento fisiopatológico, no diagnóstico e prognóstico dessas doenças. Neste artigo, apresentamos, de forma clara e objetiva, o passo a passo da cintilografia com mIBG-I123 para avaliação da atividade simpática cardíaca nos principais cenários da prática clínica.

Introdução

O sistema nervoso autônomo (SNA) é funcionalmente subdivido em sistemas simpático (SNS) e parassimpático (SNP) que trabalham juntos no controle da homeostase.[1] O controle do SNA cardíaco é um processo dinâmico, e sua disfunção pode ser intrínseca ou extrínseca. A primeira é decorrente de doenças que afetam diretamente os nervos autonômicos, como o *diabetes mellitus* e as síndromes de insuficiência autonômica. A segunda se manifesta como uma condição secundária a uma doença cardíaca ou sistêmica.[2]

A doença cardíaca pode causar alterações tanto anatômicas (primárias) quanto funcionais (secundárias) na função autonômica do coração. Estas alterações, por sua vez, podem contribuir para a progressão da doença cardíaca e/ou estar envolvidas na gênese de arritmias.[2] Além disso, algumas doenças neurodegenerativas podem afetar o SNA. Nesse contexto, a imagem neuronal cardíaca pode ajudar no entendimento fisiopatológico, no diagnóstico e prognóstico dessas doenças.[3,4] No presente artigo, apresentamos de forma clara e objetiva o passo a passo da cintilografia com metaiodobenzilguanidina marcada com o iodo-123 (mIBG-I123) para avaliação da atividade simpática cardíaca nos principais cenários da prática clínica (Figura Central).

Palavras-chave

123-metaiodobenzilguanidina; Frequência Cardíaca; Insuficiência Cardíaca; Doença de Parkinson.

Correspondência: Adriana Soares Xavier de Brito •
Instituto Nacional de Cardiologia. Rua das Laranjeiras, 374. CEP: 22240-006. Rio de Janeiro, RJ – Brasil
E-mail: adrijsoares@hotmail.com
Artigo recebido em 15/02/2024; revisado em 22/02/2024; aceito em 23/02/2024.
Editor responsável pela revisão: Marcelo Dantas Tavares de Melo

DOI: https://doi.org/10.36660/abcimg.20240009

Cintilografia cardíaca com mIBG-I123

O coração normal é densamente inervado pelo SNS, e a avaliação da atividade adrenérgica cardíaca de forma não invasiva é possível por meio da cintilografia cardíaca com mIBG-I123, um falso neurotransmissor análogo da guanetidina.[5] O mIBG foi descoberto no início de 1980 durante uma pesquisa em tumores da medula adrenal, devido à sua estrutura molecular semelhante à norepinefrina (NE). Além disso, o mIBG utiliza os mesmos mecanismos de captação (*uptake*-1) e estocagem da NE nas vesículas neurossecretórias das terminações nervosas pré-sinápticas cardíacas.[6]

Após a estimulação adrenérgica, o mIBG é liberado na fenda sináptica cardíaca. No entanto, diferentemente da NE, ele não é metabolizado pelas enzimas monoamino-oxidase e catecol-orto-metil-transferase, apresenta baixa afinidade pelos receptores pós-sinápticos e não exerce ação farmacológica (Figura 1). Estudos têm demonstrado que a captação cardíaca de mIBG *in vivo* se correlaciona à concentração de NE, representando a inervação do SNS cardíaco em condições fisiológicas e patológicas.[5] O mIBG-I123 permite a visualização da inervação simpática global e regional do miocárdio ventricular esquerdo através da aquisição de imagens cintilográficas cardíacas, planas e tomográficas (SPECT, do inglês *Single Photon Emission Computed Tomography*).

Como eu faço o exame?

A injeção intravenosa do mIBG-123I é feita em repouso, pelo menos 30 minutos após a administração oral de xarope de iodeto de potássio ou solução contendo iodo, para bloqueio e proteção da tireoide. Os medicamentos que potencialmente podem interferir na captação de catecolaminas, tais como antidepressivos, antipsicóticos e alguns bloqueadores dos canais de cálcio devem ser suspensos antes do exame.[7] Por outro lado, os betabloqueadores, inibidores da enzima conversora da angiotensina (IECA) e/ou bloqueadores dos receptores da angiotensina não precisam ser descontinuados.[8]

O exame é habitualmente realizado em gama-câmaras tomográficas, equipadas com colimadores de furos paralelos, de alta resolução e baixa energia, utilizando uma janela simétrica de 20% centrada no fotopico do iodo-123 de 159 keV e uma matriz de 128 x 128. Cerca de 15 a 20 minutos e 3 a 4 horas após a administração do mIBG-123I (com uma atividade de 185 a 370 MBq ou 5 a 10 mCi), são obtidas imagens planares em projeção anterior, além de tomográficas (SPECT) do tórax, enquanto o paciente permanece em

Contents

Figura Central: Como Eu Faço a Avaliação da Atividade Simpática Cardíaca

Arq Bras Cardiol: Imagem cardiovasc. 2024;37(1):e20240009

SPECT: Single Photon Emission Computed Tomography.

decúbito dorsal, com o braço esquerdo levantado acima do tórax.[7] Embora as imagens SPECT sejam opcionais, elas auxiliam na avaliação da atividade simpática miocárdica regional e podem ser comparadas com as imagens da cintilografia de perfusão miocárdica para avaliação de áreas perfundidas, mas desnervadas (*mismatch*), que são mais suscetíveis a arritmias.[9]

Nas imagens planares anteriores de tórax, avaliamos a relação entre a captação de mIBG-I123 no coração e no mediastino (C/M) e a taxa de clareamento miocárdico (taxa de *washout* - TW). A relação C/M precoce e tardia é calculada através da média de contagens por pixel em regiões de interesse desenhadas no mediastino superior (7x7 pixels) e no coração como um todo (Figura 2). A relação C/M precoce representa a integridade dos terminais nervosos pré-sinápticos e a densidade dos receptores β-adrenérgicos. Já a relação C/M tardia combina informações da função neural, incluindo captação, liberação e estocagem da NE nas vesículas pré-sinápticas. A TW, por sua vez, reflete o tônus adrenérgico cardíaco.[10] A TW do radiotraçador é calculada através da fórmula: TW = [(C - M precoce) - (C - M tardio)]/(C - M precoce) x 100 (%), que pode ser corrigida pelo fator de decaimento do iodo-123 (fator de 1,21, caso o intervalo de tempo entre as imagens precoces e tardias sejam de 3 horas e 45 minutos, por exemplo).[7]

Os valores normais da relação C/M variam de 1,8 a 2,8, com uma média aproximada de 2,2 ± 0,3 nas imagens tardias. O valor médio da TW de controles normais é cerca de 10 ± 9%. A variabilidade intra e interobservador dessas medidas é inferior a 5%. Vale destacar que, quanto menor a relação C/M e maior a TW, pior é a atividade simpática cardíaca.[8]

As imagens tomográficas (SPECT) são obtidas com 60 projeções, cada uma com duração de 30 segundos, cobrindo um arco de 180° armazenadas em matriz 64 x 64. Essas imagens são usadas para análise e quantificação da distribuição global e segmentar do mIBG-I123 no miocárdio ventricular esquerdo, de forma visual semiquantitativa nos três eixos tomográficos (eixo curto, eixo longo vertical e eixo longo horizontal).

Aplicações clínicas

A cintilografia cardíaca com mIBG-123I pode ser útil em vários cenários clínicos (Tabela 1), sendo usada com mais frequência na insuficiência cardíaca (IC) e como auxiliar no diagnóstico de doenças neurodegenerativas.

Seu uso na IC

O coração do paciente com IC, quando exposto cronicamente a concentrações elevadas de NE circulante, tende a desenvolver um bloqueio na função responsiva dos receptores agonistas β-adrenérgicos.[11] Diversos mecanismos podem contribuir para esse fenômeno, como o *downregulation* dos receptores β-adrenérgicos, não acoplamento dos subtipos de β-receptores, *upregulation* da enzima β-adrenoreceptor quinase, aumento da atividade da proteína G e redução da atividade da adenilciclase. O próprio remodelamento ventricular, que envolve hipertrofia e apoptose dos miócitos provocados pela NE, está associado à reexpressão dos genes fetais com consequente *downregulation* dos genes adultos. Isto demonstra que a estimulação adrenérgica crônica direta dos receptores β-adrenérgicos nos miócitos e fibroblastos é cardiotóxica, contribuindo para diversas mudanças bioquímicas e estruturais na IC (Figura 3).[11,12]

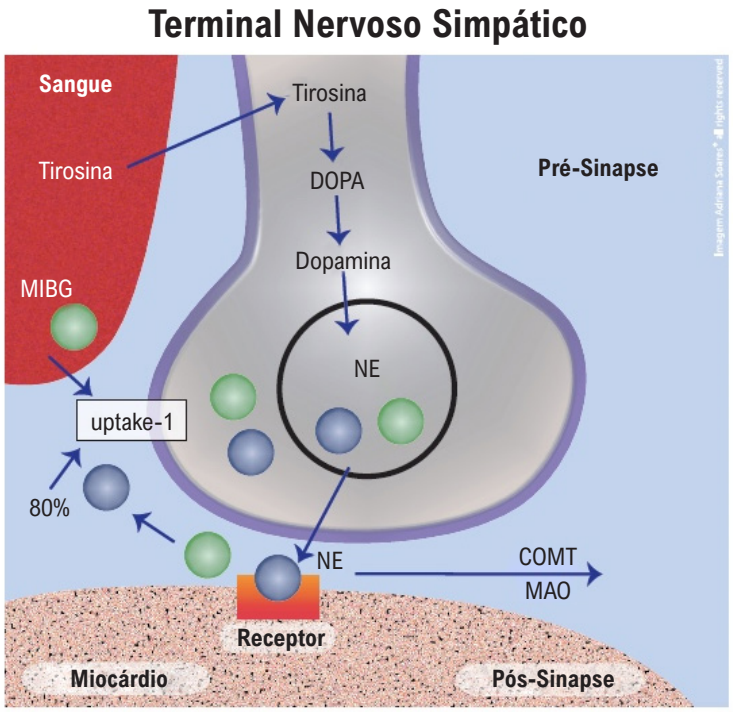

Figura 1 – *Imagem representativa da captação e liberação da metaiodobenzilguanidina (mIBG) nas terminações nervosas sinápticas cardíacas pelos receptores uptake-1 de forma similar a norepinefrina (NE). DOPA: L-Dopa; COMT: Catecol-O-Metiltransferasae; MAO: Monoaminoxidase. Fonte: Acervo pessoal dos autores.*

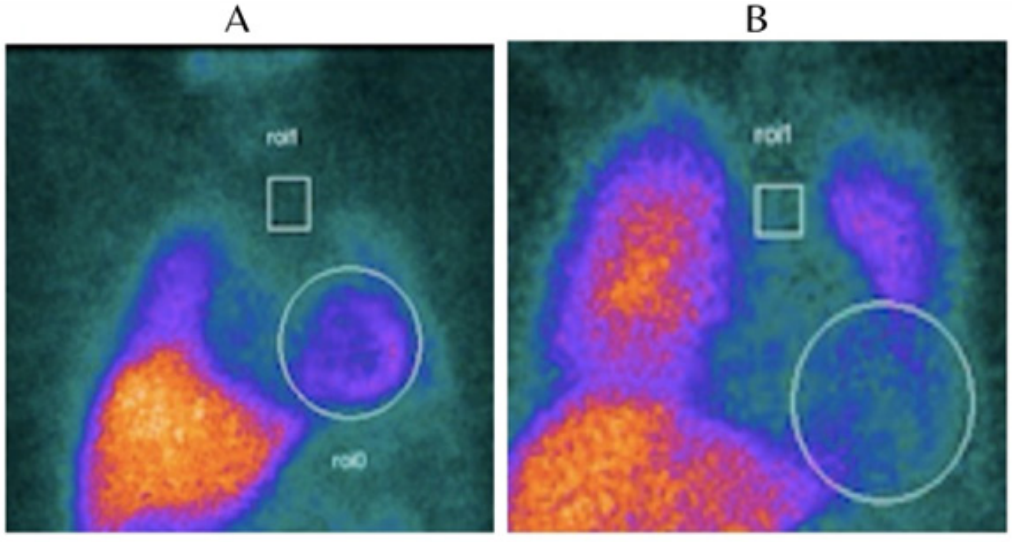

Figura 2 – *Cintilografia cardíaca com mIBG-I123. Em A: imagem planar tardia de tórax anterior demonstrando padrão normal de captação de mIBG-I123 no miocárdio do ventrículo esquerdo (VE), com áreas de interesse desenhadas sobre o VE (círculo) e o mediastino superior (retângulo) para cálculo da relação coração/mediastino (C/M); em B: imagem de um paciente com insuficiência cardíaca (IC) com hipocaptação acentuada de mIBG-I123 em topografia de VE (círculo) e índice C/M muito reduzido, indicativo de hiperatividade simpática cardíaca. Fonte: Acervo pessoal dos autores.*

Tabela 1 – Principais aplicações clínicas da cintilografia cardíaca com mIBG-I123.

Cenários clínicos	Estabelecidos	Potenciais
ICFEr	Estratificação de risco, independentemente de outros parâmetros, avaliação de progressão de IC, eventos arrítmicos e mortalidade cardíaca total até 2 anos. Identificação de um subgrupo de baixo risco para eventos cardíacos e morte. Seguimento clínico de terapias médicas indicadas nas diretrizes.	Identificar os pacientes mais prováveis a se beneficiarem da TRC ou DAVE. Guiar o tratamento de pacientes com DAVE: ponte para transplante, possível explante. Marcador substituto para avaliar benefício de novas terapias médicas e dispositivos.
ICFEp	Subanálises de estudos maiores mostram capacidade de estratificação de risco similar àquela vista em pacientes com ICFEr.	Identificar pacientes que podem ser de maior risco do que aquele aparentado clinicamente.
Arritmias associadas à IC	Estratificação de risco para arritmias ventriculares letais ou potencialmente letais até 2 anos. Identificação de pacientes de muito baixo risco de eventos arrítmicos letais até 2 anos.	Refinar critérios de indicação para pacientes que se beneficiarão de CDI. Ajudar a identificar pacientes que não mais necessitarão de CDI, em fim de vida da bateria ou com quadro de infecção do dispositivo.
Condições arrítmicas primárias	Identificação de pacientes de risco a desfechos piores, incluindo eventos arrítmicos e mortalidade total.	Melhorar entendimento da fisiopatologia das condições arrítmicas primárias. Guiar conduta de pacientes com condições arrítmicas primárias.
Transplante cardíaco	Acompanhar reinervação cardíaca após transplante.	Identificar pacientes mais prováveis de terem complicações após transplante, incluindo rejeição e transplante por DAC.
Doença cardíaca isquêmica	Avaliação da área de risco em pacientes com síndromes coronárias agudas. Estratificação de risco de pacientes com miocárdio hibernante.	Guiar conduta de pacientes com síndromes coronárias agudas. Guiar conduta de pacientes após evento isquêmico. Memória isquêmica.
Diabetes mellitus	Identificação de anormalidades autonômicas cardíacas, incluindo pacientes sem manifestações extracardíacas.	Identificar pacientes de maior risco clínico do que o aparente, auxiliando o diagnóstico e orientando tratamentos apropriados.
Cardiotoxicidade por quimioterápico	Identificar e quantificar lesão cardíaca em pacientes sob estes tratamentos.	Guiar conduta quimioterápica. Melhorar entendimento da fisiopatologia de toxicidade por fármacos.
Doenças neurodegenerativas	Diagnóstico diferencial de tremores (parkinsonismo). Ajudar no diagnóstico da DP e na diferenciação entre demência de Alzheimer e por corpos de Lewy. Identificar e quantificar lesão autonômica cardíaca.	Definição de conduta.
Doença de Chagas	Identificar e quantificar lesão autonômica cardíaca. Identificação de pacientes de risco a desfechos piores, incluindo eventos arrítmicos e mortalidade total.	Guiar tratamento.
Síndrome de Takotsubo	Identificar e quantificar lesão autonômica cardíaca.	Guiar tratamento. Melhorar entendimento da fisiopatologia.
Cardiomiopatias	Diagnóstico precoce. Estratificação de risco cardiovascular.	Guiar tratamento. Melhorar entendimento da fisiopatologia da doença.

CDI: cardioversor-desfibrilador implantável; DAC: doença arterial coronária; DAVE: dispositivo de assistência ventricular esquerda; IC: insuficiência cardíaca; ICFEp: IC com fração de ejeção preservada; ICFEr: IC com fração de ejeção reduzida; mIBG-123I: metaiodobenzilguanidina marcada com iodo-123; TRC: terapia de ressincronização cardíaca; DP: doença de Parkinson. Adaptada de JCS Joint Working Group e da diretriz brasileira de cardiologia nuclear.[8]

Devido a essas mudanças, a cintilografia cardíaca com mIBG-I23 na IC é caracterizada pela captação miocárdica reduzida do radiotraçador e aceleração da TW quando comparada à de indivíduos saudáveis.[5,13] Vários estudos têm demonstrado que a relação C/M diminuída, bem como a TW elevada, são fatores preditivos independentes de desfechos adversos cardíacos, como morte, progressão da IC e arritmia ventricular, em pacientes com disfunção ventricular esquerda. Esse prognóstico é ainda mais robusto que a fração de ejeção do ventrículo esquerdo (FEVE), a classe funcional pela *New York Heart Association* (NYHA), o tamanho do ventrículo esquerdo (VE) e os valores de NE plasmática.[14,15]

Os resultados do ensaio clínico ADMIRE-HF, prospectivo e multicêntrico, revelaram que os pacientes portadores de IC com classe funcional II ou III da NYHA, com relação C/M inferior a 1,6 apresentaram uma taxa de morte cardíaca de 19,1% em comparação com 1,8% no grupo com valores acima de 1,6, um valor preditivo negativo para esses desfechos em dois anos, atingindo 98,8%.[16]

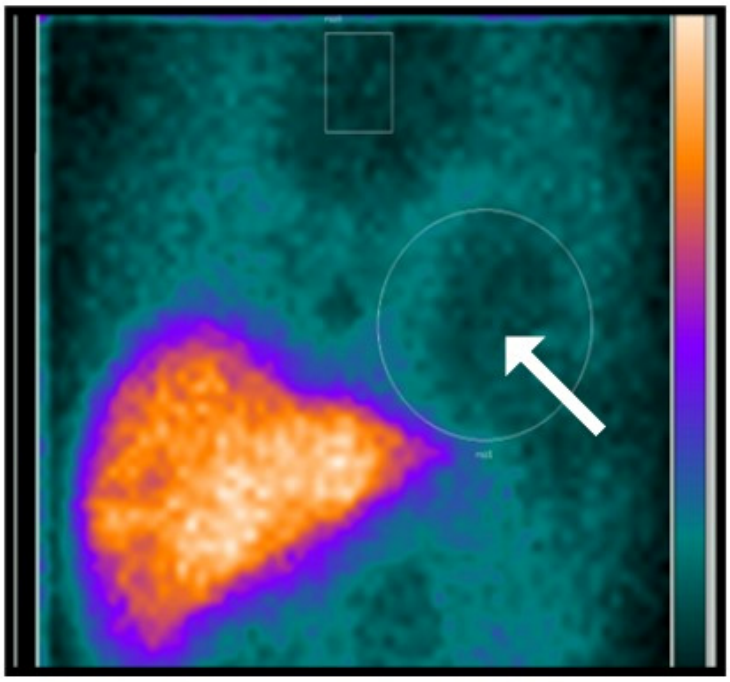

Figura 3 – *Imagem planar tardia da cintilografia cardíaca com mIBG-I123. Observa-se hipocaptaçao acentuada do radiotraçador em topografia do ventrículo esquerdo (círculo). A relação tardia da captação de mIBG-I123 entre o coração e o mediastino foi de 1,21 e a taxa de washout de 42%, indicando hiperatividade simpática cardíaca. Fonte: Acervo pessoal dos autores.*

No que tange à avaliação terapêutica da disfunção ventricular, numerosas pesquisas que utilizaram a cintilografia cardíaca com mIBG-I123 demonstraram que o uso de betabloqueadores, IECA e espironolactona podem melhorar expressivamente a atividade do SNS cardíaco.[15,17,18] Estudos também evidenciaram que o uso de carvedilol nos pacientes com IC resultou em melhorias na captação cardíaca e a TW de mIBG-I123, a FEVE, os volumes sistólico e diastólico do VE, a classe funcional, e na redução significativa dos níveis de peptídeo natriurético cerebral (BNP). Esses resultados sugerem que o uso de carvedilol pode contribuir para a melhoria da disfunção adrenérgica e do remodelamento ventricular.[14]

Em relação ao uso de dispositivos intracardíacos, uma pesquisa demonstrou que a terapia de ressincronização biventricular (TRC) resultou em um aumento na captação precoce e tardia de mIBG-I123, evidenciando uma melhora significativa na atividade do SNS cardíaco em pacientes com IC após o implante desse tipo de marca-passo. Essa descoberta sugere que este pode ser o mecanismo potencial dos benefícios observados nos grandes estudos sobre morbidade e mortalidade na TRC.[19] Além disso, um estudo brasileiro destacou que a cintilografia cardíaca com mIBG-I123 pode auxiliar no refinamento dos critérios de indicação para a TRC. Pacientes com IC grave e uma relação C/M tardia inferior a 1,36 apresentaram menor probabilidade de resposta favorável à TRC.[20,21]

Alguns autores também correlacionaram a denervação adrenérgica na cintilografia à morte súbita em pacientes com disfunção ventricular esquerda, mesmo naqueles com disfunção leve e classe funcional I da NYHA. As alterações do SNS também foram identificadas como preditores independentes de recorrência de taquicardia e fibrilação ventricular nos pacientes com história prévia destas arritmias. Conclui-se, portanto, que a cintilografia cardíaca com mIBG-I123 pode ser uma boa opção para *screening* de pacientes com alto risco de morte súbita.[21,22]

Além das indicações acima descritas, outras aplicações estão destacadas na Tabela 1.

Seu uso no parkinsonismo e no diagnóstico diferencial do tipo de demência

A doença de Parkinson (DP) é a doença neurodegenerativa mais comum que causa parkinsonismo. Caracteriza-se pelo acometimento de neurônios dopaminérgicos e não dopaminérgicos, evidenciando-se pela agregação anormal de α-sinucleína na substância negra compacta, formando inclusões intracitoplasmática neuronal, conhecidas como corpos de Lewy. Apesar de já existirem critérios diagnósticos consensuais para DP e outras doenças neurodegenerativas que apresentam parkinsonismo, como a paralisia supranuclear progressiva, atrofia de múltiplos sistemas e degeneração corticobasal, um diagnóstico preciso desses distúrbios continua a ser um grande desafio para os neurologistas.[23]

Pesquisas têm demonstrado uma redução na captação cardíaca de mIBG-I123 em pacientes afetados por doenças com inclusão de corpos de Lewy, como a DP[24,25] e a própria demência por corpos de Lewy (DLB). A avaliação da inervação simpática miocárdica pela cintilografia cardíaca com mIBG-I123 é útil em

diferenciar DP de outras causas de parkinsonismo, incluindo os tremores essenciais, bem como diferenciar a DLB da doença de Alzheimer.[26]

A neurodegeneração dependente da α-sinucleína na DP afeta os neurônios autonômicos pré e pós-ganglionares, prejudicando a captação cardíaca de mIBG-I123. Em contrapartida, em outras doenças como a atrofia de múltiplos sistemas, em que a insuficiência autonômica é predominantemente pré-ganglionar, a captação cardíaca de mIBG-I123 permanece preservada. Um estudo *post-mortem* mostrou uma significativa diminuição no número de axônio imunorreativos da tirosina hidroxilase, um marcador para axônios simpáticos do coração, na DP e na DLB. Esse achado corroboram com os resultados que indicam uma redução na captação cardíaca de mIBG-I123 nessas doenças, apresentando valores muito baixos dos índices C/M precoce e tardia, e demonstrando alta sensibilidade e especificidade do método (em torno de 90%), mesmo nos estágios iniciais da doença.[26,27]

Em um estudo brasileiro, Leite et al. avaliaram pacientes com DP de início esporádico, sem disautonomia clinicamente definida, e observaram que a captação cardíaca de mIBG-I123 nas imagens SPECT foi baixa ou ausente em todos os pacientes, concluindo que o exame foi capaz de identificar alterações da neurotransmissão simpática cardíaca em pacientes com DP, mesmo sem sintomas de disautonomia.[27]

Atualmente a cintilografia cardíaca com mIBG-I123 já é recomendada (nível A) pela *European Federation of Neurological Societies* e pela força-tarefa da *Movement Disorder Society* para o diagnóstico diferencial das síndromes com parkinsonismo.[28]

Exemplos ilustrativos da prática clínica

Caso 1: Homem, 66 anos, ICFER (classe funcional III da NYHA), cardiopatia isquêmica, com queixa de cansaço e palpitações. Ecocardiograma com FEVE de 37%, BNP de 2180 pg/mL e com episódios de taquicardia ventricular não sustentada (TVNS) ao holter de 24 horas. Realizou cintilografia cardíaca com mIBG-I123 (Figura 3) que indicou um comprometimento acentuado da inervação simpática miocárdica, denotando pior prognóstico e maior risco de arritmias ventriculares fatais. O paciente foi encaminhado para implante de cardiodesfibrilador implantável (CDI) e, seis meses após o procedimento, recebeu choques apropriados do dispositivo.

Caso 2: Mulher, 42 anos, doença de Chagas na fase indeterminada, com queixa de lipotimia. Ecocardiograma com FEVE de 63% (Simpson); holter de 24h que mostrou ectopias ventriculares frequentes e episódios curtos de TVNS. Realizou cintilografia cardíaca com mIBG-I123 e de perfusão miocárdica com sestamibi-Tc99m (Figura 4) que revelou tecido miocárdico denervado com perfusão normal (*mismatch*), sugerindo maior risco de arritmias ventriculares potencialmente fatais.

Caso 3: Mulher, 62 anos, jornalista, procurou o neurologista devido a leve rigidez matinal do membro superior direito. Negava outros sintomas ou doenças crônicas. Encaminhada para o exame de cintilografia cardíaca com mIBG-I123 (Figura 5) para investigação de DP. O exame revelou grave comprometimento da inervação simpática miocárdica, achados característicos na DP.

Considerações finais

A cintilografia com mIBG-I123 proporciona uma perspectiva detalhada sobre o estado da inervação simpática cardíaca, refinando a estratificação do risco cardiovascular e facilitando o diagnóstico precoce de cardiopatias e doenças neurodegenerativas. No entanto, aprimoramentos na experiência clínica são essenciais para otimizar os valores preditivos positivos e negativos deste método, o que permitirá uma melhor distinção entre pacientes de baixo e alto risco cardiovascular. Além disso, a escassez de dados sobre custo-efetividade e a limitada disponibilidade em ambientes clínicos representam desafios significativos para sua implementação em larga escala.

Contribuição dos Autores

Concepção e desenho da pesquisa, obtenção de dados, análise e interpretação dos dados, análise estatística, redação do manuscrito, revisão crítica do manuscrito quanto ao conteúdo intelectual importante: Brito ASX, Leite JC, Brandão SCS.

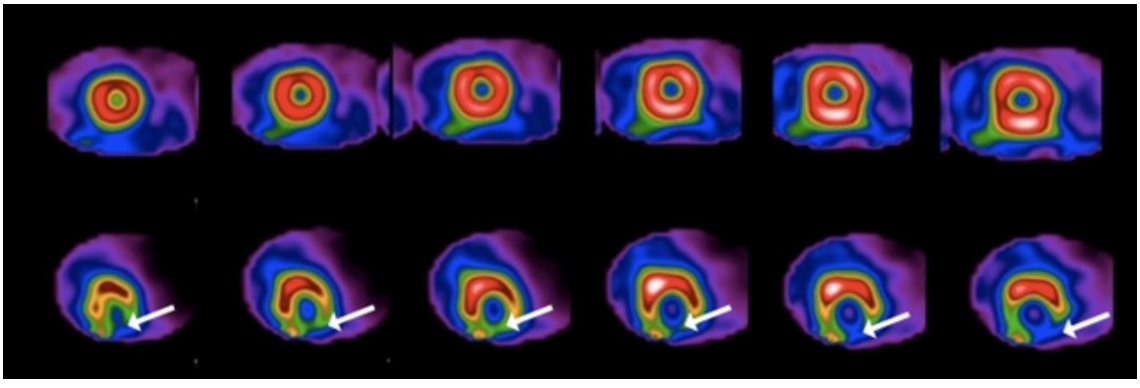

Figura 4 – *Cintilografia cardíaca com mIBG-I123 (fileira inferior) e de perfusão miocárdica com sestamibi-Tc99m (fileira superior). As imagens SPECT do curto eixo mostram um padrão mismatch entre perfusão/inervação simpática do miocárdio ventricular esquerdo, com perfusão normal e hipocaptaçao acentuada do mIBG-I123 nos segmentos apicais, inferiores e inferolaterais (setas), sugestivo de tecido miocárdico denervado nestas regiões. Fonte: Acervo pessoal dos autores.*

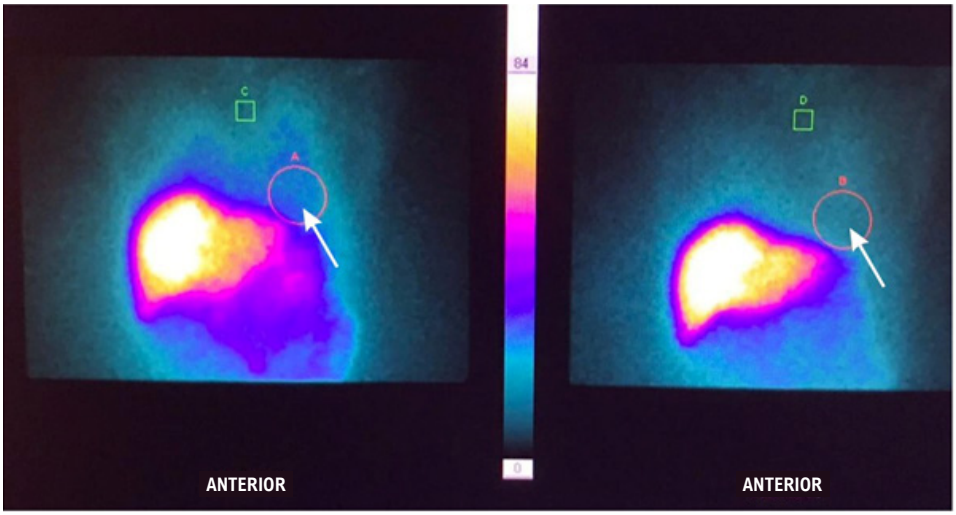

Figura 5 – *Imagem planar da cintilografia cardíaca com mIBG-I123. Observa-se hipocaptaçao acentuada do radiotraçador em topografia cardíaca (seta). A relação da captação de mIBG-I123 entre o coração e o mediastino foi de 1,31 (precoce) e 1,23 (tardia). A taxa de washout foi 35%. Esses dados sugerem comprometimento grave da inervação simpática miocárdica, característicos na doença de Parkinson. Fonte: Acervo pessoal dos autores.*

Potencial Conflito de Interesse

Declaro não haver conflito de interesses pertinentes.

Fontes de Financiamento

O presente estudo não teve fontes de financiamento externas.

Vinculação Acadêmica

Não há vinculação deste estudo a programas de pós-graduação.

Aprovação Ética e Consentimento Informado

Este artigo não contém estudos com humanos ou animais realizados por nenhum dos autores.

Referências

1. Gibbons CH. Basics of Autonomic Nervous System Function. Handb Clin Neurol. 2019;160:407-18. doi: 10.1016/B978-0-444-64032-1.00027-8.
2. Goldberger JJ, Arora R, Buckley U, Shivkumar K. Autonomic Nervous System Dysfunction: JACC Focus Seminar. J Am Coll Cardiol. 2019;73(10):1189-206. doi: 10.1016/j.jacc.2018.12.064.
3. Brito AX, Glavam A, Bronchtein AI, Rosado-de-Castro PH. Autonomic Innervation Evaluation in Cardiac Disease. Int J Cardiovasc Sci. 2021;34(6):702-13. doi: 10.36660/ijcs.20200171.
4. Leite J, Brandão S. Assessment of Cardiac Sympathetic Activity by Nuclear Medicine: Many Clinical Benefits but Weak Recommendation. Int J Cardiovasc Sci. 2021;34(6):714-6. doi: 10.36660/ijcs.20210213.
5. Carrió I. Cardiac Neurotransmission Imaging. J Nucl Med. 2001;42(7):1062-76.
6. Nakajo M, Shapiro B, Copp J, Kalff V, Gross MD, Sisson JC, et al. The Normal and Abnormal Distribution of the Adrenomedullary Imaging Agent m-[I-131] Iodobenzylguanidine (I-131 MIBG) in Man: Evaluation by Scintigraphy. J Nucl Med. 1983;24(8):672-82.
7. Flotats A, Carrió I, Agostini D, Le Guludec D, Marcassa C, Schäfers M, et al. Proposal for Standardization of 123I-Metaiodobenzylguanidine (MIBG) Cardiac Sympathetic Imaging by the EANM Cardiovascular Committee and the European Council of Nuclear Cardiology. Eur J Nucl Med Mol Imaging. 2010;37(9):1802-12. doi: 10.1007/s00259-010-1491-4.
8. Mastrocola LE, Amorim BJ, Vitola JV, Brandão SCS, Grossman GB, Lima RSL, et al. Update of the Brazilian Guideline on Nuclear Cardiology - 2020. Arq Bras Cardiol. 2020;114(2):325-429. doi: 10.36660/abc.20200087.
9. Brito ASX, Moll-Bernardes RJ, Pinheiro MVT, Camargo GC, Siqueira FPR, Oliveira RS, et al. Autonomic Denervation, Myocardial Hypoperfusion and Fibrosis May Predict Ventricular Arrhythmia in the Early Stages of Chagas Cardiomyopathy. J Nucl Cardiol. 2023;30(6):2379-88. doi: 10.1007/s12350-023-03281-9.
10. Agostini D, Carrio I, Verberne HJ. How to Use Myocardial 123I-MIBG Scintigraphy in Chronic Heart Failure. Eur J Nucl Med Mol Imaging. 2009;36(4):555-9. doi: 10.1007/s00259-008-0976-x.
11. Flotats A, Carrió I. Cardiac Neurotransmission SPECT Imaging. J Nucl Cardiol. 2004;11(5):587-602. doi: 10.1016/j.nuclcard.2004.07.007.
12. Liang CS, Fan TH, Sullebarger JT, Sakamoto S. Decreased Adrenergic Neuronal Uptake Activity in Experimental Right Heart Failure. A Chamber-Specific Contributor to Beta-Adrenoceptor Downregulation. J Clin Invest. 1989;84(4):1267-75. doi: 10.1172/JCI114294.
13. Knuuti J, Sipola P. Is it Time for Cardiac Innervation Imaging? Q J Nucl Med Mol Imaging. 2005;49(1):97-105.
14. Kasama S, Toyama T, Hatori T, Sumino H, Kumakura H, Takayama Y, et al. Evaluation of Cardiac Sympathetic Nerve Activity and Left Ventricular Remodelling in Patients with Dilated Cardiomyopathy on the Treatment Containing Carvedilol. Eur Heart J. 2007;28(8):989-95. doi: 10.1093/eurheartj/ehm048.
15. Henneman MM, Bax JJ, van der Wall EE. Monitoring of Therapeutic Effect in Heart Failure Patients: A Clinical Application of 123I MIBG Imaging? Eur Heart J. 2007;28(8):922-3. doi: 10.1093/eurheartj/ehl325.

16. Jacobson AF, Senior R, Cerqueira MD, Wong ND, Thomas GS, Lopez VA, et al. Myocardial Iodine-123 Meta-Iodobenzylguanidine Imaging and Cardiac Events in Heart Failure. Results of the Prospective ADMIRE-HF (AdreView Myocardial Imaging for Risk Evaluation in Heart Failure) Study. J Am Coll Cardiol. 2010;55(20):2212-21. doi: 10.1016/j.jacc.2010.01.014.

17. Kasama S, Toyama T, Kumakura H, Takayama Y, Ichikawa S, Suzuki T, et al. Effect of Spironolactone on Cardiac Sympathetic Nerve Activity and Left Ventricular Remodeling in Patients with Dilated Cardiomyopathy. J Am Coll Cardiol. 2003;41(4):574-81. doi: 10.1016/s0735-1097(02)02855-3.

18. Fujimoto S, Inoue A, Hisatake S, Yamashina S, Yamashina H, Nakano H, et al. Usefulness of 123I-Metaiodobenzylguanidine Myocardial Scintigraphy for Predicting the Effectiveness of Beta-Blockers in Patients with Dilated Cardiomyopathy from the Standpoint of Long-Term Prognosis. Eur J Nucl Med Mol Imaging. 2004;31(10):1356-61. doi: 10.1007/s00259-004-1557-2.

19. Gould PA, Kong G, Kalff V, Duffy SJ, Taylor AJ, Kelly MJ, et al. Improvement in Cardiac Adrenergic Function Post Biventricular Pacing for Heart Failure. Europace. 2007;9(9):751-6. doi: 10.1093/europace/eum081.

20. Nishioka SA, Martinelli Filho M, Brandão SC, Giorgi MC, Vieira ML, Costa R, et al. Cardiac Sympathetic Activity pre and Post Resynchronization Therapy Evaluated by 123I-MIBG Myocardial Scintigraphy. J Nucl Cardiol. 2007;14(6):852-9. doi: 10.1016/j.nuclcard.2007.08.004.

21. Arora R, Ferrick KJ, Nakata T, Kaplan RC, Rozengarten M, Latif F, et al. I-123 MIBG Imaging and Heart Rate Variability Analysis to Predict the Need for an Implantable Cardioverter Defibrillator. J Nucl Cardiol. 2003;10(2):121-31. doi: 10.1067/mnc.2003.2.

22. Akutsu Y, Kaneko K, Kodama Y, Li HL, Kawamura M, Asano T, et al. The Significance of Cardiac Sympathetic Nervous System Abnormality in the Long-Term Prognosis of Patients with a History of Ventricular Tachyarrhythmia. J Nucl Med. 2009;50(1):61-7. doi: 10.2967/jnumed.108.055194.

23. Yoshita M. Differentiation of Idiopathic Parkinson's Disease from Striatonigral Degeneration and Progressive Supranuclear Palsy Using Iodine-123 Meta-Iodobenzylguanidine Myocardial Scintigraphy. J Neurol Sci. 1998;155(1):60-7. doi: 10.1016/s0022-510x(97)00278-5.

24. Orimo S, Ozawa E, Nakade S, Sugimoto T, Mizusawa H. (123) I-Metaiodobenzylguanidine Myocardial Scintigraphy in Parkinson's Disease. J Neurol Neurosurg Psychiatry. 1999;67(2):189-94. doi: 10.1136/jnnp.67.2.189.

25. Watanabe H, Ieda T, Katayama T, Takeda A, Aiba I, Doyu M, et al. Cardiac (123)I-Meta-Iodobenzylguanidine (MIBG) Uptake in Dementia with Lewy Bodies: Comparison with Alzheimer's Disease. J Neurol Neurosurg Psychiatry. 2001;70(6):781-3. doi: 10.1136/jnnp.70.6.781.

26. Amino T, Orimo S, Itoh Y, Takahashi A, Uchihara T, Mizusawa H. Profound Cardiac Sympathetic Denervation Occurs in Parkinson Disease. Brain Pathol. 2005;15(1):29-34. doi: 10.1111/j.1750-3639.2005.tb00097.x.

27. Leite MA, Nascimento OJ, Pereira JS, Amaral C, Mesquita CT, Azevedo JC, et al. Cardiac 123I-MIBG Uptake in de Novo Brazilian Patients with Parkinson's Disease Without Clinically Defined Dysautonomia. Arq Neuropsiquiatr. 2014;72(6):430-4. doi: 10.1590/0004-282x20140042.

28. Berardelli A, Wenning GK, Antonini A, Berg D, Bloem BR, Bonifati V, et al. EFNS/MDS-ES/ENS [corrected] Recommendations for the Diagnosis of Parkinson's Disease. Eur J Neurol. 2013;20(1):16-34. doi: 10.1111/ene.12022.

Review Article

What do Cardiologists Expect Towards Myocardial Viability Assessment

Eduardo Gomes Lima,[1,2] Eduardo Bello Martins,[1,3] Leticia Neves Solon Carvalho,[1] Diogo Freitas Cardoso de Azevedo[1,4]

Instituto do Coração do Hospital das Clínicas da Faculdade de Medicina da USP (InCor-HCFMUSP),[1] São Paulo, SP – Brazil
Dasa/ Hospital 9 de Julho,[2] São Paulo, SP – Brazil
Hospital Israelita Albert Einstein,[3] São Paulo, SP – Brazil
Hospital Aliança/ Rede D'Or,[4] Salvador, BA – Brazil

Abstract

Within the clinical spectrum of chronic coronary syndrome (CCS), the presence of coronary artery disease (CAD) alongside ventricular dysfunction has long been a focal point due to the lower survival rates seen in this population. Improving survival in these patients, whether through medications or interventions, is a key concern for clinical cardiologists. Previous observational studies suggested that myocardial viability (MV) could influence the effectiveness of revascularization strategies in patients with ventricular dysfunction. Thus, viability assessment became a standard practice in cardiology. Different imaging methods assess viability through different parameters (such as cell membrane integrity, mitochondrial function, glycolytic metabolism, contractile reserve, or evidence of fibrosis), leading to differing sensitivities and specificities. However, recent evidence from large randomized studies does not support the notion that the presence of MV, as determined by various methods, is linked to the prognostic benefit of revascularization. Furthermore, the reduction in mortality observed in these studies was not attributed to the recovery of contractile function but rather to a decrease in fatal heart attacks. As a result, the current role of MV as a decision-making tool for revascularization in patients with CCS and left ventricular dysfunction has diminished. Nonetheless, there are still situations in specialist practice where its use may be warranted, particularly in the context of constructing a comprehensive functional revascularization strategy.

Introduction

Within the clinical spectrum of chronic coronary syndrome (CCS), the presence of coronary artery disease (CAD) alongside ventricular dysfunction has long been a focal point due to the lower survival rates seen in this population. Improving survival in CCS patients, whether through medications or interventions, has been a key concern for clinical cardiologists for over 40 years. The concept of stunned and hibernating myocardium, which refers to dysfunctional myocardium capable of recovering contractile function following myocardial revascularization, has long driven efforts to improve prognosis in affected patients. The search for imaging modalities that could identify dysfunctional yet recoverable myocardium, guiding decisions on revascularization, defined a generation of cardiologists. Initially, observational studies suggested that the presence or absence of myocardial viability (MV), as determined by imaging, could significantly impact the success of revascularization surgery.[1]

However, recent randomized studies have challenged this notion, pointing to a reduction in mortality with coronary artery bypass graft surgery (CABG) in long-term follow-up, irrespective of documented viability and even in cases where there was no immediate recovery of left ventricular ejection fraction (LVEF).[2,3] This has led to a reevaluation of how we incorporate MV information into clinical practice. Here are three common questions asked by clinical cardiologists in light of recent evidence: 1) Do I still need viability documentation to assess the indication of coronary intervention in CCS patients with reduced LVEF? 2) Is LVEF recovery relevant to this decision? 3) What is the current use of viability detection methods in cardiology?

Viability assessment methods

Part of the controversy regarding the assessment of viability for decision-making in patients with CCS and ventricular dysfunction is due to its complex definition. What is viability, after all?

From a pathophysiological standpoint, viable myocytes are those that have not undergone irreversible damage, retaining their mitochondrial function and membrane integrity. In clinical terms, on the other hand, viability refers to a myocardium with systolic dysfunction at rest that can potentially recover contractile function following revascularization. These definitions are distinct, with the latter being rooted in the concepts of stunned and hibernating myocardium.

In 1912, Herrick conducted physiological research on myocardial ischemia, demonstrating that permanent coronary occlusion leads to acute myocardial infarction (AMI).[4] Intense and prolonged ischemia at the cellular level results in necrosis and eventual replacement of the affected area with fibrotic tissue. However, in cases of non-lethal ischemia, transient systolic dysfunction can occur, with contractile recovery

Keywords

Myocardial Ischemia; Left Ventricular Function; Myocardial Stunning;

Mailing Address: Eduardo Gomes Lima •
Universidade de São Paulo Instituto do Coração, Atherosclerosis. Av Dr Enéas de C Aguiar, 44. Postal code: 05403-000. São Paulo, SP - Brazil
E-mail: eduglima@yahoo.com.br
Manuscript received February 6, 2024; revised February 6, 2024; accepted February 6, 2024
Editor responsible for the review:Marcelo Dantas Tavares de Melo

DOI: https://doi.org/10.36660/abcimg.20240005i

Contents

Central Illustration: What do Cardiologists Expect Towards Myocardial Viability Assessment

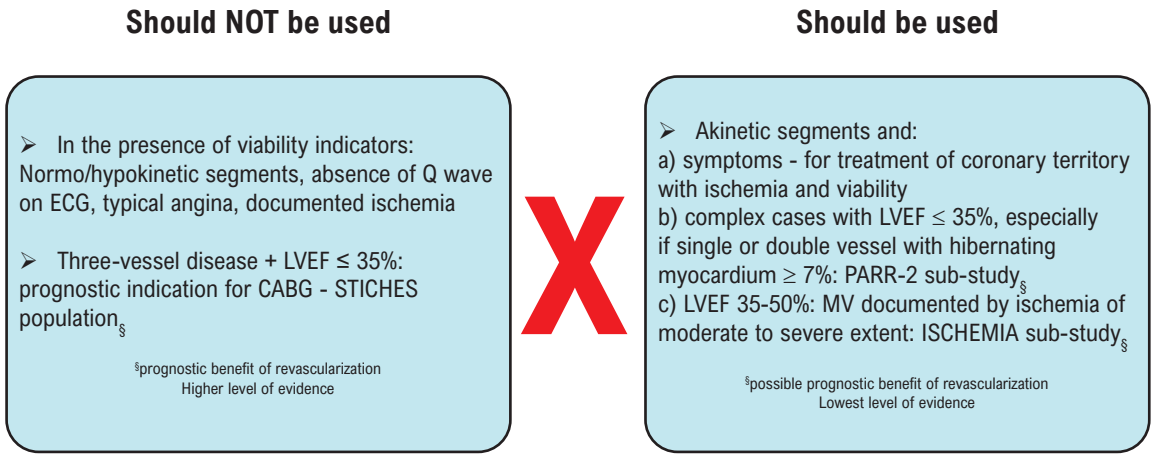

Arq Bras Cardiol: Imagem cardiovasc. 2024;37(1):e20240005

Use of MV in decision-making in ischemic heart diseasez. LVEF: left ventricular ejection fraction; CABG: coronary artery bypass graft; MV: myocardial viability; PARR-2: PET and Recovery Following Revascularization-2; ECG: electrocardiogram.

possible after reperfusion. Such dysfunction can persist for days after reperfusion, leading us to the concept of stunned myocardium, introduced in 1982.[5] In the spectrum of CCS, the combination of repeated ischemic episodes (chronic stunning) alongside the advancement of coronary stenosis results in an adaptive state involving the downregulation of myocardial function, aiming to preserve viable myocytes through cellular dedifferentiation and the loss of contractile filaments, a phenomenon known as hibernation.[6] Recovery of contractile function in hibernating myocardium can occur months after revascularization. Each complementary method evaluates a pathophysiological aspect to predict the chance of functional recovery, making it crucial for the clinician to understand the accuracy and methodology of each imaging modality.

Viability research can be simplified into a dichotomous scenario: either we look for evidence of cell death, translated as fibrosis; or signs of life, such as membrane integrity, glycolytic metabolism, and contractile reserve.

At the beginning of the investigation, we usually have a Transthoracic Doppler Echocardiogram (TTECO) of the patient at rest, an examination that demonstrates akinetic segments and motivates the viability research. Two-dimensional assessment, based on hyperechogenic myocardium and thinning of the ventricular wall (end-diastolic thickness < 6 mm), indicates significant fibrosis and lack of viability. However, this method has low specificity, as demonstrated in a study comparing it with the current gold standard, cardiac magnetic resonance (CMR) with late gadolinium enhancement (LGE).[7] LGE is the modality of choice in non-invasive evaluation to identify myocardial fibrosis, whether in ischemic or non-ischemic disease. After intravenous injection, gadolinium takes the extracellular space but is unable to cross the cell membrane of a normal myocyte. In case of increased extracellular space, as in chronic fibrosis, there is a late contrast washout, which remains visible in image acquisition after 10-15 minutes. The normal myocardial signal is annulled and scar areas appear bright, as an accurate estimate of the fibrosis percentage. Myocardial segments with transmural enhancement > 50% have a very low chance of contractile recovery after revascularization.[7]

Using these same two methods, TTECO and CMR, contractile reserve can be assessed. In low doses (2.5 - 10 mcg/kg/min), dobutamine has an inotropic effect on dysfunctional cells. At higher doses, its chronotropic effect becomes more prominent, increasing myocardial oxygen consumption. This can lead to ischemia if there is a significant lesion in the coronary artery supplying this territory. Enhanced contractile function when using low dobutamine doses, followed by declined function at higher doses, known as a biphasic response, presents the greatest specificity for recovery of contractile function.[8]

Nuclear medicine techniques combine myocardial perfusion and cellular metabolism to assess MV. In myocardial scintigraphy, the uptake and retention of radiotracers such as Thallium-201 (^{201}Tl) and technetium (^{99m}Tc)-sestamibi depend on the integrity of the cell or mitochondrial membrane, respectively. The first, a potassium analogue, has Na+/K+/ATPase channel-dependent transport. The uptake of ^{99m}Tc-sestamibi, a lipophilic compound that enters the cell passively, depends on mitochondrial transmembrane potentials. Hibernation initially compromises the uptake of radiotracers. This image is then compared with the acquisition after late redistribution (in the case of ^{201}Tl, which has a long half-life) or after the use of nitrate, in which uptake is expected to define the territory as viable.[9]

In addition to evaluating perfusion at rest, proton emission tomography (PET-CT) is based on the use of glucose by the cell. In states of ischemia, myocardial metabolism transitions from the preferential oxidation of fatty acids to glucose, given their greater energy production.[10] PET-CT uses the radiopharmaceutical fluorodeoxyglucose (^{18}F-FDG), an analog that is captured by the same glucose transporter (GLUT 1). Myocardial areas with perfusion deficit that keep glycolytic metabolism active are considered viable.

Thus, we can appreciate that various imaging modalities possess differing sensitivities and specificities in detecting MV, partly due to their assessment of MV from distinct perspectives, as illustrated in Table 1.

Clinical studies and MV

As previously mentioned, the use of MV in patient selection for myocardial revascularization was initially justified by a well-established pathophysiological rationale, with observational studies indicating that only patients with a substantial amount of viable myocardium benefited from myocardial revascularization.[1] The prospective PARR-2 (PET and Recovery Following Revascularization 2) study further investigated this by randomizing patients to a strategy guided by PET-CT results, where recommendations were based on the extent of hibernating myocardium, compared to standard care.[12] Despite the initially negative primary result, a post-hoc analysis of patients who followed the PET recommendation (75% of the randomized sample) showed a 38% reduction in events compared to standard care. Another PARR-2 sub-analysis suggested that the benefit of revascularization was significant only in patients with ≥ 7% of hibernating myocardium.[13] However, the results of the two main randomized clinical studies published in the last two decades regarding the role of myocardial revascularization in left ventricular dysfunction have raised questions about the use of MV as a primary criterion for revascularization.

STICH

The STICHES study (Surgical Treatment in Ischemic Heart Failure Extension Study), after a ten-year follow-up, demonstrated the superiority of CABG over medical therapy in patients with severe left ventricular dysfunction (LVEF ≤ 35%), particularly in cases of three-vessel disease, leading to reduced incidences of sudden death and heart failure.[2,3] Notably, subjecting the patient to specific exams to document MV was not a requirement for inclusion in STICH. However, in a sub-study evaluating 601 out of 1212 randomized patients who had MV information, the benefit of CABG was found to be independent of the presence or absence of MV.[7] Additionally, in this same sub-study, the benefit of CABG was independent of LVEF recovery, which was similar between the groups receiving medical therapy and revascularization (2% in the MV group). Despite the negative result, numerous limitations can be observed in this sub-study: 1) STICH was not designed to evaluate the role of MV in making the decision whether to revascularize or not; 2) The viability methods used (scintigraphy and echocardiography) are not the most accurate (PET-CT and CMR); 3) Binary assessment of MV (defined as ≥ 5 dysfunctional and viable segments on TTECO under stress and ≥ 11 viable segments on scintigraphy, regardless of baseline contractility); 4) Only 114 patients without MV, which undermines the power of the study to identify different results compared to the group with viability; 5) Lack of a detailed analysis of the relationship between viability, dysfunctional myocardium, and ischemia in the patients included.

The sub-analysis of the STICH mode of death,[14] documenting the benefit of revascularization surgery in reducing fatal AMIs, helps us piece together this complex puzzle, as it suggests that the reduction in mortality may not occur solely through the recovery of LVEF but also through the reduction of fatal AMIs related to viable territories.

REVIVED-BCIS2

More recently, REVIVED-BCIS2 (Revascularization for Ischemic Ventricular Dysfunction) tested percutaneous coronary intervention (PCI) in relation to clinical treatment in patients with LVEF ≤ 35%.[15]

Table 1 – Image methods for VM detection and their main characteristics

Method	Principle used	Sensitivity[11]	Specificity[11]	Relevant points
LGE	Fibrosis quantification	84%	63%	The combination of LGE with dobutamine in low doses increases the specificity of the method.
TTECO under pharmacological stress	Contractile reserve	80%	78%	Widely available method, but dependent on the examiner and the patient's acoustic window.
Scintigraphy with 201Tl	Cell membrane integrity	87%	54%	Higher radiation rate, prolonged examination time.
Scintigraphy with 99mTc-sestamibi	Mitochondrial membrane integrity	83%	65%	Required use of nitrate or pharmacological stress.
PET with 18F-FDG	Glycolytic metabolism	92%	63%	Less available, high cost.

LGE: late gadolinium enhancement; TTECO: Transthoracic Doppler Echocardiogram; PET: proton emission tomography; ^{18}F-FDG: fluorodeoxyglucose.

This study compared percutaneous treatment to drug treatment in patients with moderate to severe ventricular dysfunction. However, MV was essential as an inclusion criterion. Viability was defined by several complementary methods: TTECO under dobutamine stress, CMR (≤25% transmurality with LGE); single photon emission computed tomography and PET-CT. It is noteworthy that 70% of the viability assessments were conducted using CMR, which is considered the gold standard for its superior resolution and its ability to analyze LVEF and assess myocardial fibrosis. There was no difference in the primary endpoint (combined death from all causes and hospitalization for heart failure) between the groups at a mean follow-up of 3.4 years. The analysis of the secondary endpoint, LVEF estimated by TTECO at 6 and 12 months, was also similar for both therapeutic strategies. Similar to the STICH study, there was a slight increase of less than 5% in LVEF between the groups. In both publications, revascularization of viable territories did not translate into improved ventricular function when compared to clinical treatment. Furthermore, in REVIVED-BCIS2, angioplasty was only performed on severely injured vessels, in viable territories, and even complete revascularization did not result in changes in the primary and secondary endpoints.

In a pre-specified sub-study of REVIVED-BCIS2,[16] analyses of CMR and TTECO images under dobutamine stress, performed before randomization, including tertiles of the number of viable segments, did not influence the effect of angioplasty on any endpoint, prognosis, or likelihood of improvement in ventricular function. In contrast, the extent of non-viable myocardium was associated with a greater probability of the primary endpoint, regardless of percutaneous or clinical treatment. This effect was primarily driven by increased mortality, showing a clear correlation between non-viable myocardium and cardiovascular death. When the burden of fibrosis was semiquantitatively assessed on CMR images, the prognostic association became even stronger. However, it is important to mention the limitations of this study, including its open design, lower-than-calculated statistical power, lack of detailed information regarding the interventional procedure, and absence of documentation regarding the association between ventricular dysfunction and ischemic etiology.

Table 2 outlines some of the main differences between the STICHES and REVIVED-BCIS2 studies regarding the use of viability and profile of patients included.

ISCHEMIA

Another recent analysis involved evaluating patients with ventricular dysfunction in the ISCHEMIA study.[17] In this study, the inclusion criterion was the presence of moderate to severe ischemia and, therefore, MV. Despite excluding patients with LVEF < 35% and yielding an overall negative result, the subgroup of patients with LVEF between 35-45% (n = 398) appeared to benefit from the initial invasive strategy aimed at revascularization. This finding underscores the importance of documenting ischemia concurrently with MV.

Final considerations

The negative results of the STICHES and REVIVED-BCIS 2 studies concerning MV have complicated the establishment of clear guidelines for its clinical use.[18,19]

Nonetheless, certain conclusions can be drawn: 1) The use of MV does not appear to be a decisive factor in determining the need for myocardial revascularization in most patients, as outlined in the central figure of the study; 2) While LVEF recovery is clinically significant in managing patients with CCS, it may not be the sole mechanism responsible for reducing mortality in this population. The ability of various methods to predict LVEF recovery presents a separate challenge not addressed in this study. 3) The use of viability remains justified for planning complete functional CABG, particularly in cases where all arteries supplying ischemic and viable myocardium (≥ 1.5 mm) require treatment. Additionally, viability assessment may be beneficial in selected instances of single- or double-vessel disease where revascularization decisions could impact treatment recommendations.

Historically, the focus was on dysfunctional territories with the expectation of functional recovery post-revascularization. However, current practice involves identifying viable areas (with or without dysfunction) irrigated by coronary arteries with significant lesions, with the goal of preserving these territories and preventing potentially fatal AMIs.

Table 2 – Clinical studies that evaluated revascularization in the context of ventricular dysfunction and its main characteristics

Main characteristics:	STICHES	REVIVED-BCIS2
Revascularization procedure	Revascularization surgery	PCI
Average age	60 (CABG) and 59 (OMT)	70 (CABG) and 69 (OMT)
Follow-up time	9.8 years	3.4 years
VM mandatory for inclusion	No	Yes, ≥ 4 viable and dysfunctional segments
Most frequently used viability tests	Scintigraphy and TTECO under stress	CMR and TTECO under stress
Therapies for heart failure	Lower use of sacubitril valsartan and implantable cardiac devices	Increased use of sacubitril valsartan and implantable cardiac devices

PCI: percutaneous coronary intervention; STICHES: Surgical Treatment in Ischemic Heart Failure Extension Study; REVIVED-BCIS2: Revascularization for Ischemic Ventricular Dysfunction; CABG: coronary artery bypass graft surgery; TTECO: Transthoracic Doppler Echocardiogram; OMT: optimized medical treatment.

Author Contributions

Conception and design of the research: Lima EG, Azevedo DFC; acquisition of data: Martins EB, Carvalho LNS; analysis and interpretation of the data: Lima EG; writing of the manuscript and critical revision of the manuscript for intellectual content: Lima EG, Martins EB, Carvalho LNS, Azevedo DFC.

Potential Conflict of Interest

No potential conflict of interest relevant to this article was reported.

Sources of Funding

There were no external funding sources for this study.

Study Association

This study is not associated with any thesis or dissertation work

Ethics Approval and Consent to Participate

This article does not contain any studies with human participants or animals performed by any of the authors.

References

1. Allman KC, Shaw LJ, Hachamovitch R, Udelson JE. Myocardial Viability Testing and Impact of Revascularization on Prognosis in Patients with Coronary Artery Disease and Left Ventricular Dysfunction: A Meta-Analysis. J Am Coll Cardiol. 2002;39(7):1151-8. doi: 10.1016/s0735-1097(02)01726-6.
2. Velazquez EJ, Lee KL, Jones RH, Al-Khalidi HR, Hill JA, Panza JA, et al. Coronary-Artery Bypass Surgery in Patients with Ischemic Cardiomyopathy. N Engl J Med. 2016;374(16):1511-20. doi: 10.1056/NEJMoa1602001.
3. Panza JA, Ellis AM, Al-Khalidi HR, Holly TA, Berman DS, Oh JK, et al. Myocardial Viability and Long-Term Outcomes in Ischemic Cardiomyopathy. N Engl J Med. 2019;381(8):739-48. doi: 10.1056/NEJMoa1807365.
4. Braunwald E, Kloner RA. The Stunned Myocardium: Prolonged, Postischemic Ventricular Dysfunction. Circulation. 1982;66(6):1146-9. doi: 10.1161/01.cir.66.6.1146.
5. Kloner RA. Stunned and Hibernating Myocardium: Where are We Nearly 4 Decades Later?. J Am Heart Assoc. 2020;9(3):e015502. doi: 10.1161/JAHA.119.015502.
6. Shah DJ, Kim HW, James O, Parker M, Wu E, Bonow RO, et al. Prevalence of Regional Myocardial Thinning and Relationship with Myocardial Scarring in Patients with Coronary Artery Disease. JAMA. 2013;309(9):909-18. doi: 10.1001/jama.2013.1381.
7. Kim RJ, Wu E, Rafael A, Chen EL, Parker MA, Simonetti O, et al. The use of Contrast-Enhanced Magnetic Resonance Imaging to Identify Reversible Myocardial Dysfunction. N Engl J Med. 2000;343(20):1445-53. doi: 10.1056/NEJM200011163432003.
8. Senior R, Lahiri A. Enhanced Detection of Myocardial Ischemia by Stress Dobutamine Echocardiography Utilizing the "Biphasic" Response of Wall Thickening During Low and High Dose Dobutamine Infusion. J Am Coll Cardiol. 1995;26(1):26-32. doi: 10.1016/0735-1097(95)00139-q.
9. Garcia MJ, Kwong RY, Scherrer-Crosbie M, Taub CC, Blankstein R, Lima J, et al. State of the Art: Imaging for Myocardial Viability: A Scientific Statement From the American Heart Association. Circ Cardiovasc Imaging. 2020;13(7):e000053. doi: 10.1161/HCI.0000000000000053.
10. Martí V, Ballester M, Udina C, Carrió I, Alvarez E, Obrador D, et al. Evaluation of Myocardial Cell Damage by in-111-Monoclonal Antimyosin Antibodies in Patients Under Chronic Tricyclic Antidepressant Drug Treatment. Circulation. 1995;91(6):1619-23. doi: 10.1161/01.cir.91.6.1619.
11. Schinkel AF, Bax JJ, Poldermans D, Elhendy A, Ferrari R, Rahimtoola SH. Hibernating Myocardium: Diagnosis and Patient Outcomes. Curr Probl Cardiol. 2007;32(7):375-410. doi: 10.1016/j.cpcardiol.2007.04.001.
12. Beanlands RS, Nichol G, Huszti E, Humen D, Racine N, Freeman M, et al. F-18-Fluorodeoxyglucose Positron Emission Tomography Imaging-Assisted Management of Patients with Severe Left Ventricular Dysfunction and Suspected Coronary Disease: a Randomized, Controlled Trial (PARR-2). J Am Coll Cardiol. 2007;50(20):2002-12. doi: 10.1016/j.jacc.2007.09.006.
13. D'Egidio G, Nichol G, Williams KA, Guo A, Garrard L, deKemp R, et al. Increasing Benefit from Revascularization is Associated with Increasing Amounts of Myocardial Hibernation: a Substudy of the PARR-2 Trial. JACC Cardiovasc Imaging. 2009;2(9):1060-8. doi: 10.1016/j.jcmg.2009.02.017.
14. Carson P, Wertheimer J, Miller A, O'Connor CM, Pina IL, Selzman C, et al. The STICH Trial (Surgical Treatment for Ischemic Heart Failure): Mode-of-Death Results. JACC Heart Fail. 2013;1(5):400-8. doi: 10.1016/j.jchf.2013.04.012.
15. Perera D, Clayton T, O'Kane PD, Greenwood JP, Weerackody R, Ryan M, et al. Percutaneous Revascularization for Ischemic Left Ventricular Dysfunction. N Engl J Med. 2022;387(15):1351-60. doi: 10.1056/NEJMoa2206606.
16. Perera D, Ryan M, Morgan HP, Greenwood JP, Petrie MC, Dodd M, et al. Viability and Outcomes with Revascularization or Medical Therapy in Ischemic Ventricular Dysfunction: a Prespecified Secondary Analysis of the REVIVED-BCIS2 Trial. JAMA Cardiol. 2023;8(12):1154-61. doi: 10.1001/jamacardio.2023.3803.
17. Lopes RD, Alexander KP, Stevens SR, Reynolds HR, Stone GW, Piña IL, et al. Initial Invasive versus Conservative Management of Stable Ischemic Heart Disease in Patients with a History of Heart Failure or Left Ventricular Dysfunction: Insights from the ISCHEMIA Trial. Circulation. 2020;142(18):1725-35. doi: 10.1161/CIRCULATIONAHA.120.050304.
18. Lawton JS, Tamis-Holland JE, Bangalore S, Bates ER, Beckie TM, Bischoff JM, et al. 2021 ACC/AHA/SCAI Guideline for Coronary Artery Revascularization: a Report of the American College of Cardiology/American Heart Association Joint Committee on Clinical Practice Guidelines. J Am Coll Cardiol. 2022;79(2):e21-e129. doi: 10.1016/j.jacc.2021.09.006.
19. Rohde LEP, Montera MW, Bocchi EA, Clausell NO, Albuquerque DC, Rassi S, et al. Diretriz Brasileira de Insuficiência Cardíaca Crônica e Aguda. Arq Bras Cardiol. 2018;111(3):436-539. doi: 10.5935/abc.20180190.

Rare Presentation of Pseudoaneurysm Obstructing the Left Ventricular Inflow Tract in a Patient With Acute Myocardial Infarction

Janine Daiana Stürmer,[1] Raphael dos Santos Silva,[1] Willer Cesar Bica,[1] Tiago Hansel Basile Vigil,[1] Gabriel Soder,[1] Renata Pibernat de Moraes,[1] Mathias Silvestre de Brida,[1] Rodrigo Moraes Reis[1]

Institute of Cardiology,[1] Porto Alegre, RS – Brazil

Introduction

Left ventricular (LV) pseudoaneurysm is nowadays a rare but still potentially fatal complication of myocardial infarction (MI). Recent studies have estimated that following ST-elevation MI, 0.27 to 0.91% of patients develop mechanical complications.[1] LV free wall rupture (VFWR) is estimated to occur in 0.01 to 0.52% of patients, showing a clear decrease in incidence associated with the widespread adoption of reperfusion therapy.[2] Nonetheless, there has been no significant decrease in associated mortality rates and this complication remains an important determinant of outcomes after MI.[1]

A pseudoaneurysm is formed when a cardiac rupture is contained by adherent pericardium or scar tissue, with no myocardial tissue.[3] Transmural MI is the most common cause, usually following occlusion of the right coronary artery or the circumflex artery, therefore more often occurring on the posterior or lateral wall.[4]

The clinical presentation is vast and patients with pseudoaneurysms can present with chest pain, dyspnea, cardiac tamponade, or the condition may be even incidentally detected. The risk of sudden death due to pseudoaneurysm rupture is 30-45%, and a significant proportion of patients are probably not diagnosed in the acute phase due to early and fatal rupture.[5]

Transthoracic echocardiogram (TTE) should be the first test to be performed, however, establishing the definitive diagnosis frequently poses a substantial challenge. Further assessment with cardiac computed tomography (CT) or magnetic resonance imaging (MRI) may be helpful in patients without hemodynamic instability.[6]

We describe a very rare presentation of LV pseudoaneurysm after MI producing severe extrinsic compression with obliteration of the LV inflow tract diagnosed with TTE in an acute presentation.

Case Report

A 60-year-old male with a history of smoking and no other comorbidities was admitted with typical chest pain lasting 20 hours. The initial examination at emergency department showed a regular heart rate of 80 beats per minute, a systolic blood pressure of 110 mmHg, wheezing on lung auscultation in addition to rales in both lungs bases, with 85% of peripheral saturation of oxygen (class II of Killip classification), and no other remarkable findings at physical examination.

The electrocardiogram showed ST-elevation in I, aVL, V5 and V6 leads with a small Q wave (Figure 1), suggestive of a lateral MI. He received dual antiplatelet therapy and was immediately transferred to the cardiac catheterization laboratory. The coronary angiography displayed occlusion of the mid-circumflex coronary artery, a severe proximal stenosis in the anterior descending artery and no significant lesions in the right coronary artery.

During the exam, he presented acute deterioration of hemodynamic state requiring the use of vasoactive drugs. A TTE was requested urgently to evaluate mechanical complications and decide whether to perform primary angioplasty. The TTE was performed with the patient in supine position and at regular and tachycardic heart rhythm. Pericardial effusion was immediately ruled out on subcostal view (Figure 2, panel A). At the apical four-chamber-view, a mild segmental systolic dysfunction affecting the lateral wall of the left ventricle was observed. At this view, the most impressive finding was that the mitral valve was not visualized and where seems to be its topography there was a muscular band-like image (Figure 2, panel B). It was possible to observe a continuity solution between the lateral wall and that muscular image, with bidirectional flow at color Doppler acquisition (Figure 2, panel C/D). This image can suggest rupture of LV free wall, with a pericardial hematoma potentially exerting mass effect through the left atrium (asterisk, Figure 2, panel B). Finally, at the apical three-chamber-view this inference became more evident by the visualization of a posterior pericardial hematoma compressing the left atrium (figure 2, panel E/F). This observation substantiates the main hypothesis of a LV pseudoaneurysm. At this moment, a left ventriculography was performed (Figure 3) confirming a rupture of lateral LV wall and showing an image suggestive of lateral pseudoaneurysm.

We theorize that as the pseudoaneurysm progressed, it obstructed the LV inflow, as seen by the limited mitral valve diastolic flow at color Doppler (Figure 2, panel F). The patient suffered a pulseless arrest a few minutes later. Multiple resuscitation attempts failed.

Discussion

VFWR is an important cause of death from acute MI and the short-term mortality remains very high even with rapid diagnosis and timely surgery.[7] The clinical manifestation is contingent upon the rate at which the tear unfolds. An abrupt

Keywords

Myocardial Infarction; Pseudoaneurysm; Echocardiography.

Mailing Address: Janine Daiana Stürmer •
Institute of Cardiology. Avenida Princesa Isabel, 395. Postal code: 90040-371. Bairro Santana, Porto Alegre, RS – Brazil.
E-mail: janinedsturmer@gmail.com
Manuscript received November 17, 2023; revised January 8, 2024; accepted January 26, 2024
Editor responsible for the review: Marcelo Dantas Tavares de Melo

DOI: https://doi.org/10.36660/abcimg.20230106i

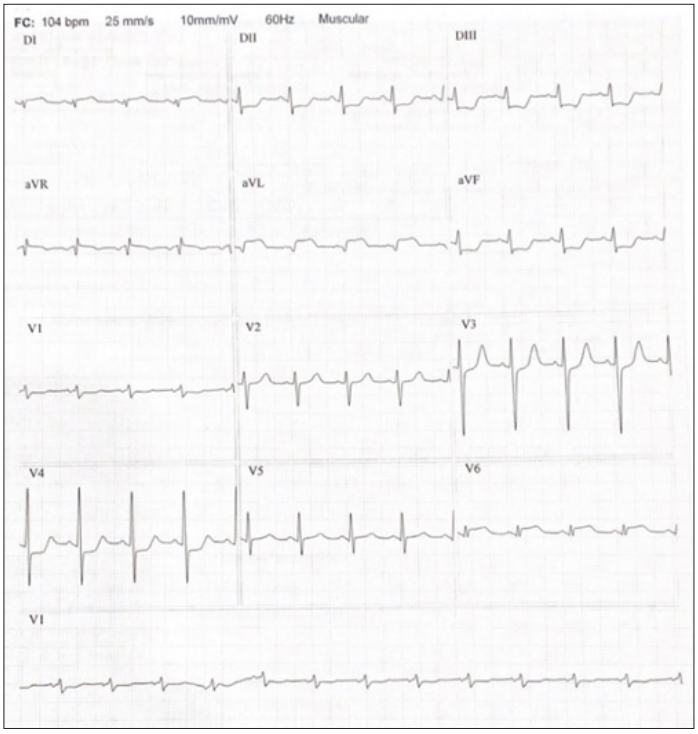

Figure 1 – *ECG at presentation showing ST elevation and small Q waves in lateral leads.*

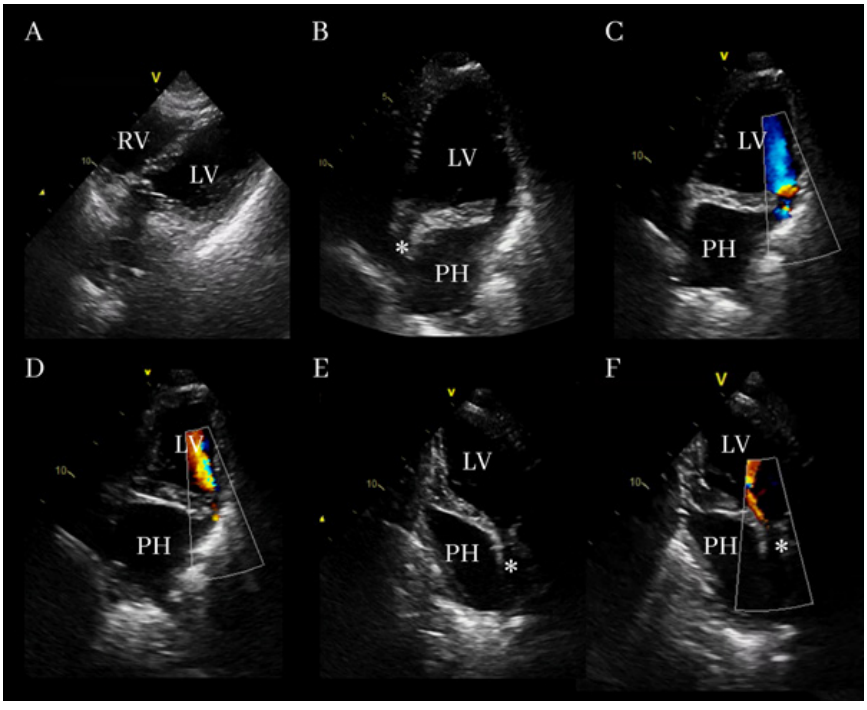

Figure 2 – *Transthoracic echocardiogram showing (A) subcostal-view with no evident pericardial effusion, (B) apical 4-chamber-view; (C and D) apical 4-chamber-view with a bidirectional flow at color Doppler; (E) apical 3-chamber-view; (F) mitral valve color Doppler at apical 3-chamber-view. LV = left ventricle; RV = right ventricle; PH = pericardial hematoma; * = left atrium compressed by the pericardial hematoma.*

tear would likely lead to sudden cardiac tamponade whereas a smaller and more gradual tear may be limited by thrombus formation or a compliant pericardium, eventually developing a pseudoaneurysm.[1] In a comprehensive analysis of 290 patients by a systematic literature review, symptoms among patients with pseudoaneurysm included congestive heart failure, chest pain and dyspnea, with sudden death identified as the initial symptom in merely 3% of patients. In a separate case series involving 52 patients,[4] acute presentation occurred in only 8% of cases. As highlighted in a recent review,[1] LVFWR typically manifests within seven days post-MI, with an average time to diagnosis of 2.6 days.

In this case, the patient presented acutely and probably had already developed a tear tamponaded by a clot. Possibly the use of heparin and antiplatelet therapy may have contributed to the expansion of the pseudoaneurysm. The peculiarity of our case is the location of pseudoaneurysm producing severe extrinsic compression of the mitral valve complex and obstructing the LV inflow tract, with a very restrictive flow registered by the color Doppler through the mitral valve, leading to a progressive obstructive shock. In the literature review, there was no previous report of this exotic condition.

The diagnosis of a LV pseudoaneurysm can be made by several imaging modalities, including the TTE, cardiac ventriculography, transesophageal echocardiography, cardiac MRI and the cardiac CT scan, but none is 100% accurate.[8] Ventriculography demonstrates notable diagnostic precision and, in this case, was useful to corroborate the diagnosis given the constraints in accessing alternative imaging modalities due to patient hemodynamic instability.

The findings that suggest pseudoaneurysm at the TTE are: (1) narrow neck, (2) lack of the normal structural elements found in an intact cardiac wall, (3) bidirectional flow with a to-and-fro pattern, consisting of systolic flow entering the pseudoaneurysm and diastolic flow exiting back into the left ventricle, and (4) the presence of turbulent flow by pulsed Doppler at the neck of a cavity or within the cavity itself.[9]

Although the TTE is a readily available non-invasive method and should be the first imaging modality to use, it is not so effective in making a definitive diagnosis. Several factors contribute to this: (1) poor transthoracic acoustic window, (2) unstable patients, (3) posterior location of the pseudoaneurysm cavity in most cases, (4) rare condition, with low suspicion and expertise for this particular images.

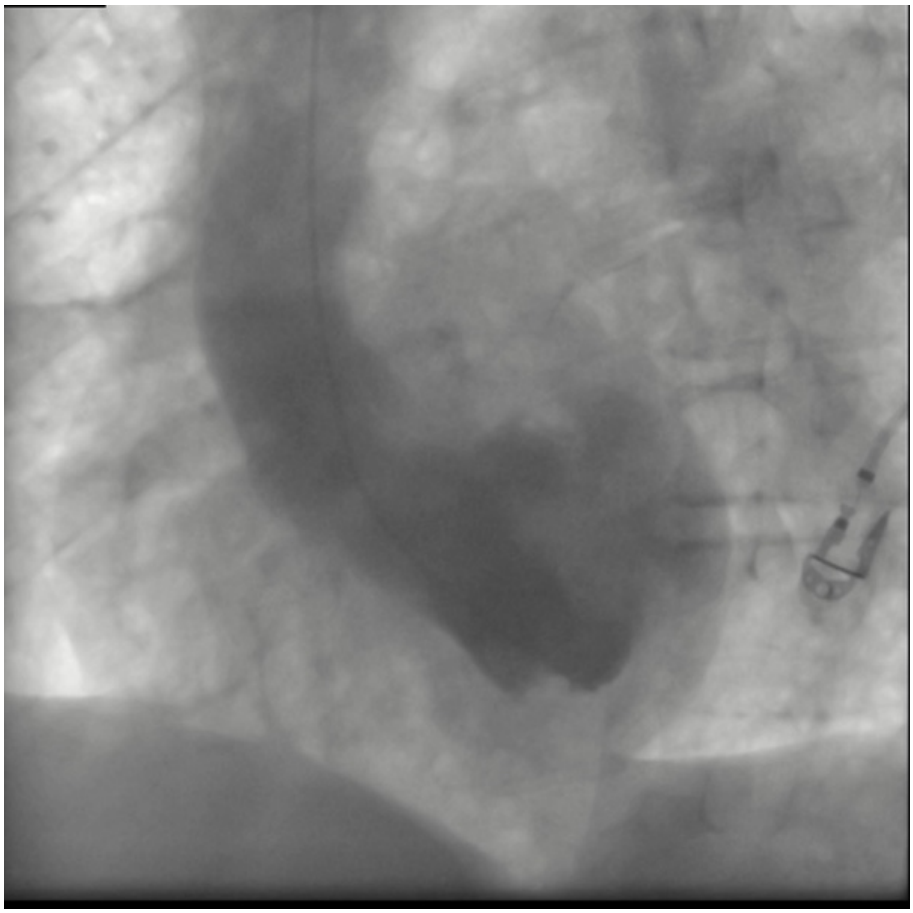

Figure 3 – *Left ventriculogram showing presence of left ventricular pseudoaneurysm*

The present case is unique in a sense that it provided diagnostic images by TTE of a rare condition with an acute presentation. This case emphasizes the need for a high clinical index of suspicion and the prompt recognition of these non-usual images for the successful diagnosis and treatment of this potentially lethal condition.

Author Contributions

Conception and design of the research and acquisition of data: Stürmer JD, Silva RS; analysis and interpretation of the data: Stürmer JD, Silva RS, Vigil THB, Bica WC, Soder G; writing of the manuscript: Stürmer JD; critical revision of the manuscript for intellectual content: Stürmer JD, Silva RS, Vigil THB, Bica WC, Soder G, Moraes RP, Brida MS, Reis RM.

Potential Conflict of Interest

No potential conflict of interest relevant to this article was reported.

Sources of Funding

There were no external funding sources for this study.

Study Association

This study is not associated with any thesis or dissertation work.

Ethics Approval and Consent to Participate

This article does not contain any studies with human participants or animals performed by any of the authors.

References

1. Elbadawi A, Elgendy IY, Mahmoud K, Barakat AF, Mentias A, Mohamed AH, et al. Temporal Trends and Outcomes of Mechanical Complications in Patients with Acute Myocardial Infarction. JACC Cardiovasc Interv. 2019;12(18):1825-36. doi: 10.1016/j.jcin.2019.04.039.
2. Honda S, Asaumi Y, Yamane T, Nagai T, Miyagi T, Noguchi T, et al. Trends in the Clinical and Pathological Characteristics of Cardiac Rupture in Patients with Acute Myocardial Infarction Over 35 Years. J Am Heart Assoc. 2014;3(5):e000984. doi: 10.1161/JAHA.114.000984.
3. Frances C, Romero A, Grady D. Left Ventricular Pseudoaneurysm. J Am Coll Cardiol. 1998;32(3):557-61. doi: 10.1016/s0735-1097(98)00290-3.
4. Yeo TC, Malouf JF, Oh JK, Seward JB. Clinical Profile and Outcome in 52 Patients with Cardiac Pseudoaneurysm. Ann Intern Med. 1998;128(4):299-305. doi: 10.7326/0003-4819-128-4-199802150-00010.
5. Atik FA, Navia JL, Vega PR, Gonzalez-Stawinski GV, Alster JM, Gillinov AM, et al. Surgical Treatment of Postinfarction Left Ventricular Pseudoaneurysm. Ann Thorac Surg. 2007;83(2):526-31. doi: 10.1016/j.athoracsur.2006.06.080.
6. Faustino M, Ranchordás S, Abecasis J, Freitas A, Ferreira M, Gil V, et al. Left Ventricular Pseudoaneurysm - A Challenging Diagnosis. Rev Port Cardiol. 2016;35(6):373.e1-6. doi: 10.1016/j.repc.2015.09.008.
7. Bajaj A, Sethi A, Rathor P, Suppogu N, Sethi A. Acute Complications of Myocardial Infarction in the Current Era: Diagnosis and Management. J Investig Med. 2015;63(7):844-55. doi: 10.1097/JIM.0000000000000232.
8. El Ouazzani J, Jandou I. Aneurysm and Pseudoaneurysm of the Left Ventricle. Ann Med Surg (Lond). 2022;75:103405. doi: 10.1016/j.amsu.2022.103405.
9. Loperfido F, Pennestrì F, Mazzari M, Biasucci LM, Vigna C, Laurenzi F, et al. Diagnosis of Left Ventricular Pseudoaneurysm by Pulsed Doppler Echocardiography. Am Heart J. 1985;110(6):1291-3. doi: 10.1016/0002-8703(85)90026-2.

A Bridging Vein Connecting Left Atrium and Coronary Sinus: Coronary Computed Tomography Angiography Findings

Sercan Şahin,[1] *Nilgün Işıksalan Özbülbül*[1]
Ankara Bilkent City Hospital, Department of Radiology,[1] *Cankaya, Ankara – Turkey*

Introduction

Until recent years, coronary venous system imaging was overshadowed by coronary artery imaging.[1] However, in recent times, the significance of coronary venous system imaging has risen markedly, particularly due to its pivotal role in diverse interventional cardiology procedures.[2] These interventions encompass a spectrum of tasks, including left ventricular pacing, mapping and ablation of arrhythmias, and retrograde cardioplegia. These procedures are facilitated by utilizing the potential of the coronary sinus (CS). As a result, comprehending the anatomy and anomalies of the CS holds paramount importance, and coronary computed tomography (CT) angiography has proven invaluable for achieving this objective.[3]

In this case report, we present an extraordinary cardiac venous anomaly: a bridging vein connecting the left atrium to the CS with non-specific chest pain. We believe that this case serves as an illustrative example for understanding rarely observed cardiac venous vascular anomalies, while also making a valuable contribution to the existing literature through the utilization of clear and direct coronary CT angiography images.

Case presentation

A 55-year-old male presented to the cardiology department with non-specific chest pain. He had a medical history of hypertension for 9 years and type 2 diabetes mellitus for 6 years. His biochemical test results were within normal limits, and the chest X-ray revealed no abnormalities. The electrocardiogram showed a slow R-wave progression in the precordial leads from V1 to V3. Transthoracic echocardiography indicated normal left ventricular function with an ejection fraction of 62%. Due to his family history of cardiac ischemic disease and non-specific chest pain, he was referred for coronary CT angiography to assess the coronary arteries.

Keywords

Coronary Sinus; Computed Tomography Angiography; Heart Atria

Mailing Address: Sercan Şahin •
Ankara Bilkent City Hospital, Radiology. Üniversiteler Mahallesi, 1604. Cadde No: 9. Postal code: 06800. Cankaya, Ankara – Turkey
E-mail: sercansahinmd@gmail.com
Manuscript received December 1, 2023; revised December 18, 2023; accepted January 26, 2024
Editor responsible for the review: Marcelo Dantas Tavares de Melo

DOI: https://doi.org/10.36660/abcimg.20230111i

For coronary CT angiography, a 256-slice General Electric Revolution™ CT scanner was utilized. Non-obstructive atherosclerotic calcified plaques were identified in the middle segment of the left anterior descending artery and the proximal segment of the circumflex artery. Additionally, enlargement of the CS was observed, with a diameter reaching 12 mm before its opening into the right atrium. A bridging vein, measuring 2.5 mm in diameter, was identified connecting the left atrium to the enlarged CS (Figures 1 and 2).

Discussion

The CS is the central venous structure of the heart, and it provides most of its venous return. Positioned within the left atrioventricular groove, the CS opens into the right atrium.[1] Left ventricular pacing, mapping and ablation of arrhythmias, and retrograde cardioplegia procedures are facilitated through the use of the CS.[2] For this reason, it is crucial to understand its anatomy, variations, and anomalies. In 1966, Mantini et al. classified CS anomalies into the following 4 groups:[4]

I. Enlargement of the CS
   A. Without left-to-right shunt into the CS
   B. With left-to-right shunt into the CS
II. Absence of CS
III. Atresia of the right atrial CS ostium
IV. Hypoplasia of the CS

In our patient, we identified a bridging vein connecting the CS and the left atrium, which was consistent with the subtype B enlargement of the CS.

Anomalies of the CS are receiving increasing attention due to their relevance in interventional cardiac procedures and their connection to other congenital heart abnormalities,[3] despite the fact that many of these anomalies are clinically insignificant, as observed in our patient. In symptomatic patients, the clinical manifestation will differ based on the occurrence of arrhythmia and the extent and direction of shunting. If there is no increased pressure in the right heart or stenosis at the CS ostium, blood will primarily move from the left atrium through the CS into the right atrium. This forms a left-to-right shunt, as observed in our case during coronary CT angiography. When right-sided pressure increases due to conditions such as right-sided valve issues and pulmonary hypertension, there is a possibility for the direction of the shunt to be reversed. Even after isolating the pulmonary veins, atrial fibrillation can continue, potentially indicating that the arrhythmia's origin might be attributed to the suspected interaction between the CS and the left atrium.[5,6]

Contents

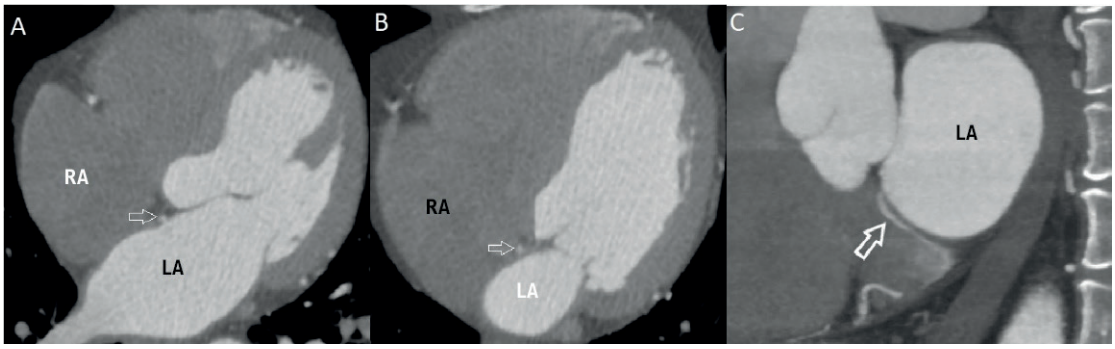

Figure 1 – *Coronary computed tomography angiography. Four chamber views (A, B) and sagittal view (C) showing a bridging vein with a 2.5 mm diameter (arrow) connecting the left atrium and coronary sinus. LA: left atrium; RA: right atrium.*

Coronary CT angiography has emerged as a highly effective option for visualizing cardiac vasculature, particularly owing to recent advancements in spatial, temporal, and contrast resolution.[7] In the context of CS anomalies, these can be successfully detected during the delayed phase of coronary CT angiography, as was observed in our patient's case. Cardiac MRI stands as an additional non-invasive technique for diagnosing cardiac anomalies, without the need for contrast agents or exposure to ionizing radiation. Furthermore, both transthoracic and transesophageal echocardiography serve as valuable tools to identify enlarged CS; however, they are operator-dependent and are limited in their ability to provide intricate details of the cardiac venous vasculature. While an alternative option for imaging the CS involves a CS venogram, its utilization is hindered by its invasive nature and challenges in execution, particularly when dealing with the presence of Thebesian valve at the CS ostium. Consequently, this method has found more application for therapeutic rather than diagnostic purposes.[5,8]

An unroofed CS refers to a communication between the CS and the left atrium, arising from the partial or complete absence of the roof of the CS, and this condition is typically accompanied by other cardiac anomalies.[9] Differentiating between a CS-to-left atrium shunt via a bridging vein and an unroofed CS is mainly accomplished through coronary CT angiography and cardiac MRI. The latter distinction is significant as unroofed CS cases usually require surgical intervention.

In conclusion, many patients with CS anomalies are typically asymptomatic and may not require intervention, similar to our patient's case. As previously mentioned, awareness of CS anomalies holds significant importance in various interventional cardiac procedures, such as electrophysiological studies and ablation for arrhythmias, ventricular pacing, and the management of high-flow shunting in coronary bypass graft surgery.[5,10]

Author Contributions

Conception and design of the research, writing of the manuscript and critical revision of the manuscript for intellectual content: Şahin S, Özbülbül NI; analysis and interpretation of the data: Şahin S.

Potential Conflict of Interest

No potential conflict of interest relevant to this article was reported.

Sources of Funding

There were no external funding sources for this study.

Study Association

This study is not associated with any thesis or dissertation work.

Ethics Approval and Consent to Participate

This article does not contain any studies with human participants or animals performed by any of the authors.

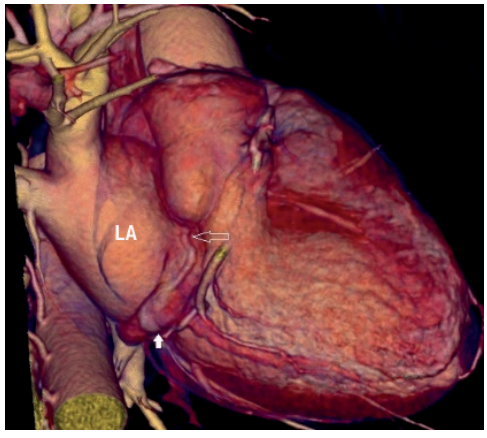

Figure 2 – *Coronary computed tomography angiography. Volume-rendered image depicting an enlarged coronary sinus (opaque arrow) with a 12 mm diameter, connected to the left atrium via a bridging vein (transparent arrow). LA: left atrium.*

References

1. Habib A, Lachman N, Christensen KN, Asirvatham SJ. The Anatomy of the Coronary Sinus Venous System for the Cardiac Electrophysiologist. Europace. 2009;11(Suppl 5):15-21. doi: 10.1093/europace/eup270.
2. Shah SS, Teague SD, Lu JC, Dorfman AL, Kazerooni EA, Agarwal PP. Imaging of the Coronary Sinus: Normal Anatomy and Congenital Abnormalities. Radiographics. 2012;32(4):991-1008. doi: 10.1148/rg.324105220.
3. Chen YA, Nguyen ET, Dennie C, Wald RM, Crean AM, Yoo SJ, et al. Computed Tomography and Magnetic Resonance Imaging of the Coronary Sinus: Anatomic Variants and Congenital Anomalies. Insights Imaging. 2014;5(5):547-57. doi: 10.1007/s13244-014-0330-8.
4. Mantini E, Grondin CM, Lillehei CW, Edwards JE. Congenital Anomalies Involving the Coronary Sinus. Circulation. 1966;33(2):317-27.
5. Justaniah A, Mckee B, Silver J, Wald C, Flacke S. Coronary Sinus to Left Atrium Communication. J Radiol Case Rep. 2013;7(12):16-20. doi: 10.3941/jrcr.v7i12.1678.
6. Haïssaguerre M, Hocini M, Takahashi Y, O'Neill MD, Pernat A, Sanders P, et al. Impact of Catheter Ablation of the Coronary Sinus on Paroxysmal or Persistent Atrial Fibrillation. J Cardiovasc Electrophysiol. 2007;18(4):378-86. doi: 10.1111/j.1540-8167.2007.00764.x.
7. Ghekiere O, Salgado R, Buls N, Leiner T, Mancini I, Vanhoenacker P, et al. Image Quality in Coronary CT Angiography: Challenges and Technical Solutions. Br J Radiol. 2017;90(1072):20160567. doi: 10.1259/bjr.20160567.
8. Shafter AM, Almeida SO, Syed U, Shaikh K, Budoff MJ. Anomalous Coronary Sinus Communication to the Left Atrium. J Cardiol Cases. 2019;20(4):122-4. doi: 10.1016/j.jccase.2019.06.007.
9. El-Eshmawi A, Tang GH, Pawale A, Anyanwu AC, Adams DH. Unroofed Coronary Sinus in an Adult. J Card Surg. 2013;28(1):19-22. doi: 10.1111/jocs.12035.
10. Chou MC, Wu MT, Chen CH, Lee MH, Tzeng WS. Multidetector CT Findings of a Congenital Coronary Sinus Anomaly: A Report of Two Cases. Korean J Radiol. 2008;9 (Suppl):S1-6. doi: 10.3348/kjr.2008.9.s.s1.

Left Ventricular Aneurysm With Contained Rupture

Priscila Nasser de Carvalho,[1] Mariane Higa Shinzato,[2] Roberto Tadeu Magro Kroll,[2] Andrea Cunha Cortellazzi,[1] Aloysio Abdo Silva Campos[2]

Hospital de Transplantes do Estado de São Paulo Euryclides de Jesus Zerbini,[1] São Paulo, SP – Brazil
Instituto Dante Pazzanese de Cardiologia,[2] São Paulo, SP – Brazil

Introduction

Left ventricular aneurysms (LVA) and left ventricular pseudoaneurysms (LVPA) are serious complications resulting from transmural myocardial infarction. Their incidence has decreased considerably with the advancements of interventional cardiology, using early revascularization of the compromised coronary artery, preventing ventricular remodeling.[1] Differential diagnosis is often not easy; however, it must be made early.

An LVA occurs months or years after acute myocardial infarction. It is formed by an area of scar tissue and contains the three layers of the ventricular wall (endocardium, myocardium, and pericardium). Its wall is preserved and may contain thrombi. An LVPA is a rare complication that can occur days or months after the infarction. It is formed by the weakened wall that ruptures after the infarction, in a way that this rupture is contained by the pericardium, resulting in discontinuity of the endocardial border.[2] Usually, an LVA is located in the apical and anterior regions, while an LVPA is located in the posterolateral region of the left ventricle.[3]

Surgical resection of an LVA is necessary in cases of refractory angina, heart failure, systemic embolization, and refractory arrhythmia.[2,3] A pseudoaneurysm has a high risk of rupture (30% to 45%) and sudden death due to cardiac tamponade. Therefore, surgical treatment is recommended immediately after detection.[4,5]

Rupture of a true left ventricular aneurysm in the chronic phase is an uncommon phenomenon.[2] The purpose of this study was to report the case of a patient with a ruptured left ventricular aneurysm, developing chest pain and needing heart surgery.

Case report

Male patient, 70 years old, hypertensive, diabetic, dyslipidemic, and former smoker. He experienced an acute myocardial infarction with ST-segment elevation of the anterior wall, undergoing angioplasty of the anterior descending artery in July 2022. In September 2022, he was admitted to the emergency department of a general hospital with ventilator-depending chest pain and dyspnea. Physical examination revealed that his condition was hemodynamically stable.

Due to the presence of a massive pleural effusion on the left side, as detected on the chest X-ray, a relief thoracentesis was performed, removing 1000 ml of serum and blood-stained fluid. Subsequently, a computed tomography scan of the chest was performed, which revealed the partial collapse of the left lung due to massive pleural effusion, in addition to a small pleural effusion on the right and sacculation of the left ventricle, with foci of gas present in contiguity with the apex, suggesting a contained ruptured aneurysm in the left ventricle (Figures 1 and 2). On the transthoracic echocardiogram (Figure 3), a large aneurysmal image can be seen in the apical region of the left ventricle with mobile formations, suggesting the presence of a thrombus, contiguous with the pericardial sac, in addition to apical dyskinesia, hypokinesia of the anterior wall, and significant left ventricular dysfunction.

Surgical correction was recommended. The patient was transferred to a tertiary hospital, where he underwent left ventricular reconstruction and thrombectomy (Figure 4). Postoperatively, the patient developed several complications, including cardiogenic and vasoplegic shock, requiring the use of vasoactive drugs and an intra-aortic balloon pump. After being hospitalized for months, he was discharged from the hospital for rehabilitation.

Discussion

Ventricular aneurysms contain a narrowed area in a scarred region of the myocardium that has a dyskinetic movement. Most of the time, they result from occlusion of the anterior descending artery in cases where there is no well-developed collateral circulation.[1] They occur due to intraventricular pressure that leads to the expansion of the necrotic area of the infarction.[4,6] Patients are generally asymptomatic and this condition is often found during a routine transthoracic echocardiogram (TTE).[1]

The TTE has good sensitivity and specificity for the diagnosis of LVA.[1] The thinner wall of the infarct region communicates with the ventricle through a wide neck, unlike the pseudoaneurysm, in which this neck is narrow. However, the differential diagnosis between the two can be difficult, especially when they are located posteriorly.[6,7]

A Chest Computed Tomography **Angiography** not only confirms the echocardiographic findings, but also

Keywords

Myocardial Infarction; Heart Aneurysm; Thoracic Surgery

Mailing Address: Priscila Nasser de Carvalho •
Hospital de Transplantes do Estado de São Paulo Euryclides de Jesus Zerbini, Cardiologia. Avenida Brigadeiro Luís Antônio, 2651. Postal code: 01401-000. São Paulo, SP – Brazil
E-mail: priscilanasser@yahoo.com.br
Manuscript received July 30, 2023; revised October 19, 2023; accepted November 21, 2023
Editor responsible for the review: Daniela do Carmo Rassi Frota

DOI: https://doi.org/10.36660/abcimg.20230072i

Contents

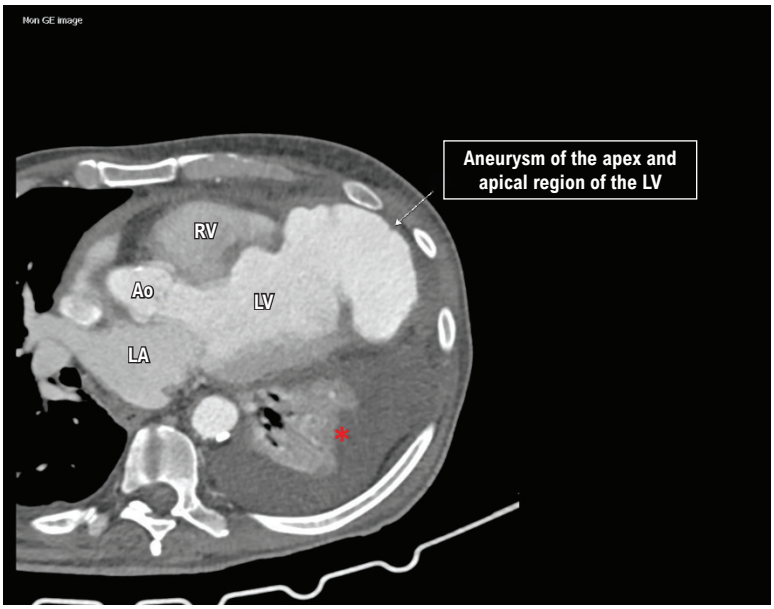

Figure 1 – *Three-chamber long-axis tomographic image (left ventricular outflow tract) showing aneurysm of the left ventricular apex (white arrow). Pleural effusion on the left with compressive atelectasis (red asterisk) is also noted.*

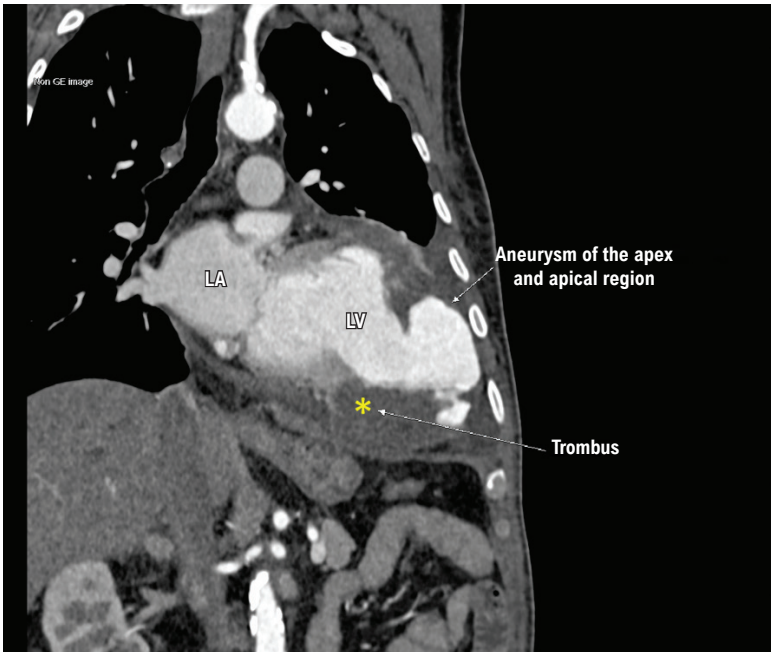

Figure 2 – *Two-chamber long-axis tomographic image showing partially thrombosed aneurysm of the left ventricular apex (yellow asterisk and white arrow)*

allows a very accurate description of the anatomy of the left ventricle. The thin wall thickness, the anatomical characteristics (regular expansion of the cavity and the pericardium surrounding the myocardial scar), and the absence of discontinuity in the endocardial wall are characteristic signs of LVA.[2] Due to its better spatial resolution, Cardiac Computed Tomography helps visualize segments that are difficult to evaluate by TTE.[1] By allowing tissue characterization, magnetic resonance imaging of the heart is the right exam to distinguish LVA from LVPA,[1] which is highly valued since it allows the assessment of size and location.[2]

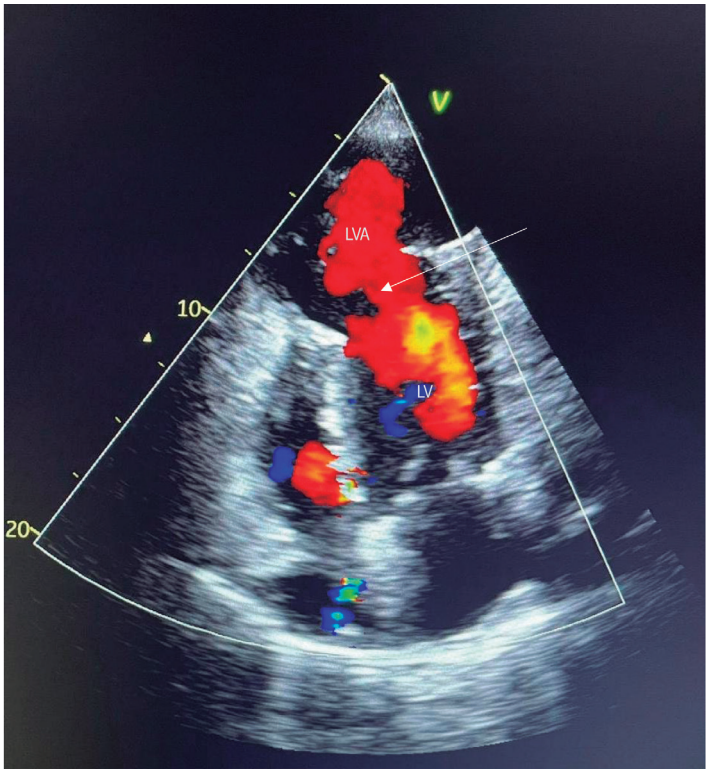

Figura 3 – *Transthoracic echocardiogram with a four-chamber apical view showing the communication of the intact wall of the left ventricle with the cystic cavity through a wide lap (white arrow). LVA: Left Ventricle Aneurysm; LV: Left Ventricle.*

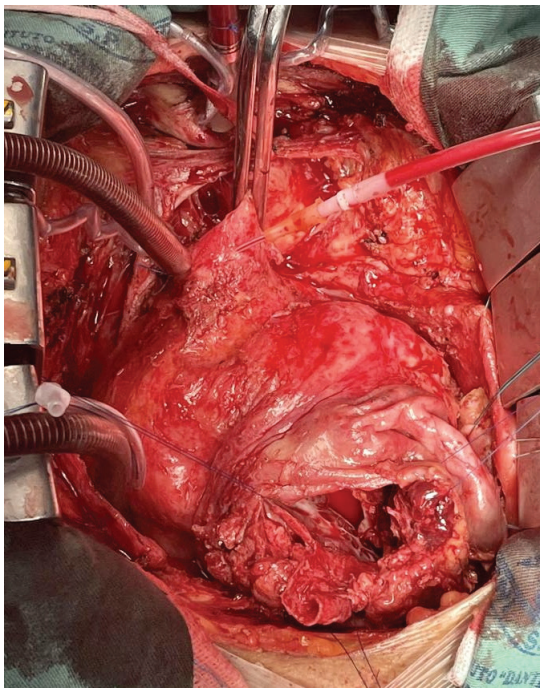

Figure 4 – *Intraoperative image showing ruptured left ventricular aneurysm*

Preoperative left ventricular ejection fraction (LVEF) is an important determinant of survival. Patients with a left ventricular ejection fraction (LVEF) < 30% have a much lower survival rate than those with LVEF > 30%.[4]

Surgical intervention is intended to improve left ventricular function and reverse remodeling, reducing the likelihood of malignant arrhythmias and embolic events.[6,7] Surgical correction of an LVA consists of an aneurysmectomy and ventricular reconstruction with a patch, implantation of an arterial graft when necessary, and correction of other mechanical complications, such as mitral insufficiency.[1]

The early diagnosis of LVA or LVPA is key for establishing the right treatment at the right time and avoiding even greater complications.

Author Contributions

Conception and design of the research and writing of the manuscript: Carvalho PN, Shinzato MH; acquisition of data:_Carvalho PN, Shinzato MH, Kroll RTM, Cortelazzi AC, Campos AAS; analysis and interpretation of the data:_Kroll RTM; critical revision of the manuscript for intellectual content: Carvalho PN, Shinzato MH,_Kroll RTM; tomography images: Shinzato MH; echocardiogram image (Figure 3): Cortelazzi AC; intraoperative image: Campos AAS.

Potential Conflict of Interest

No potential conflict of interest relevant to this article was reported.

Sources of Funding

There were no external funding sources for this study.

Study Association

This study is not associated with any thesis or dissertation work.

Ethics Approval and Consent to Participate

This study was approved by the Ethics Committee of the Hospital Brigadeiro UGA V – SP under the protocol number 6/80705. All the procedures in this study were in accordance with the 1975 Helsinki Declaration, updated in 2013. Informed consent was obtained from all participants included in the study.

References

1. El Ouazzani J, Jandou I. Aneurysm and Pseudoaneurysm of the Left Ventricle. Ann Med Surg (Lond). 2022;75:103405. doi: 10.1016/j.amsu.2022.103405.
2. Kumbasar B, Wu KC, Kamel IR, Lima JA, Bluemke DA. Left Ventricular True Aneurysm: Diagnosis of Myocardial Viability Shown on MR Imaging. AJR Am J Roentgenol. 2002;179(2):472-4. doi: 10.2214/ajr.179.2.1790472.
3. Pontone G, Andreini D, Ballerini G, Pompilio G, Alamanni F, Nobili E, et al. An Unusual Case of Large Left Ventricular Aneurysm: Complementary Role of Echocardiography and Multidetector Computed Tomography in Surgical Planning. Eur J Radiol. 2005;54(2):51-4. doi: 10.1016/j.ejrex.2005.03.010.
4. Habertheuer A, Andreas M, Wiedemann D, Rath C, Kocher A. Giant Lateral Left Ventricular Wall Aneurysm Sparing the Submitral Apparatus. J Cardiothorac Surg. 2013;8:201. doi: 10.1186/1749-8090-8-201.
5. Jacob JL, Buzelli G, Machado NC, Garzon PG, Garzon SA. Pseudoaneurysm of Left Ventricle. Arq Bras Cardiol. 2007;89(1):e1-2. doi: 10.1590/s0066-782x2007001300012.
6. Zoffoli G, Mangino D, Venturini A, Terrini A, Asta A, Zanchettin C, et al. Diagnosing Left Ventricular Aneurysm from Pseudo-Aneurysm: A Case Report and a Review in Literature. J Cardiothorac Surg. 2009;4:11. doi: 10.1186/1749-8090-4-11.
7. Aguiar J, Barba Mdel M, Gil JA, Caetano J, Ferreira A, Nobre A, et al. Left Ventricular Aneurysm and Differential Diagnosis with Pseudoaneurysm. Rev Port Cardiol. 2012;31(6):459-62. doi: 10.1016/j.repc.2012.04.001.

Ischemic Stroke in a Patient with Challenging Pseudoaneurysm in the Left Ventricular Outflow Tract

Saulo Rodrigo Cunha,[1] Fernanda Pandolfo,[1] Fernando Colares Barros,[1] Eduardo Gatti Pianca,[1] Pedro Tregnago Barcellos[1]

Serviço de ecocardiografia, Hospital Nossa Senhora da Conceição, Ecocardiografia,[1] Porto Alegre, RS – Brazil

Introduction

Literature shows cases of cardiac neocavities, often associated with pseudoaneurysms resulting from traumatic injuries or fistulized periprosthetic abscesses involving the left ventricle (LV).[1]

Cardiac pseudoaneurysms are typically complications of acute myocardial infarction but can also occur in the late postoperative period of valve surgery. Certain areas are particularly prone to the development of ascending aortic pseudoaneurysms. Generally, these events occur in sites where aortic cannulation and clamping take place, as well as in the areas of graft sutures.[2]

This case report highlights the challenges and difficulties handled in some clinical cases associated with the development of pseudoaneurysms despite advancements in therapy.

Case report

This 39-year-old patient was admitted to the emergency room of a tertiary public hospital, with a clinical condition compatible with ischemic stroke (aphasia of expression and decreased strength in the right upper limb). A computed tomography scan of the skull revealed hypodense areas in the frontal region, frontal operculum, and left insular lobe. During the etiological investigation, ultrasound of the carotid and vertebral arteries revealed no abnormalities, and a transthoracic echocardiogram (TTE) was performed (Figure 1).

The patient had a previous pathological history of bicuspid aortic valve, and underwent cardiac surgery in 2021, in another hospital service, due to infectious endocarditis with valve abscess and significant aortic insufficiency. In May 2021, the patient underwent aortic valve replacement with a No. 23 mechanic prosthesis and correction of the aortic-cavitary fistula. However, in control TTE, maintenance of the aorto-cavitary fistula and sequelae of periaortic abscess were observed. A month later, the patient underwent new heart surgery to close the fistula. However, postoperative imaging exams revealed the persistence of the fistula connecting the pseudoaneurysm and the left ventricular cavity. Thirty days after the second surgery, a new attempt at closure was made using a different technique, involving the placement of two Amplatzer® prostheses to promote thrombosis within the developed pseudoaneurysm. The procedure was performed via left thoracotomy with apical puncture. Despite these efforts, the closure was again unsuccessful, as confirmed by a follow-up echocardiogram showing the fistula still present.

Going back to the current hospitalization procedures, given the challenging characterization of the neocavity on TTE, a transesophageal echocardiogram (TEE) (Figure 2) was performed, revealing a pseudoaneurysm adjacent to the aortic prosthesis with the Amplatzer® prostheses inside. The mechanical aortic valve prosthesis exhibited good disc mobility and mild perivalvular regurgitation. The LV showed normal dimensions, preserved systolic function, and mild diastolic dysfunction. The left atrium was slightly enlarged. The patient had mild functional mitral regurgitation.

Considering the risk of new cardioembolic events and the patient's wish to address the pseudoaneurysm surgically, cardiac surgery was performed on August 25, 2023. During the procedure, a pseudoaneurysm was identified in the ascending aorta, involving the infra and supravalvular planes, containing two Amplatzer® prostheses. After entering cardiopulmonary bypass, the aortic prosthesis and large LV pseudoaneurysm with two-hole aorta were removed. Two Amplatzer® devices were extracted, and the communicating apertures were closed using 4-0 prolene. A pericardial patch was used to widen the aortic ring, and a mechanical valve No. 19 was implanted in the aortic position. However, due to the aorta's high fragility, upon removal of the clamp, the ascending aorta ruptured at the beginning of the aortic arch, resulting in significant bleeding. Despite efforts to control the hemorrhage, including refractory measures, the patient succumbed to hemorrhagic shock.

Discussion

Aorto-cavitary fistulas are rare abnormal connections between the aorta and the heart cavities. These can be congenital or acquired, with the most common etiology being iatrogenic (38%), followed by infectious (25%), traumatic (14%) and rupture of the sinus of Valsalva (8%). The most common locations are aorta to right atrium

Keywords

False Aneurysm; Stroke; Heart Valve Prosthesis.

Correspondência: Saulo Rodrigo Cunha •
Hospital Nossa Senhora da Conceição, Ecocardiografia. Av. Francisco Trein, 596. CEP: 91350-200. Bairro Cristo Redentor, Porto Alegre, RS – Brasil
E-mail: saulo_rodrigom@hotmail.com
Artigo recebido em 10/01/2024; revisado em 23/01/2024; aceito em 01/03/2024.
Editor responsável pela revisão: Marco Lofrano-Alves

DOI: https://doi.org/10.36660/abcimg.20240001i

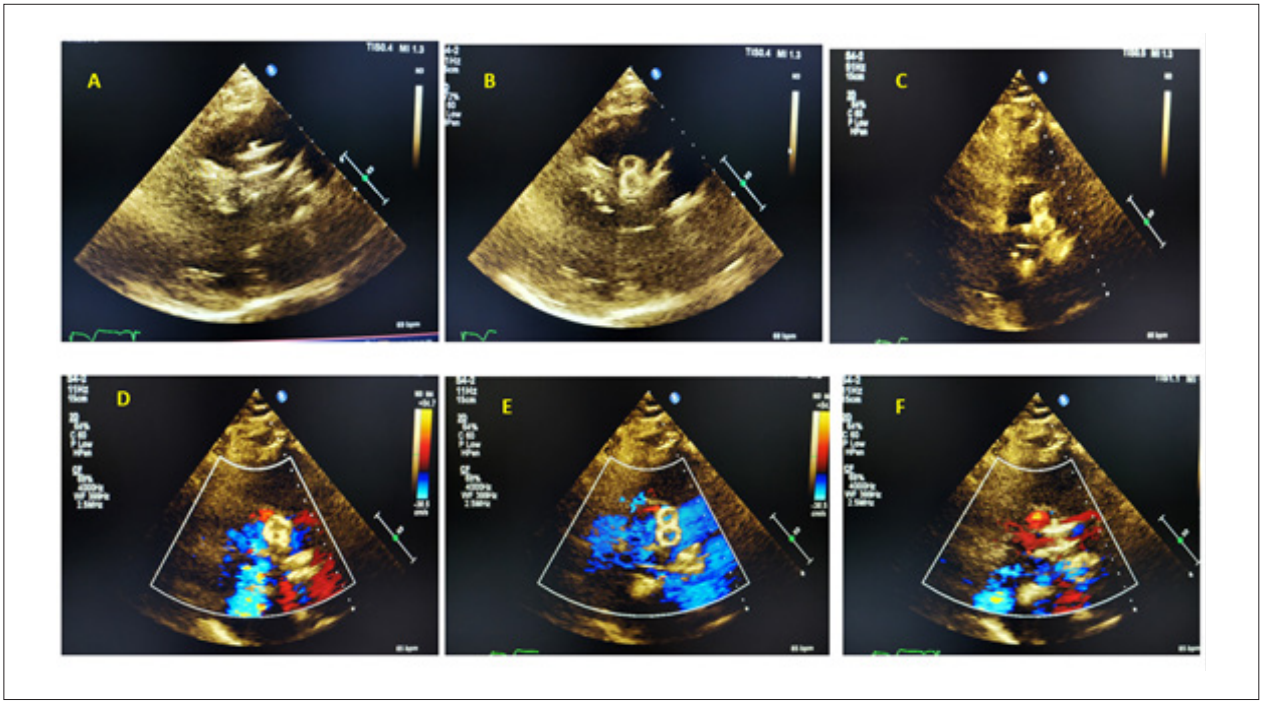

Figure 1 – *TTE in parasternal window. Tables A, B and C show two moving and independent images in a position anterior to the LV and the aortic valve. Tables D, E and F show images suggestive of Amplatzer® prostheses highlighted when applying the color Doppler effect.*

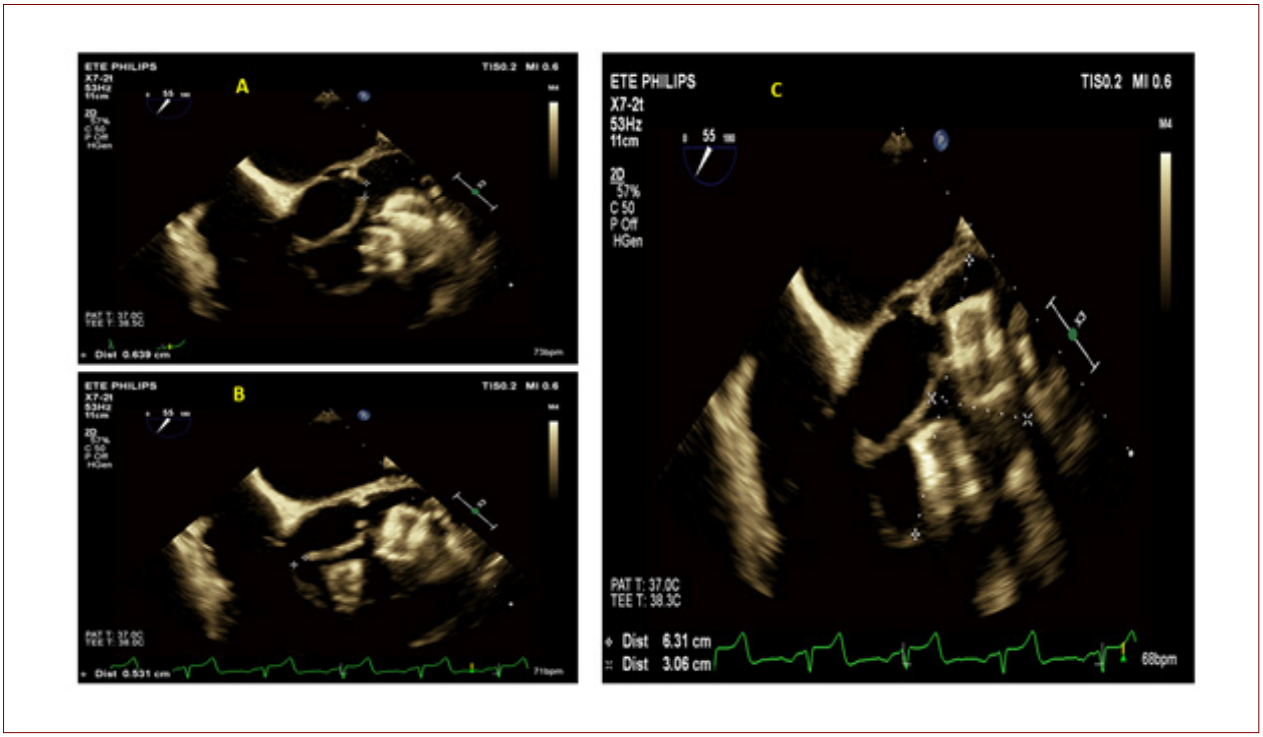

Figure 2 – *TEE. A) Anterior aortic periprosthetic pseudoaneurysm with thin walls and two communications with the left ventricular outflow tract, one measuring 0.6 cm at 2 o'clock. B) Communication with the LV outflow tract measuring 1 cm at 8 o'clock. C) Anterior aortic pseudoaneurysm measuring 6.3 x 3 cm, with two Amplatzer® prostheses inside.*

(37%), to pulmonary artery (25%), to left atrium (18%), to right ventricle (18%) and to LV (2%). Management of this disease includes symptomatic treatment and surgical or percutaneous interventions, which is a common treatment option in the 21st century.[3]

Amplatzer® prostheses are currently used in several percutaneous procedures. However, with the increasing use of Amplatzer® devices, an increasing number of device-related complications have been observed, such as device migration, patency of the embolized vessel and late reperfusion of the vessel or orifice.[4] In a single-center study following 803 patients for up to 25 years after Amplatzer® closure of interatrial septal defects, major complications occurred in 0.5% of cases, including device embolization, thrombus formation on the occluder's surface, post-procedure cardiac erosion, and infective endocarditis.[5]

For cases of device embolization, management depends on factors such as location, timing, clinical manifestations, and the type of device employed.[6]

Given the current situation of cardioembolic ischemic stroke with potential recurrence, pseudoaneurysm in the left ventricular outflow tract, and displaced Amplatzer® prostheses, the patient, in consultation with the medical team, decided to attempt resolution, despite the high surgical risk associated with the patient's medical history.

Conclusion

In this case, surgical attempts were made to resolve the aorto-cavitary fistula and the pseudoaneurysm in the LV outflow tract, but they were all unsuccessful. The clinical evolution was unfavorable, and the patient died intraoperatively.

Even with substantial advancements in therapeutic medicine, there are still clinical cases that pose challenges and are difficult to resolve. Discussions within the Heart team regarding the therapeutic measures adopted are crucial, as is involving patients in the decision-making process.

Author Contributions

Conception and design of the research and acquisition of data: Cunha SR; analysis and interpretation of the data, writing of the manuscript and critical revision of the manuscript for intellectual content: Cunha SR; Pandolfo F, Barros FC, Pianca EG, Barcellos PT.

Potential Conflict of Interest

No potential conflict of interest relevant to this article was reported.

Sources of Funding

There were no external funding sources for this study.

Study Association

This article is part of the scientific production of the Medical Residency Program in Echocardiography at Hospital Nossa Senhora da Conceição.

Ethics Approval and Consent to Participate

This article does not contain any studies with human participants or animals performed by any of the authors.

References

1. Almeida DT, Silva LBP, Andrioli VGE, Resende MV, Vieira MLC. Abscesso Periprotético Aórtico Fistulizado para o Ventrículo Esquerdo Visualizado ao Ecocardiograma Transesofágico Tridimensional. Arq Bras Cardiol: Imagem Cardiovasc. 2019;32(2):134-7. doi: 10.5935/2318-8219.20190028.
2. Manica JL, Bender LP, Borges MS, Prates PRL, Rossi-Filho RI. Percutaneous Treatment of Left Ventricle and Aortic Pseudoaneuryms: Three Case Series. Rev Bras Cardiol Invasiva. 2015;23(1):73-6. DOI: 10.1016/j.rbci.2015.02.002.
3. Foster TJ, Amin AH, Busu T, Patel K, Farjo P, Hallak AA, et al. Aorto-cardiac Fistula Etiology, Presentation, and Management: A Systematic Review. Heart Lung. 2020;49(3):317-23. doi: 10.1016/j.hrtlng.2019.11.002.
4. Chessa M, Carminati M, Butera G, Bini RM, Drago M, Rosti L, et al. Early and Late Complications Associated with Transcatheter Occlusion of Secundum Atrial Septal Defect. J Am Coll Cardiol. 2002;39(6):1061-5. doi: 10.1016/s0735-1097(02)01711-4.
5. Olejnik P, Tittel P, Venczelova Z, Kardos M, Tomko J, Bartova M, et al. Long-term Follow-up of Percutaneous Secundum-type Atrial Septal Defect Closure Using Amplatzer Septal Occluder Since 1995: A Single-centre Study. Cardiol Young. 2024;34(3):643-6. doi: 10.1017/S1047951123003190.
6. Silvestre JMS, Silvestre GS, Sardinha WE, Ramires ED, Morais Filho D, Schimit GTF, et al. Complication After Percutaneous Treatment of Inter-atrial Communication: Amplatzer© Device Migration to the Aortic Bifurcation – A Case Report. J Vasc Bras. 2015;14(3):271-4. doi: 10.1590/1677-5449-0010.

Ultrasound in the Diagnosis of Carotid Web: Report of Two Cases and Review

Ana Claudia Gomes Pereira Petisco,[1,2] Paulo Magno Martins Dourado,[2,3] Larissa Almeida Dourado,[2] João Paulo Almeida Dourado,[2] Ricardo Thomaz Tebaldi[2]

Instituto Dante Pazzanese de Cardiologia,[1] São Paulo, SP – Brazil

Clínica Procoração Cardiologia Preventiva,[2] São Paulo, SP – Brazil

Universidade de São Paulo Faculdade de Medicina,[3] São Paulo, SP – Brazil

Introduction

Carotid web (CW) is a nonatherosclerotic disease of the extracranial carotid artery, described as an atypical, still little known, and poorly diagnosed focal fibromuscular dysplasia (FMD). CW has been associated with the occurrence of cerebral vascular accidents (CVAs) and transient ischemic attacks (TIAs), affecting young patients, with no other known causes.

Case report

Case 1: A 51-year-old female teacher, married, asymptomatic until September 2022, when she developed sudden motor deficit of left hemibody, and was admitted with the diagnosis of CVA. The patient reported complete regression of motor deficit one month after hospital discharge, and use of atorvastatin 40mg and aspirin 100mg. The patient has smoked for 30 years and denied diabetes and hypertension. Her mother has a history of cerebral aneurysm. Physical examination was normal (blood pressure: 120x80mmHg; heart rate = 76bpm).

The patient underwent laboratory tests, electrocardiogram (ECG), transthoracic and transesophageal echocardiograms, 24h Holter monitoring, and treadmill test, with normal results. Vascular ultrasound (VUS) of carotid and vertebral arteries revealed an echogenic image in left carotid bifurcation, projecting into the carotid artery lumen, apparently fixed, without significant stenosis, raising the possibility of CW. On the surface, there was a small pedunculated echogenic mobile mass, towards the flow, measuring 0.66 mm (possible thrombus) – Figures 1A-F. Computed tomography angiography (CTA) of cervical vessels corroborated the ultrasound findings, showing a luminal thin band or folding, at the bulb of the left internal carotid artery (Figures 2A and 2B). Contrast angiography was performed, which revealed a filling defect, compatible with CW, projecting into the left bulb in a turbulent flow, and no intracranial changes (Figures 2C and D). A surgical intervention was indicated.

Case 2: A 42-year-old woman, service assistant, single. The patient was asymptomatic, with a history of hypertension, using losartan 75 mg/d, and preparing for elective hysterectomy. The patient underwent a cardiovascular *check-up* and reported that her mother had dyslipidemia and hypertension. The VUS of carotid and vertebral arteries showed an echogenic image in the posterolateral wall, near the right carotid bifurcation, projecting into the arterial lumen, apparently fixed, suggestive of CW, with flow disturbance, peak systolic velocity (PSV) = 134 cm/s and narrowing of the lumen by nearly 50%. A cross-sectional view reviewed that the membrane acted as a "web" (Figures 3A-F).

CTA of carotid arteries corroborated the ultrasonographic diagnosis, showing a filling defect in the right carotid bulb / origin of the right internal carotid artery, suggestive of CW (variant of FMD), and causing discrete stenosis (Figures 4A and B). The patient is still asymptomatic and clinically followed-up.

Discussion

CW was first described in 1968.[1] It consists of a little known and poorly diagnosed nonatherosclerotic disease of the extracranial carotid artery.[2] CW is described as a discrete membrane (web or net) defined as an intraluminal filling defect that usually affects the posterolateral wall of the carotid artery, more commonly in the proximal internal carotid artery. Of unknown cause, CW is considered an atypical focal carotid FMD, with intimal fibrous proliferation.[2,3] CWs are more prevalent in proximal internal carotid artery and carotid bifurcation and may be unilateral or bilateral.[3]

CW may be the cause of CVA and TIAs, accounting for 9.4-37% of cryptogenic stroke, mainly in young patients.[3-5] CW patients may be asymptomatic or develop recurrent neurological events.[3,5] Sajedi et al.[5] assessed cryptogenic stroke patients and demonstrated a CW prevalence of 21.2% (95% CI, 8.9–38.9%). Mean age was 38.9 years, and CW was more common among African American (86%) and women (86%). The mechanism by which CW leads to neurological events is not well established. Although CW does not commonly result in significant stenosis, flow disturbance may occur, with blood recirculation and stasis, which would increase the risk of platelet aggregation. CW is

Keywords

Carotid Artery Diseases; Carotid Arteries Ultrasonography; Fibromuscular Dysplasia.

Mailing Address: Ana Claudia Gomes Pereira Petisco •
Instituto Dante Pazzanese de Cardiologia. Rua Dr. Dante Pazzanese, 500. Postal code: 04012-909. São Paulo, SP – Brazil
E-mail: anapetisco@outlook.com
Manuscript received December 19, 2023; revised January 26, 2024; accepted February 14, 2024
Editor responsible for the review: Simone Nascimento dos Santos

DOI: https://doi.org/10.36660/abcimg.20230117i

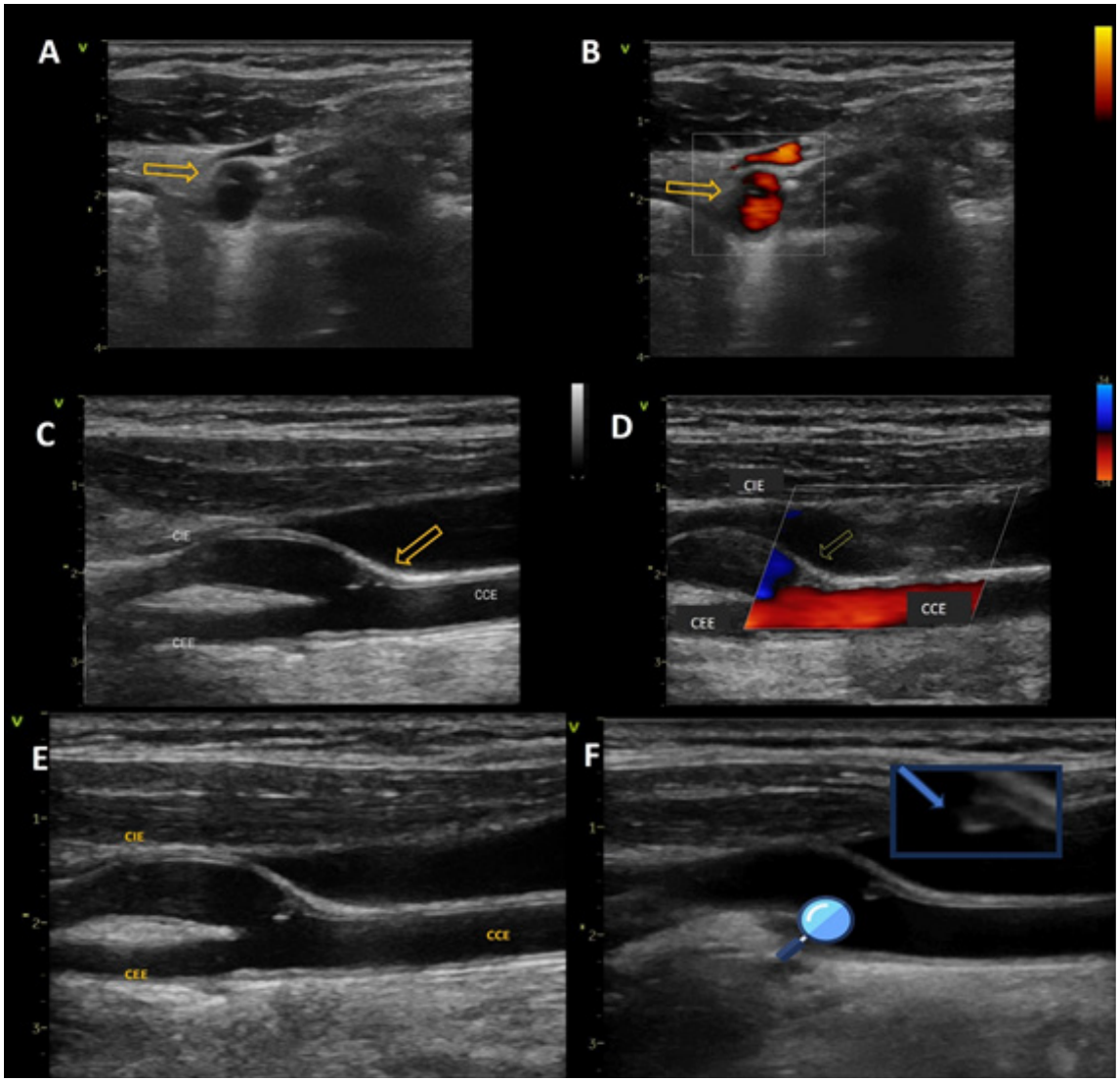

Figure 1 – *Case 1 – Visualization of the carotid web (yellow arrows) by Vascular Ultrasonography; A – B mode cross section view; B- Power Doppler cross section view; C- B mode longitudinal section view; D – Color Doppler longitudinal section view; E- B mode longitudinal section view; F – Pedunculated and mobile image in the direction of flow (magnifying glass – suggests a small thrombus).*

a shelf-like membrane that allows the blood to be retained and in longer contact with the endothelium, favoring thrombus formation and thromboembolic events.[3,5] It is believed that the pattern of flow abnormalities caused by CWs differs from those caused by atherosclerotic plaques, since while CWs are focal lesions, atherosclerotic plaques may affect longer segments of the artery and have more irregular surface.[6] The detection of a thrombus adherent to CW, similar to that found in our first case, was reported in 16.2% of the cases.[7]

CW may be diagnosed by CTA, contrast angiography, magnetic resonance angiography, or VUS.[8] It is radiologically described as a focal protrusion, a tissue fold from the posterior wall of the carotid bulb, on sagittal or on oblique sagittal image, also visible on the axial image as a septum.[4]

As described in the two cases presented here, VUS can detect CW. In the two-dimensional image, CW is seen as a thin membrane formed by an abnormal endothelial fold, with variable-diameter orifices, similar to a web, causing a partial flow in the carotid artery.[4,6,9] The use of the VUS resources like color Doppler, power Doppler, and contrast VUS whenever possible, helps in MW visualization.[9] Madaelil et al.[6] reported a moderate agreement between VUS and contrast angiography (k=0.62; p=0.01). However, a more recent study reported an 85.7% agreement between CTA and contrast-enhanced VUS.[8]

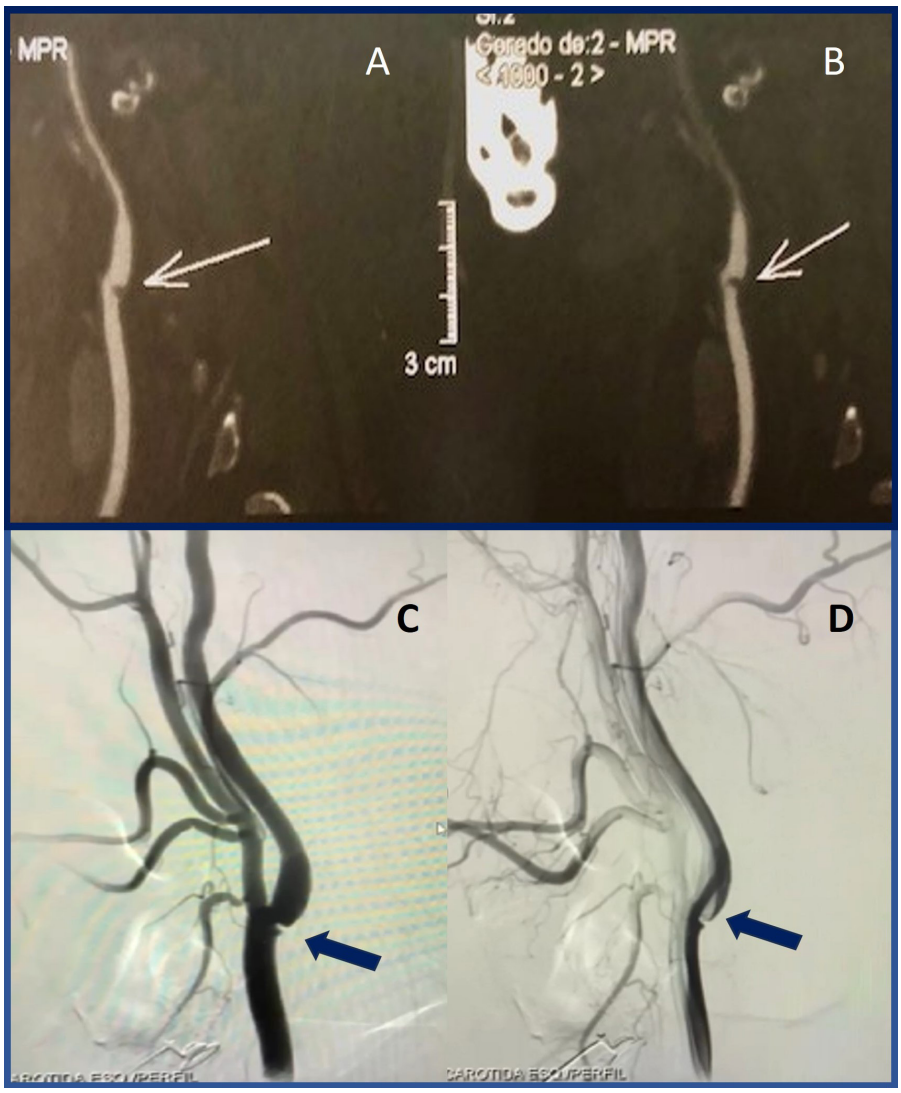

Figure 2 – *A and B) Case 1: Carotid web visualization in the bulb-emergence of the left internal carotid artery by tomography angiography (white arrows); C and D) Case 1: filling failure on contrast angiography, compatible with carotid web with flow turbulence.*

Due to is high resolution and images in multiple planes, CTA allows the identification of filling defect projecting from the carotid wall into the lumen, in addition to thrombi and calcium. It is useful for the exclusion of atherosclerosis and other vascular lesions and, so far, it is considered the method of choice for the diagnosis of CW.[4,6-8]

Digital subtraction angiography can be used in the CW diagnosis, however, since CW usually affects the posteromedial and posterolateral carotid artery wall, different angiographic projections may be necessary, with the disadvantage of being an invasive procedure.[7] Magnetic resonance angiography can evaluate the morphology and composition of CW, but there are few data in this regard.[4,8]

Differential diagnoses of CW are atherosclerotic plaque, carotid dissection, and intraluminal thrombus.[4] Fontaine et al.[10] compared ultrasound images (B-mode and microflow imaging) of 24 patients with CW and 24 patients with atherosclerotic plaques and reported that none of patients with atherosclerotic plaques presented ultrasonographic features suggestive of CW. The treatment of CW patients is still debatable. Therapeutic options include medical treatment with antiplatelet or anticoagulant agents, and/or interventions via stents or endarterectomy. Patel et al.[7] conducted a systematic review of 289 symptomatic CW patients across 15 series. Interventional management was performed in 151 (52.2%) (stent implantation in 87 and carotid endarterectomy in 64) and medical management was performed in 138 (47.8%), including antiplatelet therapy and anticoagulants. Baseline characteristics and time from index CVA were similar between medical and interventional patients. In the interventional group, no

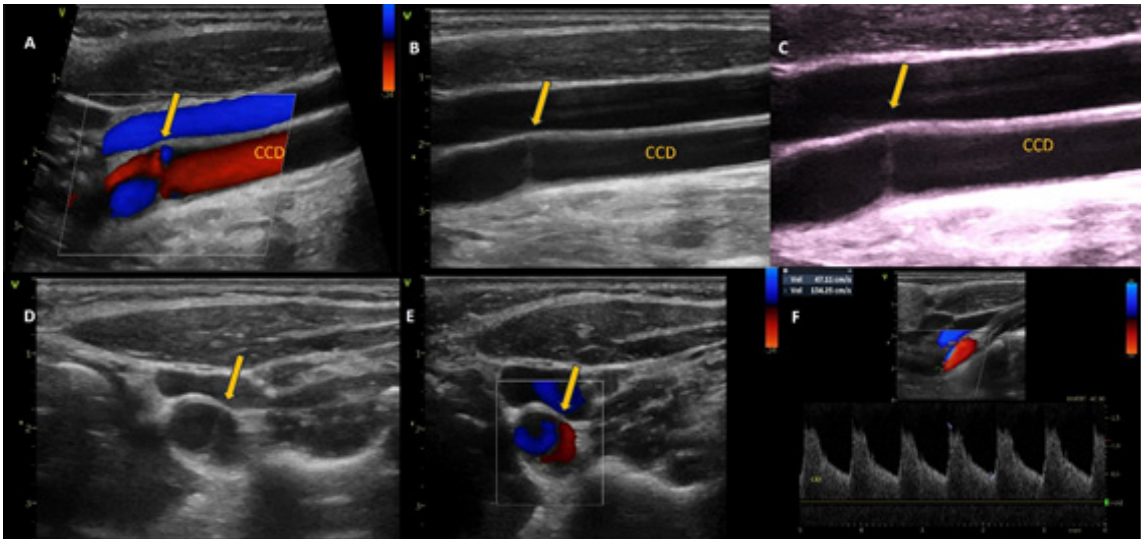

Figure 3 – *Case 2: Visualization of the carotid web (yellow arrows) by Vascular Ultrasonography; A) Longitudinal section with color Doppler; B and C) B mode longitudinal section view; D) B mode cross section view; E) Color Doppler cross section view; F) Pulsed Doppler demonstrating flow turbulence (peak systolic velocity = 134cm/s).*

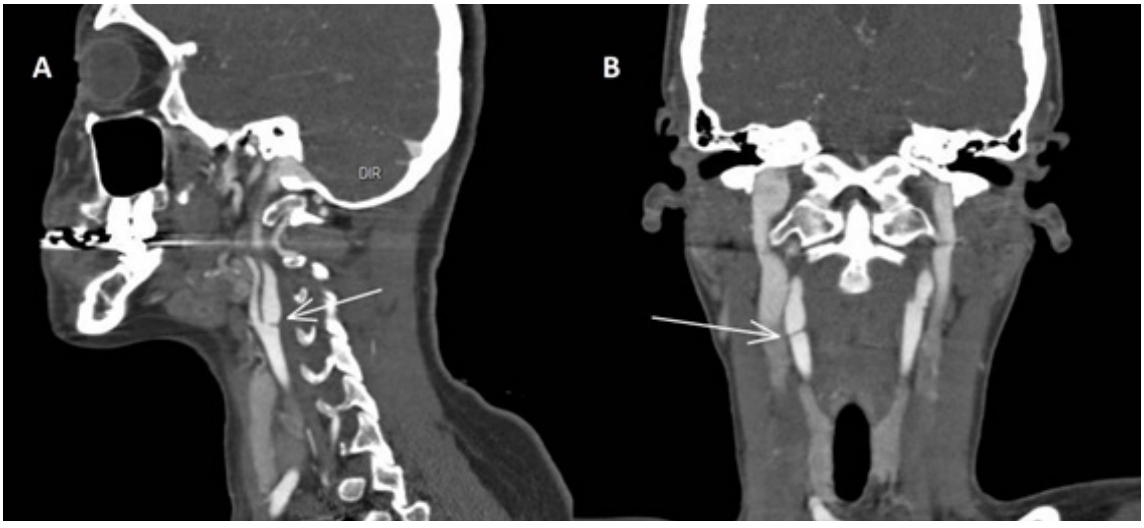

Figure 4 – *A and B) Case 2: Visualization of the carotid web (white arrows) by CT angiography*

recurrent ischemic events were observed over a follow-up of up to 60 months. In the medical group, over a follow-up of up to 55 months, recurrence rate was 26.8%, with no statistical difference between patients receiving any antithrombotic vs. no antithrombotic.

Therefore, the diagnosis of CW depends on a greater knowledge about the disease, to identify those patients with neurological events, frequently young patients, to provide proper treatment and prevent recurrence. In this context, VUS stands out as a low-cost, reliable, and accessible diagnostic method.

Author Contributions

Conception and design of the research: Petisco ACGP, Dourado JPA, Dourado LA; acquisition of data and analysis and interpretation of the data: Petisco ACGP, Dourado PM, Tebaldi RT; writing of the manuscript: Petisco ACGP; critical revision of the manuscript for intellectual content: Petisco ACGP, Dourado PM, Tebaldi RT, Dourado JPA, Dourado LA.

Potential Conflict of Interest

No potential conflict of interest relevant to this article was reported.

Sources of Funding

There were no external funding sources for this study.

Study Association

This study is not associated with any thesis or dissertation work.

Ethics Approval and Consent to Participate

This article does not contain any studies with human participants or animals performed by any of the authors.

References

1. Rainer WG, Cramer GG, Newby JP, Clarke JP. Fibromuscular Hyperplasia of the Carotid Artery Causing Positional Cerebral Ischemia. Ann Surg. 1968;167(3):444-6. doi: 10.1097/00000658-196803000-00021.
2. Zhang AJ, Dhruv P, Choi P, Bakker C, Koffel J, Anderson D, et al. A Systematic Literature Review of Patients with Carotid Web and Acute Ischemic Stroke. Stroke. 2018;49(12):2872-6. doi: 10.1161/STROKEAHA.118.021907.
3. Compagne KCJ, van Es ACGM, Berkhemer OA, Borst J, Roos YBWEM, van Oostenbrugge RJ, et al. Prevalence of Carotid Web in Patients with Acute Intracranial Stroke Due to Intracranial Large Vessel Occlusion. Radiology. 2018;286(3):1000-7. doi: 10.1148/radiol.2017170094.
4. Mac Grory B, Emmer BJ, Roosendaal SD, Zagzag D, Yaghi S, Nossek E. Carotid Web: An Occult Mechanism of Embolic Stroke. J Neurol Neurosurg Psychiatry. 2020;91(12):1283-9. doi: 10.1136/jnnp-2020-323938.
5. Sajedi PI, Gonzalez JN, Cronin CA, Kouo T, Steven A, Zhuo J, et al. Carotid Bulb Webs as a Cause of "Cryptogenic" Ischemic Stroke. AJNR Am J Neuroradiol. 2017;38(7):1399-404. doi: 10.3174/ajnr.A5208.
6. Madaelil TP, Grossberg JA, Nogueira RG, Anderson A, Barreira C, Frankel M, et al. Multimodality Imaging in Carotid Web. Front Neurol. 2019;10:220. doi: 10.3389/fneur.2019.00220.
7. Patel SD, Otite FO, Topiwala K, Saber H, Kaneko N, Sussman E, et al. Interventional Compared with Medical Management of Symptomatic Carotid Web: a Systematic Review. J Stroke Cerebrovasc Dis. 2022;31(10):106682. doi: 10.1016/j.jstrokecerebrovasdis.2022.106682.
8. Liang S, Qin P, Xie L, Niu S, Luo J, Chen F, et al. The Carotid Web: Current Research Status and Imaging Features. Front Neurosci. 2023;17:1104212. doi: 10.3389/fnins.2023.1104212.
9. Luo X, Li Z. Ultrasonic Risk Stratification of Carotid Web. Echocardiography. 2019;36(11):2103-7. doi: 10.1111/echo.14521.
10. Fontaine L, Guidolin B, Viguier A, Gollion C, Barbieux M, Larrue V. Ultrasound Characteristics of Carotid Web. J Neuroimaging. 2022;32(5):894-901. doi: 10.1111/jon.13022.

Brief Communication

Correlation of Telemedicine-guided POCUS Echocardiography and In Situ Data: Pilot Study in a Remote Area in Brazil

Juliane Rompkoski,[1] Tarso Augusto Duenhas Accorsi,[1] Bruna Dayanne Reges Amaral,[1] Christian Barbosa de Freitas,[2] Flavio Tocci Moreira,[1] Karen Francine Kohler,[1] Karine De Amicis Lima,[1] Renata Albaladejo Morbeck,[1] Carlos Henrique Sartorato Pedrotti[1]

Hospital Israelita Albert Einstein,[1] São Paulo, SP – Brazil

Sistema de Saúde Governamental, Unidade Básica de Saúde de Almeirim,[2] Almeirim, PA – Brazil

Abstract

Cardiovascular diseases remain the leading cause of mortality in Brazil. Nevertheless, a significant portion of the Brazilian population still faces challenges in accessing specialized care and undergoing complementary exams, especially in remote areas. Currently, data transmission and remote specialized assessment are possible, but obtaining echocardiographic images still relies on a trained professional on-site. This pilot study aimed to assess the feasibility of Point-of-Care Ultrasound (POCUS) tele-echocardiography administered by a general physician with specialist guidance to improve accessibility to cardiovascular exams. Ten patients (mean age was 58.6±8 years, 50% female) from the North region participated, undergoing remote-guided tests using Philips Lumify™ ultrasound and Facetime for transmission. These patients had recent official echocardiographic exams. As part of the POCUS examination, seven echocardiographic views were obtained — parasternal long axis, parasternal short axis (PSAX), apical four chambers (A4C), apical five chambers (A5C), apical two chambers (A2C), subcostal (SC), and suprasternal (SSN). The procedure included linear measurements of cardiac chambers, and valve analysis was performed using color flow. The on-site examinations were carried out by a general physician who underwent brief training prior to the official exams. Despite encountering technical challenges, the study demonstrated the viability of acquiring echocardiographic images. Overall agreement in examination results was observed, except for left ventricular segmental contractility in two cases and the systolic diameter of the left ventricle. The approach, though performed by untrained professionals, showed promise in screening cardiovascular diseases in remote locations, focusing on ventricular function and valvular diseases. Nevertheless, further research is necessary to improve the quality of this process.

Keywords

Echocardiography; Telemedicine; Ultrasonography; Telediagnostics; Telecardiology

Mailing Address: Juliane Rompkoski •
Hospital Israelita Albert Einstein – Telemedicina. Av. Albert Einstein, 627, Bloco B, 2º andar. Secretaria da Unidade de Telemedicina São Paulo. Postal code: 05652-900. São Paulo, SP – Brazil
E-mail: jurompkoski@gmail.com
Manuscript received December 1, 2023, revised manuscript January 18, 2024, accepted January 30, 2024
Editor responsible for the review: Marcelo Dantas Tavares de Melo

DOI: https://doi.org/10.36660/abcimg.20230110i

Introduction

Performing echocardiography is a challenging task in areas that are remote and have a low human development index.[1] Although data transmission is currently available and there is ample evidence of remote specialized evaluation, it depends on a professional trained *in loco* to obtain the echocardiographic views.[2] The use of artificial intelligence is still in the development stage and requires more scientific evidence.[3]

In recent years, tele-echocardiography has expanded all over the world, involving experimental studies with non-cardiologist physicians, non-physicians, and even remotely operated robotic devices, combined with remote interpretation by cardiologist echocardiographers.[4]

Handheld imaging platforms and remote interpretation have introduced these developments to the realm of echocardiography. The increasing accessibility of mobile computers and handheld imaging devices opens up new avenues for delivering and optimizing cardiovascular healthcare.[5] Various types of handheld ultrasounds with differing capabilities are available; a laptop-based system covers almost every 2D echocardiographic application, whereas a pocket-size ultrasound may not have full-scale color-flow and spectral Doppler capabilities. POCUS has demonstrated good accuracy. For instance, in a study by Abe et al., which involved 130 patients with aortic stenosis, pocket ultrasound successfully differentiated moderate-to-severe aortic stenosis with a sensitivity of 84% and specificity of 90%, even without quantitative Doppler information.[6]

In Brazil, there is an ongoing program for screening congenital heart diseases in the northeastern region of the country, where telemedicine and tele-echocardiography are utilized for early diagnosis and patient monitoring.[7]

While tele-echocardiography has proven useful in detecting cardiac abnormalities, it still lacks robust evidence, particularly concerning image quality compared to traditional echocardiography. Furthermore, its implementation in remote areas necessitates discussions on digital infrastructure, cost-effectiveness, regulation, and legal challenges.[5]

The feasibility of untrained medical professionals obtaining POCUS echocardiography data using a handheld device, guided synchronously by a mobile device under the supervision of an echocardiographer, is still under investigation.[8]

This pilot study aims to assess the feasibility and correlation of echocardiography data obtained in person versus those guided by telemedicine, conducted by untrained general practitioners using simple devices.

Materials and methods

This pilot prospective unicentric study analyzed ten consecutive patients in the North Region of Brazil who were part of the specialized medical assistance program through the telemedicine health system development program (PROADI, in the Portuguese acronym) by the Ministry of Health, Brazil. The study was performed at Almeirim in Pará, Brazil, a remote city that could be reached mainly through water transport, which comprised the Telemedicine Center and an echocardiographer.

The inclusion criteria for the participants comprised age ≥ 18 years old, returning for the medical telemedicine appointment and bringing an echocardiography performed *in loco*. The exclusion criteria were incomplete echocardiographic data. *In situ* echocardiograms were performed by different echocardiographers.

Data collection took place from June to July 2023. This study was approved by the local institutional review board under the registration of the name TeleECO. All data can be accessed from the institutional digital records.

All remote-guided tests were performed using a portable Philips Lumify® ultrasound (Figure 1). Seven echocardiographic views were defined to be performed on all patients: parasternal long axis (PLAX), PSAX, A4C, A5C, A2C, SC, and SSN.

The professional who conducted the examinations locally is a general practitioner from the local basic health unit. Two pre-exam meetings were held to train the general practitioner, with each meeting including training on performing a complete examination.

The exams were transmitted via the Facetime platform.

It was a POCUS approach, so it was obtained linear measurements of cardiac chambers (septum, posterior wall, aortic root, ascending aorta, left atrium, systolic diameter of the left ventricle and diastolic diameter of the left ventricle) taken in the parasternal long axis view (APLAX), and measurements of the right ventricle were taken in the A4C view. Valve analysis was conducted using color flow, as the continuous Doppler function was not available on the portable device. Free tracing for the assessment of cardiac chamber volumes, such as the left atrium, and for determining ventricular function using the Simpson method was also not feasible.

When there was left ventricular dysfunction, the ejection fraction was estimated by the echocardiography specialist who was guiding the examination remotely. The time taken to perform each exam was recorded. The IBM-SPSS for Windows version 22.0 software was used, and the statistics were descriptive.

Results

The first ten consecutive patients screened were included in the study. Seven patients with cardiovascular risk factors had

Figure 1 – *Portable Philips Lumify® ultrasound used to perform the exams.*

in situ exams requested to investigate end-organ damage, two for risk stratification in patients with chronic coronary artery disease, and one for evaluating mitral biological prosthesis. The mean age of the patients was 58.6±8 years, and 50% were female.

The mean time taken to perform the POCUS echocardiography exam was 23.1 minutes. All proposed cardiac seven views were obtained, some with window limitation due to patient biotype. We had imaging limitations in one patient with obesity in the SC and SSN windows. Guidance and image interpretation were feasible through mobile screen calls. The results of the main continuous variables for each patient are shown in Figure 2, and examples of images interpreted by the cell phone screen are shown in Figure 3. Regarding regional wall motion abnormalities, eight patients showed conformity between tests. In these two cases, remote evaluation identified segmental abnormalities that were not observed previously, but both patients underwent cardiac catheterization immediately after the virtual encounter, and the clinical context of the procedure may explain the disparity in results. Concerning valvular heart disease, there was agreement in nine exams (five with no regurgitation jets and four with mild mitral regurgitation jets). However, in one test, the remote assessment noted mild mitral regurgitation that had not been reported earlier.

The echocardiographs performed *in situ* were done four to twelve months prior to the remotely guided test. One of the patients had a biological mitral prosthesis, and its evaluation was limited due to the absence of continuous Doppler in the device. In general, the assessment of cardiac function through ejection fraction was reasonably equivalent between the tests.

Discussion

Echocardiogram is a simple and non-invasive diagnostic test that is difficult to access in remote places, and the main factors that contribute to this are the availability of the device and a trained professional. Although specialized cardiological

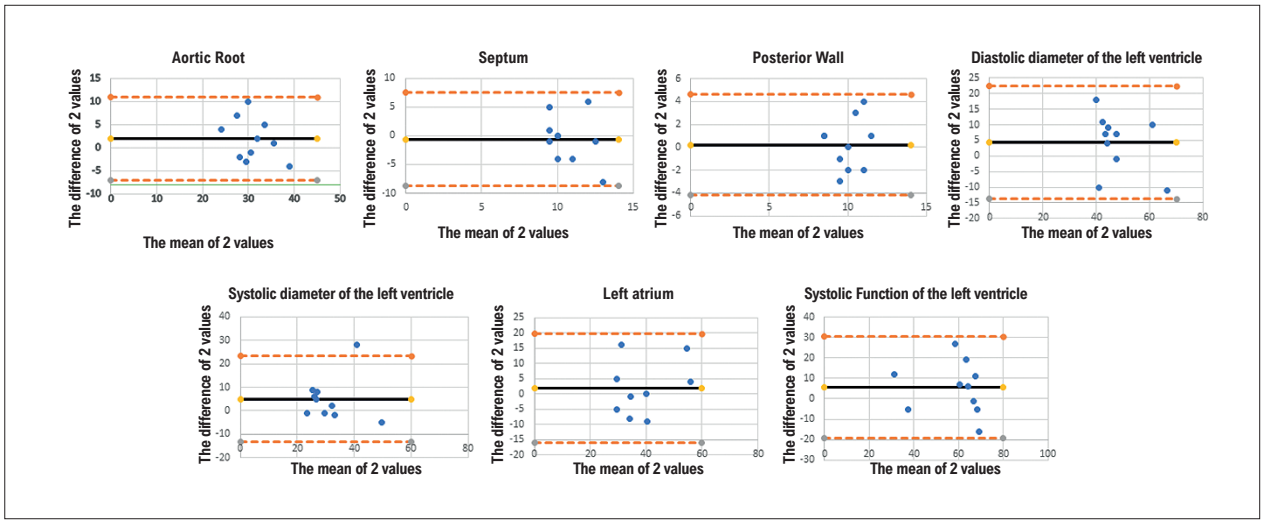

Figure 2 – *Based on the analysis of the Bland-Altman plots obtained from linear measurements, it can be observed that, despite a difference in the mean of the measurements, most elements showed agreement between the measurements, remaining within the confidence interval. The exception was the systolic diameter of the left ventricle, where one measurement fell outside the interval.*

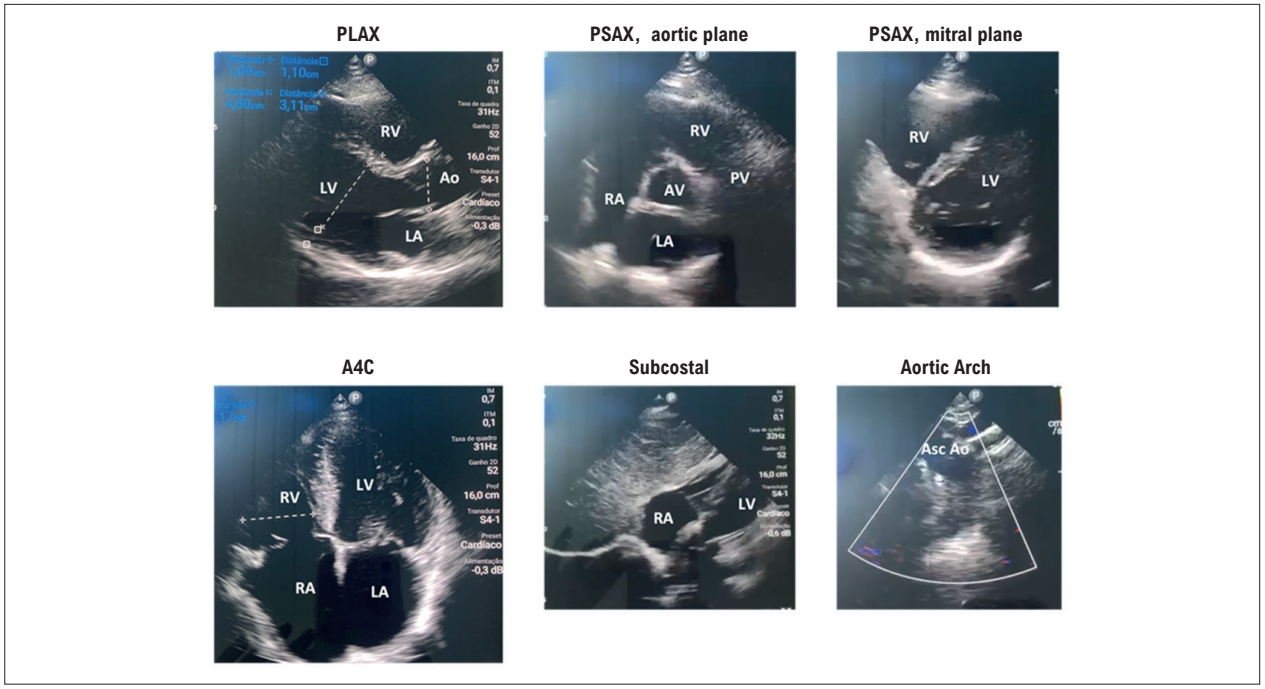

Figure 3 – *Six basic echocardiography views analyzed remotely by cell phone screen. PLAX: parasternal long axis; PSAX: parasternal short axis; A4C: apical four chambers; SC: subcostal.*

care provided virtually is possible, it is focused on clinical reasoning in teleconsultation, and the problem of carrying out complementary exams is still worrying.

Tele-echocardiography is usually based on images obtained by non-medical professionals with an asynchronous echocardiographer interpretation.[9] A Brazilian study with this methodology included more than 1,000 patients. It showed a high correlation for detecting cardiovascular alterations between the tests, but led to the overestimation of regurgitation jets, ventricular dysfunction, and ventricular hypertrophy.[10]

Our study had an untrained general practitioner performing echocardiographic views with a portable device. All remote-guided tests were performed using a portable Philips Lumify® ultrasound. Seven echocardiographic views were defined to be performed on all patients: PLAX, PSAX, A4C, A5C, A2C, SC, and SSN. The professional who conducted the examinations locally is a general practitioner from the local

basic health unit. Two pre-exam meetings were held to train the general practitioner, with each meeting including training on performing a complete examination.

We faced some technical difficulties during the conduction of the guided test. The first pertains to the necessity of a third person who would be responsible for recording the real-time execution of the test for the specialist to guide hand movements and probe angulation to improve the quality of the acquired image. The second lies in the examination's guidance, particularly in the fine movements required to optimize the image quality. Despite these challenges, all patients obtained results that could be analyzed and compared to the official *in situ* echocardiogram.

There were some discrepancies in the linear measurements obtained, especially in the dimensions of the systolic diameter of the left ventricle, besides the septum and posterior wall, which resulted in an overestimation of the hypertrophy and can be attributed to the examination executor's lack of experience.

As the examinations progressed, the time required for their execution decreased. The mean time was 23 minutes, which is a feasible timeframe for integrating this examination into primary care services.

Lastly, it's important to highlight that this pilot study presents certain limitations. The first relates to the portable Ultrasound device. While the promises of POCUS are substantial, one of the major concerns is standardizing the quality of scanning and interpretation, in addition to its limited capabilities in terms of image quality and applications like pulsed-wave Doppler. Due to its availability, POCUS can be more easily utilized than standard echocardiography, and the image quality and interpretation issues can be addressed by having a specialist during real-time exams.

The second involves the inclusion of consecutive patients without any regular clinical follow-up. Furthermore, using different echocardiography devices to conduct the *in-situ* tests may lead to variations in the quality of the obtained images.

Conclusion

Timely telemedicine-guided echocardiography performed by a generalist professional appears to be feasible for screening cardiovascular diseases in remote locations, especially for the assessment of ventricular function and screening for valvular diseases. Future research must be done to address the quality development of this task.

Acknowledgment

We thank Mrs. Bárbara Costa Roim, clinical coordinator of the POCUS Program at Philips do Brazil, for her invaluable collaboration with the device used.

Author Contributions

Conception and design of the research: Rompkoski J, Accorsi TAD, Freitas CB, Moreira FT, Kohler KF, Lima KA, Morbeck RA, Pedrotti CHS; acquisition of data: Rompkoski J, Amaral BDR, Freitas CB, Morbeck RA; analysis and interpretation of the data, statistical analysis and writing of the manuscript: Rompkoski J, Accorsi TAD; critical revision of the manuscript for intellectual content: Accorsi TAD, Moreira FT, Kohler KF, Lima KA, Pedrotti CHS; study supervision: Pedrotti CHS.

Potential Conflict of Interest

No potential conflict of interest relevant to this article was reported.

Sources of Funding

There were no external funding sources for this study.

Study Association

This study is not associated with any thesis or dissertation work.

Ethics Approval and Consent to Participate

This study was approved by the Ethics Committee of the Hospital Israelita Albert Enstein under the protocol number 63709222.0.000.0071/5.934.573. All the procedures in this study were in accordance with the 1975 Helsinki Declaration, updated in 2013. Informed consent was obtained from all participants included in the study.

References

1. Peters A, Patil PV. Tele-Echocardiography: Enhancing Quality at the Point-of-Care. Heart. 2019;105(4):264-5. doi: 10.1136/heartjnl-2018-313969.
2. Salerno A, Kuhn D, El Sibai R, Levine AR, McCurdy MT. Real-Time Remote Tele-Mentored Echocardiography: A Systematic Review. Medicina. 2020;56(12):668. doi: 10.3390/medicina56120668.
3. Zhou J, Du M, Chang S, Chen Z. Artificial Intelligence in Echocardiography: Detection, Functional Evaluation, and Disease Diagnosis. Cardiovasc Ultrasound. 2021;19(1):29. doi: 10.1186/s12947-021-00261-2.
4. Arbeille P, Chaput D, Zuj K, Depriester A, Maillet A, Belbis O, et al. Remote Echography between a Ground Control Center and the International Space Station using a Tele-operated Echograph with Motorized Probe. Ultrasound Med Biol. 2018;44(11):2406-12. doi: 10.1016/j.ultrasmedbio.2018.06.012.
5. Seetharam K, Kagiyama N, Sengupta PP. Application of Mobile Health, Telemedicine and Artificial Intelligence to Echocardiography. Echo Res Pract. 2019;6(2):R41-R52. doi: 10.1530/ERP-18-0081.
6. Abe Y, Ito M, Tanaka C, Ito K, Naruko T, Itoh A, et al. A Novel and Simple Method Using Pocket-Sized Echocardiography to Screen for Aortic Stenosis. J Am Soc Echocardiogr. 2013;26(6):589-96. doi: 10.1016/j.echo.2013.03.008.
7. Ramos JVB, da Silva MHA, de Sousa TMMA, de Araújo KDT, de Araújo JSS. The Impact of the Telemedicine Network on the Epidemiology of Congenital

Malformations in the State of Paraíba-Brazil: A Comparison with Worldwide Incidences. Res Soc Dev. 2022;11(7):e41211730233. doi: 10.33448/rsd-v11i7.30233.

8. Lopes MACQ, Oliveira GMM, Ribeiro ALP, Pinto FJ, Rey HCV, Zimerman LI, et al. Guideline of the Brazilian Society of Cardiology on Telemedicine in Cardiology - 2019. Arq Bras Cardiol. 2019;113(5):1006-56. doi: 10.5935/abc.20190205.

9. Evangelista A, Galuppo V, Méndez J, Evangelista L, Arpal L, Rubio C, et al. Hand-Held Cardiac Ultrasound Screening Performed by Family Doctors with Remote Expert Support Interpretation. Heart. 2016;102(5):376-82. doi: 10.1136/heartjnl-2015-308421.

10. Nascimento BR, Beaton AZ, Nunes MCP, Tompsett AR, Oliveira KKB, Diamantino AC, et al. Integration of Echocardiographic Screening by Non-Physicians with Remote Reading in Primary Care. Heart. 2019;105(4):283-90. doi: 10.1136/heartjnl-2018-313593.